Shedding light on adhesion and biofilms of *Halobacterium salinarum* R1

TECHNISCHE UNIVERSITÄT DARMSTADT

Vom Fachbereich Biologie der Technischen Universität Darmstadt

zur

Erlangung des akademischen Grades

eines Doctor rerum naturalium

genehmigte

Dissertation von

Dipl.-Biol. Gerald Losensky

aus Groß-Umstadt

1. Referentin: Prof. Dr. Felicitas Pfeifer

2. Referent: PD Dr. Arnulf Kletzin

Tag der Einreichung: 12.05.2016

Tag der mündlichen Prüfung: 11.07.2016

Darmstadt 2016

D 17

„For science, play is not a luxury, but a necessity.“

-- Sir Edwin Southern

Publications

Parts of the present work have already been published or have been submitted for publication.

[1]**Losensky, G.**, Vidakovic, L., Klingl, A., Pfeifer, F. and Fröls, S. (2014). Novel pili-like surface structures of *Halobacterium salinarum* strain R1 are crucial for surface adhesion.
Front Microbiol, 5, 755. doi:10.3389/fmicb.2014.00755

[2]**Losensky G.**, Fröls S., Jung K., Pfeifer F., Urlaub H. and Lenz C. (2016). Shedding light on biofilm formation of *Halobacterium salinarum* R1 by SWATH-LC/MS/MS analysis of planktonic and sessile cells.
PROTEOMICS. Submitted February 2016, under revision.

[1]Gene deletion mutants were generated by L. Vidakovic. Single and double gene deletion mutants were originally characterized by L. Vidakovic. Transmission electron microscopic studies were performed by L. Vidakovic in cooperation with A. Klingl at Cell Biology and LOEWE Research Center for Synthetic Microbiology, Philipps University, Marburg.
[2]Mass spectrometric analyses and technical evaluations were performed by C. Lenz in the group of H. Urlaub at the Institute for Clinical Chemistry, University Medical Center, Göttingen and the Bioanalytical Mass Spectrometry group, Max Planck Institute for Biophysical Chemistry, Göttingen. Statistical calculations were carried out by K. Jung at the Institute for Animal Breeding and Genetics, University of Veterinary Medicine, Hannover.

Contents

Summary

Biofilms, *i.e.* multicellular microbial communities, are widely accepted as the predominating mode of prokaryotes living in nature. However, knowledge about this lifestyle is still limited, especially in Archaea. The present work focuses on the formation of archaeal biofilms by the extremely halophilic archaeon *Halobacterium salinarum* R1.

Surface adhesion of *Hbt. salinarum* R1 was monitored by phase contrast microscopy and quantified in a fluorescence-based adhesion assay, and demonstrated that abiotic surfaces were successively colonized by the cells. The formation of complex three-dimensional cell clusters with tower-like structures up to 25 μm in height was observed within 15 days by scanning electron microscopy and confocal laser scanning microscopy. Extracellular polymeric substances, *i.e.* a complex biofilm matrix containing extracellular DNA and glycosidic residues, was detected using suitable molecular probes, as well as a high viability of the biofilm cells. The sequence of events observed during the biofilm formation consisted of adhesion, accumulation and maturation. Adherent cells contained different types of cell surface structures, since filaments with two predominant diameters (7-8 and 10 nm) were observed. One of the diameters belongs to the archaellum, whereas the smaller one belongs to pili involved in adhesion.

The *Hbt. salinarum* R1 genome was searched for genes potentially associated with the synthesis of cell surface structures by bioinformatical analyses. Two gene loci, pil-1 and pil-2, putatively encoding type IV pilus-like structures were identified. It was demonstrated by RT-PCR that both loci were transciptionally active and cotranscribed. Moreover, qRT-PCR yielded 5.2- and 8.5-fold induction of the respective ATPase genes, *pilB1* and *pilB2*, in adherent cells compared to planktonic cells. Deletion of the archaella ATPase gene, *flaI*, resulted in cells lacking the 10 nm filaments. These cells were non-motile but still showed the 7-8 nm appendages and strong adhesion. An additional deletion of *pilB1* in a Δ*flaI*/Δ*pilB1* mutant severely impaired the ability of the cells to adhere, which was reduced to 20% compared to the parental strain. In contrast, an additional deletion of *pilB2* did not have further effects on adhesion. A search for genes encoding the filament subunits, *i.e.* pilins, yielded more than 30 candidates. Transcriptional analyses of the most likely candidates demonstrated differential expression of the genes in planktonic and adherent samples, with the genes *pilA5*, *pilA6* and *pilA7* showing 2.5- to 7.1-fold induction in initial biofilms.

A proteome analysis of the biofilm formation was performed investigating planktonic as well as initial and mature biofilm cells of *Hbt. salinarum* R1. A molecular differentiation of the protein pattern was already observed by SDS-PAGE in samples derived from biofilms after one day

compared to planktonic cells. Employing label-free mass spectrometric SWATH-LC/MS/MS analysis a high coverage of the predicted proteome was achieved, reflected by 1629 different proteins identified and 1464 proteins quantified (63.2% and 56.8% of the total proteome, respectively). A relative quantification was performed, showing between 55 and 245 proteins strongly altered (> 2-fold) when two of the cellular states were compared. 882 proteins showed statistically significant abundance changes, correspoding to 60.8% of the quantified proteins and 34.2% of the total proteome, respectivly, reflecting the high diversity of the processes affected. The relative changes detected ranged between 195-fold increase of an uncharacterized glutamine-rich alkaline protein (OE3542R) and 22.8-fold decrease of ribonucleoside-diphosphate reductase subunit beta (NrdB1). The most striking effects were observed with proteins involved in energy conversion, as well as proteins acting in nucleotide-, amino acid- and lipid metabolism. In addition, proteins associated with protein biosynthesis and cellular processes like cell motility and signal transduction were strongly affected. The proteomic data of selected proteins was validated by qRT-PCR transcriptional analyses.

This work represents the first comprehensive description of haloarchaeal biofilm formation using the example of *Hbt. salinarum* R1.

1. Introduction

1.1. Archaea – The third domain of life

In the late 1970s Carle Woese supposed that Archaea represent a distinct phylogenetic group (domain) besides Eukarya and Bacteria. This became clear by comparative sequence analysis of the 16S and 18S rRNA of many different microorganism, resulting in their separation into the three superkingdoms (Woese & Fox, 1977). The Archaea were originally further subdivided into the Euryarchaeota, dominated by methanogenic, halophilic and several thermophilic organisms, and the Crenarchaeota, comprising sulfur-dependent and hyperthermophilic microorganisms (Woese *et al.*, 1990). Later on, these phyla were complemented by the Korarchaeota, Nanoarchaeota and Thaumarchaeota (Barns *et al.*, 1996; Brochier-Armanet *et al.*, 2008; Huber *et al.*, 2002) (Figure 1). Moreover, additional archaeal phyla have been proposed recently, namely Aigarchaeota, Geoarchaeota, Bathyarchaeota and Lokiarchaeota. The latter ones represent the closest relatives of eukaryotes in phylogenomic analyses, potentially filling the gap between prokaryotes and eukaryotes (Kozubal *et al.*, 2013; Meng *et al.*, 2014; Nunoura *et al.*, 2011; Spang *et al.*, 2015).

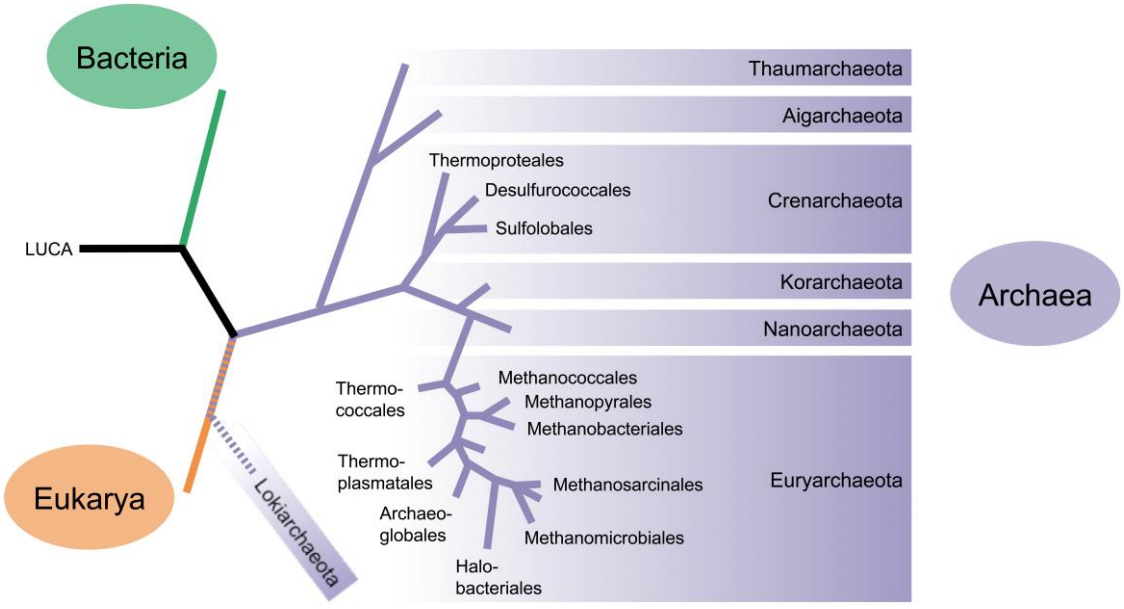

Figure 1 Schematic three-domains tree of life. The two archaeal phyla Bathyarchaeota and Geoarchaeota branching with the Thaumarchaeota and Aigarchaeota, respectively, are not shown for reasons of clarity. LUCA, last universal common ancestor. (Modified from Bang & Schmitz, 2015)

Archaea combine several bacterial and eukaryotic properties, but also show unique features. Archaeal cells resemble bacteria with respect to their sizes and regarding the organization of their genomes. They usually contain circular chromosomes often complemented by plasmids, while the genes are commonly found in polycistronic operons (Koonin & Wolf, 2008; Zillig *et al.*, 1988). Moreover, central metabolic processes in Archaea resemble those found in Bacteria

(Koonin *et al.*, 1997). In contrast, components involved in the cellular information processing (DNA replication, transcription, translation or DNA repair) display similarities to the processes in eukaryotes (Nasir *et al.*, 2014; Rivera *et al.*, 1998). However, Archaea also possess a number of distinct characteristics, such as the unique membrane ether lipids or methanogenesis, *i.e.* methane production from H_2 and CO_2, which represents a pathway exclusively present in methanogenic archaea (Falkowski *et al.*, 2008; Kandler & Konig, 1998; van de Vossenberg *et al.*, 1998).

Many extremophilic species are found among the Archaea, *i.e.* microorganisms adapted to extreme environmental conditions, like high temperature, very acidic or alkaline pH, radiation or high salinity (Rothschild & Mancinelli, 2001). Though Archaea are more widespread and diverse than initially assumed. They are found in virtually all habitats, which can be as disparate as deep-sea hydrothermal vents or the human gut (DeLong, 1998; Gaci *et al.*, 2014; Takai & Nakamura, 2011). Over the years it has become evident that Archaea play an elementary role in the global geochemical cycles (Falkowski *et al.*, 2008; Offre *et al.*, 2013). Nevertheless, it is especially their adaptations to extreme conditions that make Archaea of special interest, also affecting questions of the origin of life as well as its natural limitations (Tych *et al.*, 2015). Moreover, the potential exploitation of extremophiles for biotechnological applications, like enzymes or new biomaterials, makes them popular objects of investigations (Elleuche *et al.*, 2015; Ventosa & Nieto, 1995).

1.2. Halophilism – Coping with high salt concentrations

Microorganisms adapted to environments with extreme salt concentrations are referred to as 'halophilic' and are found in all three domains of life (Oren, 1999). Moderate halophilic microbes show optimal growth at NaCl concentrations between 0.5 and 2.5 M. Extremely halophilic representatives depend on salt concentrations of at least 1.5 M, while they grow best at 2.5 to 4.5 M salt and tolerate concentrations up to saturation (Andrei *et al.*, 2012). Eukaryotic examples comprise algae of the genus *Dunaliella* and diverse fungi. Halophilic bacteria are found within the phyla Cyanobacteria, Proteobacteria, Firmicutes, Actinobacteria, Spirochaetes, and Bacteroidetes. Regarding halophilic archaea, they are restricted to the euryarchaeota, with several species found among the methanogens. In addition, the family Halobacteriaceae solely contains halophilic members, also referred to as haloarchaea (Oren, 2008).

Halophiles thrive in habitats with high salt content, like salt lakes, the Dead Sea or salt crystallizer ponds used for salt manufacture (Figure 2A). For osmotic adaptation to their high salt environments, two major strategies are used to avoid a loss of water. The first one is based on the accumulation of *compatible solutes* in the cytoplasm, *i.e.* small organic molecules like

glycerol, amino acids or sugars, which can be adjusted depending on the outside salinity and do not interfere with the cells' proteins and enzymes. The second mechanism is termed *salt-in strategy* and used by *Salinibacter* as well as members of the Halobacteriaceae. They accumulate potassium ions in the cytoplasm, that are exchanged against sodium ions (Oren, 2002). Since less water molecules are coordinated by the potassium ions, this results in a higher water availability inside the cell. Nonetheless, the accumulation of molar salt concentrations inside the cells necessitates an adaptation of the intracellular constituents and proteins. In general halophilic proteins contain higher proportions of acidic and hydrophilic but reduced amounts of hydrophobic amino acids on their surfaces, to stabilize the protein structure and prevent aggregation under high salt conditions (Dennis & Shimmin, 1997; Nath, 2015; Oren, 2013).

1.3. *Halobacterium salinarum* R1 – An extremely halophilic archaeon

The extremely halophilc species *Halobacterium salinarum* R1 (DSM 671) is a member of the Halobacteriaceae, which comprise a number of 48 genera with 177 species (Gupta *et al.*, 2015). *Halobacterium* is a rod shaped microbe with a length of 3 to 7 μm (Figure 2B). It shows optimal growth at a salinity of 4.2 M NaCl and a temperature of 42 °C resulting in a doubling time of 7.5 hours. The genome sequence is available since 2008 and comprises 2.67 Mbp distributed to a 2 Mbp circular chromosome and four megaplasmids (Pfeiffer *et al.*, 2008b). The genome contains 2687 predicted genes and encodes 2592 proteins (NCBI). Also, the genome sequence of the closely related strain *Hbt. salinarum* NRC-1 is available (Ng *et al.*, 2000). Both strains originate from the same natural isolate and diverged in the laboratory. Their chromosomes are virtually identical, while the numbers and overall structures of the plasmids are different (Pfeiffer *et al.*, 2008b). The closely related *Hbt. salinarum* strains PHH1 and PHH4 display altered plasmid populations, as well.

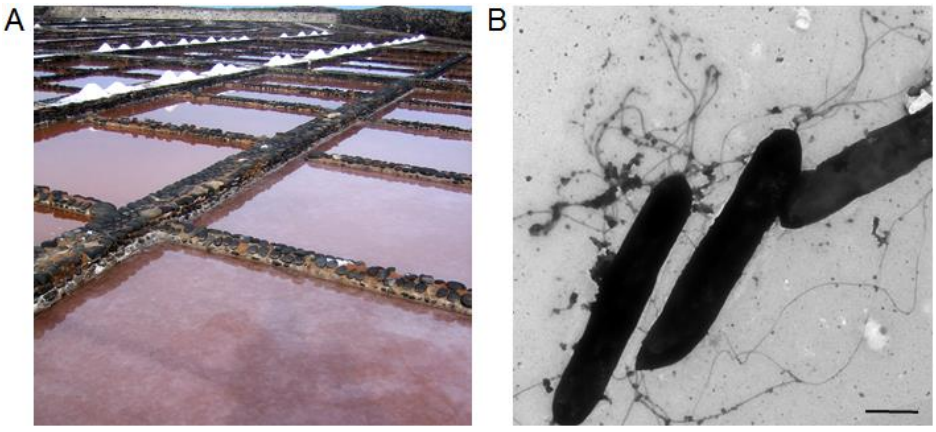

Figure 2 Typical habitat of haloarchaea and cell morphology of *Halobacterium salinarum*. **A**, Salt crystallizer pond at Salinas del Carmen, Fuerteventura (Courtesy of S. Fröls). **B**, Electron micrograph illustrating the typically rod shaped *Hbt. salinarum* R1 cells with cellular appendages. Cells contrasted with uranyl acetate. Scale bar 1 µm.

Halobacteriaceae in general are aerobic or facultative anaerobic heterotrophic microorganisms utilizing different organic substrates. Some species from the genera *Haloferax*, *Haloarcula* or *Halococcus* use carbohydrates, as opposed to *Halobacterium* species that grow solely on amino acids (Falb *et al.*, 2008). Under aerobic conditions *Halobacterium* uses a respiratory chain with oxygen as terminal electron acceptor for generation of a proton gradient across the cell membrane and the synthesis of ATP by ATP-synthase. The respiratory chain is adjustable depending on the oxygen availability, also allowing anaerobic respiration and the use of alternative electron acceptors like DMSO or TMAO under anaerobic conditions (Müller & DasSarma, 2005). An alternative important energy conservation mechanism is photophoshorylation by the light-driven proton pump bacteriorhodopsin under anoxic conditions, using light to generate a proton gradient across the cell membrane (Hartmann & Oesterhelt, 1977). *Halobacterium* is also capable of arginine fermentation for the generation of ATP by substrate level phosphorylation (Hartmann *et al.*, 1980; Ruepp & Soppa, 1996).

Halobacterium salinarum possesses archaella (archaeal flagella) for motility, which are encoded by the *fla* operon (Alam & Oesterhelt, 1984; Houwink, 1956; Patenge *et al.*, 2001). In combination with an array of signal transducing systems this enables chemotactic responses of the cells (Rudolph & Oesterhelt, 1995; Schlesner *et al.*, 2012; Schlesner *et al.*, 2009). Some haloarchaeal species possess an additional motility mechanism by the production of cytoplasmic gas vesicles. These are proteinaceous hollow organelles filled with gas, allowing the regulation of cell buoyancy and floatation in the water column to reach favored oxygen and light conditions. In strain R1 the corresponding genes are present but the operon is dysfunctional due to the insertion of an ISH-element (Pfeifer *et al.*, 2002).

Halobacterium species exhibit yellow to orange or pink to red pigmentation (Figure 3) of their cell membranes, which is typical for members of the Halobacteriaceae. This is due to the production of C_{40} and C_{50} carotenoids, like lycopene or bacterioruberin, protecting the cells from UV-light and oxidative damage (Mandelli *et al.*, 2012). High intracellular KCl concentrations protect the cells from oxidative damage, as well (Mandelli *et al.*, 2012; Shahmohammadi *et al.*, 1998). In combination with different DNA repair mechanisms, for instance photolyases and the UV repair (Uvr) system, this results in high UV resistance of the microorganisms, which is important in their natural habitats marked by intensive sun exposure (Baliga *et al.*, 2004).

Figure 3 Photograph of different *Halobacterium salinarum* strains in liquid cultures illustrating the varying and characteristic pigmentation of the cells. From left to right the strains S9, R1, DSM 3754^T, NRC-1, PHH1, and PHH4 are shown.

Furthermore, *Halobacterium* species resist extreme desiccation, ionizing radiation as well as starvation (Kottemann *et al.*, 2005; Norton & Grant, 1988; Stan-Lotter & Fendrihan, 2015). To cope with this, the microorganism has additional protection mechanisms. A number of physiological changes, most importantly DNA repair by homologous recombination, cell cycle progression and nucleotide metabolism, are associated with the responses to gamma irradiation (Kish *et al.*, 2009; Whitehead *et al.*, 2006). Another important resistance factor promoting growth and survival of haloarchaea is polyploidy of the cells, *i.e.* the presence of multiple chromosomal copies per cell (Jaakkola *et al.*, 2014). It was shown that *Hbt.* cells from the exponential growth phase contain up to 25 genome copies, while stationary cells have 15 copies (Breuert *et al.*, 2006). This facilitates an efficient DNA repair via homologous recombination and low mutation rates. Moreover, haloarchaea use the DNA provided by polyploidy as a storage polymer for phosphate (Zerulla *et al.*, 2014; Zerulla & Soppa, 2014). Another microbial process associated with cell survival and environmental adaptation is biofilm formation, which is observed with several haloarchaeal species that are capable of adhesion (Fröls *et al.*, 2012).

1.4. Biofilms – Microbial living communities

Microbial multicellular communities of a single or several species embedded in a matrix are referred to as biofilms. They are usually formed at interfaces, *e.g.* at the air-liquid or solid-liquid boundaries of aquatic habitats (Davey & O'Toole G, 2000). Biofilms are the preferred mode of how microorganisms live, with 3.5 billion year old microfossils representing the oldest proof of life on earth (Noffke *et al.*, 2013). Biofilms are found in natural, industrial and clinical environments (Parsek & Singh, 2003).

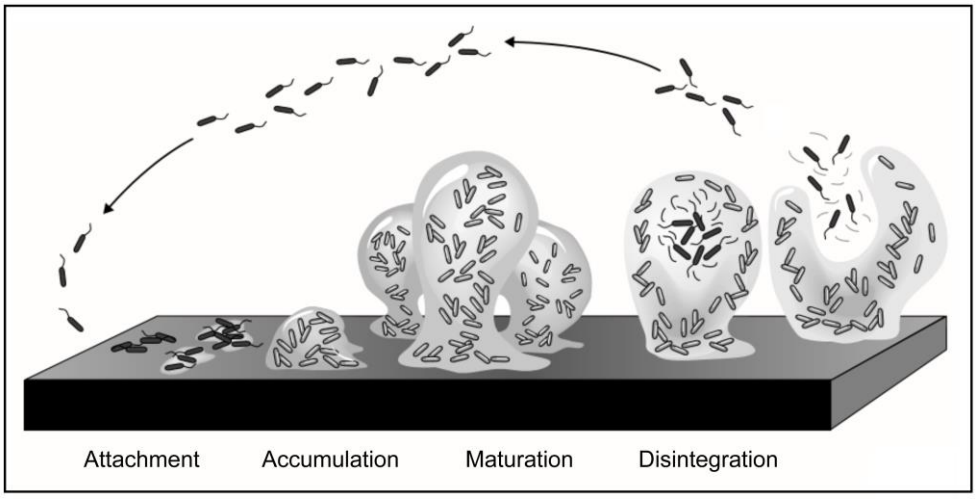

Figure 4 Developmental stages during biofilm formation. (Modified from Sauer, 2003)

The biofilm formation is initiated by the attachment of the cells to a substratum, *i.e.* planktonic cells change from a freely motile mode of life to an immobilized sessile lifestyle (Figure 4). The

adhesion is a reversible process at the beginning and often mediated by cellular surface structures, like flagella or pili (An & Friedman, 1998). As the attachment becomes irreversible, the cells start to accumulate on the surface and form aggregates referred to as microcolonies. The cells produce a biofilm matrix embedding them, which is composed of hydrated extracelluar polymeric substances (EPS), consisting of different types of biopolymers, like proteins, carbohydrates, lipids or nucleic acids. The biofilms grow and undergo a maturation process ending up with a characteristic three-dimensional structure, *e.g.* flat, rough, filamentous or mushroom-shaped. Finally, cells can detach from the biofilms and disperse to colonize other locations (Flemming & Wingender, 2010; Hall-Stoodley *et al.*, 2004).

The properties of biofilms depend on the EPS, which form the scaffold for the complex architecture and can account for over 90% of the dry mass. The EPS can vary greatly depending on the respective species or external conditions like temperature and nutrient availability (Sutherland, 2001). Living in biofilms provides several advantages for the microorganisms. One important aspect is protection from unfavorable environmental conditions, which is largely dependent on the biochemical EPS composition. The hydrated biofilm matrix protects the cells from desiccation, UV radiation, pH shifts and osmotic shock (Davey & O'Toole, 2000; Flemming & Wingender, 2010). In addition, the matrix provides a protective barrier against antimicrobial agents or toxic metals (Evans *et al.*, 1991; Harrison *et al.*, 2007) and in pathogenic species it protects from the host immune defense (Hänsch, 2012). Spatial closeness of the cells enables exchange of genetic material, which occurs with enhanced efficiency in biofilms (Molin & Tolker-Nielsen, 2003). Moreover, the proximity of cells allows for substrate interchange and removal or distribution of metabolites, thereby facilitating metabolic and syntrophic cooperations (Bryant *et al.*, 1967; Schink, 1997). Biofilms represent a heterogenous cell population, due to diffusional constraints and metabolic activities that lead to the formation of chemical gradients and thereby generate local cellular niches (Stewart & Franklin, 2008).

Most current knowledge of biofilm formation is based on bacterial examples, due to their clinical, industrial and domestic relevances. However, it was realized that Archaea are capable to form complex biofilms, as well. They are often found associated with bacterial species in environmental biofilms in diverse habitats (Fröls, 2013). Biofilm formation and the production of extracellular polysaccharide-containing EPS has been studied in different crenarchaeote as well as euryarchaeote species (Anton *et al.*, 1988; Nicolaus *et al.*, 2003; Rinker & Kelly, 1996) and the presence of extracellular DNA (eDNA) is detected (Fröls *et al.*, 2012; Koerdt *et al.*, 2010). It was shown that *Archaeoglobus fulgidus* forms biofilms in response to stress factors, like low temperatures, antibiotics, pH, radiation or NaCl, however, the regulatory mechanisms are unknown (Lapaglia & Hartzell, 1997). First functional genomic analyses on archaeal biofilm formation were performed in the extremely acidophilic *Ferroplasma acidarmanus*. A proteomic

approach was used to examine protein expression patterns differing between planktonic and biofilm cells. The results suggest an association of mature biofilms with anaerobic growth (Baker-Austin *et al.*, 2010). Moreover, biofilm formation has been investigated in detail with regard to three closely related *Sulfolobus* species using a combination of transcriptomic and proteomic analyses. The studies demonstrate that the sessile lifestlye is strain-specific. Differential expression is observed with 1 to 15% of the genes depending on the species, affecting diverse cellular processes. Only a few factors are shared by all three strains, among them putative transciptional regulators, *i.e.* Lrs14 proteins (Koerdt *et al.*, 2011). Subsequent mutational analyses showed that they are key factors in the regulation of *Sulfolobus* biofilm formation and the archaella-driven cell motility (Orell *et al.*, 2013b). Furthermore, Archaea possess additional cell surface structures, some of which have influences on biofilm formation, as demonstrated in *Sulfolobus* and *Haloferax* species (Lassak *et al.*, 2012a; Pohlschröder & Esquivel, 2015).

1.5. Cell surface structures of archaea – Varieties and functions

Microorganisms interact with their environment by cell surface structures. Similar to bacteria, archaea possess a variety of such structures with functions in motility, adhesion, DNA-exchange, or substrate binding (Lassak *et al.*, 2012a). While some of these structures were shown to have bacterial equivalents, others are unique to the archaeal domain (Jarrell *et al.*, 2013).

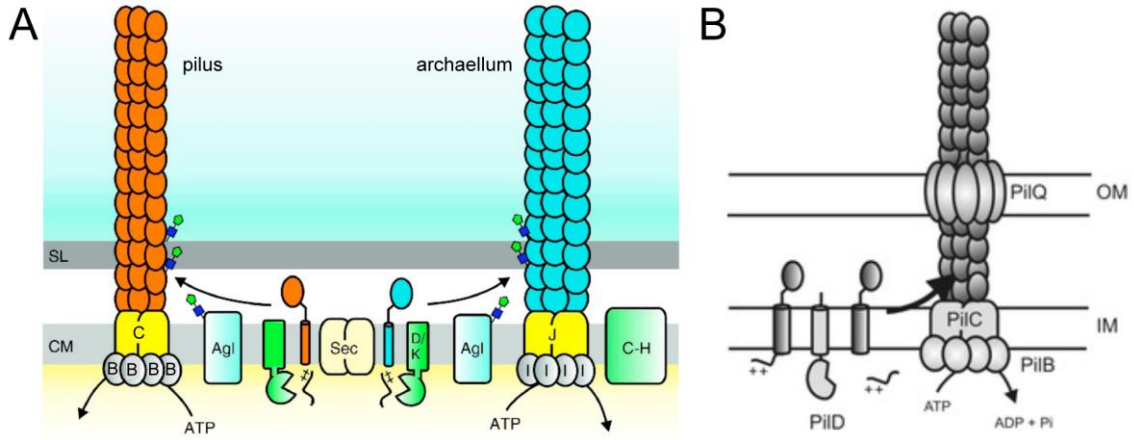

Figure 5 Assembly of archaeal type IV pilus-like cell appendages and bacterial type IV pili. **A**, Schematic view of archaeal type IV pilus-like structures (pilus and archaellum). Prepilin/archaellin monomers (orange and blue, respectively) are processed by the prepilin/archaellin peptidase (FlaK) before they are incorporated at the basal end. Energy for assembly is supplied by the assembly ATPase (PilB/FlaI), while the transmembrane protein (PilC/FlaJ) serves as the platform located in the cytoplasmic membrane (CM). C-H, accessory archaella proteins; Agl, archaeal glycosylation pathway; Sec, protein secretion pathway; SL, protein cell surface layer. **B**, Illustration of a type IV pilus of Gram-negative bacteria. Sequence is similar to A, with the protein nomenclature: PilA, prepilin monomers; PilB, assembly ATPase; PilC, transmembrane protein; PilD, prepilin peptidase, PilQ, pore-forming outer membrane (OM) protein; IM, inner (cytoplasmic) membrane. (Modified from Pohlschröder *et al.*, 2009 and Albers & Pohlschröder, 2009)

Archaeal cell appendages can be devided into two major categories, type IV pilus-like (T4P-like) and non-type IV pilus-like structures. T4P-like refers to the core components and the assembly mechanism (Figure 5), which are similar to those found in bacterial type IV pili (Lassak *et al.*, 2012a). The T4P filaments consist of pilins, which are secreted via the Sec pathway. The precursor proteins (prepilins) are integrated into the cytoplasmic membrane by a conserved hydrophobic stretch and processed by a class III signal peptidase (PibD/PilD) at the cytoplasmic side. For the assembly of the pilins at the basal end of the filament, the ATPase, PilB, and the transmembrane protein, PilC, are necessary, providing the energy and a platform formed by the transmembrane protein. Additional proteins may be involved in the biosynthesis of T4P-like structures, but they are not conserved across the prokaryotic domains (Pohlschröder *et al.*, 2011).

The archaellum (archaeal flagellum) is the best-studied example among the T4P-like structures. It performs the same function as the bacterial flagellum, but the assembly systems and structures of both organelles are different. Bacterial flagella are assembled via a type III secretion system that governs the flagellin subunits through the hollow filament to the distal tip. In contrast, archaella have smaller diameters and are assembled by the integration of the subunits in a T4P-like manner at the base. The archaellin subunits are processed by a prearchaellin peptidase (Shahapure *et al.*, 2014). The correspoding genes are organized in operons (Albers & Jarrell, 2015). Most genes involved in the formation of the *Hbt. salinarum* R1 archaellum are encoded by the *fla* gene cluster [Figure 6, (Patenge *et al.*, 2001)]. They are complemented by the prearchaellin peptidase encoding gene (*flaK*) as well as the five archaellin genes from the A and B loci (*flgA1-2* and *flgB1-3*). The archaellins encoded by the A locus are the major components forming the filaments, while the B locus is involved in formation of a curved basal structure of the archaella, with FlgB2 as the major subunit (Beznosov *et al.*, 2007; Tarasov *et al.*, 2000).

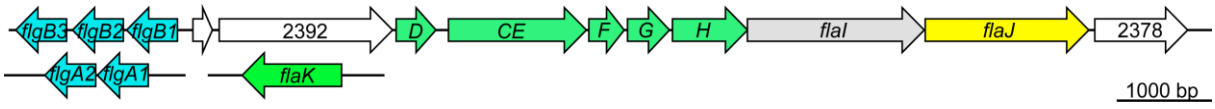

Figure 6 Schematic representation of the *Hbt. salinarum* R1 *fla* operon and associated genes. Letters indicate the respective accessory *fla* genes (C–H). The archaella motor/assembly ATPase (*flaI*) and the transmembrane protein (*flaJ*) enoding genes are shown in grey and yellow, respectively. Archaellin genes of the A and B loci in blue and the gene coding for the prearchaellin peptidase (*flaK*) in light green. The color code corresponds to the archaella assembly model in Figure 5, p. 9.

FlaI and FlaJ represent the central unit of the archaellum. The polytopic transmembrane protein FlaJ serves as the basis for archaellum assembly, and FlaI forms an ATP-dependent hexamer providing the energy for the assembly of the archaellins into the filaments. Moreover, FlaI is thought to drive archaella rotation by its ATP-hydrolyzing activity (Albers & Jarrell, 2015).

The rotation of the archaellum facilitates cell motility. However, in some species of *Methanococcus*, *Pyrococcus* or *Sulfolobus* the archaellum is also involved in cell-cell contacts or adhesion (Bellack *et al.*, 2011; Näther *et al.*, 2006; Zolghadr *et al.*, 2010). In contrast, *Hfx. volcanii* adhesion is independent of the archaella (Tripepi *et al.*, 2010), but depends on T4P-like adhesion filaments (Esquivel *et al.*, 2013). Also, *Ingicoccus hospitalis* produces cell surface structures that consist of T4P-like proteins (Iho670 fibers) and are crucial for adhesion (Müller *et al.*, 2009; Yu *et al.*, 2012). In addition, *Sulfolobus acidocaldarius* possesses specialized T4P-like structures mediating adhesion, referred to as Aap pili (Henche *et al.*, 2012a). The same species forms aggregates using T4P-like pili upon UV-irradiation, called Ups pili (Fröls *et al.*, 2008). This mechanism facilitates DNA exchange of the cells and promotes DNA repair (van Wolferen *et al.*, 2013). Moreover, the *Sulfolobus* Aap and Ups pili influence biofilm formation of the organisms (Henche *et al.*, 2012b).

A number of distinct cell appendages deviating from the T4P model, *i.e.* non-type IV pilus-like structures, were characterized in archaea. The uncultured SM1 euryarchaeon produces hook-like structures with a sophisticated architecture, referred to as hami, which are involved in attachment and biofilm formation of the cells, as well as cell-cell contacts with presumed synthrophic bacterial partners (Henneberger *et al.*, 2006; Moissl *et al.*, 2005; Moissl *et al.*, 2002). In contrast, the Mth60 fimbriae produced by *Methanococcus thermoautotrophicus* are specialized adhesins (Thoma *et al.*, 2008).

1.6. Label-free MS quantitation – State of the art in proteomics

Proteomics have proven to be a valuable tool to uncover molecular mechanisms associated with the biofilm lifestyle of microorganisms (Seneviratne *et al.*, 2012). Classical proteomic approaches are based on two-dimensional gelelectrophoresis (2-DE). The staining patterns of proteins from different samples are compared for the detection of proteins with differential abundances, which are subsequently identified by mass spectrometry (MS). However, 2-DE is restricted by low resolution, sensitivity and biases against hydrophobic proteins as well as extreme molecular weights and pI values (Zhu *et al.*, 2010). Therefore non-gel-based proteomic techniques have become the methods of choice allowing for higher data throughput and better sensitivity in protein detection even in complex protein samples. The ‘shotgun‘ MS approach is based on the digestion of proteins into peptides using site-specific proteases such as trypsin (Figure 7A). The peptide samples are separated by liquid chromatography (LC), online electrosprayed and subjected to tandem mass spectrometry (MS/MS) analysis for peptide identification. This is achieved by fragmentation of selected peptide ions (Figure 7B), referred to as precursors, into smaller pieces in a processes called collision-induced dissociation (CID).

The acquired MS/MS spectra of the resulting fragment ions facilitate the determination of the amino acid sequences of the peptides which in turn allow for identification of the corresponding proteins by database search [Figure 7C, (Nesvizhskii, 2007)].

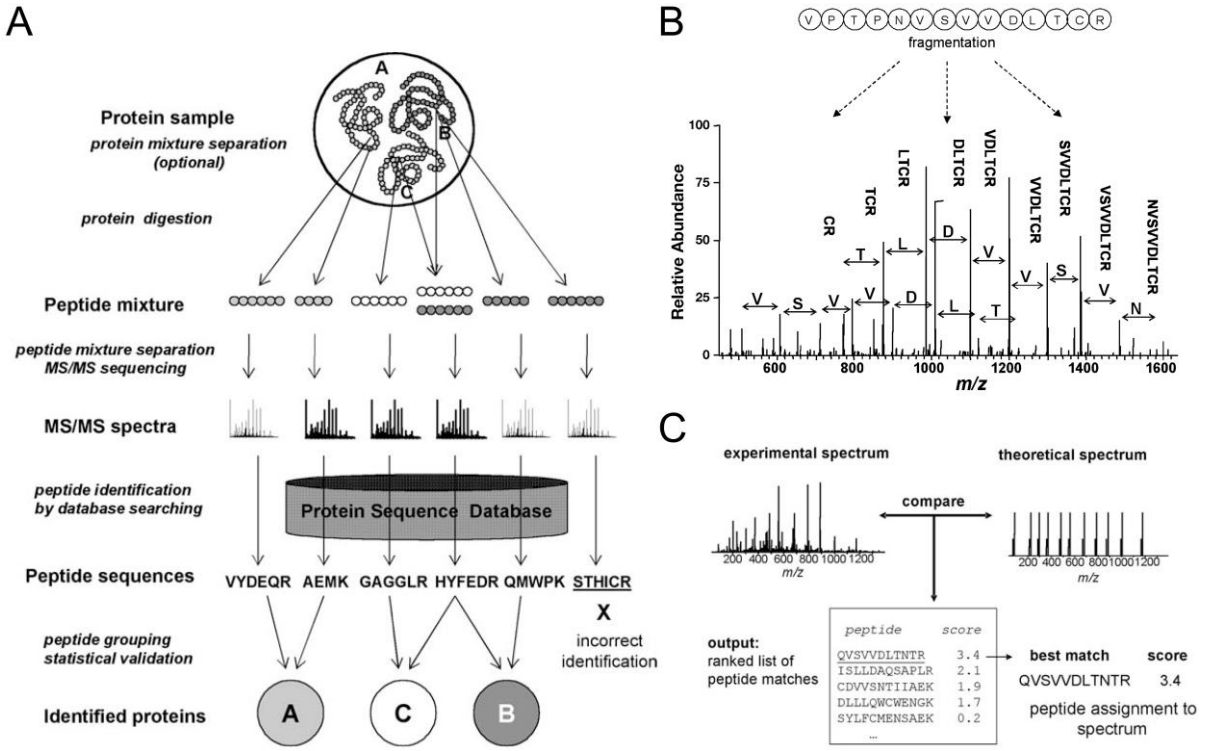

Figure 7 Shotgun mass spectrometrical proteomics. **A**, Experimental steps and flow of data in shotgun proteomics analysis. **B**, Example of a tandem mass spectrometry (MS/MS) spectrum obtained from precursor peptide fragmentation. **C**, Depiction of MS/MS database searching. (Modified from Nesvizhzkii, 2007)

The general approaches of MS-based quantitative proteomics can be divided into two groups, *i.e.* methods based on labeling and label-free quantitation methods (Figure 8). For quantitation differently labeled samples are combined and analyzed by LC-MS/MS (Figure 8A). The quantitation is computed accurately on the basis of the intensity ratio of isotope-labeled peptide pairs. Labeling methods have limitations such as the effort of sample preparation, high cost of reagents, insufficient labeling or the maximum number of multiplexed samples. Some of these issues are overcome by label-free quantitative proteomics (Figure 8B), where the different samples are analyzed in individual LC-MS/MS analyses and the quantitation is calculated *e.g.* based on the spectral counts or the respective peak intensity, respectively the peak area, of the same peptide (Zhu *et al.*, 2010).

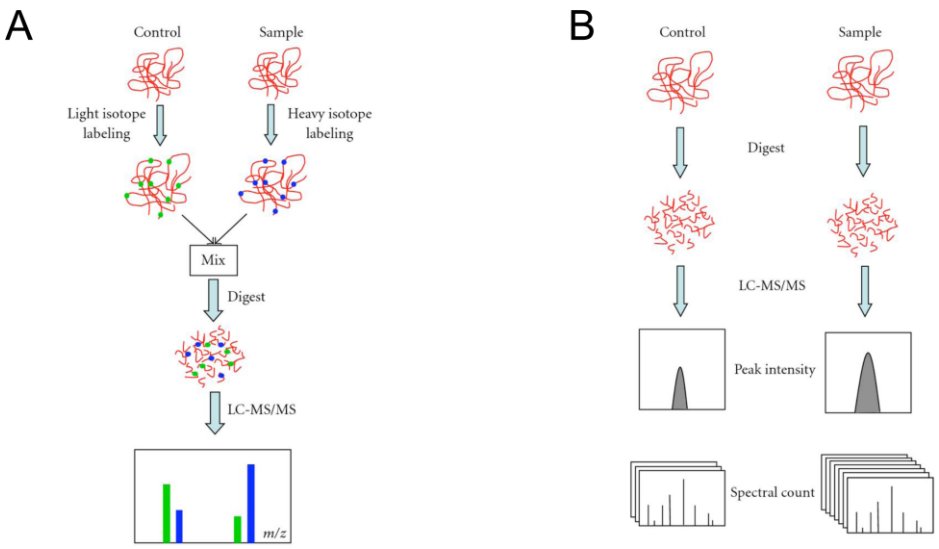

Figure 8 General strategies of quantitative proteomics. **A**, Schematic representation of an isotope labeling method. **B**, Depection of a label-free quantitation procedure. Explanations are given in the text. (Adapted from Zhu *et al.*, 2010)

An innovative label-free MS quantitation strategy is the sequential window acquisition of all theoretical fragment ion spectra (SWATH) approach, which combines data-independent acquisition (DIA) of trypsinized protein samples with *in silico* targeted analysis of the acquired complete fragment ion maps. The method acquires fragment ion spectra of all precursors in a space defined by the 400–1200 m/z precursor range and a user-specified retention time window, by repeatedly cycling through 32 consecutive 25 Da precursor isolation windows (swaths). Using a spectral library, which is prior generated in data-dependent MS mode, groups of signals that uniquely identify a specific peptide can be extracted and used for quantification (Gillet *et al.*, 2012). The method was applied firstly for the identificaton and quantification of yeast proteomes on a global scale (Selevsek *et al.*, 2015).

1.7. Aims of this study

Although living in biofilms is the predominant microbial mode of life in nature, the formation of biofilms by haloarchaea came into focus recently and knowledge on the structural and compositional characteristics of these multicellular archaeal communities is sparse. Also, little is known about the underlying processes facilitating the development of sophisticated archaeal living communities. The present work is aimed to shed light on adhesion and biofilm development of the extremely halophilic *Halobacterium salinarum* R1.

The first part of this study aims to describe the adhesion and biofilm formation of *Hbt. salinarum* R1. The adhesion process and biofilm development was monitored by microscopic and quantitative techniques.

The second part aims to identify the adhesion mechanism of *Hbt. salinarum* R1. Bioinformatical analyses were used to search for putative genes involved in the assembly of cell surface structures and the transcriptional activity of these genes was analyzed in planktonic cells and adherent cells. Mutant strains lacking distinct genes were characterized with regard to adhesion and biofilm formation. Also, a genotyping analysis was pursued to investigate a possible correlation between the adhesion capabilities and the presence of putative adhesion associated genes.

In the third part *Hbt. salinarum* R1 biofilm cells were analyzed in comparison to planktonic cells with regard to their proteomes. The proteins of planktonic cells as well as initial and mature biofilm cells were examined. A label-free mass spectrometric protein quantitation method was established and evaluated with regard to biophysical parameters of the identified and quantified proteins. Proteins showing the strongest increase or decrease were identified and categorized at a functional level to recognize biological processes associated with the different cellular states. The quantitative proteomic results were also validated by an analysis of mRNA levels by qRT-PCR.

2. Materials and methods

2.1. Materials

2.1.1. Chemicals

Chemicals and materials that were used but not listed below were purchased from Merck KGaA, Darmstadt, Germany; Carl Roth GmbH, Karlsruhe, Germany or LS Labor-Service GmbH, Griesheim, Germany.

2-Propanol	LS Labor-Service GmbH, Griesheim, Germany
3-(N-Morpholino)-propane sulfonic acid (MOPS)	Carl Roth GmbH, Karlsruhe, Germany
Acetic acid	Carl Roth GmbH, Karlsruhe, Germany
Acridine orange	Merck KGaA, Darmstadt, Germany
Acrylamide/bisacrylamide Rotiphorese® Gel 30 (37.5 : 1)	Carl Roth GmbH, Karlsruhe, Germany
Agarose ME	Biozym Scientific GmbH, Hessisch Oldendorf, Germany
Ammonium persulfate (APS)	Carl Roth GmbH, Karlsruhe, Germany
Ampicillin	Roche Diagnostics, Mannheim, Germany
Bacto Agar	Becton Dickinson GmbH, Heidelberg, Germany
Blocking reagent	Roche Diagnostics, Mannheim, Germany
Boric acid	Carl Roth GmbH, Karlsruhe, Germany
Bromothymol blue	Merck KGaA, Darmstadt, Germany
Chloroform	Carl Roth GmbH, Karlsruhe, Germany
Coomassie Brilliant Blue G250	Serva Electrophoresis GmbH, Heidelberg, Germany
Deoxyribonucleotide triphosphates (dNTPs)	Carl Roth GmbH, Karlsruhe, Germany
Ethanol	Carl Roth GmbH, Karlsruhe, Germany
Ethidium bromide	Carl Roth GmbH, Karlsruhe, Germany
Ethylendiaminetetraacetic acid di-sodium salt (EDTA)	LS Labor-Service GmbH, Griesheim, Germany
Filter paper (Whatman paper)	Macherey & Nagel GmbH, Düren, Germany
Formaldehyde, 37%	LS Labor-Service GmbH, Griesheim, Germany
Formamid	LS Labor-Service GmbH, Griesheim, Germany
Glutaraldehyde, 25%	Serva Electrophoresis GmbH, Heidelberg, Germany
Glycerol	Carl Roth GmbH, Karlsruhe, Germany
Guanidinium thiocyanate	Carl Roth GmbH, Karlsruhe, Germany
Hydrochloric acid fuming, 37%	Merck KGaA, Darmstadt, Germany
Isoamyl alcohol	Merck KGaA, Darmstadt, Germany
Magnesium sulfate (heptahydrate)	AppliChem GmbH, Darmstadt, Germany
β−Mercaptoethanol	Serva Electrophoresis GmbH, Heidelberg, Germany
Methanol	LS Labor-Service GmbH, Griesheim, Germany
N-Lauroylsarcosine sodium salt, 30%	Serva Electrophoresis GmbH, Heidelberg, Germany
N'N'N'N'-Tetramethylethylendiamine (TEMED)	Carl Roth GmbH, Karlsruhe, Germany
Ortho-Phosphoric acid	Merck KGaA, Darmstadt, Germany
Oxoid™ Peptone	Thermo Fisher Scientific, Braunschweig, Germany
Paraformaldehyde	Serva Electrophoresis GmbH, Heidelberg, Germany
Phenol solution (pH 7.5 - 8.0)	Carl Roth GmbH, Karlsruhe, Germany
Phenol solution (water saturated)	Carl Roth GmbH, Karlsruhe, Germany
Phenol/chloroform/isoamyl alcohol	Carl Roth GmbH, Karlsruhe, Germany
Potassium chloride	Carl Roth GmbH, Karlsruhe, Germany
Propidium iodide	Carl Roth GmbH, Karlsruhe, Germany
Random Hexamer Primer	Thermo Fisher Scientific, Braunschweig, Germany
Roti® Blue colloidal Coomassie	Carl Roth GmbH, Karlsruhe, Germany
Rotisolv® HPLC gradient grade water	Carl Roth GmbH, Karlsruhe, Germany
Silver nitrate	Merck KGaA, Darmstadt, Germany
Sodium acetate	LS Labor-Service GmbH, Griesheim, Germany
Sodium carbonate	Carl Roth GmbH, Karlsruhe, Germany
Sodium chloride	AppliChem GmbH, Darmstadt, Germany
Sodium dodecylsulfate (SDS), 20%	Carl Roth GmbH, Karlsruhe, Germany
Sodium thiosulfate	Merck KGaA, Darmstadt, Germany
Sucrose	Serva Electrophoresis GmbH, Heidelberg, Germany
Toluidine blue	Carl Roth GmbH, Karlsruhe, Germany
Tris(hydroxymethyl)aminomethane (Tris)	Carl Roth GmbH, Karlsruhe, Germany
Tri-sodium citrate dihydrate	LS Labor-Service GmbH, Griesheim, Germany
Tween 20	Carl Roth GmbH, Karlsruhe, Germany
Uranyl acetate	Serva Electrophoresis GmbH, Heidelberg, Germany
Urea	Carl Roth GmbH, Karlsruhe, Germany

2.1.2. Microorganisms

Strain	Adhesion[1]	Origin	Reference
Hbt. salinarum R1	strong	Derived from DSM670	Pfeiffer *et al.*, 2008
Hbt. salinarum DSM 3754^T	strong	Type strain	Elazari-Volcani 1957 emended Gruber *et al*. 2004
Hbt. salinarum NRC-1	no	Derived from DSM670	Ng *et al.*, 2000
Hbt. salinarum PHH1	no	Derived from DSM670	Pfeifer *et al.*, 1988
Hbt. salinarum PHH4	weak	Derived from PHH1	Pfeifer & Blaseio, 1989
Hbt. salinarum SB3	weak	Natural isolate	Ebert *et al.*, 1984
Hbt. salinarum GN101	no	Natural isolate	Ebert *et al.*, 1984
Hbt. salinarum R1 Δ*flaI*	strong	In frame deletion of OE2380R	Losensky *et al.*, 2014; Master thesis L. Vidakovic, 2014
Hbt. salinarum R1 Δ*flaI*/Δ*pilB1*	weak	In frame deletion of OE2380R and OE2215R	Losensky *et al.*, 2014; Master thesis L. Vidakovic, 2014
Hbt. salinarum R1 Δ*flaI*/Δ*pilB1*/Δ*pilB2*	weak	In frame deletion of OE2380R, OE2215R and OE1347R	Master thesis L. Vidakovic, 2014

[1] According to Fröls *et al.*, 2012

2.1.3. Enzymes and kits

DIG DNA Labeling Mix (10-fold conc.)	Roche Diagnostics GmbH, Mannheim, Germany
DNase I (RNase free)	Thermo Fisher Scientific Inc., Dreieich, Germany
Dream*Taq*™ DNA Polymerase	Thermo Fisher Scientific Inc., Dreieich, Germany
Pfu DNA Polymerase	Thermo Fisher Scientific Inc., Dreieich, Germany
Phototope®-Star Detection Kit	New England Biolabs GmbH, Frankfurt, Germany
Q5® High-Fidelity DNA Polymerase	New England Biolabs GmbH, Frankfurt, Germany
Restriction endonucleases	Thermo Fisher Scientific Inc., Dreieich, Germany
	New England Biolabs GmbH, Frankfurt, Germany
RevertAid™ Reverse Transcriptase	Thermo Fisher Scientific Inc., Dreieich, Germany
RiboLock RNase Inhibitor	Thermo Fisher Scientific Inc., Dreieich, Germany
SensiFAST™ SYBR® Hi-ROX Kit (2-fold conc.)	Bioline GmbH, Luckenwalde, Germany
T4 Polynucleotide Kinase	Thermo Fisher Scientific Inc., Dreieich, Germany
T7 RNA Ligase	Thermo Fisher Scientific Inc., Dreieich, Germany
T7 RNA Polymerase	Thermo Fisher Scientific Inc., Dreieich, Germany
TOPO® TA Cloning® Kit	Life Technologies, Darmstadt, Germany

2.1.4. Synthetic oligonucleotides

Synthetic oligonucleotides were purchased from biomers.net GmbH (Ulm, Germany) and Sigma-Aldrich Chemie GmbH (München, Germany). Primers were dissolved in HPLC-grade water and stored at -20°C.

Name	Oligonucleotide sequence (5'-3')
ARF-TSS [1]	
TSS-pil-1-P1-RT	TCCTCGTAGTCCGCCACC
TSS-pil-1-P2-PCR	GTACGGTGGAACGTCGACG
TSS-pil-1-P3-PCR	CCGCTGGTCGAGTTTGACG
Generation of bgaH in vitro transcription template [2]	
bgaH_IvT_T7-fwd	TAATACGACTCACTATAGGG AGACCGATATCAGTCAGA[5]
bgaH_IvT_T7-rev	GGACTCACCCGAGCAGGAAC

Name	Oligonucleotide sequence (5'-3')
Screening of mutants [2]	
flaI-Seq-fwd	GCAGCATCGTCCTCGTCGAGG
flaI-Seq-rev	GTTGGCCCTCGTAGGTGGTCG
pilB1-Seq-fwd	TGTGGACCGACACTCATGGTGATGG
pilB1-Seq-rev	GTACTCCTGTTTGAGGAACGCCGG
pilB2-Seq-fwd	AGGCGAGCACGACGAACAGCAC
pilB2-Seq-rev	CGCGCTGCCGTACACGAGCAG

Name	Oligonucleotide sequence (5'-3')
RT-PCR analyses [3]	
pil-1-RT-1-fwd	GGAGCGACGACTTCACGTAT
pil-1-RT-1-rev	GACGTACAGCGGACGTACAA
pil-1-RT-2-fwd	CACACTCCTCGTCCAGGAAC
pil-1-RT-2-rev	CACCCAGTCGCAGTTCCTC
pil-1-RT-3-fwd	CGATCACCACCAGAATCGT
pil-1-RT-3-rev	TCGCGAAGCGACCTGCTC
pil-1-RT-4-fwd	GGCTCTTGTTGGATTCGATG
pil-1-RT-4-rev	CAGCTTCATGGACGTGGATA
pil-1-RT-5-fwd	GTTCGAAACACCGGTCTCA
pil-1-RT-5-rev	ATGCAGGTACTCACCGTCGT
pil-2-RT-1-fwd	CGCGGTAGACCTCGTTGT
pil-2-RT-1-rev	GATCACCCGCCGGTGTTTG
pil-2-RT-2-fwd	CACCTGCTCCGAGAGATCG
pil-2-RT-2-rev	CACGACACTGCGTACACAC
pil-2-RT-3-fwd	GGTGTTGGTGGCGATCATC
pil-2-RT-3-rev	CCGCAAGCTGGGTATCGAC
pil-2-RT-4-fwd	GGCGACTCTACCACGAGAAG
pil-2-RT-4-rev	GCCGGCGAGATAGGTGA
pil-2-RT-5-fwd	ATCGAAACCACGCACACC
pil-2-RT-5-rev	GATCGTAAGCGACCCTGTG
pil-2-RT-6-fwd	CGACACGCACTCCCAAAC
pil-2-RT-6-rev	TGGTGGTGTCCACACTGAAC
pil-2-RT-7-fwd	CGCGACGATCATCGAGAC
pil-2-RT-7-rev	CTCGCATCGCTTCCCACC
pil-2-RT-8-fwd	GCGTGAGGACAGTGACCA
pil-2-RT-8-rev	ATCGCGGACTCTCCTCTGT
qRT-PCR [4]	
bgaH-qPCR-fwd	TCGTCAAGGGCAAGAACAG
bgaH-qPCR-rev	ACCGAATCCAAGTCGAACAG
rpoB1-qPCR-fwd	GTCCTACGAGGGGTTCAACA
rpoB1-qPCR-rev	CTCGTACGTGCGGAAGAAAT
fdx-qPCR-fwd	ACGAGGAAGTCGAGGAGAAGG
fdx-qPCR-rev	CAGGTAGTCGAGGTGCTTGG
flaI-qPCR-fwd	ACGTCCAGGAGCGCATCCT
flaI-qPCR-rev	ACTTGTCGTCGGAGATGCGAA
pilB1-qPCR-fwd	CCGGAAGTACAGCGAGGAG
pilB1-qPCR-rev	GGCTCTTGTTGGATTCGATG
pilB2-qPCR-fwd	CGAAGGTGAACCTCGAACC
pilB2-qPCR-rev	CTTCCGGATGGAGACGTGG
flgA1-qPCR-fwd	GCTTCCTCCAGTCAAAAGGC
flgA1-qPCR-rev	CACTAGCGGTCTTGACGTTG
flgB1-qPCR-fwd	CAACCGCATCAACATCGTCT
flgB1-qPCR-rev	GAGGTTGATGTTGTCGGCTC
flgX-qPCR-fwd	CAGGATAGCTTCTCGGGCAC
flgX-qPCR-rev	GGAACCGAAACCCAGTACGT
pilA1-qPCR-fwd	TGACAGACCTCAGCCTCTTC
pilA1-qPCR-rev	GTCACCGAATCCAAGCACTG
pilA2-qPCR-fwd	CGCGACGATCATCGAGAC
pilA2-qPCR-rev	TGGTGGTGTCCACACTGAAC
pilA3-qPCR-fwd	CGACACGCACTCCCAAAC
pilA3-qPCR-rev	GATCGTAAGCGACCCTGTG
pilA4-qPCR-fwd	ATCGAAACCACGCACACC
pilA4-qPCR-rev	GAGACGCTCACCGTCGTT
pilA4-qPCR-2nd-fwd	CGCGTCCTGAACGAGAC
pilA4-qPCR-2nd-rev	GCCGGCGAGATAGGTGA
pilA5-qPCR-fwd	ATCCTGGCTGTCAAGGAGTC
pilA5-qPCR-rev	TACACCACGGACAGAACTCC
pilA6-qPCR-fwd	TTCGAACACGGTCTCCCATC
pilA6-qPCR-rev	CAGTGAGCGTCGTGTACAG
pilA7-qPCR-fwd	TTGAAGTGGCCAGGGAATCC
pilA7-qPCR-rev	TTCGAGCTCTGTCGGTTGTC
pilA8-qPCR-fwd	GCTACGCGGTCTCCTATCTG
pilA8-qPCR-rev	CGTCTGTGTCATGTCCGCT
pilA9-qPCR-fwd	ACGGACACCATCAGCAGTC
pilA9-qPCR-rev	ATGTGGGTGAGTCGAACGAT
pilA10-qPCR-fwd	CTTCTACAGCGGGCCGAC
pilA10-qPCR-rev	GGCAGTGGATCGTTCGTC
pilA10-qPCR-2nd-fwd	CTTCTACAGCGGGCCGAC
pilA10-qPCR-2nd-rev	GGCAGTGGATCGTTCGTC
pilA11-qPCR-fwd	ACACGACCATCACCGAGGT
pilA11-qPCR-rev	ACGTCCTGCTCTTCGATGAC
pilA12-qPCR-fwd	GCGACAGATGATGGTGATGG
pilA12-qPCR-rev	CTTCCTCTTGCGCGATAACC
Southern analyses [2]	
pil-1-probe-fwd	CCACACGACGTATTCGACGATGC
pil-1-probe-rev	TCCGTGATCGAGTCCAGGTAGACC
pil-2-probe-fwd	GATGTCCGGGTTGAGGTAGTTG
pil-2-probe-rev	CGTACTACGTGGTGCGTGATCT
pilA1-probe-fwd	TGACAGACCTCAGCCTCTTC
pilA1-probe-rev	AGGCAACAACACTGGCGTTC
pilA2-4-probe-fwd	AAGCGAACCTGGTGGCGCTTGTGG
pilA2-4-probe-rev	GATCGTAAGCGACCCTGTGGTCGTC
pilA5-probe-fwd	ATCCTGGCTGTCAAGGAGTC
pilA5-probe-rev	TACACCACGGACAGAACTCC
pilA6-probe-fwd	TTCGAACACGGTCTCCCATC
pilA6-probe-rev	CAGTGAGCGTCGTGTACAG
pilA7-probe-fwd	TTGAAGTGGCCAGGGAATCC
pilA7-probe-rev	TTCGAGCTCTGTCGGTTGTC
pilA8-probe-fwd	GCTACGCGGTCTCCTATCTG
pilA8-probe-rev	CGTCTGTGTCATGTCCGCT
pilA9-probe-fwd	ACGGACACCATCAGCAGTC
pilA9-probe-rev	CCTCGATCACAACCGTCTC
pilA10-probe-fwd	GCCGTGACACTGCTTTCC
pilA10-probe-rev	GGCAGTGGATCGTTCGTC
pilA11-probe-fwd	TGATGTTCGTGCTTGCGGTG
pilA11-probe-rev	ACGTCCTGCTCTTCGATGAC
pilA12-probe-fwd	ACACTTGAGATTCCGGACCG
pilA12-probe-rev	CTTCCTCTTGCGCGATAACC
carA-qPCR-fwd	GAAAATGGACTTCGGCCACC
carA-qPCR-rev	ATAGCCGTGGTTCTGTGTGG
cbiG-qPCR-fwd	GACATCCTCGACTACCACGG
cbiG-qPCR-rev	GTCCTCCCACTTGTCGTCG
nrdA1-qPCR-fwd	TCAAATCCAACATGAGCGGC
nrdA1-qPCR-rev	GTGAGTTTGTCGCGGAGTTC
dmsR-qPCR-fwd	TCAAGCTCACCGACAAACAG
dmsR-qPCR-rev	GCTCAGTCGCTGTGAAACC
pykA-qPCR-fwd	CGTGCCGATGATCCAAAAGC
pykA-qPCR-rev	ACCATCGAGTCCAGCATCTC
rps13-qPCR-fwd	CCGTCGATAGCTTCACCGAG
rps13-qPCR-rev	TACCCGTGATGTGCTGGTTC
lrpA2-qPCR-fwd	AACGATCCTACACGCACTCC
lrpA2-qPCR-rev	GTGGTAGCCGGTCAGAATCC
OE1974R-qPCR-fwd	TGCTCAGTGACACCGAAACA
OE1974R-qPCR-rev	GCCGTGTGCCTGATAGAAGT
OE4416R-qPCR-fwd	CGTACTCGGAGCTGTTGACC
OE4416R-qPCR-rev	ATCTCCGAACTCTCCAAGCG
OE2097F-qPCR-fwd	GTTGTTACACGTCACCACCG
OE2097F-qPCR-rev	TTCGTCGATGGTGTACGTGA
OE3073R-qPCR-fwd	GTGGTGTGGGCGGAAGTC
OE3073R-qPCR-rev	TACTGGGAGCCGTCGAGTT
OE3542R-qPCR-fwd	GTTCGAGCAGTCCCCGATG
OE3542R-qPCR-rev	CCACCAGCAGTTTCGTGTTC
dmsA-qPCR-fwd	TACCGGCGACTCAAGGAGCTAGT
dmsA-qPCR-rev	CATGTTCGAGTTCATGCCGTACA
arcC-qPCR-fwd	GGACGAAGCCTCAGAGAAGG
arcC-qPCR-rev	GCGTCTTGATGTGTTCTGCC
bop-qPCR-fwd	ATGGCCTCACAATGGTACCG
bop-qPCR-rev	AGCAACGCGAGGTCTAACAA

*Oligonucleotides listed were used for [1] ARF-TSS, [2] Standard/DIG-PCR, [3] RT-PCR or [4] qRT-PCR; [5] T7 RNA polymerase promoter is underlined.

2.1.5. Molecular markers

GeneRuler™ DNA Ladder Mix	Thermo Fisher Scientific Inc., Dreieich, Germany
Unstained Protein MW Marker	Thermo Fisher Scientific Inc., Dreieich, Germany
PageRuler Prestained Protein Ladder	Thermo Fisher Scientific Inc., Dreieich, Germany
0.5 – 10 kb RNA Ladder	Thermo Fisher Scientific Inc., Dreieich, Germany

2.1.6. Buffers and solutions

TE-buffer	20 mM Tris/HCl (pH 8.0), 1 mM EDTA
TEN-buffer	20 mM Tris/HCl (pH 8.0), 1 mM EDTA, 100 mM NaCl
TAE-buffer (50-fold conc.)	2 M Tris, 1 M acetate, 50 mM EDTA (pH 8.0)
TBE-buffer (10-fold conc.)	890 mM Tris, 890 mM borate, 20 mM EDTA
Bradford reagent	0.01% (w/v) Coomassie R-Brilliant blue G-250, 5% (v/v) EtOH, 8.5% (v/v) ortho-phosphoric acid
Protein loading buffer (3-fold conc.)	125 mM Tris/HCl (pH 6.8), 20% (w/v) glycerol, 4% (w/v) SDS, 0.2% (w/v) bromophenol blue, 10% (v/v) β-mercaptoethanol
DNA loading buffer (10-fold conc.)	0.25% (w/v) bromophenol blue, 50% (w/v) sucrose, 100 mM EDTA (pH 8.0)
RNA loading buffer	50% (v/v) formamide, 6% (v/v) formaldehyde, 10% (v/v) MOPS buffer (10-fold conc.), 10% (v/v) DNA loading buffer (10-fold conc.)
MOPS buffer (10-fold conc.)	200 mM MOPS, 50 mM sodium acetate, 10 mM EDTA (pH 7.0)
SSC buffer (20-fold conc.)	3 M NaCl, 0.3 M sodium citrate (pH 7.0)
Solution D	4 M guanidinium thiocyanate, 25 mM sodium citrate, 0.3% (v/v) sarkosyl, 0.1 M β-mercaptoethanol

2.2. Microbiological methods

2.2.1. Cultivation of *Halobacterium salinarum* R1

Halobacterium salinarum strain R1 (ATCC 29341, DSM 671) was grown under aerobic conditions at 37 °C in complex medium (250 g NaCl, 20 g $MgSO_4$ x $7H_2O$, 2 g KCl, 15 g Oxoid peptone, 50 mL 1M Tris/HCl pH 7.5 per liter). For cultivation of planktonic and sessile cells, an overnight culture with an optical density of 0.35 at 600 nm (OD_{600}) was used for inoculation. OD_{600} was set to 0.002 before cultivation. Planktonic cells were grown in liquid media in flasks shaking at 180 rpm and harvested at different stages, *i.e.* early exponential (OD_{600} 0.1 – 0.2), late exponential (0.3 – 0.4) and stationary (0.8 – 0.9) growth phase. Sessile cells were grown in large Petri dishes (150/20 mm, Sarstedt AG & Co. KG, Nümbrecht, Germany) in liquid media under static conditions without shaking. Biofilms were harvested after 1 to 15 days of growth. The supernatant was discarded and the dishes were washed three times with 50 mL basal salt water (complex medium without peptone) to remove non-adhering cells. Adherent cells were then scraped off the dishes using a spatula.

2.2.2. Fluorescence-based quantification of cell adhesion

Adhesion of cells was quantified by use of a fluorescence-based assay, which facilitated examination of cell adhesion in the time course and also comparison of adhesion strength between different strains. For this purpose, cells were grown in 24-well tissue culture plates. Wells were inoculated with 2 mL of the culture media and 20 μL of a cell culture (OD_{600} 0.3) or volume equivalents. As a negative control and for background normalization, at least four wells per plate were inoculated with culture media only. Cells were grown at 37 °C under static conditions for up to 21 d.

After the incubation time, the cells were stained by the addition of acridine orange (final concentration 2 μg/mL), a membrane permeating, DNA intercalating fluorescent dye. Staining was done for 15 min at room temperature in the dark. The liquid was discarded and the wells were washed three times with basal salt water. During the subsequent fluorescent signal detection procedure, wells were incubated with basal salt water. Detection of acridine orange signals was performed on a fluorescent image analyzer (FLA-5000, Fuji Photo Film Co., Ltd., Tokio, Japan), using 473 nm excitation wavelength (green filter LPG), in combination with the Image Reader FLA-5000 software (Version 1.0). ImageGauge software (Version 4.23) was used for quantification of fluorescence intensities in Light Absorbing Units per mm^2 (LAU/mm^2).

2.3. Microscopic methods

2.3.1. Phase contrast microscopy (PCM)

Progression of cell adhesion during biofilm formation was monitored by phase contrast microscopy (PCM). *Hbt. salinarum* R1 cells were grown in Petri dishes (92/16 mm, Sarstedt) containing 15 mL *Halobacterium* complex medium inoculated with cells from the exponential growth phase (OD_{600} 0.3). OD_{600} of the cultures was set to 0.002 before the cells were grown at 42 °C for 1 to 24 days. Glass coverslips were submerged in the media to allow adherence of the cells on the glass. Prior the microscopic analyses, overgrown coverslips were washed three times with basal salt water to remove non-adherent cells. Microscopic analyses were performed using an Axioskop 2 microscope equipped with an AxioCam MRm camera (Carl Zeiss Microscopy GmbH, Jena, Germany) and the software AxioVision (Release 4.8).

2.3.2. Scanning electron microscopy (SEM)

Insights into the three-dimensional structure of *Hbt. salinarum* R1 biofilms were gained by scanning electron microscopy (SEM). Carbon-coated gold grids (400 mesh, Plano GmbH, Wetzlar, Germany) were placed in static 20 mL cell cultures of *Hbt. salinarum* R1 in Petri dishes (92x16 mm, Sarstedt) to enable adherence of cells. After 10 d of incubation the culture medium

was removed carefully from the Petri dishes. 15 mL basal salt water were added to the dishes and removed carefully, to wash the grids and eliminate non-adhering cells. Cell fixation was done by modification of a protocol previously used (Gruber *et al.*, 2004). 15 mL fixation reagent (2% paraformaldehyde and 1% glutaraldehyde dissolved in basal salt water) were added to the Petri dishes for overnight fixation at 4 °C. After fixation the reagent was removed and grids were stained by placing them on a droplet of 2% uranyl acetate solution for 40 s. For removal of the straining reagent and salt, the grids were pulled through a pure ddH_2O droplet. Excess fluid was removed using filter paper and grids were stored in a desiccator containing silica gel for drying. Afterwards a scanning electron microscope (XL 30 FEG, Philips, Netherlands) was employed to visualize adherent cells.

2.3.3. Confocal laser scanning microscopy (CLSM)

The three-dimensional structure of *Hbt. salinarum* R1 biofilms as well as their development over time was visualized by confocal laser scanning microscopy (CLSM). This microscopic technique further allowed visualization of certain constituents of the biofilm extracellular polymeric substances, *i.e.* extracellular DNA and glycoconjugates within the biofilm matrix, using suitable molecular probes/stains. Cells were stained with acridine orange, a membrane permeating DNA intercalating dye. Extracellular DNA and dead cells were stained with propidium iodide which cannot permeate the cell membrane and therefore only stains extracellular DNA as well as disrupted cells. Concanavalin A (ConA) Alexa Fluor® 647 conjugates was used to stain glycosidic (α-mannopyranosyl and α-glucopyranosyl) residues in the biofilm matrix.

For CLSM analyses of biofilms, sessile cells were grown in small Petri dishes (35/10 mm, Sarstedt) on polyethylene terephthalate (PET) surfaces for 1 to 24 days. The start OD_{600} was 0.002. Prior to the analyses, biofilms were washed with basal salt water. Staining was done for 15 min with acridine orange (Merck KGaA, final concentration 10 μg/mL) and propidium iodide (Carl Roth, final concentration 30 μg/mL) plus 10 min with ConA Alexa Fluor® 647 (Life Technologies, final concentration 10 μg/mL). After the staining procedure, biofilms were washed three times and finally incubated with basal salt water. For CLSM analyses of planktonic cells, cells in the exponential growth phase (OD_{600} 0.3) were sedimented by centrifugation and resuspended in basal salt water for the staining procedure, which was done analogously to staining of the biofilms. After staining the cells were washed three times with basal salt water, sedimented by centrifugation at 6000 *g* for 5 min, and finally resuspended in the original volume of basal salt water. A confocal laser scanning microscope (TCS SP5 II, Leica Microsystems GmbH, Wetzlar, Germany) in combination with Leica Application Suite software was used to take images of planktonic cells and biofilm cells at different stages. Image processing was done using the software ImageJ (http://imagej.nih.gov/ij/).

2.4. Biochemical methods

2.4.1. Preparation of protein samples from haloarchaea

Protein samples for SDS-PAGE and MS analyses were prepared from planktonic cells, which were harvested at different growth phases (OD_{600} 0.1, 0.4 and 0.8), and sessile cells grown for different incubation times (1 through 15 days). Biofilm cells were washed three times with basal salt water and scratched off the Petri dishes while incubated with basal salt water. Planktonic and biofilm cells were sedimented by centrifugation at 6000 *g* and 4 °C for 15 min and supernatants were discarded. Cells were lysed osmotically by addition of 10 mM Tris/HCl (pH 7.5) and mixed vigorously using a Vortex until a homogenous suspension was obtained. To reduce viscosity of the cell lysates, DNA was hydrolyzed by DNase I treatment (final concentration 1 μg/mL), according to the manufacturer's protocol for 3 h. Protein concentration of the cell lysates was determined by standard Bradford assay (Bradford, 1976).

Equal amounts of proteins were prepared by standard trichloroacetic acid (TCA)/acetone precipitation. In brief, two volumes of protein solution were precipitated by addition of one volume of 30% TCA solution. The samples were chilled on ice for 1 h to precipitate proteins. Precipitates were sedimented by centrifugation at 21 000 *g* for 15 min. Supernatants were discarded and the resulting pellets were washed by addition of 1 volume of 80% acetone followed by centrifugation at 21 000 *g* and 4 °C for 10 min. The supernatants were discarded and the pellets were air-dried.

2.4.2. Sodium dodecyl sulfate polyacrylamide gel electrophoresis (SDS-PAGE)

The SDS-PAGE system invented by Schägger and von Jagow was used to separate proteins of complex cell lysates according to their relative molecular weight (Schägger & von Jagow, 1987). Since polymerized polyacrylamide (PAA) acts as a molecular sieve, variation of the PAA concentration allows for separation of proteins, depending on their expected molecular weights. Crude cell lysates were separated on 10% PAA gels, to facilitate separation over a wide molecular weight range. The following buffers were utilized for SDS-PAGE: 3-fold Schägger gel buffer (3 M Tris/HCl, 0.3 % SDS, pH 8.45), 10-fold cathode buffer (1 M Tris/HCl, 1 M Tricine, 1% SDS, pH 8.45), 10-fold anode buffer (2 M Tris/HCl, pH 8.9) and 3-fold loading buffer (125 mM Tris/HCl, 20% glycerol, 4% SDS, 0.2% bromothymol blue, 10% β-mercaptoethanol, pH 6.8).

Protein gels were cast and run using a Mini-PROTEAN Tetra Cell system (Biorad Laboratories Inc., Hercules, USA). Protein samples were mixed with an appropriate volume of loading buffer and proteins denatured by heating at 90 °C for 10 min. Samples were chilled on ice, shortly centrifuged and applied to the gels. Electrophoresis was carried out with a voltage of 100 - 120

Volts. After the gel run, Roti®-Blue colloidal Coomassie (Carl Roth GmbH + Co. KG, Karlsruhe, Germany) was used to visualize proteins in the gel according to the manufacturer's instructions. In cases where faint or no protein bands were visible, silver staining was performed for better visualization (as described in 2.4.3).

Table 1 Standard SDS-gel composition

Component	Stacking gel (5% PAA)	Separating gel (10% PAA)
Rotiphorese® Gel 30 (37.5 : 1)	2 mL	9 mL
Schägger gel buffer (3-fold conc.)	3.5 mL	9 mL
Glycerol (60% stock solution)	–	3 mL
ddH_2O	9 mL	6 mL
TEMED	0.04 mL	0.04 mL
APS (10% stock solution)	0.2 mL	0.2 mL

2.4.3. Silver staining of sodium dodecyl sulfate polyacrylamide gels

To achieve better visualization at low protein concentrations, gels were stained employing a more sensitive (Switzer *et al.*, 1979) and mass spectrometry compatible silver staining procedure (Gromova & Celis, 2006). The following solutions were used for silver staining: fixation solution [50% (v/v) ethanol, 12% (v/v) acetic acid, 0.05% (v/v) formaldehyde], washing solution [20% (v/v) ethanol], sensitizing solution [0.02% (w/v) sodium thiosulfate], silver staining solution [0.2% (w/v) silver nitrate, 0.076% (v/v) formaldehyde], developing solution [6% (w/v) sodium carbonate, 0.0004% (w/v) sodium thionate, 0.05% (v/v) formaldehyde], termination solution [12% (v/v) acetic acid]. All steps were performed with moderate shaking of the gel in the solutions. Gel fixation was done for at least 2 h in fixation solution. The gel was washed in washing solution for 20 min, with solution exchanges every 5 min. After 2 min incubation in sensitizing solution, the gel was washed twice for 1 min in ddH_2O. Silver staining was done for 20 min in silver staining solution. The gel was washed twice for 30 s with ddH_2O, before it was incubated in developing solution. When protein bands reached the desired intensities, the reaction was stopped by adding one sixth of the total volume of termination solution. If no bands appeared, the reaction was stopped after 10 min.

2.4.4. Preparation of protein samples for mass spectrometry

Protein preparations from each biological sample (planktonic, initial biofilm grown for 1 day, mature biofilm after 15 days) were digested and analyzed in duplicate to assess the variability of sample preparation. For each replicate 40 μg precipitated protein were dissolved using sodium 3-[(2-methyl-2-undecyl-1,3-dioxolan-4-yl)methoxy]-1-propanesulfonate (Rapigest,

Waters) cleavable surfactant (Yu *et al.*, 2003). After reduction and alkylation of cysteine residues with dithiothreitol and iodoacetamide, proteins were digested using sequencing grade procine trypsin (Promega GmbH, Mannheim, Germany) at a 1:50 enzyme-to-substrate ratio (w:w). Following acidic cleavage of the surfactant, the resulting fatty acids were pelleted and removed by centrifugation at 13 000 *g* for 20 min. The resulting peptide mixtures were dried in a Concentrator Plus centrifuge (Eppendorf AG, Hamburg, Germany) and stored at -20 °C prior to analysis.

2.4.5. Liquid chromatography and tandem mass spectrometry (LC/MS/MS) acquisition

Protein digests were analyzed on a nanoflow chromatography system (Eksigent nanoLC425) hyphenated to a hybrid triple quadrupole-time of flight mass spectrometer (TripleTOF 5600+) equipped with a Nanospray III ion source (Ionspray Voltage 2200 V, Interface Heater Temperature 150 °C, Sheath Gas Setting 10) and controlled by Analyst TF 1.6 software build 6211 (all AB SCIEX). In brief, peptides from each digest were dissolved in 160 μL loading buffer (2% aqueous acetonitrile vs. 0.1% formic acid in). For each analysis 1.5 μg protein were concentrated and desalted on a trap column (Waters Synergy C18 5 μm, 20 x 0.180 mm, 160 μL loading buffer) and separated by reversed phase-C18 nanoflow chromatography (Waters TSS-3 1.8 μm, 250 x 0.075 mm, linear gradient 150 min 4%>34% acetonitrile vs. 0.1% formic acid, 300 nL/min, 50 °C).

Qualitative LC/MS/MS analysis was performed using a Top30 data-dependent acquisition method with an MS survey scan of m/z 380-1250 accumulated for 250 ms at a resolution of 35.000 FWHM, 0.7 FWHM precursor isolation width. MS/MS scans of m/z 180-1750 accumulated for 100 ms at a resolution of 17.500 FWHM, resulting in a total cycle time of 3.4 s. Precursors above a threshold MS intensity of 200 cps with charge states 2+, 3+ and 4+ were selected for MS/MS, the dynamic exclusion time was set to 15 s. Three technical replicates of each sample were acquired for qualitative analysis.

For SWATH analysis, MS/MS data were acquired for 34 precursor segments of 25 m/z, resulting in a precursor m/z range of 400-1250. Fragments were produced using Rolling Collision Energy Settings and fragments acquired over an m/z range of 380-1750 for an accumulation time of 110 ms per segment. Including a 250 ms survey scan this resulted in an overall cycle time of 4.0 s. Seven technical replicates of each sample were acquired for quantitative analysis.

2.4.6. LC/MS/MS data processing

Protein identification was achieved using ProteinPilot Software version 5.0 build 4304 (AB SCIEX) at 'thorough' settings. A total of 832.416 MS/MS spectra from the combined qualitative

analyses were searched against a strain-specific *Hbt. salinarum* R1 extract from the UniProtKB protein sequence database (revision 10/2014, 2577 entries) augmented with a set of 51 known common laboratory contaminants. False discovery rates (FDR) were adjusted to 1% at both the protein and peptide level using a forward/reverse decoy database approach.

SWATH peak extraction was achieved in PeakView Software version 2.1 build 11041 (AB SCIEX) using the SWATH quantitation microApp version 2.0 build 2003. Peak areas were extracted for the ten highest scoring peptides per protein group at 6 transitions per peptide, an extracting ion current (XIC) width of 75 ppm and an XIC window of 14 min, resulting in a total of 147.747 features extracted at an estimated FDR of 1% (Lambert *et al.*, 2013). The resulting peak areas were then exported at the fragment, peptide and protein level for further statistical analysis.

2.4.7. LC/MS/MS data statistical analysis

For the purpose of variance stabilization raw peak areas were $\log_2$-transformed and quantile normalization was applied (Bolstad *et al.*, 2003) in order to make the individual MS runs comparable. Hierarchical clustering and principal component analysis was performed for quality control and to explore the separability of study groups.

The three groups were compared pairwise with respect to differentially expressed proteins using the linear models proposed by Smyth (Smyth, 2004). Resulting p-values were adjusted to control an FDR of 5% (Benjamini & Hochberg, 1995). The strength of expression change was quantified by the $\log_2$ fold change (FC) and FDR-adjusted confidence intervals (Jung *et al.*, 2011; Jung *et al.*, 2009).

In order to characterize the expression time profile (t1 = planktonic, t2 = initial biofilm 1 day, t3= mature biofilm 15 days) of each protein, a score S was set up as follows. A significant (but weak) up- or down-regulation was rewarded 1 point, a significant up- or down-regulation with an absolute FC > 1 was rewarded with 3 points. Thus, a protein with a significant and strong up-regulation from t1 to t2 and from t2 to t3 received for example an unadjusted score of S* = 6. To further distinguish between the proteins with the same value of S*, p-values from the linear model for t2 versus t1 and t3 versus t2 were combined by the method of Fisher for meta analyses (Moreau *et al.*, 2003), yielding $p_{combined}$. The final score was than calculated by $S = S^* + (1 - p_{combined})$.

All statistical analyses were performed with the free software R (version 3.1, www.r-project.org). The linear models were carried out using the 'limma'-package. For further characterization of the lists of differentially expressed proteins, annotations and functional categorizations were retrieved from the UniProtKB protein sequence database (http://www.uniprot.org) and the Archaeal Clusters of Orthologous Genes (arCOG) Browser

(http://archaea.ucsc.edu/arcogs). Metabolic pathway maps were derived from the Kyoto Encyclopedia of Genes and Genomes database (KEGG; Release 76.0, October 1, 2015; www.genome.jp/kegg/) and generated applying the 'User data mapping' tool.

2.4.8. Isolation of genomic DNA from haloarchaea

For isolation of genomic DNA, 2 mL of a cell culture (OD_{600} 0.5) were sedimented by centrifugation at 6000 *g* for 5 minutes. The supernatant was discarded and the cell pellet was resuspended in 100 μL basal salt water. 900 μL TEN-buffer (100 mM NaCl, 1mM EDTA, 20 mM Tris/HCl pH 8.0) were added to the suspension for osmolysis of the cells. The cell lysate was chilled on ice for 10 minutes. One volume phenol/chloroform/isoamyl alcohol [25:24:1, (v/v/v)] was added and mixed vigorously for 15 s on a Vortex. After centrifugation at 9000 *g* the upper, aqueous phase was transferred into a new vial. One volume of chloroform/isoamyl alcohol (49:1) was added and mixed intensely on a vortex. After centrifugation at 9000 *g* the upper, aqueous phase was transferred into a new vial. 1/10 volume 3 M sodium acetate (pH 4.6) and one volume 2-propanol was added to precipitate the DNA. Samples were incubated at -20 °C for at least 30 min and then DNA precipitates were sedimented by centrifugation at 21 000 *g* and 4 °C for 30 min. The supernatant was discarded and the DNA pellet was washed by addition of 1 volume of 70% ethanol. After centrifugation at 21 000 *g* and 4 °C for 10 minutes, the supernatant was discarded and the pellet was dried using a Concentrator 5301 centrifuge (Eppendorf AG, Hamburg, Germany). Genomic DNA pellets were resuspended in 10 mM TE-buffer (1 mg/mL RNaseA added).

2.4.9. Agarose gel electrophoresis

Agarose gel electrophoresis was performed for analytical separation of nucleic acid (RNA or DNA) fragments with expected sizes > 300 bp.

The fragments were separated on agarose gels consisting of 0.7 to 3.0% agarose (w/v) dissolved in TAE buffer. Nucleic acid samples were mixed with an appropriate volume of loading dye and loaded onto the gel. Gel electrophoresis was carried out at currents from 60 to 120 mA and stopped when the bromophenol blue added in reached 2/3 of the gel length. DNA-containing gels were stained by incubation in ethidium bromide solution (1 μg/mL in ddH_2O) and visualized using a gel documentation system. RNA-containing gels were stained with toluidine blue solution [10% acetic acid (v/v) and 0.1 % toluidine blue (w/v) in ddH_2O] and documented using a scanner.

2.4.10. Polyacrylamide gel electrophoresis

Analytical separation of small nucleic acid fragments with sizes < 300 bp was carried out by polyacrylamide (PAA) gel electrophoresis in some cases.

PAA gels consisted of 10% PAA dissolved in 0.5-fold TBE buffer. Nucleic acid samples were mixed with an appropriate volume of loading dye and loaded onto the gel. Gel electrophoresis was carried out at currents from 40 to 60 mA and stopped when the bromophenol blue band reached the lower end of the gel. PAA gels were stained by incubation in ethidium bromide solution (1 μg/mL in ddH_2O) and visualized using a gel documentation system.

Table 2 Standard PAA-gel composition

Component	Separating gel (10% PAA)
Rotiphorese® Gel 30 (37.5 : 1)	9.6 mL
ddH_2O	24.6 mL
TBE buffer (10-fold conc.)	1.8 mL
TEMED	0.04 mL
APS (10% stock solution)	0.4 mL

2.4.11. Southern analysis

The presence or absence of genes of interest in different haloarchaeal genomes was investigated by Southern analysis (Southern, 1975). For Southern analysis 3 μg of genomic DNA were hydrolyzed with restriction endonucleases yielding clearly separable restriction fragments by gel electrophoresis on 0.7% agarose gels. The restriction fragments were blotted on Roti®Nylon membranes with a pore size of 0.2 μm (Carl Roth GmbH & Co. KG, Karlsruhe, Germany). Southern blots were hybridized in standard hybridization buffer (50% formamide (v/v), 5-fold SSC, 2% blocking reagent (w/v), 0.1% N-lauroylsarcosinate (w/v) and 0.02% SDS) with digoxigenin-labeled DNA-probes. Digoxigenin (DIG) was detected by use of Anti-digoxigenin-alkaline phosphatase Fab fragments (# 11093274910, Roche Diagnostics, Mannheim, Germany) in combination with the Phototope®-Star Detection Kit (# N7020S, New England Biolabs) according to the manufacturer's protocols. After the detection procedure, alkali-labile DIG was removed by incubation of the membrane with stripping solution [(0.2 M NaOH, 0.1% SDS, SSC buffer (2-fold conc.)], twice for 15 min, which enabled reprobing.

A digoxigenin DNA labeling Kit (# 11277065910, Roche Diagnostics GmbH, Mannheim, Germany) was used to produce DNA probes by standard PCR using genomic DNA of *Hbt. salinarum* R1 as template in combination with the oligonucleotides listed in 2.1.4. DIG

nucleotide incorporation into the DNA fragments was verified by agarose gel electrophoresis, resulting in a shift of the DIG probes, *i.e.* slower migration in the gels. For the detection of the pil-1 locus, probes were generated comprising the *pilB1* 3'-end and the *pilC1* 5'-end of *Hbt. salinarum* R1, resulting in 1541 bp DIG-DNA fragments. A 686 bp segment of the gene *pilB2* (2145 bp) was amplified by DIG-PCR to yield probes for the detection of the pil-2 locus. All other DIG-DNA probes generated were directed against individual putative pilin genes (*pilA1* through *pilA11*), respectively sections of them (fragment sizes are indicated in Table 8, p. 62).

2.4.12. Polymerase chain reaction (PCR)

Standard PCR was used for the amplification of genomic DNA fragments and the generation of DIG DNA probes.

Component	Volume
DNA template (variable conc.)	1 μL
Oligonucleotide mix (stock solution: each 5 μM)	2 μL
dNTP mix (stock solution: each 2.5 mM)*	2.5 μL
Pfu buffer (10-fold conc.)	2.5 μL
HPLC-grade H_2O	14.75 - 15.75 μL
Taq/Pfu mix (19:1)*	0.25 μL

*DIG DNA Labeling Mix (10-fold conc.) was used instead of dNTP mix for probe synthesis.

The standard PCR program used was: initial step 300 s at 95 °C, 30 - 35 cycles of 30 s at 95 °C, 15 to 30 s at 54 °C to 70 °C, 30 to 180 s at 72 °C, end step 60 to 300 s at 72 °C.

2.4.13. Isolation of RNA from haloarchaea

Total RNA was isolated from *Hbt. salinarum* cells to enable examination of the transcriptional activity and cotranscription of gene loci, *i.e.* presence or absence of corresponding transcripts, and to relatively quantify transcription of genes of interest in sessile cells compared to planktonic cells. RNA was isolated from *Halobacterium* cells by standard acid guanidinium thiocyanate-phenol-chloroform extraction (Chomczynski & Sacchi, 2006). Cell pellets were thawed on ice for 5 min and afterwards resuspended in 1 mL solution D. After addition of 100 μL 2 M sodium acetate (pH 4.0), 1 mL water-saturated phenol and 210 μL chloroform/isoamyl alcohol [49:1, (v/v)] for extraction of proteins, lipids and DNA, the emulsion was mixed thoroughly on a Vortex for 15 s and incubated on ice for 15 min. Separation of the aqueous and organic phases was achieved by centrifugation at 12 000 *g* and 4 °C for 20 min. The aqueous phase was transferred carefully into a new vial, without the interphase. One volume of isopropyl alcohol was added to the aqueous solution and incubated for 1 h at -20 °C for RNA precipitation.

The RNA was sedimented by centrifugation at 21 000 *g* and 4 °C for 30 min. The supernatant was discarded and the sediment was dissolved with moderate shaking in 300 μL solution D at 65 °C for 2 min. One volume phenol/chloroform/isoamyl alcohol [25:24:1 (v/v/v)] was added for another extraction of undesired organic compounds. The emulsion was mixed thoroughly on a Vortex for 15 s and phase separation was achieved by centrifugation at 9500 *g* and room temperature for 5 min. The aqueous phase was transferred into a new vial and mixed with one volume of chloroform/isoamyl alcohol [49:1, (v/v)] on a Vortex for 15 s. The emulsion was centrifuged at 9500 *g* for 5 min to separate the organic from the aqueous phase, which was transferred into a new vial. For precipitation of RNA, 1 volume of isopropyl alcohol was added and the solution was incubated at -20 °C for at least 1 h. RNA precipitates were sedimented by centrifugation at 21 000 *g* and 4 °C for 30 min. The supernatant was discarded and the RNA pellet was washed by addition of 1 volume of 70% ethanol and centrifugation at 21 000 *g* and 4 °C for 10 min. The supernatant was discarded and the RNA precipitate was dried using a Concentrator 5301 centrifuge (Eppendorf AG, Hamburg, Germany). Total RNA pellets were dissolved in TE-buffer (pH 8.0). Genomic DNA was removed by treatment with RNase-free DNase I (# EN0523, Thermo Fisher Scientific) at 37 °C for 4 h according to the manufacturer's instructions. RNA preparation quality was tested by agarose gel electrophoresis. Purified RNA was used to generate complementary DNA (cDNA).

2.4.14. Reverse transcription polymerase chain reaction (RT-PCR)

For the investigation of the transcriptional activity and cotranscription of gene loci, 40 μg purified RNA were reversely transcribed into cDNA using Random Hexamer Primers (# SO142, Thermo Fisher Scientific) and RevertAid™ Reverse Transcriptase (# EP0441, Thermo Fisher Scientific) in a total volume of 160 μL, according to the manufacturer's protocol. To investigate cotranscription of neighboring genes, oligonucleotides were designed to amplify fragments encompassing the intergenic region and overlapping adjacent genes (oligonucleotides listed in 2.1.4). In case of cotranscription, these primers will lead to PCR products using cDNA as template. RT-PCR analysis of pil-1 was performed using *Taq/Pfu*-polymerase mix 19:1 (# EP0702 and # EP0502, Thermo Fisher Scientific) (initial step 300 s at 95 °C, 35 cycles of 60 s at 95 °C, 90 s at 54 °C to 64 °C, 135 s at 72 °C, end step 300 s at 72 °C) according to the manufacturer's protocol. For analysis of pil-2 the more sensitive Q5®-polymerase (# M0491L, New England Biolabs) was used (initial step 300 s at 98 °C, 35 cycles of 10 s at 98 °C, 30 s at 49 °C to 60 °C, 40 s at 72 °C, end step 120 s at 72 °C). Control reactions were performed using a similar RNA sample without reverse transcription to exclude a possible genomic DNA contamination. PCR was performed to validate the amplicon size and specificity of the oligonucleotides using *Hbt. salinarum* R1 genomic DNA as template.

2.4.15. Adaptor- and radioactivity-free determination of transcriptional start sites (ARF-TSS)

Transcription start sites (TSS) were determined using the adaptor- and radioactivity-free (ARF-TSS) method (Wang *et al.*, 2012). Purified RNA was utilized for the generation of first strand cDNA employing the *pilB1* gene-specific oligonucleotide TSS-pil-1-P1-RT (oligonucleotides listed in 2.1.4) complementary to a sequence located 160 bases downstream of the annotated start codon of OE2215R. Prior to the cDNA synthesis, the oligonucleotides were phosphorylated at the 5'-end using T4 polynucleotide kinase (# EK0031, Thermo Fisher Scientific) according to the manufacturer's instructions. The resulting cDNA fragments were circularized using T4 RNA ligase (# EL0021, Thermo Fisher Scientific) that fuses the 3′- and the 5′-ends. The circularized cDNA served as template for PCR using the two diverging oligonucleotides TSS-pil-1-P2-PCR and TSS-pil-1-P3-PCR, binding between the sites of the gene-specific oligonucleotide and the TSS. PCR products were inserted into pCR® 2.1-TOPO® using a TOPO® TA Cloning® Kit for Sequencing (# 450641, Life Technologies) following the protocol of the manufacturer. The resulting constructs were used for sequence analysis with standard M13 oligonucleotides.

2.4.16. Quantitative reverse transcription polymerase chain reaction (qRT-PCR)

The qRT-PCR procedure applied was based on the use of an external control RNA for data normalization, similar to a method described previously (Shibata *et al.*, 1999). For qRT-PCR 5 μg RNA supplemented with 1 ng of an external standard RNA in a total volume of 20 μL were used to generate the cDNA. External standard RNA (length 1790 nt) was produced by *in vitro* transcription of the *bgaH* gene, using T7 RNA polymerase (# EP0111, Thermo Fisher Scientific) according to the manufacturer's protocol. Since no *bgaH* gene is present in the *Hbt. salinarum* R1 genome, the external RNA detection is not prone to contamination by genomic DNA. qRT-PCR analysis was performed using the StepOne™ Real- Time PCR System (Applied Biosystems by Thermo Fisher Scientific) and the SensiFast™ SYBR® Hi-ROX Kit (# BIO-92005, Bioline) according to the manufacturer's protocol. Employing the StepOne™ software (Version 2.0) the $\Delta\Delta C_T$-method was applied to calculate relative expression changes of the target genes in adherent cells grown for different incubation times or cells from different growth phases compared to their expression in planktonic cells from the exponential growth phase (Schmittgen & Livak, 2008). C_T-values were determined by the StepOne™ software. C_T-values of the target genes were normalized to the housekeeping gene *rpoB1* (Bleiholder *et al.*, 2012) or the external standard *bgaH*. Samples were examined in triplicates. Control reactions checking for genomic DNA contamination were done using similar RNA samples as for the cDNA synthesis, which were not reversely transcribed, as a template. Gene expression was regarded

as being the case only when C_T differences between cDNA samples and the corresponding control samples were at least four cycles.

2.5. *In silico* analyses

The somewhat similar sequences (blastn), position-specific iterated (psi-blast) and protein-protein (blastp) BLAST® alignment search tools were used to analyze gene and protein identities, functions and presence in other genomes (NCBI Resource Coordinators, 2014). Additional analyses were performed using HaloLex (Pfeiffer *et al.*, 2008a), the UCSC Archaeal Genome Browser (Schneider *et al.*, 2006) and SMART (Schultz *et al.*, 1998). The predictions of transmembrane helices in proteins were performed using the software TMHMM Server v. 2.0 (Krogh *et al.*, 2001), archaeal class III (type IV pilin-like) signal peptides by use of FlaFind 1.2 (Esquivel *et al.*, 2013; Szabó *et al.*, 2007b) and the secondary structures of single stranded nucleic acids by the software mfold (Zuker, 2003). Phylogenetic dendrograms were generated by use of the MAFFT server (Katoh & Standley, 2014). The software ApE (v2.0.40) and SerialCloner (version 2.5) were used for nucleic acid sequence analyses.

Results overview

The results of this study are summarized in three chapters (chapter 3 - 5).

Chapter 3 deals with the characterization of biofilms formed by *Hbt. salinarum* R1. A fluorescence-based adhesion assay was used to monitor adhesion dynamics of the organism. Different microscopic techniques were employed to track the adhesion process and the formation of biofilms. The biofilms were characterized with respect to their architecture and composition. Moreover, it was focused on the presence and diversity of haloarchaeal cell surface structures of adherent cells.

Chapter 4 concentrates on the adhesion mechanism of *Hbt. salinarum* R1 cells. A bioinformatical search was performed to identify genes potentially associated with cell surface structure biogenesis. Candidate genes were analyzed with regard to their transcription by RT-PCR. Relative transcriptional quantification in adherent cells compared to planktonic cells was done by quantitative RT-PCR to identify target genes potentially involved in adhesion. Gene deletion mutants were characterized with respect to the adhesion phenotype of *Hbt. salinarum* R1.

Chapter 5 adresses the question what global proteomic changes go along with the transition of *Hbt. salinarum* R1 cells from the planktonic to the sessile lifestyle and the formation of complex biofilms. Protein samples were prepared from each state and compared by a shotgun tandem mass spectrometrical approach. The protein abundances were determined using a SWATH-LC/MS/MS-based quantitation procedure. The identified and quantified proteins were categorized according to arCOG (Archaeal Clusters of Orthologous Genes). Groups of co-trending proteins were determined by a 'Direction Scoring' analysis and their functional relationship with respect to biofilm formation was assessed. Some of the data was validated by an independent method, *i.e.* qRT-PCR.

The enclosed CD-ROM contains the results of the quantitative proteome analysis, *i.e.* 'Pairwise Comparison' (Supplementary tables 1) and 'Direction Scoring' (Supplementary tables 2).

3. Adhesion and biofilm formation of *Halobacterium salinarum* R1

3.1. Introduction

Many microorganisms are able to adhere to surfaces or even have the ability to colonize these by the formation of biofilms. To date this phenomenon was predominantly studied in bacterial species, due to their clinical relevance. Adhesion is a virulence factor of pathogens and often leads to contamination of medical devices (Khoury *et al.*, 1992; Soto & Hultgren, 1999). Moreover, biofilm formation has industrial and domestic relevance, resulting in problems regarding corrosion or blockage of water distribution pipes (Ibars *et al.*, 1992; Niquette *et al.*, 2001). But also positive examples are known, since biofilms are useful in bioremediation or wastewater treatment processes (Bouwer & Zehnder, 1993; Stams & Oude Elferink, 1997).

Also, archaeal species form biofilms, but in contrast to bacteria, knowledge about archaeal adhesion and biofilm formation is very limited and little is known about the underlying mechanisms and processes. Recently it was shown that several haloarchaeal species from different genera are able to adhere to solid surfaces at the interphase between culture vessels and culture medium (Fröls *et al.*, 2012). Thirteen of twenty species tested show a significant adhesion to the plastic surfaces. Among the species investigated was *Halobacterium salinarum* R1 that shows the second-strongest adherence in comparison to the other haloarchaea (Fröls *et al.*, 2012). Nevertheless, nothing is known about the molecular alterations in cells during biofilm formation or the adhesion mechanism of *Hbt. salinarum* R1.

The first part of this thesis aims to describe the events taking place when *Halobacterium salinarum* R1 adheres to solid surfaces as well as to characterize adherent cells and multicellular structures using quantitative and different microscopic techniques.

3.2. Results

3.2.1. Monitoring of *Hbt. salinarum* R1 adhesion to solid surfaces

The adhesion process of *Hbt. salinarum* R1 was monitored and quantified in a fluorescence-based adhesion assay over a time course from 1 through 21 days. For quantitation of the adhesion cells were grown in static cultures in polystyrene 24 well tissue culture plates. At the time points of investigation cell growth was checked qualitatively by observing turbidity and pigmentation of the cell cultures in the culture plate cavities. A steady increase of the turbidity throughout the incubation time was observed (Figure 9A, Top). From day six on the cultures appeared orange and reddish in color. In contrast, no turbidity or pigmentation was observed in the wells with non-inoculated media control after 21 days of incubation.

For quantitation, cells adhering to the polystyrene surface of the cavities were stained by addition of the membrane permeating fluorescent dye acridine orange (AO), which intercalates into the cellular DNA. After the staining procedure non-adherent cells were washed off by repeatedly adding basal salt water (complex medium without peptone) to the wells with subsequent discarding of the suspensions. Fluorescence was detected by a fluorescent image analyzer (Figure 9A, Bottom) and quantitation software was used for determination of fluorescence intensities (see 2.2.2). To allow for relative comparison of the adhesion at different times, all fluorescence intensities measured were set off against the value measured after 15 days of growth, which represented the highest value (Figure 9B).

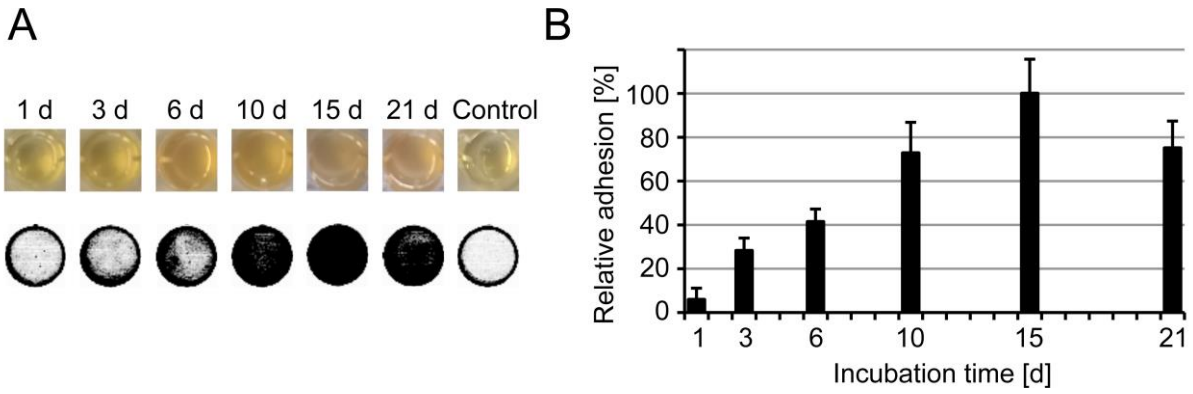

Figure 9 Quantitation of the *Hbt. salinarum* R1 adhesion to plastic surfaces by use of a fluorescence based adhesion assay. Growth and adhesion of the cells was monitored over three weeks in the cavities of 24 well tissue culture plates. **A**, Top: Photographs showing turbidity of the cells in the cavities after incubation times from 1 to 21 days (1 d through 21 d); Bottom: Corresponding fluorescence signals received in the quantitation procedure from the cavities shown above; **B**, Relative adhesion of the cells throughout the time course. Ordinate: Relative adhesion of the cells after growth for 1 to 21 days in relation to the adhesion signal after 15 days (set to 100%). Abscissa: Incubation time in days. Based on three independently cultivated samples (N=3).

A continuous increase of the fluorescence signal was detected in the cavities from day one to day fifteen (Figure 9B). After 21 d of growth the fluorescence signal decreased compared to the 15 d sample, having similar intensities as after 10 d. In contrast, no fluorescence was detected

from the non-inoculated control wells only containing culture medium, implying specificity of the signals measured. The adhesion assays demonstrated an increasing attachment of the cells to the plastic surface throughout the first two weeks. After reaching a maximum value around day fifteen, adhesion diminished as incubation proceeded.

To gain further insights into the sequence of events during the adhesion of *Hbt. salinarum* R1 at the cellular level, the morphology of attached cells as well as the adhesion progress of the cells was monitored by phase contrast microscopy (PCM) from 1 to 15 days. Microscopic glass coverslips were submerged in static *Hbt. salinarum* R1 cell cultures and incubated up to 15 days. After incubation times the glass slides were removed from the cultures and submerged several times in basal salt water to remove non-attached cells. Cells bound to the coverslips were observed by phase contrast microscopy.

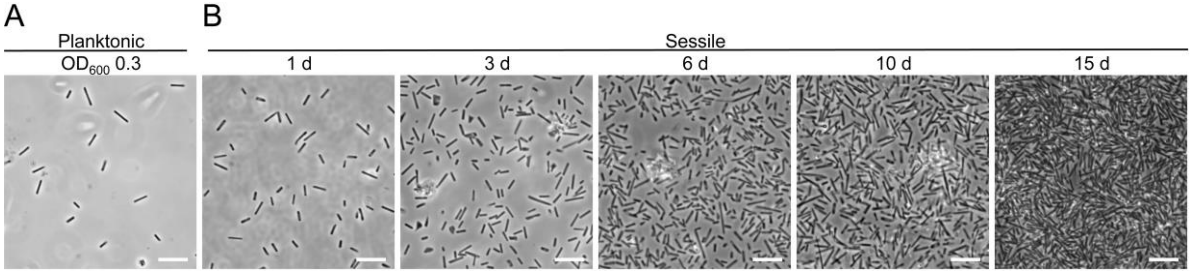

Figure 10 Phase contrast light micrographs of *Hbt. salinarum* R1 planktonic and adherent cells. **A**, cells from the exponential growth phase (OD_{600} 0.3). **B**, sessile cells adhering to microscopic glass coverslips after 1 to 15 days of growth (1 d through 15 d). Scale bars equal 10 µm.

No morphological difference was observed between planktonic and sessile cells. The typical rod-shaped cell morphology of *Hbt. salinarum* R1 appeared in both cases (Figure 10A and B). The planktonic cells were motile and freely moving in the medium, whereas in consequence of the washing procedure only immobilized cells appeared on the coverslips. An increase of the number of adherent cells on the glass surface was observed throughout the incubation (Figure 10B). At the beginning of the experiment only single cells attached to the glass, after three days already small cell accumulations were observed. These microcolonies became larger as the number of adherent cells increased during the course of incubation. After 10 d of growth gaps were still present in between the cells, whereas virtually the whole glass surface was overgrown after fifteen days. By focusing through the microscopic planes of the specimen, it was observed that the adherent cells not only formed a single cell layer, but multiple layers of cells, with regions showing cell accumulations and obviously stacks of cells extending along the z-axis. In the PCM images these appeared as bright regions, which indicated a more complex three-dimensional architecture of the attached cells on the glass surface.

3.2.2. Investigations on the complexity of *Hbt. salinarum* R1 adherent multicellular structures

For a more detailed analysis of the structures formed by *Hbt. salinarum* R1 cells adhering on plastic surfaces, confocal laser scanning microscopy (CLSM) was performed (2.3.3). The formation of attached multicellular structures was monitored over a period of time from 1 through 24 days. Viable cells were stained with the cell membrane permeating DNA intercalating dye acridine orange (AO). Moreover the presence of a biofilm matrix, *i.e.* extracellular polymeric substances (EPS), containing typical components like glycoconjugates and extracellular DNA (eDNA) as well as the viability of the cells was tested. As a marker of EPS, commonly found glycosidic residues were detected by concanavalin A Alexa Fluor® 647 conjugates (ConA), selectively binding glycosidic α-mannose and α-glucose residues. Furthermore, propidium iodide (PI) was employed for staining of extracellular DNA (eDNA) and DNA from disrupted cells.

Planktonic *Hbt. salinarum* R1 cells appeared rod-shaped and motile after AO staining (Figure 11A). Virtually no PI or ConA signals were observed with freely swimming single cells. Occasionally individual dead cells, yielding PI signals, were observed (not shown here), while weak ConA signals were only rarely detected in cell accumulations apparently floating in the medium. Adherent cells occurred as immobilized rods on the substratum after one day of growth (Figure 11B). On the first day predominantly single cells were spread all over the surface, with large spaces in between. After three days, small cellular accumulations were observed. With proceeding incubation time accumulations became larger and more of the surface area was covered with cells. Nearly the whole surface was overgrown by cells after 15 d and if incubation was continued up to 24 d.

Detection of ConA proved the production of a biofilm matrix containing glycosidic components. Significant ConA signals associated with adherent cells were firstly observed after three days of incubation. ConA signals were generally co-localized with the cellular aggregations and increased in parallel with these during the 24 d course of monitoring, indicating the presence of a biofilm matrix, in which the cells were embedded. According to the propidium iodide signals, all cells attached to the surface were viable after one day of incubation and no eDNA was detectable, while first weak PI signals were visible after three days of growth. Together with the ConA signals, this suggests the presence of EPS containing DNA and glycosidic components. Similar to ConA, PI signals were mostly associated with cellular accumulations, also increasing with proceeding biofilm development, although they were generally relatively weak. The weak PI signals indicated high viability of the cells in *Hbt. salinarum* R1 biofilms after 15 days of incubation and during later stages. This was verified by chemical fixation and

cell lysis of biofilm cells grown for 15 days, which resulted in stronger PI signals originating from virtually all cells, congruent with the AO signals (Figure 11C).

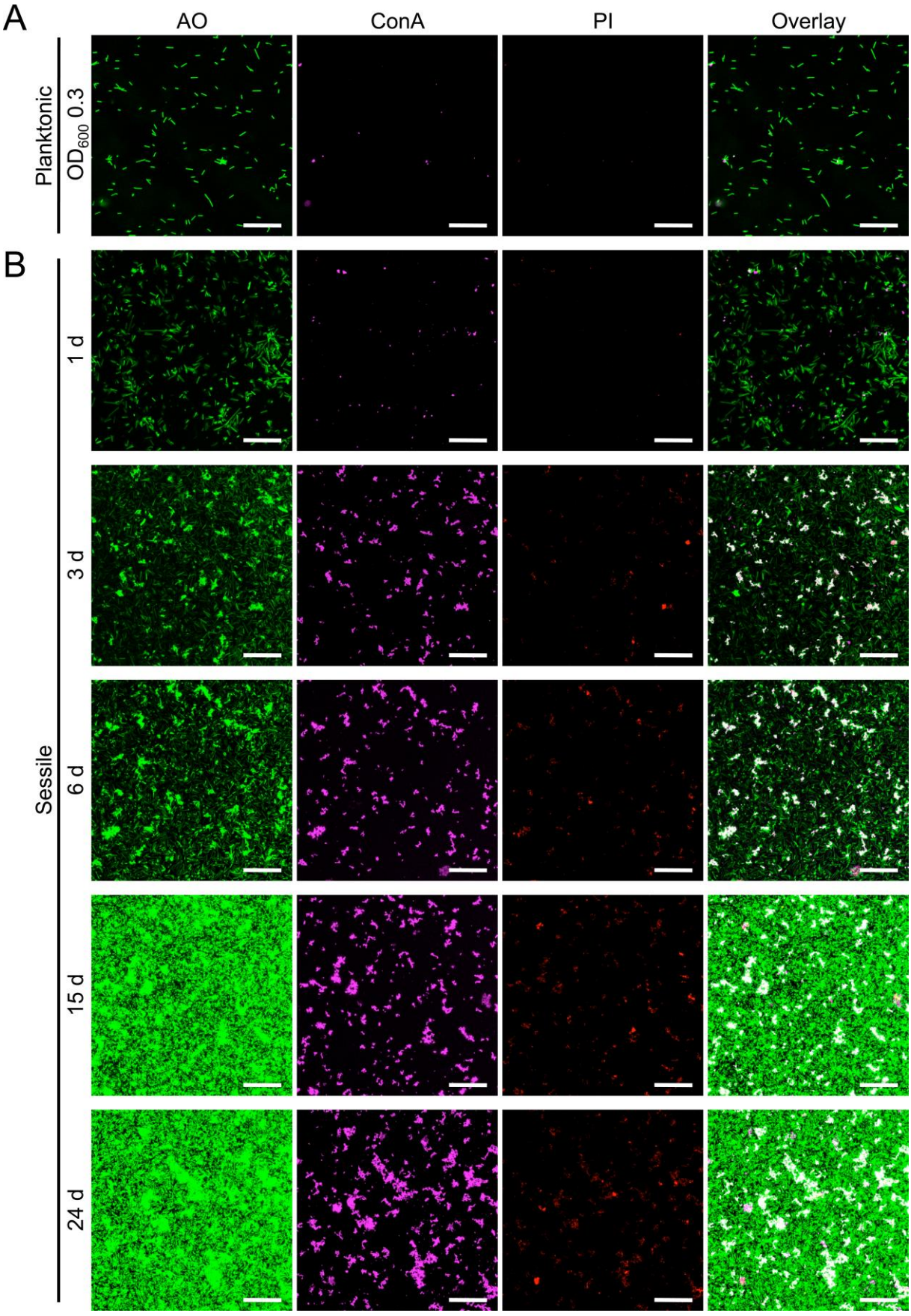

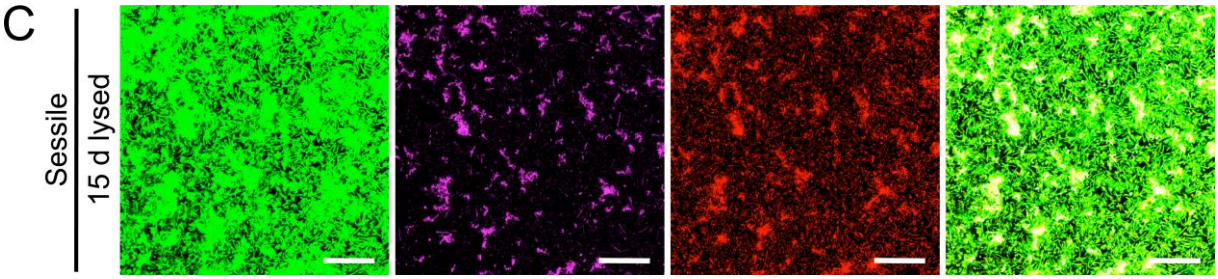

Figure 11 Confocal laser scanning micrographs of *Hbt. salinarum* R1 planktonic as well as biofilm forming cells. **A**, Planktonic cells grown at 37 °C in shaking cultures until exponential growth phase (OD_{600} 0.3). **B**, Biofilms grown for 1 to 24 days (1 d to 24 d) at 37 °C under static conditions on plastic surfaces. **C**, Biofilm cells grown for 15 days, chemically fixated and lysed (15 d lysed), to check for permeability of propidium iodide and compare cell viability to untreated cells. Fluorescent staining of cells was done using acridine orange (AO), glycoconjugates were stained with concanavalin A Alexa Fluor® 647 conjugates (ConA) and propidium iodide (PI) was employed to stain extracellular DNA and DNA associated with lysed cells. Overlay: Overlay of AO (green), PI (red) and ConA (magenta) signals. Scale bars equal 30 µm. CLSM images of the planktonic cells show one slice of a stack. CLSM images of biofilms show z-projections of stacks. (Losensky *et al.*, 2016)

Stacks of fluorescent images of the biofilms were produced to visualize the three-dimensional biofilm structures after different incubation times (Figure 12). After one day of growth only a single layer of spread cells was observed on the plastic surface. First cellular accumulations (microcolonies) were visible after three days, which were a few cell layers thick and became larger as incubation continued. They reached heights of 9 to 12 μm on day six and 15 μm after nine days. On day 15 the cells had formed up to 20 μm thick biofilms, which measured 20 through 25 μm in height after 24 d. Sometimes also tower-like structures higher than 30 μm were observed.

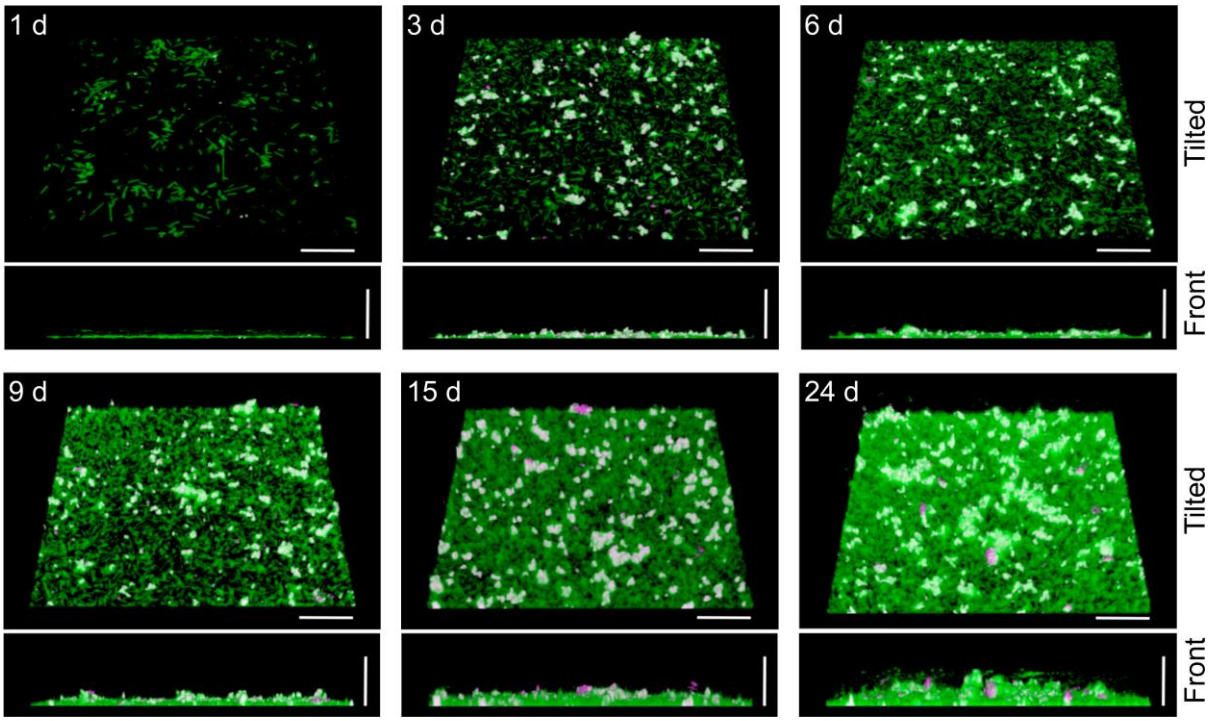

Figure 12 Stacks of confocal laser scanning micrographs taken from *Hbt. salinarum* R1 biofilm forming cells. Tilted top view (top) and corresponding side view (bottom) of 1, 3, 6, 9, 15 and 24 days old biofilms grown at 37 °C under static conditions on plastic surfaces. Genomic DNA was stained with acridine orange

(green), glycoconjugates with terminal α-mannopyranosyl and α-glucopyranosyl residues were stained with concanavalin A Alexa Fluor® 647 (magenta to white), indicating production of EPS. Scale bars equal 25 µm. (Modified from Losensky *et al.*, 2016)

For a more detailed structural investigation of the adherent *Hbt. salinarum* R1 multicellular accumulations, *i.e.* the microcolonies, scanning electron microscopy (SEM) was performed. The SEM analysis was done in cooperation with Dr. Nathalie Benker (Institute of Applied Geosciences, Environmental Mineralogy, Technische Universität Darmstadt).

Carbon coated gold grids were submersed in static *Hbt. salinarum* R1 cultures for 10 d, to allow for adhesion of the cells. Observation of the multicellular structures of attached cells and potential cell surface structures was purposed with regard to the SEM analysis. Therefore the cells on the grids were fixed in a glutaraldehyde/paraformaldehyde solution dissolved in basal salt water, using a protocol modified of Gruber *et al.* (2004). Drying of the specimen for SEM resulted in extensive salt crystal formation and impeded the observation of cells (Figure 13A). For better visualization of the cellular structures, the samples were contrasted with uranyl acetate and an additional washing step was implemented after the fixation and contrasting procedure. An improved visualization of single cells and multicellular structures was achieved (Figure 13B).

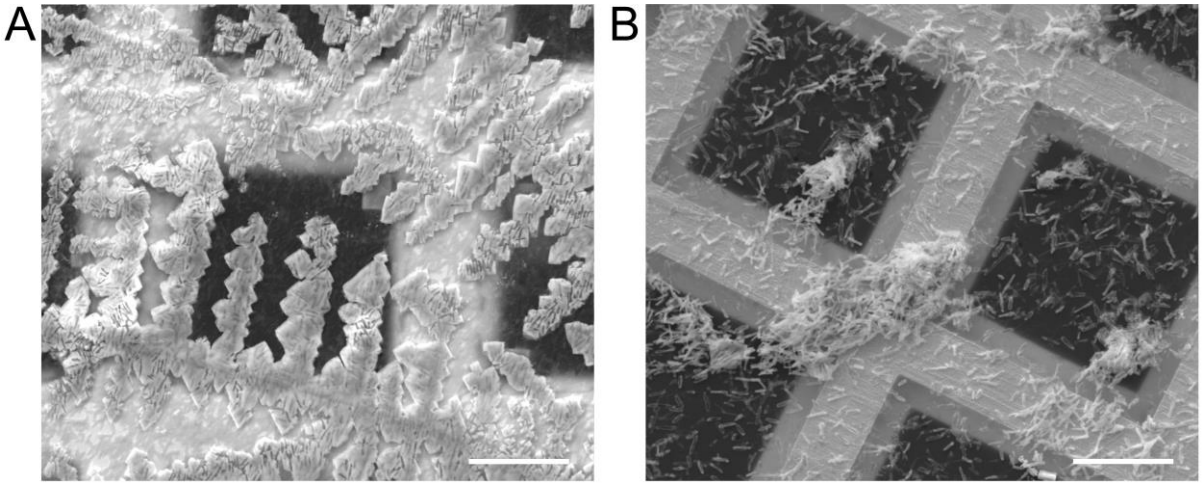

Figure 13 Optimization of sample preparation for scanning electron microscopy (SEM). Cells were grown on carbon coated gold grids for 10 d. After fixation employing a paraformaldehyde/glutaraldehyde solution in basal salt water the specimen were dried and observed directly by SEM (**A**) or following uranyl acetate contrasting and an additional wash step using water (**B**). SEM images at 2500x magnification. Scale bars equal 20 µm.

Microcolonies were visible evenly spread over the surface, measuring diameters of up to 50 μm (Figure 14A). Within these clusters the cells were often embedded in a pleomorphic matter (Figure 14B), presumed to be the biofilm matrix. With regard to visualization of the cellular structures, a better contrast was achieved by sputter coating of the specimen with gold, which revealed the presence of manifold cellular appendages in the surrounding of the adherent cells (Figure 14C and D). These were visible between different cells as well as between cells and the

surface. The identity of these cell surface structures was not clear, though possibly representing the *Hbt. salinarum* R1 archaella (archaeal flagella), which were described previously (Houwink, 1956), or other unknown cell extensions, potentially involved in adhesion or cohesion of the cells.

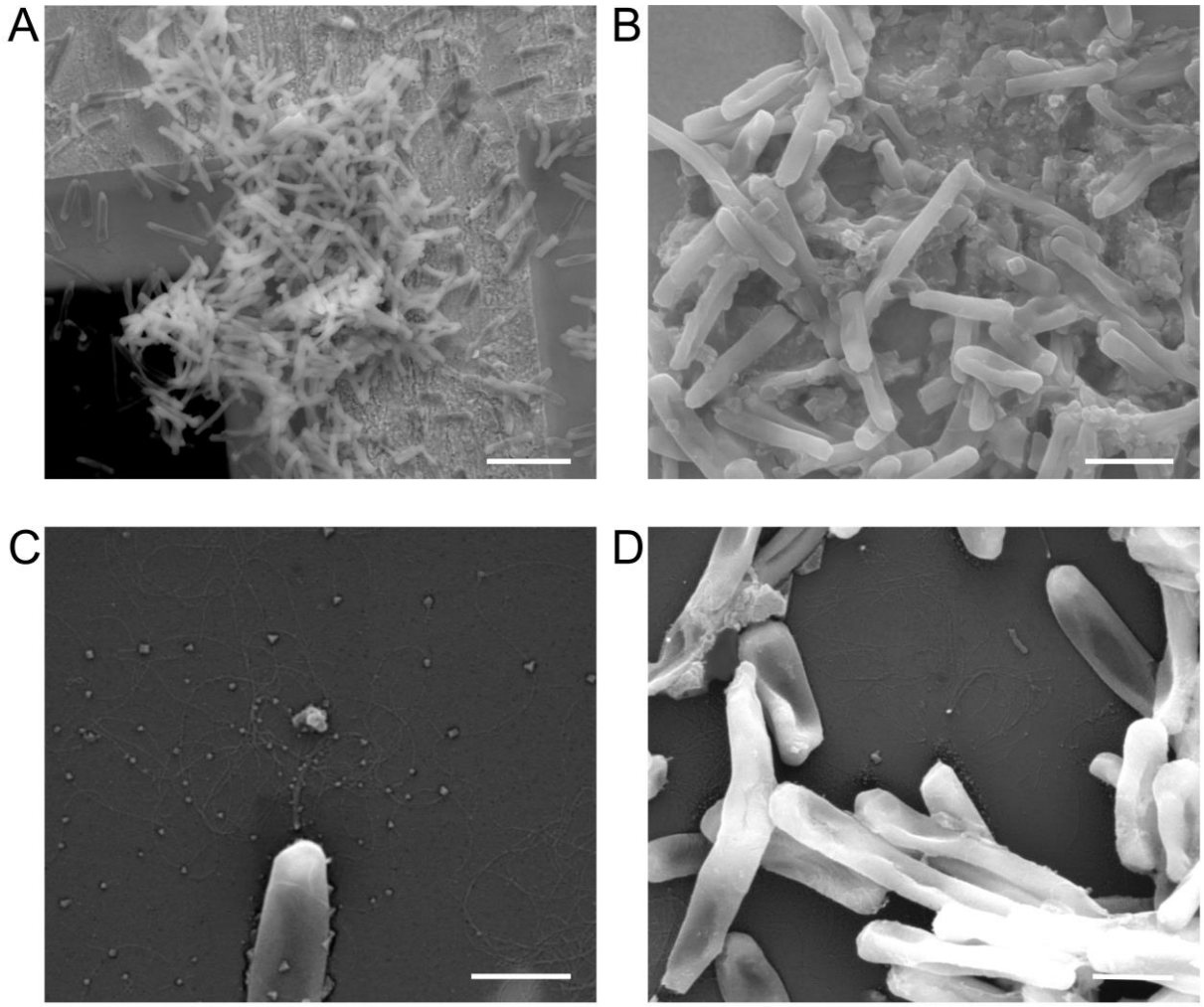

Figure 14 SEM analysis of adherent *Hbt. salinarum* R1 multicellular accumulations. Cells were grown on carbon coated gold grids for 10 d. **A**, Multilayered cell cluster (8250x magnification, scale bar 5 µm). **B**, Multilayered cell cluster with cells embedded in a biofilm matrix (20 000x magnification, scale bar 2 µm). **C**, Section of a single attached cell with manifold cellular appendages (50 000x magnification, scale bar 1 µm). **D**, Accumulation of adherent cells with cellular appendages (40 000x magnification, scale bar 1 µm).

3.3. Discussion

3.3.1. *Hbt. salinarum* R1 adheres to solid surfaces and forms complex biofilms

It was demonstrated that *Halobacterium salinarum* R1 is able to adhere to surfaces and forms characteristic multicellular structures embedded in a self-produced matrix, *i.e.* biofilms.

Unlike bacteria, biofilm formation is a recently observed trait with regard to archaea (Orell *et al.*, 2013a). Predominantly hyperthermophilic species represent the best-studied archaeal examples to date. A formation of biofilms was observed for *Archaeoglobus fulgidus* under stress conditions (Lapaglia & Hartzell, 1997). Another example is *Pyrococcus furiosus*, which is able to adhere to various surface materials, like diverse metals and silicon, as well as different types of plastics and glass, by use of its multifunctional flagella (Näther *et al.*, 2006). In addition to this, an archaeal bi-species biofilm formed by *Pyrococcus furiosus* and *Methanopyrus kandleri* was described (Schopf *et al.*, 2008). Biofilm formation was also observed with three closely related *Sulfolobus* species, which all three display different biofilm architectures (Koerdt *et al.*, 2010). Biofilm formation is also common among haloarchaea, demonstrated by the fact that members within four of five genera are able to adhere and to form biofilms (Fröls *et al.*, 2012).

The initial observation that *Hbt. salinarum* R1 showed an increasing adherence signal in a fluorescence-based adhesion assay throughout the first two weeks of incubation was also seen by phase contrast microscopy (PCM). After initial and widespread attachment of single cells, small cellular aggregations were observed after a few days, which became larger until virtually the whole surface was covered with cells after two weeks. No further changes were observed after longer incubation times by PCM. CLSM analysis demonstrated that the cells successively formed multicellular structures with a complex three-dimensional architecture. In these clusters the cells were embedded in a matrix, containing components which are typical extracellular polymeric substances (EPS) of archaeal and bacterial biofilms, like alpha-mannose/glucose glycosidic residues and extracellular DNA. The presence of glycosidic components was also detected in biofilms of other haloarchaeal biofilms, from the genera *Haloferax*, *Haloruburum* and Antarctic isolates, as well as the closely related strain *Halobacterium salinarum* DSM 3754^{T} (Fröls *et al.*, 2012). However, the exact EPS composition and function in haloarchaeal biofilms is still not known. In previously studied biofilms of *Pseudomonas aeruginosa* it was demonstrated that the EPS components play roles in mechanical stability as well as adhesion and cohesion of the cells (Flemming & Wingender, 2010). This is also possible with respect to *Hbt. salinarum* R1 biofilm formation, where the EPS components were already observed in early stages from day three on, when small attached cell aggregates were noticed. Afterwards increase of the EPS signals went hand in hand with cell accumulation and the maturation of a characteristic biofilm morphology.

Compared to biofilms formed by other haloarchaeal species, different three-dimensional morphologies are observed with some species. The biofilms of *Halorubrum lacusprofundi* DL28 and *Haloferax volcanii* DSM 3757^T on glass surfaces consist of large multicellular aggregates. In contrast, *Halobacterium salinarum* DSM 3754^T and *Halohasta litchfieldiae* (formerly denoted Antarctic isolate DL24) form carpet-like biofilms, with a thickness of multiple cell layers and exhibit small and large cell aggregates, which are similar to the biofilms of *Hbt. salinarum* strain R1 (Fröls *et al.*, 2012). This suggests a genus-specific morphology of biofilms, formed by different species of *Halobacterium*. Interestingly differing biofilm morphologies, even between species from the same genus, are also observed with *Sulfolobus*. *Sulfolobus acidocaldarius* shows dense biofilms with large tower-like structures, *S. tokodaii* forms dense biofilms with occasional cell accumulations, and *S. solfataricus* displays carpet-like biofilms with a low cell density (Koerdt *et al.*, 2010).

Additionally, different effects of environmental parameters like temperature or pH on the different *Sulfolobus* species' biofilm formation have been observed (Koerdt *et al.*, 2010). This suggests a more complex regulation of biofilm formation by *Sulfolobus*, allowing adjustments or variable developmental mechanisms. If this also holds true with *Halobacterium* is not yet clear. On the one hand it has been demonstrated by Fröls *et al*. (2012) that parameters like salt concentration, pH or growth temperature do not affect biofilm formation of *Haloferax* or the *Hbt. salinarum* strains DSM 3754^T and R1. On the other hand it has been shown that certain metal ions influence biofilm formation of *Hbt. salinarum* R1 (unpublished results S. Völkel and S. Fröls; Master thesis S. Völkel, 2015), suggesting that these biofilms also adapt to their environment and potentially provide protection from hazardous compounds or influences by so far unknown mechanisms.

In addition, the benefits that haloarchaeal cells gather from building sophisticated biofilm structures remain to be elucidated. The formation of a hydrated biofilm matrix can be interpreted as a protection mechanism from dessication in their hypersaline habitats. The matrix could also retain nutrients to persist starvation periods. In the same context extracellular DNA can be also regarded as nutrient storage, which has been demonstrated for *Haloferax volcanii* (Chimileski *et al.*, 2014a). Furthermore, eDNA can function in surface adhesion or biofilm structure, as observed with bacterial biofilms (Dominiak *et al.*, 2011; Whitchurch *et al.*, 2002).

3.3.2. Cells in *Hbt. salinarum* R1 microcolonies possesses various cell surface structures

An improved visualization of the complex *Hbt. salinarum* R1 biofilm structures on a cellular level was achieved in this work by scanning electron microscopy (SEM). In addition, SEM

facilitated visualization of various cell surface structures, which surrounded and interconnected the cells. These structures were observed between the cells and the surface, as well. Similar observations have been made with other adhering microorganisms like *Pyrococcus furiosus*, or *Sulfolobus solfataricus* (Schopf *et al.*, 2008; Zolghadr *et al.*, 2010). While *Pyrococcus* possesses one type of cell surface structures with multiple functions, it was shown that *Sulfolobus* has several types of cellular appendages with specialized functions. The resolution achieved by SEM in this report did not allow to evaluate whether the cell surface structures of *Hbt. salinarum* R1 were uniform.

Therefore the SEM preparation and fixation protocol optimized here was also applied to samples of attached *Hbt. salinarum* R1 cell clusters for investigations by transmission electron microscopy (TEM) performed by others (Master thesis L. Vidakovic, 2014). TEM resulted in an even better resolution of the ultrafine *Hbt. salinarum* R1 appendages and confirmed the presence of different cell surface structure types, which had been already observed previously with regard to biofilms of *Hbt. salinarum* DSM 3754^{T} (Fröls *et al.*, 2012). A systematic measurement of their thicknesses reveals two predominant diameters of 7.6 and 10 nm in average [Master thesis L. Vidakovic, 2014; (Losensky *et al.*, 2014)]. A diameter of 10 nm refers to the haloarchaeal archaellum (Cohen-Krausz & Trachtenberg, 2002), while the identity of the second type of structures is unclear. Their diameters of 7.6 nm are thinner in comparison to the 10 nm pili observed with *Sulfolobus solfataricus* or the 8.5 nm pili of *Methanococcus maripaludis* (Henche *et al.*, 2012a; Wang *et al.*, 2008).

Most recent studies on *Hbt. salinarum* cellular appendages only report the presence of polarly localized archaella, which form bundles referred to as super-flagella (Alam & Oesterhelt, 1984; Kupper *et al.*, 1994). Nevertheless, there is one report on another type of cell surface structures in *Hbt. salinarum*, which is observed upon knock-out of the five archaellin genes from the *flgA* and *flgB* loci. These structures, termed X-filaments, also show a thinner diameter of 7 to 8 nm compared to the archaella and are observed as single filaments distributed over the whole surface of few cells by TEM analysis (Beznosov *et al.*, 2007). The authors hypothesize that these filaments are abnormal archaella and consist of a protein encoded by the gene *flgX*, which in their opinion possibly constitutes only a minor component of the archaellum under normal circumstances. Yet, their intended identification of the X-filament constituents was not successful. The authors speculate on additional functions of the archaellum, like the adhesion or intercellular connections observed with respect to the archaella of *Pyrococcus furiosus* (Näther *et al.*, 2006), but no experimental data supports this assumption.

In the present work adherent cells of *Hbt. salinarum* R1 were investigated for the first time, which is in contrast to Beznosov *et al.* (2007) and other previous microscopic studies on planktonic halobacterial cells and their archaella. TEM analyses of adherent cells indicated the

presence of the thin filaments, summing up to about 30% of the total cell surface structures. In contrast, only two to three of these appendages were observed with planktonic cells[(Master thesis L. Vidakovic, 2014; (Losensky *et al.*, 2014)]. This suggested a potential function of the thin filaments in the adhesion mechanism. Moreover, this might explain why the thin filaments were mostly not observed or possibly overlooked before, because cells are usually kept in shaking liquid cultures in the laboratory, *i.e.* planktonic conditions. Nevertheless, a role for archaella in adhesion is possible, since they were found also with adherent cells. Additionally, the action of yet another mechanism is conceivable, like the previously discussed EPS production.

From these results it has to be pointed out, that the exact adhesion mechanism, facilitating initial attachment of the *Hbt. salinarum* R1 cells to the surface and subsequent biofilm development, could not be resolved by mere microscopic analyses. However, strong indication for an adhesion mediated by cellular surface structures was given, namely the archaella or the newly observed filaments.

4. Investigation of the *Halobacterium salinarum* R1 adhesion mechanism

4.1. Introduction

While cell motility is crucial to reach beneficial environmental conditions or to escape from unfavorable external influences, adhesion is also a common trait of microbes. Adhesion to organic or inorganic surfaces and also to other cells plays an important role to keep them in favorable niches and to prevent their removal. For both purposes bacteria and archaea have invented special organelles and mechanisms (Dufrêne, 2015; Jarrell *et al.*, 2013).

Investigation of various *Sulfolobus* species demonstrated that they possess diverse pili exerting different functions in surface adhesion and cell aggregation (Henche *et al.*, 2012a; Henche *et al.*, 2012b). Also, euryarchaeote species like the methanogenic *Methanothermobacter thermoautotrophicus* and *Methanococcus maripaludis* have pili facilitating adhesion to surfaces (Jarrell *et al.*, 2011; Thoma *et al.*, 2008). In addition, several species like *Methanococcus maripaludis* or *Pyrococcus furiosus* possess multifunctional archaella enabling motility as well as attachment to surfaces or intercellular connections (Jarrell *et al.*, 2011; Näther *et al.*, 2006; Schopf *et al.*, 2008). In contrast, the archaella of the extremely halophilic species *Haloferax volcanii* are responsible exclusively for locomotion, while attachment of the cells is mediated by distinct adhesion pili (Esquivel *et al.*, 2013; Tripepi *et al.*, 2010).

Investigations on a number of haloarchaeal species from different genera demonstrated that adhesion is a common trait (Fröls *et al.*, 2012). Adhesion is the initial step in the formation of biofilms, as demonstrated with *Hbt. salinarum* R1 (see Chapter 3). Adhesion represents the first and therefore most important event, which also marks a fundamental changeover from a free living mode to a sessile lifestyle. Motility of *Halobacterium* is mediated by archaella, that were firstly observed by electron microscopy (Houwink, 1956) and are already characterized in detail (Alam and Oesterhelt, 1984; Patenge *et al.*, 2001). In contrast, the cellular structures mediating adhesion of *Hbt. salinarum* R1 are still unknown and nothing is known about the underlying mechanism. The presence of additional cell surface structures besides the archaella was suggested by electron-microscopic studies in our lab (Chapter 3.3.2).

This chapter deals with the elucidation of the adhesion mechanism of *Hbt. salinarum* R1. A bioinformatical search for candidate genes encoding potential cell surface structures besides the archaella was conducted. The transcription of archaella encoding genes as well as genes coding for potential surface structures was analyzed and the transcripts were characterized. To connect the identified genes with cell surface structures and adhesion, gene deletion mutants were characterized in respect to these traits. Furthermore, genotyping analyses of different halobacterial strains exhibiting variable adhesion capabilities were performed, to investigate the occurrence of potentially adhesion-associated genes.

4.2. Results

4.2.1. Bioinformatical search for (putative) type IV pili encoding genes

The genome sequence of *Hbt. salinarum* R1 was searched for putative type IV pili encoding genes, because type IV pili are common as surface structures in archaea (Lassak *et al.*, 2012a). Since the halobacterial archaellum itself constitutes a type IV pilus, one of its core components was assumed to be a good starting point for a bioinformatis analysis. The amino acid sequence of the archaellum motor/assembly ATPase FlaI (OE2380R) was used for a BLASTp search against the *Hbt. salinarum* R1 proteome, to look for similar proteins which might be part of additional putative type IV pili systems besides the archaellum. Two chromosomally encoded proteins were found sharing high similarities with the archaella ATPase (Table 3). The protein encoded by the ORF OE2215R shared 35% amino acid sequence identity, while the second protein was encoded by ORF OE1347R and had 28% identical amino acids. In both cases low E-values indicated high significance of the BLASTp results, while the sequence identities of about 30% suggested similar functions. This was substantiated by the presence of conserved type IV secretory pathway VirB11 ATPase domains in all three protein sequences (Figure 15), prompting that OE2215R and OE1347R encoded putative type IV pili assembly ATPases.

Table 3 Comparison of the archaellum motor/assembly ATPase FlaI (OE2380R) with two similar putative type IV pili ATPases (OE2215R and OE1347R)

Gene number	Protein length [aa]	Sequence identity[1] [%]	Query coverage [%]	E-value	Conserved domains[2]
OE2380R	629	100	100	0	VirB11 ATPase
OE2215R	550	35	62	7E-75	VirB11 ATPase
OE1347R	714	28	48	7E-21	VirB11 ATPase

[1] Compared to OE2380R; [2] according to UniProtKB

```
OE2380R   ELAAYLWLCLENEQTVFVVGETASGKTTTLNSIMSFIPRDSKIYTA-EDTAEVIPPHDTW   417
OE2215R   DQMAYLWLAIESNKSLLFAGGTASGKTTSMNAVSMFVPPRAKILTI-EDTRELALYHDNW   331
OE1347R   GIVALLWLAYEHHRVVLFSGPTGVGKTTLMNAHMPFVPFDDRPVSIDEGSREVRLPHETG   495
             * ***. * .: ::. * *. **** :*:   *:*   :  :  * : *:   *:.

OE2380R   QQLLTREGQGENSADVDMFDLVAAALRSRPDYIIVGEVRGEEGRMA-FQAAQTGHPVMLT   476
OE2215R   LSSVTRGADGGGDTITMYDLLRSALRHRPEYIIVGEVRGEEAMTL-FQAMNTGHTTYST   390
OE1347R   VSLSTREHEQ-AFKRVSMADLMTATNYLNPDIEVIAEINTRASFESFAQILNTGHGVVGT   554
           .  **  :      : * **: ::   .*:  ::.*:. . .     *  :*** .  *

OE2380R   FHASDIVSMIQRFTGEPINVPETFMDNADVALFQNRVKQGDDVLRRVTSVQEIEGYSKE-   535
OE2215R   MHADSVQTVINRLENDPINVPRAMIQSLDILCVQTLTHVGDERVRRSSVIAEIEGIDQR-   449
OE1347R   THAAGVDPLVNRAVEQ--GVPAHLLREIDLVVFPRRTD-GDRYVGEVVEFVDDAGPTTTA   611
           **  :  :::*   :   **  :: . *:  .   .. **  : .   . :  *
```

Figure 15 Protein sequence aligment of the (putative) type IV pili ATPases of *Hbt. salinarum* R1. The archaella motor/assembly ATPase FlaI (OE2380) was aligned with the two putative type IV pili ATPases (OE2215R and OE1347R). Only part of the alignment is shown, comprising segments of the conserved VirB11 ATPase domains (shaded in grey) including Walker A and B motifs (bold) involved in nucleotide binding. Numbers indicate amino acid positions. Asterisk, fully conserved residue. Colon, conservation between groups of strongly similar properties. Period, conservation between groups of weakly similar properties. Alignment performed by use of ClustalOmega (www.ebi.ac.uk/Tools/msa/clustalo/).

Further inspection of the corresponding gene loci revealed for both identified type IV pili ATPase encoding genes the presence of downstream ORFs (OE2212R and OE1344R) encoding putative transmembrane proteins. These ORFs displayed similarities to the flagella transmembrane protein FlaJ (OE2379R), as predicted by TMHMM server v. 2.0 and BLASTp alignments. While the FlaJ sequence contains nine transmembrane helices (TMH), the ORF OE2212R encoded a protein containing seven TMH, with 23% sequence identity (query coverage 35%, E-value 2E-7) compared to FlaJ. ORF OE1344R was predicted to encode a six TMH protein and had an identity of 24% (query coverage 40%, E-value 9E-3) compared to FlaJ. Although the protein sequences differed with regard to their length and the number of TMH predicted, the topologies of their TMH appeared partially similar (Table 4).

Table 4 Comparison of the (putative) type IV pili transmembrane proteins

Gene number	Protein length [aa]	Sequence identity[1] [%]	No. of TMH[2]	TMH topology[3]
OE2379R	581	100	9	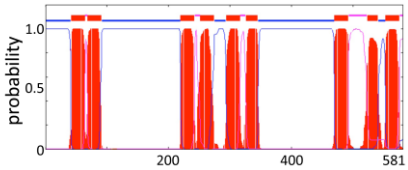
OE2212R	692	23	7	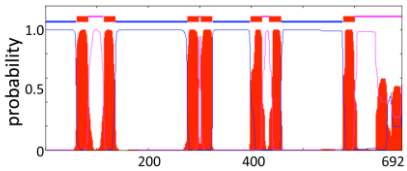
OE1344R	609	24	6	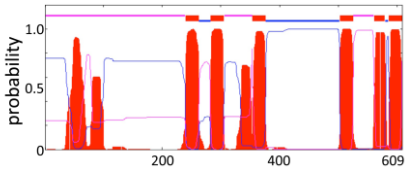

[1] In comparison to OE2379R; [2] according to TMHMM prediction server v. 2.0; [3] probability of TMH occurrence dependent on the amino acid sequence (http://www.cbs.dtu.dk/services/TMHMM/)

Based on the protein sequence similarities of the ATPases and transmembrane proteins and with respect to the analogous spatial organization of the genes, the two loci likely represented type IV pili encoding systems and were therefore termed pil-1 and pil-2 (Figure 16A and B). The corresponding ATPase and transmembrane protein encoding genes were referred to as *pilB1* and *C1*, respectively, *pilB2* and *C2*. Further bioinformatical analysis of the neighboring genes located at the pil-1 locus did not yield any association with type IV pili assembly, whereas several putative prepilin encoding genes (OE1340R, OE1336R and OE1334R) were located at the pil-2 locus (Figure 16B).

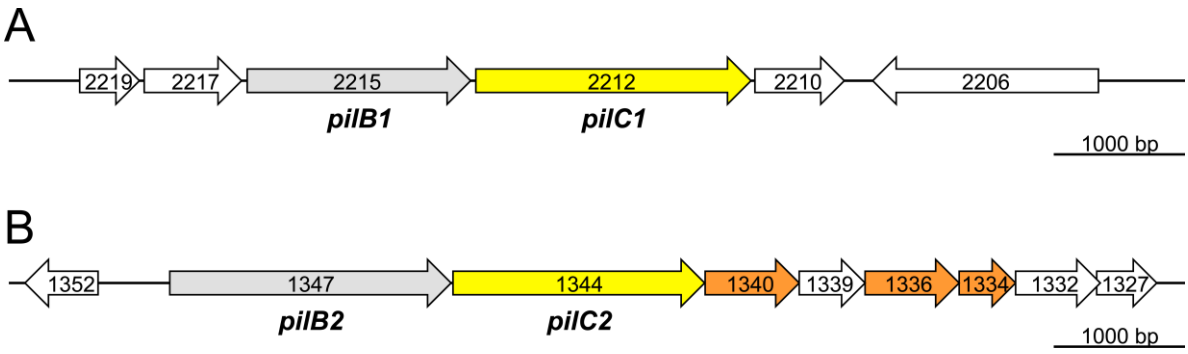

Figure 16 Genomic regions of the pil-1 and pil-2 loci. **A**, pil-1 locus with genes encoding a putative type IV pili assembly ATPase (*pilB1*) and putative transmembrane protein (*pilC1*). **B**, pil-2 locus comprising genes coding for a putative type IV pili assembly ATPase (*pilB2*) and putative transmembrane protein (*pilC2*). Putative prepilin encoding ORFs (OE1340R, OE1336R and OE1334R) are shown in orange. Color code corresponding to the type IV-like pilus assembly model in **Figure 5**, p. 9. (Modified from Losensky *et al.*, 2014)

4.2.2. Analysis of cotranscription of the putative type IV pili systems in *Hbt. salinarum* R1

The identification of the two novel type IV pili-like systems raised the question whether these genes were transcriptionally active and if the respective genes were cotranscribed. Since some of the neighboring ORFs were located on the same chromosomal strand, their cotranscription appeared to be possible.

Transcription of the pil-1 and pil-2 loci was investigated by reverse transcription PCR (RT-PCR). Total RNA was extracted from planktonic *Hbt. salinarum* R1 cells and genomic DNA contamination was hydrolyzed by extensive DNase I treatment of the RNA samples. The treated RNA was transcribed into cDNA that was used as a template in PCR reactions employing primers for amplification of specific target genes from both *pil* loci. To check for genomic DNA contamination, similar RNA samples were used as template and should not result in amplification products. To check for correct product formation on cDNA template, genomic DNA was used as a template. The cotranscription of neighboring genes was investigated using primers amplifying overlapping regions between two adjacent genes. Amplification products are observed only when cotranscription occurred.

With regard to pil-1, cotranscription of the three genes *pilB1* through OE2210R was detected, suggesting a 4.4 kb cotranscript (see Figure 17A). In some experimental repetitions an overlapping fragment of OE2217R and *pilB* was obtained, as well. To test whether this was due to incomplete transcription termination of OE2217R, the transcription start of *pilB* was determined by ARF-TSS (adaptor- and radioactivity-free determination of transcriptional start sites; see 2.4.15). The sequence analyses of four PCR-products identified the guanine at position +4 nt downstream of the annotated ATG translation start codon as the start site of the *pilB1*-containing transcript (Figure 17B). A GTG motif, which might serve as an alternative translational start codon is located at position +76 nt, suggesting the presence of a 5′-

untranslated region (5′-UTR) in the *pilB1*-mRNA. This would also implicate that the OE2217R/OE2215R fragment previously observed in RT-PCR resulted from incomplete transcription termination of OE2217R.

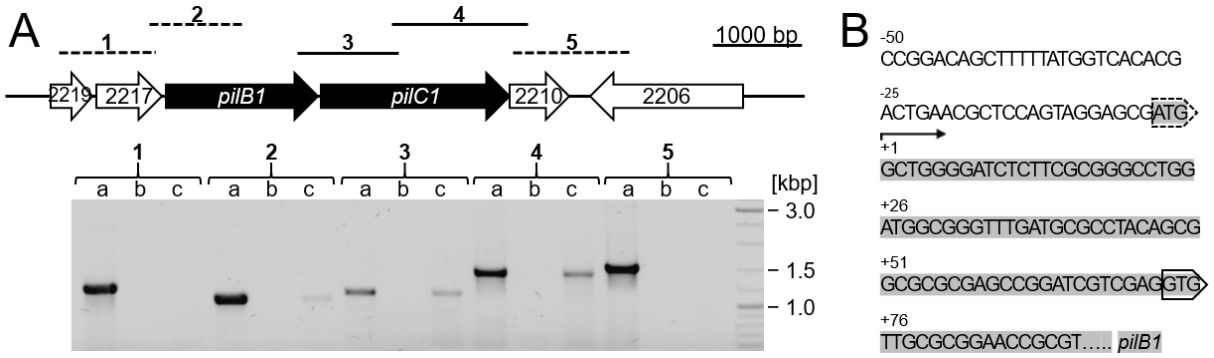

Figure 17 Transcription analysis of the pil-1 locus. **A**, *Top:* pil-1 locus with genes encoding the putative type IV pili assembly ATPase (*pilB1*) and transmembrane protein (*pilC1*) marked in black. *Bottom:* RT-PCR to determine a putative cotranscription using oligonucleotides amplifying fragments across the intergenic regions (brackets numbered 1 to 5 above the gel correspond to fragments 1 through 5 in the gene map; dashed lines, no cotranscription detected; full lines, cotranscription detected). For each pair of adjacent genes the three lanes in the gel represent: (a) PCR product using *Hbt. salinarum* R1 genomic DNA as template to validate the amplicon size and oligonucleotide specificity; (b) PCR product with RNA of planktonic *Hbt. salinarum* R1 cells without reverse transcription; (c) RT-PCR product. **B**, Upstream and 5' nucleotide sequence of *pilB1* (OE2215R, shown in grey). The AUG translation start codon annotated for OE2215R is marked by a dashed box. The transcription start site determined by ARF-TSS is labeled +1. The alternative GUG translation start codon is boxed. (Modified from Losensky *et al.*, 2014)

Regarding pil-2, a cotranscription including ORFs located upstream of *pilB2* was not detectable (Figure 18). The results of the RT-PCR experiments suggested that *pilB2* and *pilC2* as well as several ORFs downstream of *pilC2* were cotranscribed. The cotranscript consisted of the seven genes *pilB2* through OE1332R, including three putative prepilin encoding ORFs (OE1340R, OE1336R and OE1334R; see also section 4.2.5). A cotranscript spanning the seven ORFs is 6.9 kb in size.

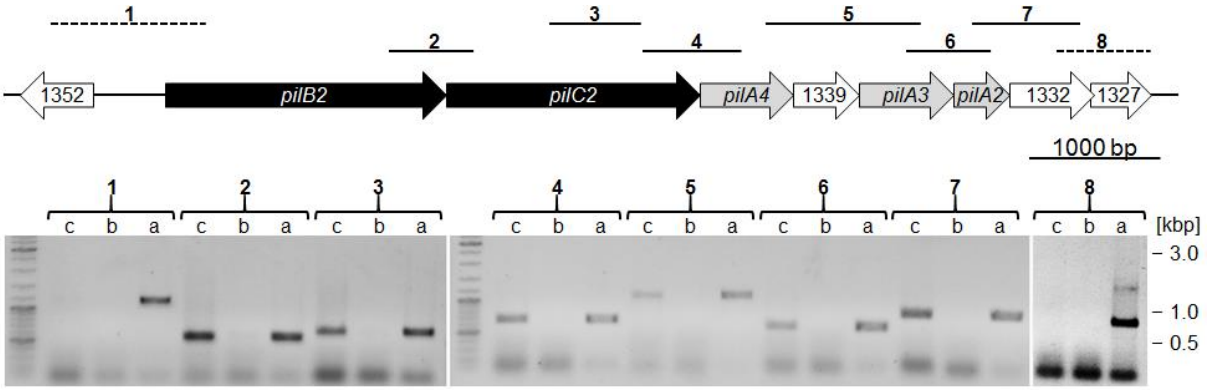

Figure 18 Transcription analysis of the pil-2 locus. *Top:* pil-2 locus with genes encoding the putative type IV pili assembly ATPase (*pilB2*) and transmembrane protein (*pilC2*) marked in black. Putative prepilin encoding genes shown in grey. *Bottom:* RT-PCR experiment investigating cotranscription of the pil-2 genes similar to pil-1 in **Figure 17**. Brackets numbered 1 to 8 in the gel correspond to fragments 1 to 8 in the gene map (dashed lines, no cotranscription; full lines, cotranscription). For each adjacent gene pair the three lanes represent: (a) PCR product using genomic DNA as template; (b) PCR product obtained from RNA without reverse transcription; (c) RT-PCR product. (Modified from Losensky *et al.*, 2014)

4.2.3. Relative quantification of the *pilB1* and *pilB2* transcription in adherent cells

To investigate a possible involvement of the *Halobacterium salinarum* R1 type IV pili systems in adhesion, the relative transcription of the respective ATPase encoding genes, *i.e. pilB1*, *pilB2* as well as *flaI*, was investigated in adherent and planktonic cells by quantitative reverse transcription PCR (qRT-PCR). Total RNA was extracted from planktonic cells from the exponential growth phase and adherent cells after 6 days of growth. Purified RNA was transcribed into cDNA and used as template for qRT-PCR. Specificity of the product formation was verified by PAA-gel electrophoresis for short DNA-fragments (Figure 19A and B) and by melting profile analysis (Figure 19C), expecting one defined product band, respectively, one distinct melting peak. In the relative quantification by qRT-PCR, the housekeeping gene *rpoB1* was used for normalization of the data (Bleiholder *et al.*, 2012), applying the $\Delta\Delta C_T$ method (Figure 19D).

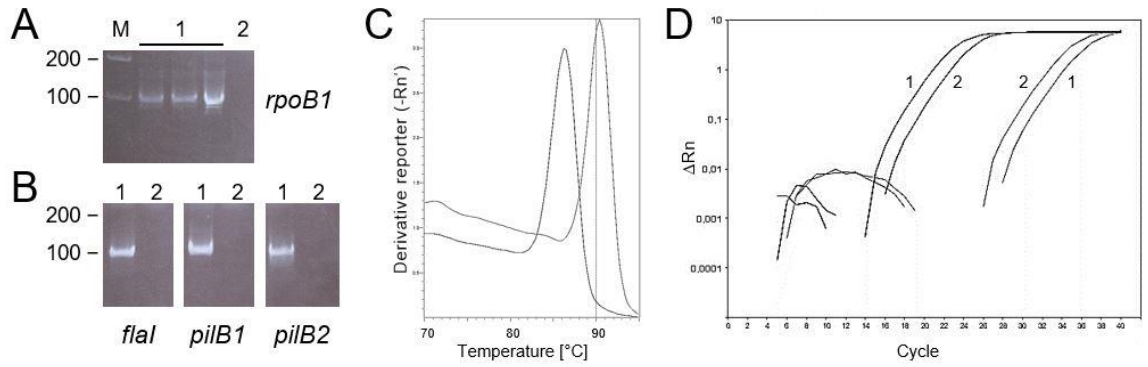

Figure 19 Quantitative RT-PCR analysis of the *Hbt. salinarum* R1 genes coding for the archaella motor/assembly ATPase (*flaI*) and the putative type IV pili assembly ATPases (*pilB1* and *pilB2*). **A**, Analytical PAA gel for short DNA fragments. Lane M: DNA marker 200 bp and 100 bp fragments. Lane 1: Triplicate of qRT-PCR products by use of *rpoB1* specific oligonucleotides in combination with cDNA generated from *Hbt. salinarum* R1 cells producing 97 bp fragments. Lane 2: qRT-PCR product using similar RNA samples as used in (1) for cDNA generation but without reverse transcription, to check for genomic DNA contamination. **B**, Analytical PAA gels, showing qRT-PCR products produced by use of *flaI* (105 bp fragment), *pilB1* (110 bp fragment) and *pilB2* (107 bp fragment) specific oligonucleotides in combination with cDNA (lane 1) and analogous RNA without reverse transcription (lane 2). One distinct DNA-fragment is observed in each case. **C**, Melting profiles of two exemplary qRT-PCR products amplified by use of *rpoB1* (black) and *pilB2* (dark grey) specific oligonucleotides, showing product specificity. Both profiles display one defined melting peak. Plot shows fluorescence intensity change dependent on the temperature. **D**, Exemplary amplification plots from a qRT-PCR experiment for relative quantification of *pilB2* (dark grey curves) by use of the housekeeping gene *rpoB1* (black curves) for data normalization. Amplification plots resulting from qRT-PCR using cDNA generated from planktonic cells (1), respectively, sessile cells (2) RNA samples in combination with the respective oligonucleotides are shown. Single example amplification curves for each cDNA and oligonucleotide combination are depicted. Plot shows fluorescence increase of the reporter SYBR® Green I dependent on the PCR cycle.

All three ATPase genes exhibited higher expression in adherent cells compared to the planktonic state (Figure 20A). Interestingly, *pilB1* and *pilB2* expression in adherent cells was stronger induced compared to the change observed for the archaellum ATPase encoding *flaI*, which exhibited a similar transcriptional change as the ferredoxin encoding housekeeping gene *fdx*.

Although relative expression change of *pilB2* appeared the strongest, its transcription was difficult to detect and obviously weaker compared to the expression of *pilB1*. This was inferred from the cycle of threshold (C_T) values of both genes (C_T = 21 for *pilB1* and C_T = 31 for *pilB2*) (Figure 20B). Even though no absolute quantification of transcript amounts was performed, the C_T values of both genes differed by ten cycles and therefore clearly indicated higher expression of *pilB1*, while *pilB2* was expressed only weakly.

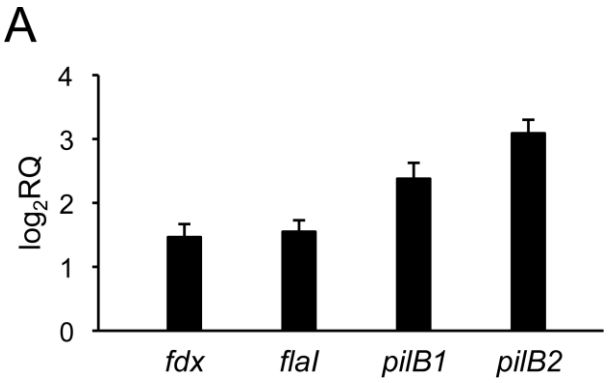

B

Target gene	Threshold cycle C_T
fdx	20
flaI	20
pilB1	21
pilB2	31

Figure 20 Transcription analysis of the *Hbt. salinarum* R1 type IV pili system assembly ATPase encoding genes. **A**, Relative transcriptional quantification of the assembly ATPase encoding genes of the archaellum (*flaI*) and the putative type IV pilus biogenesis systems pil-1 (*pilB1*) and pil-2 (*pilB2*) as well as the constitutively expressed ferredoxin gene (*fdx*). The bars represent the fold change of gene expression shown in base 2 logarithmic scale in adherent cells compared to the planktonic state, which is defined by the baseline. **B**, Average C_T values of the taget genes *fdx*, *flaI*, *pilB1* and *pilB2* detected in adherent cells.

In summary, cotranscription of the genes *pilB1* and *pilB2* with downstream genes from the pil-1 and pil-2 *loci*, respectively, was demonstrated. The transcription patterns of both genes, *i.e.* higher expression in adherent cells of *Hbt. salinarum* R1, prompted a role in the adhesion.

4.2.4. Characterization of type IV pili gene deletion mutants

Gene deletion mutants were characterized to test the involvement of the various *Halobacterium salinarum* R1 type IV pili systems (T4P) in adhesion. These mutants lacked *flaI* or *flaI* together with *pilB1*, respectively, a combination of the three genes *flaI*, *pilB1* and *pilB2*. The gene deletion mutants were provided by Lucia Vidakovic (Master thesis L. Vidakovic, 2014). These mutants were generated using a pop-in/pop-out strategy, as described previously (Koch & Oesterhelt, 2005).

Validation of the gene deletion mutants was carried out by PCR employing oligonucleotides flanking the genomic sites of the genes which were intended for deletion, *i.e. flaI*, *pilB1* and *pilB2*. Mutants with a successful deletion yielded a shorter PCR product by about the length of the target gene, in contrast to the *Hbt. salinarum* R1 parental strain. Successful deletions of the archaella ATPase gene (Δ*flaI*), the archaella ATPase plus the presumed pil-1 ATPase encoding

genes (Δ*flaI*/Δ*pilB1*) as well as a combination of all three *Halobacterium* T4P ATPase genes (Δ*flaI*/Δ*pilB1*/Δ*pilB2*) were verified (Figure 21).

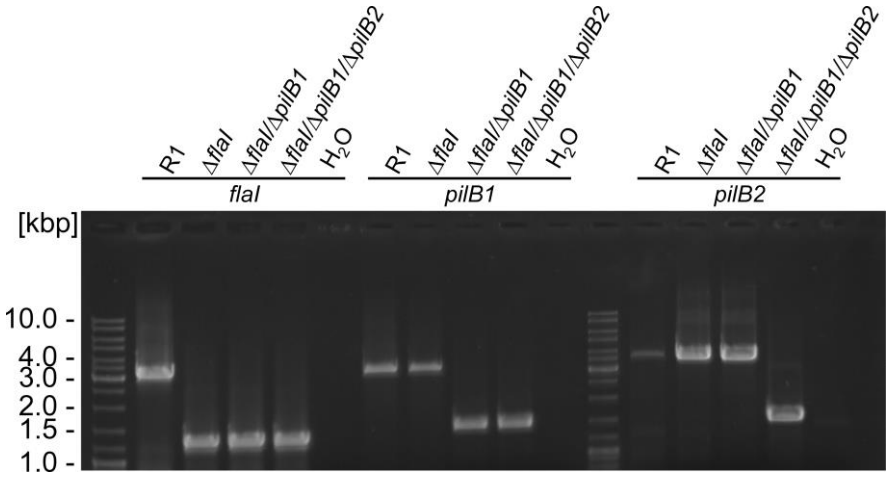

Figure 21 Verification of *Hbt. salinarum* R1 parental, Δ*flaI* single deletion, Δ*flaI*/Δ*pilB1* double deletion and Δ*flaI*/Δ*pilB1*/Δ*pilB2* triple deletion mutant strains. PCRs using genomic DNA isolated from the respective strains as template were carried out with oligonucleotides flanking the *flaI*, *pilB1* and *pilB2* genomic regions (listed in section 2.1.4). The absence of *flaI*, *pilB1* or *pilB2* genes leads to a reduced fragment size of 1.2 kbp, 1.5 kbp and 1.6 kbp respectively. Control reactions using water as template were performed.

Growth of the *Hbt. salinarum* R1 parental strain as well as the Δ*flaI*, Δ*flaI*/Δ*pilB1* and the Δ*flaI*/Δ*pilB1*/Δ*pilB2* mutant strains was compared by monitoring the increase of the optical density at a wavelength of 600 nm (OD_{600}) over a time course of about 100 h.

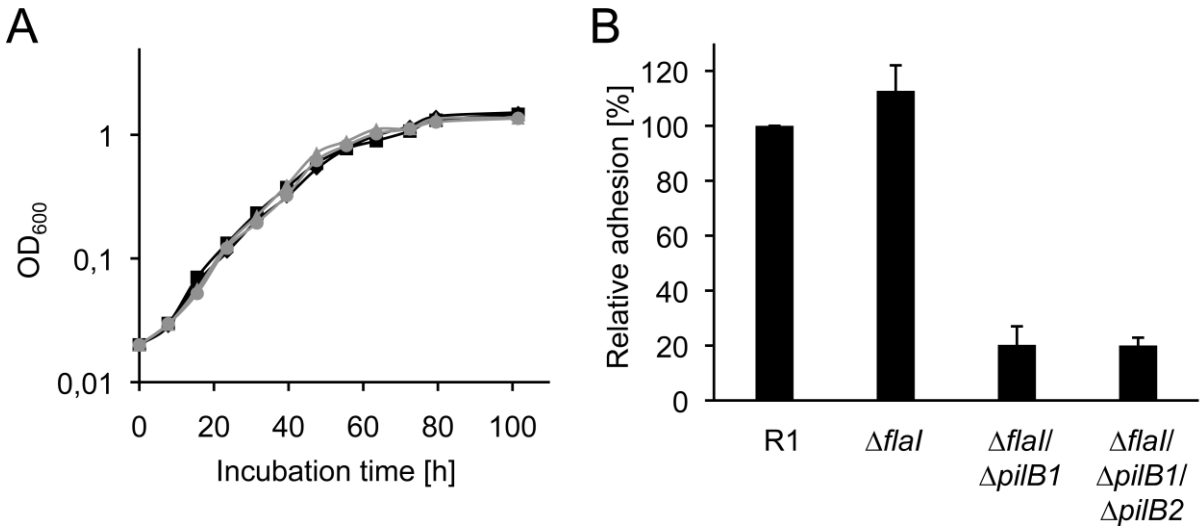

Figure 22 Growth and adhesion of the *Hbt. salinarum R1* parental strain in comparison to the gene deletion mutants. **A**, Growth of *Hbt. salinarum* R1 parental strain (black squares) and the Δ*flaI* (black diamonds), Δ*flaI*/Δ*pilB1* (grey triangles) and the Δ*flaI*/Δ*pilB1*/Δ*pilB2* (grey dots) mutants. Diagram shows semilogarithmic plot of the optical density at 600 nm (OD_{600}) as a function of incubation time in hours. **B**, Fluorescence-based adhesion assay of the *Hbt. salinarum* R1 parental strain and Δ*flaI*, Δ*flaI*/Δ*pilB1* and the Δ*flaI*/Δ*pilB1*/Δ*pilB2* mutants. Relative adhesion of the mutant strains in relation to the parental strain after 15 days of growth is illustrated.

The resulting growth curves did not show notable differences (Figure 22A). All four strains entered a logarithmic growth phase after 16 h, which lasted until the 48 h point of time, when the curves start flattening. A plateau was reached after 80 h of incubation, with no noteable further increase of OD_{600}. The final optical density was similar in all four strains. From these results no negative impacts on growth of the cells appeared as consequence of the mutations. Nevertheless, differing adhesion properties to plastic surfaces were observed with the four strains, in a fluorescence-based adhesion assay (Figure 22B). The parental strain and the Δ*flaI* mutant exhibited strong adhesion, whereas the double and triple gene deletion mutants both displayed relative adhesion signals of only 20% in comparison to the parental strain (Master thesis L. Vidakovic, 2014).

Differences with regard to motility were observed in swimming motility assays of the four strains, using semi-solid agar plates, which were inoculated in the centre with a droplet of cell suspension of the different strains. While the parental strain displayed motility and a swarming radius of about 2.5-3.0 cm after three days of static incubation, all three deletion mutant strains did not spread on the surface of the semi-solid agar plates (Figure 23A). Planktonic cells of all four strains had a regular rod-shaped cell morphology, as observed by light microscopy (Figure 23B). Only the parental strain was motile and freely swimming, whereas no motility was observed for planktonic cells of any of the three gene deletion strains.

Adhesion of the cells to glass coverslips and biofilm formation on plastic surfaces was investigated by phase contrast microscopy (PCM) and confocal laser scanning microscopy (CLSM). Extensive adhesion was only observed in the case of the *Hbt. sainarum* R1 parental and the Δ*flaI* strain (Figure 23C). In contrast, only few attached cells and cell accumulations were visible with the double and triple gene deletion strains. The parental and Δ*flaI* strains both formed biofilms on plastic surfaces, although there existed apparently differences regarding the biofilm architecture (Figure 23D). The biofilms formed by the Δ*flaI* mutant appeared flat and dense, showing less microcolonies or tower-like structures. After 15d of incubation dense adherence of the Δ*flaI* cells over the surface was observed including the formation of 15 to 20 μm thick biofilms, whereas the other two mutant strains adhered only weakly to the plastic surface.

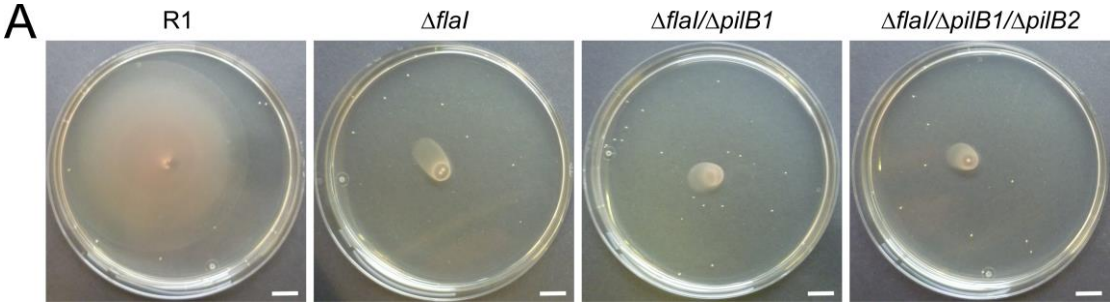

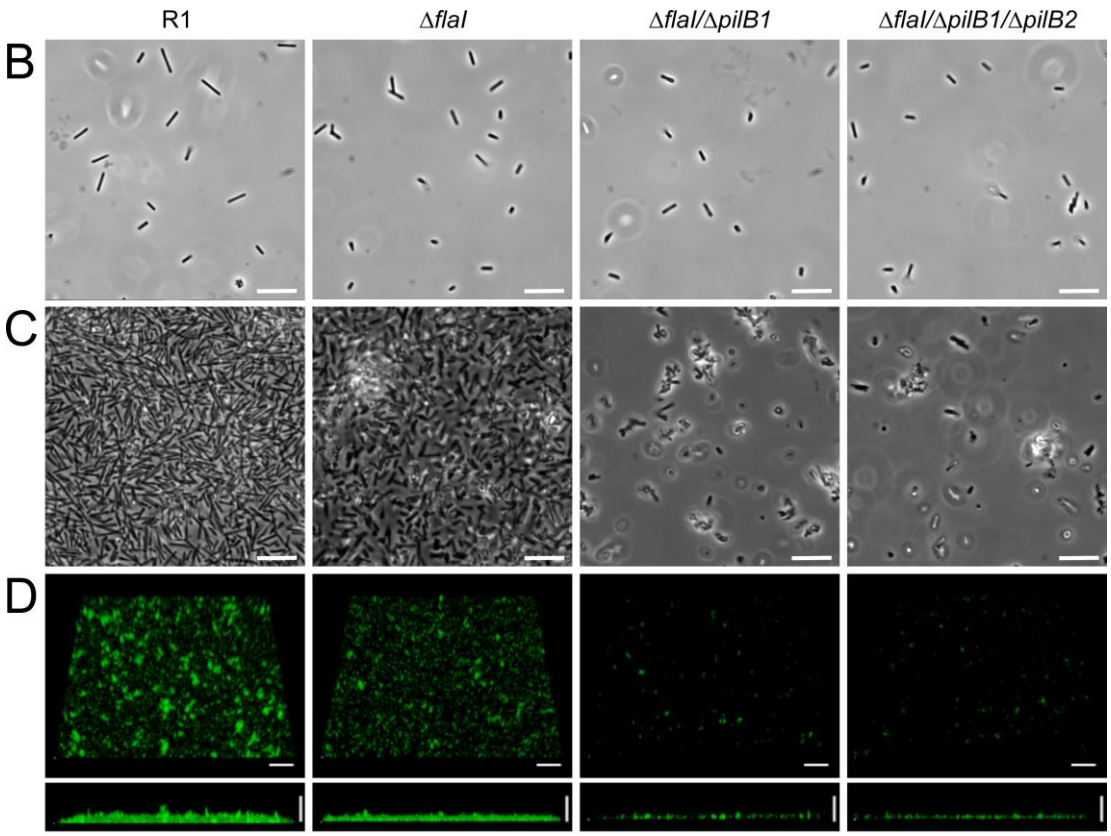

Figure 23 Characterization of the *Hbt. salinarum* R1 parental strain in comparison to the gene deletion mutants. **A**, Swimming assay of *Hbt. salinarum* R1 parental strain (R1) and the Δ*flaI*, Δ*flaI*/Δ*pilB1* and the Δ*flaI*/Δ*pilB1*/Δ*pilB2* mutants on semi solid agar plates. Scale bars: 1 cm. **B**, Corresponding phase contrast micrographs depicting planktonic cells of the four strains. **C**, Phase contrast micrographs of cells adhering to glass coverslips after 15 d of growth. B and C: 100x magnification, scale bars 10 µm. **D**, Corresponding CLSM projections depicting biofilms formed. Cells stained with acridine orange. Tilted top views (top) and side views (bottom) of biofilms grown for 15 d. 63x magnification, scale bars 30 µm.

Table 5 Overview of the characterization of the *Hbt. salinarum* R1 parental and gene deletion strains

Strain	Motility	Adhesion	Biofilm formation	Filament types*
R1	yes	strong	yes	2
Δ*flaI*	no	strong	yes	1
Δ*flaI*/Δ*pilB1*	no	weak	no	0
Δ*flaI*/Δ*pilB1*/Δ*pilB2*	no	weak	no	n.d.

*According to TEM analyses (Master thesis L. Vidakovic, 2014); n.d. not determined

In summary, in contrast to the motile parental strain strain, all three mutants investigated were non-motile, because Δ*flaI* leads to the deletion of the archaella. Nevertheless, the Δ*flaI* strain showed adhesion comparable to the parental strain as well as biofilm formation, but with altered architectures. In comparison, the ability to adhere and to form biofilms was strongly reduced upon additional deletion of the *pilB1* gene in the Δ*flaI*/Δ*pilB1* mutant. Further deletion of *pilB2* had no additional effects on adhesion in the Δ*flaI*/Δ*pilB1*/Δ*pilB2* mutant.

4.2.5. Bioinformatical search for putative prepilin encoding genes

The identification of the *Hbt. salinarum* R1 adhesion pili raised the question what proteins are involved in the Pil-1 biogenesis. While the assembly ATPase, PilB1, and the transmembrane protein, PilC1, only represent the platform on which the type IV-like pili are assembled, at least one type of pilin monomers is necessary to complete the core components (Pohlschröder *et al.*, 2011). Inspection of the pil-1 locus demonstrated that it contains no predicted pilin encoding genes. The pilins of type IV pilus-like structures are variable depending on the organism investigated. The archaellum of *Sulfolobus acidocaldarius* consists of a single archaellin subunit (Ghosh & Albers, 2011), while its adhesion pili (Aap) are composed of at least two pilin modules (Henche *et al.*, 2012a). The halobacterial archaellum has five different archaellin subunits (Tarasov *et al.*, 2000), whereas a repertoire of six adhesion pilins is found in *Haloferax volcanii*, each of them sufficient to produce functional pili (Esquivel *et al.*, 2013). Because of this, a search for putative pilin candidates was performed, considering all protein sequences of *Hbt. salinarum* R1 available in UniProtKB (12/2014).

The proteins possessing archaeal type IV pilin-like signal peptides (Szabó *et al.*, 2007b) were predicted by use of the search tool FlaFind 1.2 (http://signalfind.org/flafind.html). The search algorithm is based on the presence of a hydrophobic segment, starting within the first 30 amino acids of the protein sequence preceded by a four amino acid cleavage motif containing a positively charged residue at the first position. This sequence represents the prepilin peptidase cleavage site. It was reported that *Haloferax volcanii* adhesion pilins contain a highly conserved domain of unknown function (DUF) at the N-terminus (DUF1628). Several *Hbt. salinarum* R1 proteins contain DUF1628 domains (www.haloex.mpg.de).

The search for putative prepilins revealed more than 30 candidates (Table S1, p. 141). Some of these proteins were precisely annotated in the protein database, whereas others represented functional predictions. Additional BLASTp searches were performed to improve functional annotations and to examine whether any similarities to known pilin proteins from other species existed. The main fraction (22 proteins) were hypothetical proteins. Candidates with positive FlaFind results were excluded from further analysis, if annotations assigned them to other processes different from type IV-like pilus biogenesis. Furthermore, candidates were disregarded if they had a molecular mass >45 kDa, since type IV pilins are typically < 20 kDa (Giltner *et al.*, 2012).

Among the positive proteins detected with FlaFind were the six highly conserved archaellins of *Hbt. salinarum* R1 [FlgA1-A3, FlgB1-B2, FlgX (Gerl *et al.*, 1989)]. They all had identical prearchaellin peptidase cleavage motifs (Table 6, p. 55).

Most prepilin candidate genes were distributed throughout the genome. Interestingly, three genes were located in a gene cluster at the pil-2 locus, *i.e.* OE1340R, OE1336R and OE1334R

(Table 7), directly downstream of the putative T4P assembly ATPase and transmembrane protein encoding genes (also see Figure 16, p. 47). In contrast, no genes encoding putative prepilins were found within a 100-kbp range surrounding the pil-1 locus.

Table 6 Characteristics of the six *Hbt. salinarum* R1 flagellins.

Symbol	Gene number	Length [aa]	FlaFind[1]	Cleavage motif[2]	No. of TMH[2]	DUF1628[3]	Comments
flgA1	OE2469F	196	+	RGQV	1	–	
flgA2	OE2470F	194	+	RGQV	1	–	
flgB1	OE2397F	193	+	RGQV	1	–	*fla* locus
flgB2	OE2398F	196	+	RGQV	1	–	*fla* locus
flgB3	OE2399F	193	+	RGQV	1	–	*fla* locus
flgX	OE2695F	207	+	RGQV	1	–	

[1]Plus, positive FlaFind results, *i.e.* presence of type IV pilin-like signatures; hyphen, negative results.
[2]Prearchaellin peptidase cleavage motifs and numbers of TMH predicted by FlaFind 1.2.
[3]According to HaloLex (www.halolex.mpg.de); hyphen, no DUF1628.

According to the HaloLex database five DUF1628-containing proteins were present in *Hbt. salinarum* R1, encoded by the ORFs OE1186A1F, OE3768F, OE3996R, OE4050F, as well as OE6130F. Two of these were FlaFind 1.2 negative, since their N-terminal peptides deviated from the consensus, and the putative signal peptides were assigned manually. All five exhibited similarities to adhesion pilins of *Haloferax volcanii*. These results were complemented by two putative prepilins encoded by the ORFs OE2531F and OE2586F, which were relatively large compared to the other proteins, with calculated molecular masses of 37 kDa and 41 kDa.

Table 7 Characteristics of *Hbt. salinarum* R1 putative prepilins

Symbol*	Gene number	Length [aa]	FlaFind[1]	Cleavage motif[2]	No. of TMH[2]	DUF1628[3]	NetNGlyc[4]	Comments[5]
pilA1	OE1186A1F	122	+	RAVS	1	+	3	*Hfx. pilA4*
pilA2	OE1334R	122	+	RGQA	1	−	1	pil-2 locus
pilA3	OE1336R	225	+	RGQA	1	−	2	pil-2 locus
pilA4	OE1340R	240	+	RGQS	1	−	1	pil-2 locus
pilA5	OE1476R	136	+	RGLL	1	−	0	
pilA6	OE1501F	129	+	RAAT	2	−	0	
pilA7	OE2531F	326	+	RGLL	1	−	0	
pilA8	OE2586F	394	+	DAMV	1	−	6	
pilA9	OE3768F	173	+	RAAT	1	+	0	*Hfx. pilA5*
pilA10	OE3996R	153	−	(RGSA)	1	+	0	*Hfx. pilA3*
pilA11	OE4050F	125	–	(RATS)	1	+	1	*Hfx. pilA2*
pilA12	OE6130F	163	+	RGVS	1	+	2	*Hfx. pilA3*

*Gene symbols based on the ascending gene numbers of the putative pilins. [1]Plus, positive FlaFind 1.2 results, *i.e.* presence of type IV pilin-like signatures; hyphen, negative results. [2]Predicted by FlaFind 1.2, motifs in brackets assigned manually. [3]According to HaloLex (www.halolex.mpg.de); plus, DUF1628 present; hyphen, no DUF1628. [4]Number of potential N-glycosylation sites predicted by NetNGlyc 1.0 Server. [5]Based on BLASTp search against *Hbt. salinarum* R1 and *Haloferax* sp., respectively.

In summary, twelve putative pilin-like proteins were assigned in *Hbt. salinarum* R1 (Table 7). The corresponding candidate genes were denoted *pilA1* through *pilA12*, based on their

ascending gene numbers. Comparison of their N-terminal regions revealed that they contained sections ranging from 1 to 21 amino acids in front of their predicted prepilin peptidase cleavage sites (Figure 24). The cleavage motifs were followed by hydrophobic stretches dominated by aliphatic and aromatic amino acids.

```
PilA2   ---------------MPERGRRGQASLPAVEAAIGVFVILAVAATFTVGVPGDGGHTRTAQLDRYAADAATIIETTPPHG 65
PilA3   --------------------MQRGQANLVALVVGVLLVGAAVTLAVGAGADAFARADRSPAEARLAASLADRLVSPRGPLA 61
PilA1   --------MTDLSLFDTDADERAVSPVIGVILMVAITVILAAVIATAVLGFGDGNLQSNAQAGVTVEQNATDTYDVTLTK 72
PilA12  --------MKKVTLEIPDRDERGVSPVIGVILMVAITVILAAVIASFVLGFGGSVNETVQAGADVSENGDGTATVTWISE 72
PilA11  -----------MHMALAPSDERATSPATGVAVMFVLAVLIAAAVGVGAFTNNEEVTATVQVAATDGGATVLWTDQGTANY 69
PilA9   ---------------------MRAATSVTAVVLMVAVVVVLAGTVAVFTLGSTDTISSPAPLIGQTSGELVRDTAGGGDQI 60
PilA10  --------------------MPRGSAPVVAVVAVVAITVLAGAAVFAVAPSVTTPPLPQRGVSVSAAADGTVAVTLLSGPP 61
PilA4   --------------------MTRGQSAVVGVAVLVAATVVAVAALTASVGTVVTEHAAAADSRRVAADLRTALHPARTTGT 61
PilA8   ---------------MTQICDDAMVSVRLCLILALVVLGGCVFVLTDDHTGAPSSTAVAAGLNDIESVSATEVSGIRFGN 65
PilA6   ------------------MDAKRAATHSSKYFLAITTLGIVALALIGYGGVLAQPAFEHGLPSGPHLADAVPGLALAAAGV 63
PilA7   MAGNLRGWIKEHRAKIRASPLRGLLHAVFTAYLGFWYTLTSRWPFGTHVYDEDWDLLVILDACRVDVLDDVADEYAFIET 80
PilA5   -----------------MANRRGLLAGVLAFVYPGLGHIYLRAWVRAIAWFGLSMAVAALVIPDAAYQAIEARGVQGAID 63
```

Figure 24 Comparison of the N-terminal regions of the putative prepilins of *Hbt. salinarum* R1. Amino acid sequences of the putative pilins (PilA1 through A12) were aligned manually based on the positions of the predicted prepilin peptidase cleavage motifs (shown in bold). Positions with at least 60% functional conservation of the respective amino acid residues are shaded in red (basic) and grey (hydrophobic). Only parts of the corresponding protein sequences are shown, with the numbers indicating their lengths. The sequences are arranged based on the dendrogram shown in Figure 25.

A dendrogram was constructed by use of the MAFFT server, based on a multiple protein sequence alignment of the pilin candidates and the archaellins of *Hbt. salinarum* R1, as well as exemplaric adhesion pilins of *Haloferax volcanii* and the more distantly related *Sulfolobus acidocaldarius* (Figure 25). A clustering among the *Halobacterium* archaellins was observed, separated from the pilins. Some of the DUF1628-containing pilins of *Hbt. salinarum* R1 clustered the closest with the adhesion pilin of *Hfx. volcanii* (HVOA0633). However, the *Halobacterium* pilins only show a weak similarity, as becoming clear from the alignment (Figure S1, p. 142), while type IV pilins generally share little sequence similarity apart from their signal peptides (Esquivel *et al.*, 2013).

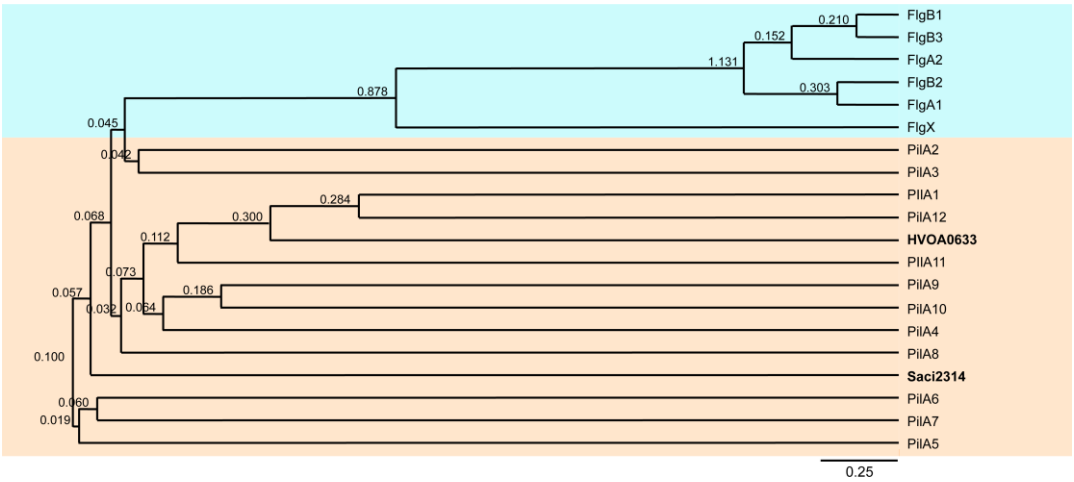

Figure 25 Dendrogram of *Hbt. salinarum* R1 archaellins (Flg, shaded light blue) and putative pilins (Pil, shaded orange) in relation to exemplaric *Haloferax volcanii* (HVOA0633) and *Sulfolobus acidocaldarius* (Saci2314) adhesion pilins (bold). [http://mafft.cbrc.jp/alignment/server; (Katoh & Standley, 2014)].

4.2.6. Transcriptional analysis of putative prepilin encoding genes

The transcriptional activity of the identified candidate genes coding for the putative prepilins was investigated by qRT-PCR. The transcription was analyzed in planktonic cells in comparison with adherent cells from different biofilm stages. In contrast to the previously performed qRT-PCR experiments, in this case, external control RNA was used for normalization as described in 2.4.16. *In vitro* transcripts of the *bgaH* gene were an appropriate external standard, since the gene is not present in the *Hbt. salinarum* R1 genome. The *bgaH* RNA was added in constant amounts to the different RNA samples under investigation prior to the cDNA synthesis.
To test whether the external RNA standard produced plausible resultes, total RNA was isolated from cells of the *Hbt. salinarum* R1 parental strain as well as the Δ*flaI* deletion mutant and treated as described before. The archaellum assembly/motor ATPase gene *flaI* as well as the putative type IV pili ATPase genes *pilB1* and *pilB2* were chosen for relative quantification. Also, transcription of the housekeeping gene *rpoB1* was examined. The Δ*flaI* mutant showed strongly reduced expression of *flaI* compared to the parental strain (Figure 26). In contrast, the transcription of *pilB1*, *pilB2* and *rpoB1* was not or only marginally changed in the mutant strain. This was in accordance with the expectation that only *flaI* should be affected in the corresponding gene deletion mutant strain (Δ*flaI*), representing a proof of principle with respect to the qRT-PCR quantitation method established.

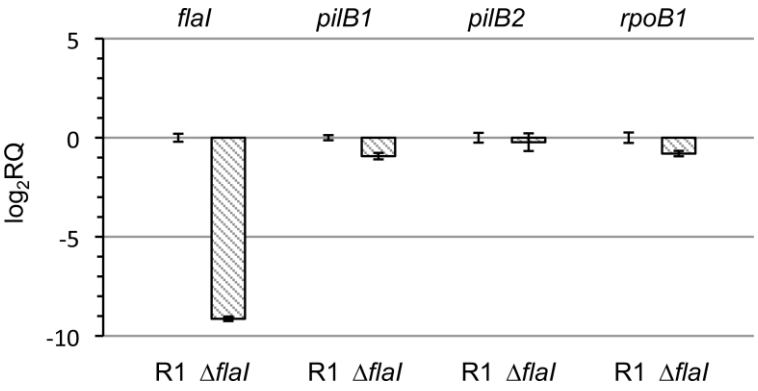

Figure 26 Relative transcriptional quantification (RQ) of the assembly ATPase encoding genes of the archaellum (*flaI*) and the putative type IV pilus biogenesis systems pil-1 (*pilB1*) and pil-2 (*pilB2*) as well as the RNA polymerase subunit B' (*rpoB1*). Bars represent the fold change (base 2 logarithmic scale) of transcript levels in the *Hbt. salinarum* R1 Δ*flaI* strain in comparison to the parental strain (baseline).

Total RNA was isolated from different planktonic and adherent cell samples for transcriptional quantification of several archaellin genes as well as the putative prepilin genes. Planktonic cells were harvested during the early and late exponential as well as the stationary growth phase (OD_{600} 0.15, 0.4 and 0.8). Adherent cells were harvested after one, six and fifteen days of growth (initial, mid and mature biofilm stages). RNA treatment, cDNA preparation and the quantitation procedure were performed as described earlier.

The two archaellin genes *flgA1* and *flgB1* are encoded by the archaellin loci A and B, respectively, at different genomic sites (Gerl & Sumper, 1988). Both genes showed similar transcription profiles in almost all planktonic and biofilm samples investigated (Figure 27A). Their transcription was not altered markedly in the planktonic samples, but a slight decrease was observed in the early biofilms, followed by stronger down-regulation during the mid and mature biofilm stages. Moreover, quantitation of the sixth archaellin gene (*flgX*) was intended, which is encoded at another genomic locus (Beznosov *et al.*, 2007). No qRT-PCR quantification of *flgX* was achieved, because no specific amplification products were obtained using either of the cDNA samples as templates. RT-PCR did not yield amplification of the desired 116 bp fragment of *flgX*, as well, whereas the use of genomic DNA as template resulted in amplification of the fragment (Figure 27B), suggesting that transcription of *flgX* did not occur. In contrast, fragments of the two putative pilin genes *pilA7* and *pilA8* were amplified using cDNA as well as genomic DNA templates (Figure 27B), indicating transcription of the genes.

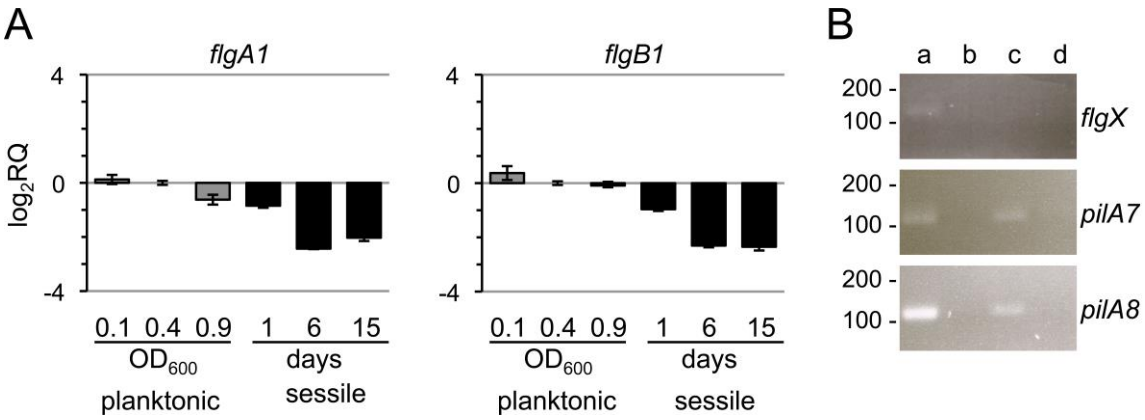

Figure 27 Transcription analyses of *Hbt. salinarum* R1 archaellin encoding genes. **A**, Relative quantification (RQ) of the transcription of the genes *flgA1* and *flgA2*. Grey bars represent from left to right three different planktonic samples, *i.e.* cells from the early exponential (OD_{600} 0.15), late exponential (OD_{600} 0.4) and stationary (OD_{600} 0.9) growth phase. Black bars constitute from left to right three different sessile samples harvested after different incubation times, *i.e.* biofilm cells grown for 1 day (1 d), 6 days (6 d) and 15 days (15 d). Bars indicate fold change (base 2 logarithmic scale) of the respective gene transcription compared to the transcription in the OD_{600} 0.4 sample (baseline). **B**, RT-PCR amplification of fragments of putative archaellin and pilin encoding genes. 116 bp, 113 bp and 104 bp PCR products obtained by use of *flgX*-, *pilA7*- and *pilA8*-specific oligonuleotides, respectively, combined with gDNA (a), H_2O (b), 1 d sessile cDNA (c) and RNA withouth reverse transcription (d) templates.

Similar transcription quantitation experiments were performed with regard to the putative prepilin genes spread all over the genome. The mRNA species successfully quantitated showed various expression profiles (Figure 28). The *pilA2* and *pilA3* transcriptions were very similar to the archaellin genes, with weak changes regarding the planktonic samples, but distinct down-regulation in the biofilm samples. Furthermore, *pilA1*, *pilA8*, *pilA9* and *pilA11* transcriptions were slightly down-regulated in the stationary growth phase, whereas their expression was only marginally changed in the initial biofilm samples and again weakly decreased in the mid and mature biofilms. In contrast, *pilA12* expression was virtually constant in all samples under

investigation. Detection of *pilA4* transcripts failed and the results obtained for *pilA10* did not allow an accurate quantitation, although in both cases different oligonucleotide pairs were tested in the qRT-PCR amplification.

Distinct patterns were observed with respect to the expression profiles of the three genes *pilA5*, *pilA6* and *pilA7*, which displayed inductions in the early exponential growth phase and reductions in the stationary phase of growth. Interestingly these three genes showed a clear transcriptional up-regulation in the initial biofilm stage, with *pilA7* displaying the strongest 7.1-fold induction, while *pilA5* and *pilA6* were 3.4- and 2.5-fold higher expressed in comparison to planktonic cells derived from the exponential growth phase. Transcription of *pilA6* was still slightly induced in the mid and mature biofilm stage, while the amount of transcripts derived from *pilA5* and *pilA7* did not change notably.

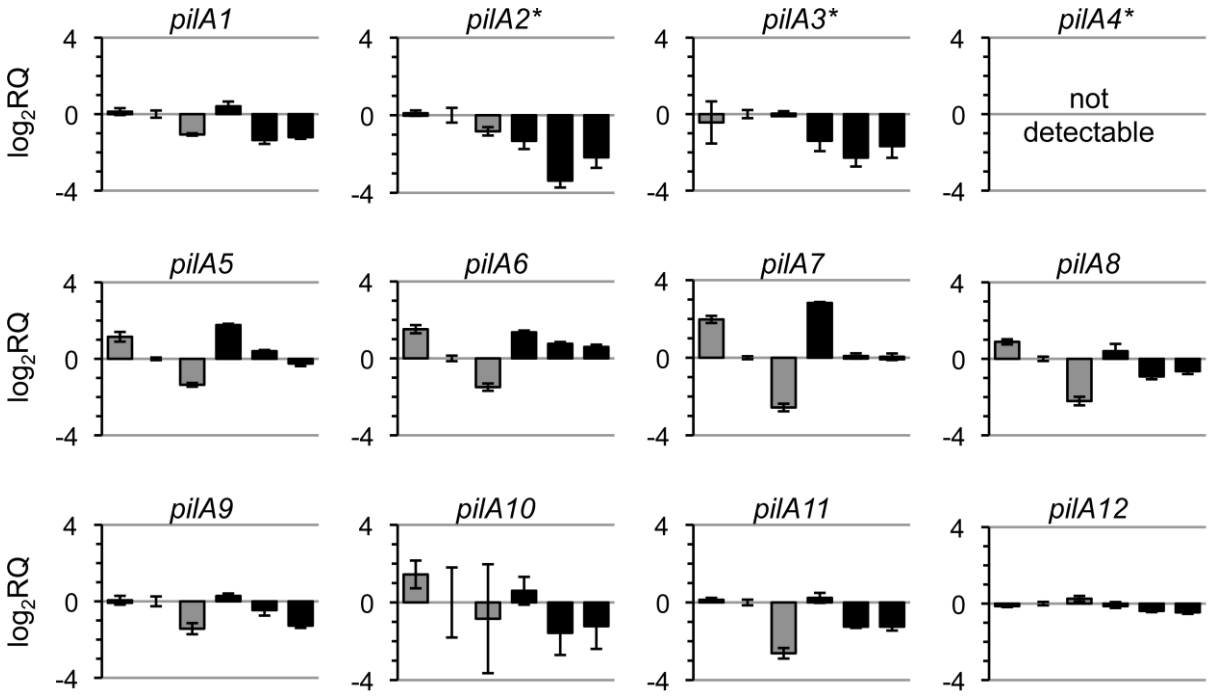

Figure 28 Putative prepilin genes transcription profiles. Relative quantification (RQ) of the transcription of the putative prepilin encoding genes *pilA1* through *pilA12* (asterisks mark genes located at the pil-2 locus). Grey bars represent from left to right three different planktonic samples, *i.e.* cells from the early exponential (OD_{600} 0.15), late exponential (OD_{600} 0.4) and stationary (OD_{600} 0.9) growth phase. Black bars constitute from left to right three different sessile samples harvested after 1 day, 6 days and 15 days. Bars indicate fold change (base 2 logarithmic scale) of the respective gene transcription compared to the transcription in the OD_{600} 0.4 sample (baseline).

In summary, the qRT-PCR quantification of the transcription of two archaellin and twelve putative prepilin encoding genes was perfomed. A virtually constant expression of the archaellin genes (*flgA1* and *flgB1*) in planktonic cells from different growth phases, but strong down-regulation of their transcription in biofilms was observed. In contrast, the putative prepilin encoding genes showed varying expression patterns, with the three genes *pilA5*, *pilA6* and *pilA7* displaying up-regulated expression, especially with regard to the initial biofilm stage.

4.2.7. Genotyping of different *Hbt.* strains with respect to putative type IV pili genes

Previous studies of several halobacterial strains had shown differences in their abilities to adhere to surfaces (Fröls *et al.*, 2012). Among the strains investigated were the type strain DSM3754^{T}, the three closely related wild type strains R1, NRC-1, PHH1 and the PHH1 derivative PHH4, as well as the two natural isolates strains SB3 and GN101. All strains share 16S rRNA sequence identities of 98 to 99% to *Hbt. salinarum* R1, but possess distinct plasmid populations different from the three wild type strains (Ebert *et al.*, 1984). *Hbt. salinarum* R1 and DSM 3754^{T} show strong, *Hbt. salinarum* PHH4 and SB3 moderate adhesion to plastic surfaces, whereas no significant adhesion is observed for *Hbt. salinarum* NRC-1, PHH1, and GN101 (Fröls *et al.*, 2012).

A genotyping analysis was applied to test for a correlation between the identified type IV pili systems pil-1 and pil-2, as well as the putative pilin genes and the adhesion capabilities of these seven halobacterial strains. Total DNA of the strains was hydrolyzed with *Aat*II and blotted as described in 2.4.11. Southern hydridizations were done using probes specific for genes of the *pil* loci as well as for genes putatively encoding pilins.

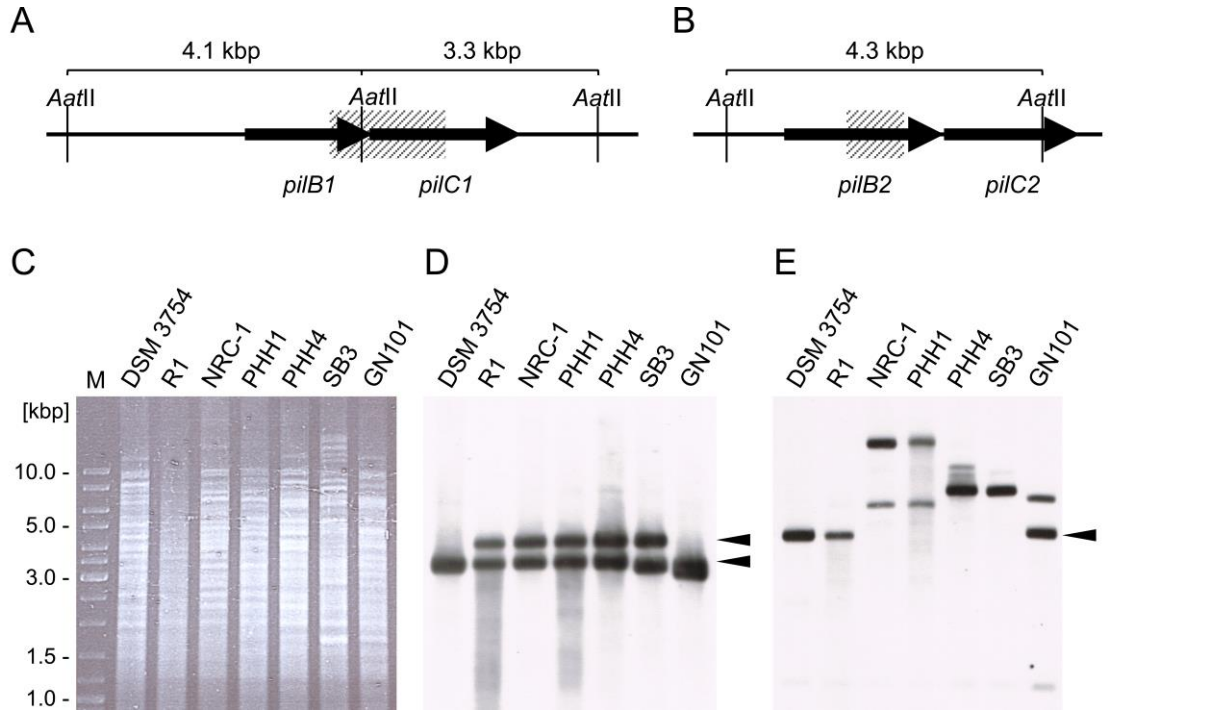

Figure 29 Southern analyses investigating the occurrence of the pil-1 and pil-2 loci in different strains of *Hbt. salinarum*. Total DNA samples were digested with *Aat*II. **A**, *Hbt. salinarum* R1 pil-1 locus with the central genes *pilB1* and *pilC1*. *Aat*II restriction sites and resulting DNA fragment sizes are indicated. Probe hybridization region is shaded. **B**, *Hbt. salinarum* R1 pil-2 locus with the central genes *pilB2* and *pilC2*, *Aat*II restriction sites and resulting DNA fragment size as well as probe hybridization region (shaded). **C**, Restriction patterns obtained after hydrolysis of genomic DNA of different *Halobacterium salinarum* strains (DSM 3754, R1, NRC-1, PHH1, PHH4, SB3 and GN101). M, DNA marker. **D**, Probe hybridization signals obtained with the DNA samples shown in C by use of a *pilB1/C1* probe. The binding region is highlighted in A. Arrow heads mark restriction fragments expected for strain *Hbt. salinarum* R1 (3.3 and 4.1 kbp). **E**, Hybridization signals detected using a *pilB2* probe binding to the region indicated in B. Arrow head marks restriction fragment expected for strain *Hbt. salinarum* R1 (4.3 kbp).

The *pilB1/C1* probe hybridized with DNA of all strains, but strain-specific variations were observed with regard to the restriction fragments detected (Figure 29D). Five of the seven strains tested (R1, NRC-1, PHH1, PHH4, and SB3) displayed probe hybridizations with two fragments of 4.1 kbp and 3.3 kbp, corresponding to the theoretical sizes calculated from the genome sequence of *Hbt. salinarum* R1 (Figure 29A). However, only one size of the hybridizing restriction fragment (3.3 kbp) was detected for *Hbt. salinarum* DSM 3754^{T} and GN101, while the thick bands might also result from two similar-sized fragments.

The *pilB2* probe yielded even more divergent patters. The probe was expected to label a single fragment of 4.3 kbp, based on the *Hbt. salinarum* R1 genetic sequence (Figure 29B). Such a fragment was detected in *Hbt. salinarum* R1, DSM 3754^{T} and GN101 (Figure 29E). In contrast, *Hbt. salinarum* strains PHH4 and SB3 contained a 7 kbp fragment, whereas regarding the strains PHH1 and NRC-1 the fragments hybridizing were larger than 10 kbp.

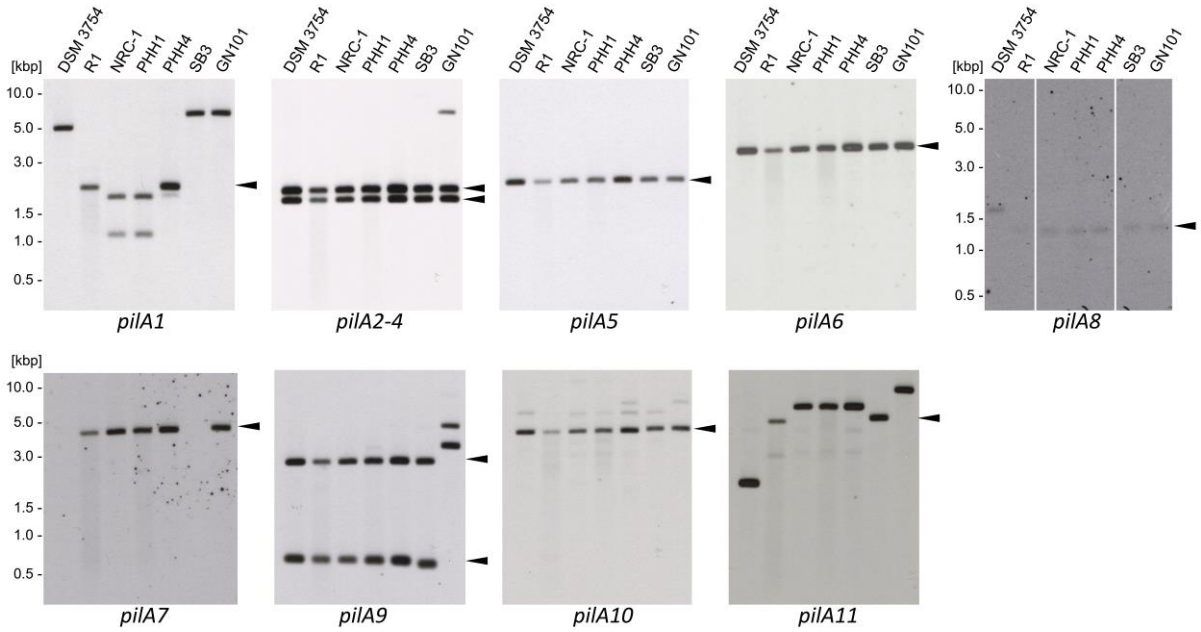

Figure 30 Southern analyses examining the presence of putative pilin encoding genes in different strains of *Hbt. salinarum* (DSM 3754, R1, NRC-1, PHH1, PHH4, SB3 and GN101). Total DNA samples were digested with *Aat*II. Pilin gene-specific probes were employed. The respective gene/s tested is/are indicated below the hybridization patterns. A simultaneous detection of *pilA2-4* was possible by use of *pilA3*-specific probes, since the three genes are part of a cluster. All probes were hybridized with the same blot after stripping, except for the *pilA8* probes hybridized with a separate blot. Arrow heads mark restriction fragments expected with respect to strain *Hbt. salinarum* R1. Fragment sizes are indicated in Table 8.

Eight out of nine pilin probes tested gave hybridization signals in all *Hbt. salinarum* strains under investigation, suggesting that the putative pilin genes are conserved, with the exception of *pilA7* (Figure 30). The *pilA7* probe did not yield signals in the strains DMS 3754^{T} and SB3, representing the best adhering and a weakly adhering strain of *Halobacterium*, respectively [Table 8; (Fröls *et al.*, 2012)], while the signals in the other stains were similar to strain R1.

Although the other probes gave rise to signals in all strains, in some cases differing restriction fragments were detected. With regard to the *pilA1* and *pilA11* probes, only one of the other strains yielded the same signal as strain R1, *i.e.* PHH4 and SB3, respectively. Both strains have weak adhesion capabilities as demonstrated previously (Fröls *et al.*, 2012). In both cases strain DSM 3754^{T}, which displays the strongest adhesion of the halobacterial strains tested (Fröls *et al.*, 2012), resulted in unique hybridization signals. A unique restriction fragment of strain DSM 3754^{T} was also detected using a *pilA8* specific probe, while the other strains gave similar signals as strain R1. With regard to the *pilA2-4*, *pilA5*, *pilA6* and *pilA10* specific probes, similar restriction fragments were observed in all strains. Regarding the *pilA9* probe, only the non-adherent strain GN101 (Fröls *et al.*, 2012) displayed a unique fragment, while the other strains appeared similar.

Table 8 Adhesion properties of different *Hbt.* strains and detection of putatively T4P associated genes

		***Hbt. salinarum* strains**						
		DSM 3754^{T}	**R1**	**NRC-1**	**PHH1**	**PHH4**	**SB3**	**GN101**
	Adhesion	**strong**	**strong**	**no**	**no**	**weak**	**weak**	**no**
Target genes	***pilB1-C1***	(+)	3.3 4.1	+	+	+	+	(+)
	pilB2	+	4.3	(+)	(+)	(+)	(+)	+
	pilA1	(+)^{U}	2.1	(+)	(+)	+	(+)	(+)
	pilA2-4	+	1.8 2.0	+	+	+	+	+
	pilA5	+	2.2	+	+	+	+	+
	pilA6	+	3.6	+	+	+	+	+
	pilA7	–	4.0	+	+	+	–	+
	pilA8	(+)^{U}	1.3	+	+	+	+	+
	pilA9	+	0.6 2.6	+	+	+	+	(+)
	pilA10	+	3.9	+	+	+	+	+
	pilA11	(+)^{U}	4.7	(+)	(+)	(+)	+	(+)

Detected fragment sizes [kbp]

*Information on adhesion properties obtained from Fröls *et al.* (2012).
+, similar restriction fragment size detected as for strain R1
(+), hybridization signal of different size compared to strain R1
^{U}, unique restriction fragment in a certain strain
–, no hybridization signal

Taken together, no direct correlation between the adhesion capabilities and the occurrence of any of the type IV pili systems in different strains of *Hbt. salinarum* was observed. Possibly, the 7 kbp pil-2 fragments of *Halobacterium* strains SB3 and PHH4 correlate with their moderate

adhesion ability, while the 10 kbp fragments of strains NRC-1 and PHH1 coincide with their inability to adhere. Regarding the putative pilin genes, differential restriction patterns were observed upon hybridization with the *pilA1*, *pilA8*, *pilA9* and *pilA11* probes, while the other probes resulted in similar signals in all strains tested. Only the *pilA7* probe did not show hybridizations in all strains.

4.3. Discussion

4.3.1. *Hbt. salinarum* R1 possesses two type IV pili systems besides the archaella operon

It was shown recently that *Hbt. salinarum* R1, like serveral other haloarchaea, is able to adhere to surfaces, but the adhesion mechanism was not known (Fröls *et al.*, 2012). There were no reports on cellular structures mediating adhesion, while the archaellum acting in motility was the only cell surface structure described (Alam & Oesterhelt, 1984). A potential role of the archaella in adhesion to surfaces was possible, while electron microscopic analyses in our lab suggested the existence of additional cellular appendages.

Searching for homologs of the archaella (*fla*) operon by bioinformatical analyses of the *Hbt. salinarum* R1 genome identified the two gene loci pil-1 and pil-2. These loci encode homologous proteins of type IV pili (T4P) system core components. In both cases a similar arrangement of a putative T4P assembly ATPase and a multispanning transmembrane protein encoding gene was found. The presence of the two *pil* systems is conserved among different *Halobacterium* species, as suggested by Southern analysis, where all seven species tested yielded pil-1 and pil-2 specific hybridization signals. Nevertheless, the restriction patterns observed also indicated genetic variability within the genus *Halobacterium*, which might explain differences in adhesion strength observed with different closely related *Hbt. salinarum* strains (Fröls *et al.*, 2012).

The occurrence of the pil-1 and pil-2 loci in other archaeal genomes was examined by bioinformatical analyses (Blastn) using the gene sequences of the pil-1 and pil-2 transcription units (4.7 kbp and 6.9 kbp, respectively). It was shown that pil-1 homologs exist in a wide array of Halobacteriaceae (Losensky *et al.*, 2014). Interestingly, its *Hfx. volcanii* D2 equivalent comprises the genes *pilB3* and *pilC3*, which are necessary for the synthesis of PilA adhesion pili (Esquivel & Pohlschröder, 2014). Moreover, pil-1 homologs are found in the genomes of methanogenic and hyperthermophilic euryarchaeota but not in the genomes of crenarchaeota or other archaeal phyla, suggesting that the system represents a general adhesion factor in euryarchaeota (Losensky *et al.*, 2014). In contrast, the occurrence of the pil-2 locus is confined to haloarchaea and it is not detected with other euryarchaeota. Low identities were found in comparison to high GC gram-positive actinobacteria, like the biofilm forming *Microbacterium xylanilyticum* (Kim *et al.*, 2005; Losensky *et al.*, 2014). It is possible that the pil-2 genes were acquired from bacteria by horizontal gene transfer (HGT). Comparative genome analyses of archaea and bacteria yielded over 2000 genes of bacterial origin in archaea and more than 1000 in haloarchaea. Most of these genes were attained from actinobacteria, which have members tolerating high salt environments (Hamedi *et al.*, 2013; Nelson-Sathi *et al.*, 2012; Nelson-Sathi *et al.*, 2015).

T4P are virtually universal in prokaryotes (Berry & Pelicic, 2015) and homologs of T4P assembly genes were identified in many archaeal genomes (Jarrell *et al.*, 2013; Szabó *et al.*, 2007b). The occurrence of multiple T4P is also the case with regard to other archaeal species. *Methanococcus maripaludis* possesses one additional kind of pili besides the archaella (Nair *et al.*, 2014). *Sulfolobus acidocaldarius* was shown to possess three kinds of type IV pilus-like appendages, the archaellum as well as adhesion pili (Aap) and UV-inducible pili (Ups) (Henche *et al.*, 2012b). The genome of *Hfx. volcanii* even encodes five putative T4P besides the archaella operon (Hartman *et al.*, 2010), while only two of these were transcriptionally active under the experimental conditions tested previously (Pohlschröder & Esquivel, 2015).

4.3.2. The pil-1 and pil-2 loci of *Hbt. salinarum* R1 are cotranscribed

RT-PCR studies suggested that the genes found in the pil-1 and pil-2 loci of *Hbt. salinarum* R1 are cotranscribed. Regarding pil-1, the cotranscript comprised the putative T4P assembly ATPase gene *pilB1*, the polytopic transmembrane protein encoding *pilB2*, as well as a third gene of unknown function, which did not show an association with T4P assembly. Extensive investigation of the genes surrounding the pil-1 locus did not yield further essential T4P components, like prepilins or prepilin peptidases. With respect to pil-2, cotranscription of seven ORFs was indicated. These comprised the assembly ATPase and transmembrane protein encoding genes *pilB2* and *pilC2*, respectively, as well as three putative prepilin encoding genes and in addition two ORFs with unknown functions. Although lacking a prepilin peptidase encoding gene, as well, pil-2 seems to be a complete T4P, with respect to the other basic components necessary (Albers & Pohlschröder, 2009).

Based on bioinformatical analyses *Hbt. salinarum* R1 possesses only one archaeal class III signal peptidase encoding gene (*flaK*), which encodes the enzyme used to process the prearchaellins. For the assembly of other type IV-like pili the enzyme has to be able to process the corresponding prepilins, as well. Promiscuitiviy of type III signal (prearchaellin/pilin) peptidases was reported for *Haloferax volcanii* (Esquivel *et al.*, 2013; Tripepi *et al.*, 2010) as well as *Sulfolobus solfataricus* (Albers *et al.*, 2003), both of which use the same enzyme (PibD) to processes their archaellins and pilins. In contrast, *Methanococcus voltae* possesses two distinct type III signal (type IV archaellin/pilin-like) peptidases. Prearchaellins are processed by the specific peptidase FlaK, while a second type IV prepilin-like peptidase, EppA, is present and specifically processes type IV prepilins (Szabó *et al.*, 2007b).

A cotransription of the *Hbt. salinarum* R1 pil-1 and pil-2 loci is similar to the transcription of the *fla* locus of the organism (Patenge *et al.*, 2001). In *Hbt. salinarum* one polycistronic mRNA is synthesized, comprising the essential *fla* genes for archaella assembly and function

(*flaDEFGHIJ*) (Patenge *et al.*, 2001). In addition, the archaellin genes from the A and B loci (*flgA1-2* and *flgB1-3*) are also transcribed into polycistronic messages. Archaella are generally encoded by gene clusters (*fla* operons) that are cotranscribed, as determined for all the aforementioned species (Albers & Jarrell, 2015). In contrast, the production of different transcripts was reported for the archaella operon of *S. acidocaldarius* that contains two promoters, with one promoter located upstream of the single archaellin subunit encoding gene (*flgB*) and a second promoter located within the *flaB* sequence regulating the downstream genes (Lassak *et al.*, 2012b). The organization of the *Halobacterium* pil-1 is similar to the situation described for the *Methanococcus maripaludis* adhesion pili system, since the additional components, *i.e.* putative pilin genes and peptidase, are spread around the genome (Nair *et al.*, 2014). In contrast, the large cotranscript formed by the *Halobacterium* pil-2 resembles the transcription of archaeal *fla* operons or the diverse T4P systems (adhesion pili, UV-inducible pili, and bindosome) of *Sulfolobus* (Henche *et al.*, 2012a; van Wolferen *et al.*, 2013; Zolghadr *et al.*, 2007).

A clustering and transcription of polycistronic mRNAs makes sense with respect to regulation, since it facilitates simultaneous induction or repression of all genes necessary to form a pilus. On the other hand it is reasonable to assume that the filament subunits are needed in larger quantities to form the macromolecular pilus structures, which can reach lengths of several microns, corresponding to thousands of subunits (Giltner *et al.*, 2012). From this point of view, distinct regulation mechanisms for the respective archaellin or pilin encoding genes appears advantageous. This may also explain, why no pilin genes were found located at the *Hbt. salinarum* R1 pil-1 locus and why the putative candidates are distributed throughout the genome.

4.3.3. T4P-like ATPase genes of *Hbt. salinarum* R1 show differential expression

In the qRT-PCR analysis both newly identified T4P-like ATPase genes of *Hbt. salinarum* R1 (*pilB1* and *pilB2*) showed stronger induction in adherent cells versus planktonic cells compared to the archaella ATPase gene *flaI*. This suggests a role for pil-1 and pil-2 in adhesion of the organism and a potential adhesion-dependent up-regulation of the genes by an unknown mechanism. In contrast, the archaellum, whose major function is motility, might be of minor importance when the cells adhere to surfaces and switch to a sessile lifestyle. Differential expression of various T4P systems was also observed with other archaeal species under certain conditions, although examples are sparse and little is known about the underlying regulational processes.

Increased archaella synthesis was observed with the hydrogenotrophic species *Methanocaldococcus janaschii* under hydrogen limitation conditions (Mukhopadhyay *et al.*, 2000). In contrast transcription of the archaella genes of *Methanococcus maripaludis* was reduced in consequence of specific nutrient limitations (Hendrickson *et al.*, 2008). While the first example was interpreted as an escape reaction of the cells, the latter might save resources under starvation conditions (Lassak *et al.*, 2012a).

Induction of the archaella operon was also observed during tryptone starvation of *Sulfolobus acidocaldarius*. Morover, it was shown that the core genes for assembly of the *S. acidocaldarius* archaellum are constitutively expressed, while transcription of the gene encoding the single filament subunit (*flaB*) is strongly induced in consequence of starvation. This is possible by two distinct promoters, which allow for a specific transcriptional regulation (Lassak *et al.*, 2012b). Transcription is controlled by the archaellum regulation network [Arn, (Reimann *et al.*, 2012)]. In addition, the protein Saci0446 was found to bind to the promoters of *flaB* and the adhesive pili gene *aapA*, presumably activating *flaB* and repressing *aapA* (Orell *et al.*, 2013b). This suggests a complex regulatory network of archaellation and piliation in *S. acidocaldarius*. If this also holds true for other archaeal species remains to be seen as more T4P and associated factors are identified (Chimileski & Papke, 2015).

4.3.4. Adhesive pili in *Hbt. salinarum* R1 are dependent on *pilB1*

Deletion of the *Hbt. salinarum* R1 archaella ATPase gene (*flaI*) led to non-motile cells, lacking the 10 nm thick surface structures, *i.e.* archaella. This was in agreement with a mutational analysis of the *fla* operon of the closely related strain *Hbt. salinarum* S9, which showed the same effects upon Δ*flaI* (Patenge *et al.*, 2001). Nevertheless, the Δ*flaI* mutant showed adhesion comparable to the parental strain, implying that the archaella are not the major determinant for cell adhesion. Moreover, strain R1 still showed the thinner 7.6 nm filaments, which was in contrast to the findings of Patenge *et al.* (2001) who had observed no filaments at all with the Δ*flaI* mutant. Though, observation of the 7.6 nm filaments in the present study might have been favored due to the investigation of adherent cells. The 7.6 nm filaments observed here are presumably identical to the so-called X-filaments observed by Beznosov *et al.* (2007). However, the Δ*flaI* mutant phenotype contradicts their hypothesis that the thinner filaments were abnormal versions of the archaella, since the archaella assembly apparatus of the mutant is inactivated. In addition, no *flgX* transcripts were detected in the present study by RT-PCR.

Additional deletion of the assembly ATPase gene *pilB1* of strain R1 resulted in a complete absence of cell surface structures, as observed by transmission electron microscopy (Master thesis L.Vidakovic, 2014). This was accompanied by a defect in adhesion of the cells, only

amounting to 20% of the parental strain. It was concluded that *pilB1* is crucial for the formation of the 7.6 nm filaments, which mediate adhesion of the cells. This suggests that pil-1 encodes core components of archaeal type IV pili that facilitate adhesion of *Hbt. salinarum* R1.

Although no appendages are observed with the Δ*flaI*/Δ*pilB1* double mutant, the existence of further cell surface structures is possible, which might account for the residual adherence of the cells. Nevertheless, the remaining adherence of the double deletion mutant is an open question. A complementary adhesion mechanism depending on *pilB2* from the pil-2 locus is excluded, because its deletion does not have an effect on adhesion in the Δ*flaI*/Δ*pilB1*/Δ*pilB2* triple mutant. A possible explanation is presented by Esquivel & Pohlschröder (2014), proposing that pilins in the membrane cause weak residual adhesion even when they are not assembled into pili. This might be the case in consequence of the assembly ATPase (*pilB1*) deletion, which prevents incorporation of the pilins (of so far unknown identities) into a functional filament.

To exclude another type IV pili-like mechanism responsible for the residual adhesion of *Hbt. salinarum* R1, a knock-out of the prearchaellin/pilin peptidase gene (*flaK*) is desireable, as performed with the *Haloferax volcanii* homolog *pibD* (Tripepi *et al.*, 2010). Attempts made in this direction were not successful (L. Vidakovic & S. Fröls, unpublished results), suggesting that *flaK* is essential for *Hbt. salinarum*, possibly due to further proteins containing archaeal class III signal peptides, which might necessarily be processed by the enzyme FlaK.

However, the existence of other adhesion mechanisms different from type IV pili is possible. For instance other types of appendages, different from the type IV pilus architecture, were observed with diverse species, like the amyloid protein recognized in association with biofilms of *Hfx. volcanii* (Chimileski *et al.*, 2014b). Moreover, *Methanococcus thermoautotrophicus* produces non-type IV pili-like Mth60 fimbriae which function as adhesins (Thoma *et al.*, 2008). In addition, the production of a biofilm matrix containing components like adhesive exopolysaccharides or extracellular DNA was shown to greatly influence cellular adhesion in bacterial biofilms of *Pseudomonas aeruginosa* (Myszka & Czaczyk, 2009; Wang *et al.*, 2015). The presence of biofilm matrices containing similar components was also demonstrated for archaeal biofilms, for instance with *S. acidocaldarius* (Jachlewski *et al.*, 2015) as well as *Hbt. salinarum* R1 (see Chapter 3). Also, unspecific processes caused by functional groups on the cell surface of *Hbt. salinarum* R1 cannot be excluded.

4.3.5. *Hbt. salinarum* R1 possesses a repertoire of archaellins and putative pilin encoding genes

Bioinformatical analyses revealed more than 30 proteins with archaeal class III prepilin/archaellin peptidase signal peptides in the *Hbt. salinarum* R1 genome. The occurence of

multiple type IV pilin-like genes, *i.e.* prearchaellins or prepilins, is common in microorganisms (Szabó *et al.*, 2007b), which often possess an array of these molecular modules excerting versatile functions (see also Chapter 1.5).

Archaellins

At least one archaellin gene is found in 75% of the sequenced archaeal genomes, with the highest number of archaellin genes (six) found in *Hbt. salinarum* (Syutkin *et al.*, 2014a). The similar expression patterns of *flgA1* and *flgB1* in the present study suggest a co-regulation of the A and B loci in *Hbt. salinarum* R1, although they are located in a distance of 40 kbp. However, there is no information available on how this regulon is controlled. While the growth phase seems to have a weak influence on archaellin gene transcription in planktonic cells, the switch to a sessile biofilm lifestyle goes along with marked down-regulation. This suggests minor importance of archaellation in sessile cells and also implies that archaella are not important for adhesion.

The role of the archaellin gene multiplicity is not fully understood in *Hbt salinarum*, but there is evidence that the archaellin subunits perform different structural functions [see also chapter 1.5 (Beznosov *et al.*, 2007; Tarasov *et al.*, 2000)]. This is similar to the specialized functions of the four *Methanococcus voltae* archaellins, where two major subunits (FlaB1 and FlaB2) as well as one minor subunit (FlaA) form the archaella filament, while another minor archaellin (FlaB3) composes its hook region (Bardy *et al.*, 2002; Kalmokoff *et al.*, 1988). *Hfx. volcanii* has two archaellin genes, *flgA1 and flgA2*. The protein FlgA1 is the major subunit of the archaella. FlgA2 is a minor structural component, which also exerts regulational functions, since deletion of the corresponding gene results in hypermotile cells, which possess longer archaella and a larger number of these (Tripepi *et al.*, 2013). Also, two archaellins (FlaB and FlaA2) are encoded in the genome of *Haloarcula marismortui*. The organism produces distinct archaella filaments consisting mainly of either of these two proteins (Pyatibratov *et al.*, 2008). The different filament types provide advantages dependent on environmental conditions like salinity or temperature (Syutkin *et al.*, 2014b). In comparison, *Halorubrum lacusprofundi* and *Sulfolobus* species only possess one single archaellin encoding gene which is sufficient to form functional archaella (Syutkin *et al.*, 2014a; Szabó *et al.*, 2007a).

***flgX* and pilins**

Transcription was not detectable with regard to the sixth archaellin gene of *Hbt. salinarum* R1, *flgX*, although RNA was isolated from various planktonic and sessile cell samples. This is in accordance with the fact that only the archaellins of the A and B loci were identified in archaella preparations (Gerl *et al.*, 1989). In contrast, it contradicts the assumption that the 7-8 nm X-

filaments observed previously upon *flgA1-2* plus *flgB1-3* deletion are constituted of the *flgX* gene product, which was not proven experimentally (Beznosov *et al.*, 2007). Since the X-filaments are presumably equivalent to the 7.6 nm adhesion pili (Pil-1) of *Hbt. salinarum* R1 (Losensky *et al.*, 2014), this implies that other genes might be involved.

At least one pilin monomer is necessary to form the Pil-1 filaments of *Hbt. salinarum* R1. Nevertheless, pilins sometimes exhibit redundant functions, like the multiple adhesion pilins of *Hfx. volcanii*, each of which is sufficient to form functional pili (Esquivel *et al.*, 2013). The role of this redundancy is unclear, but one can assume that it might provide advantages under certain environmental conditions, like it was observed with the two archaellins of *Haloarcula marismortui* acting as ecoparalogs (Syutkin *et al.*, 2014b). Twelve putative prepilin encoding genes were identified in *Hbt. salinarum* R1, based on their predicted class III prepilin peptidase signal peptides and the similarities to known adhesion pilins of other species. Their transcription in different planktonic and sessile cell samples of *Hbt.* was quantified, resulting in diverse expression patterns. Most of the genes tested showed down-regulation or only weak changes in sessile cells and therefore appeared of minor importance in biofilm formation. In contrast, the genes *pilA5*, *pilA6* and *pilA7* were significantly induced in the initial biofilm stage. Due to the fact that this is the phase when adhesion takes place, these three genes represent the most promising candidates potentially encoding the adhesion (Pil-1) pilins of *Hbt. salinarum* R1, but this has to be tested by gene deletion studies.

Several unsuccessful attempts were made to identify the Pil-1 monomers in *Hbt. salinarum* R1 (data not shown). There exist diverse protocols that were employed for the isolation of archaeal cell surface structures and subsequent mass spectrometrical (MS) identification of the protein subunits (Gerl *et al.*, 1989; Henche *et al.*, 2012a; Kupper *et al.*, 1994). Variants of these protocols based on shearing, solubilization and precipitation of the cellular appendages were tested. But the same difficulties in identification of the *Hbt. salinarum* surface structure components were encountered as described previously by others (Beznosov *et al.*, 2007; Klein *et al.*, 2005). Possible explanations for this are the low abundance of the adhesion pili and the potential stickiness of the pilin monomers. Moreover, archaeal type IV pilins are often subject to post-translational protein modifications, namely N-glycosylation (Esquivel *et al.*, 2016; Jarrell *et al.*, 2014), which might complicate their MS identification.

Modifications and regulation

Protein modifications even expand the diversity and complexity of archaellins and pilins. It was shown that the *Hfx. volcanii* major archaellin (FlgA1) is N-glycosylated at different positions and the modifications are necessary for the assembly of functional archaella (Tripepi *et al.*, 2012). The four archaellins of *Methanococcus voltae* possess altogether 15 potential N-

glycosylation sites, 14 of which are modified by glycans (Voisin *et al.*, 2005), while disruption of the corresponding machinery had negative effects on archaella assembly (Chaban *et al.*, 2006). N-glycosylation is also the case with respect to the archaellin (FlaB) of *S. solfataricus*, where all six predicted sites show glycosidic modifications, but they are not essential for assembly and functionality of the archaella (Meyer *et al.*, 2015). Growth parameters influence the protein modification in different species. N-glycosylation in *Methanococcus maripaludis* is affected by the growth temperature (Ding *et al.*, 2015), whereas it is dependent on the salinity in *Hfx. volcanii* (Eichler *et al.*, 2013). Whether this is also the case with adherent cells or in consequence of biofilm formation in *Hbt. salinarum* R1, is not yet known, while seven of the twelve putative pilin candidates in the present study have at least one predicted N-glycosylation site. Interestingly, N-glycosylation sites are also predicted with four (PilA1-PilA4) of the six adhesion pilins of *Hfx. volcanii* (Pohlschröder & Esquivel, 2015). The pilin N-glycans act in biosynthesis of the corresponding pili, adhesion and microcolony formation, while a role in the regulation of the transition between planktonic and sessile cell states is suggested for their differential glycosylation (Esquivel *et al.*, 2016).

4.3.6. Do additional roles for the putative pilin genes or the pil-2 locus exist?

Assuming that one or even a few of the *Hbt. salinarum* R1 putative pilins might be involved in adhesion, the question arises what the functions of the residual 'FlaFind positives' are. Type IV-like pilins represent versatile molecular modules, which are involved in a diversity of processes (see Chapter 1.5). Regarding bacterial type IV pilins the functional repertoire is even expanded by actions in electron transfer and twitching motility, host cell manipulation or protein export (Berry & Pelicic, 2015; Giltner *et al.*, 2012). Moreover, novel functions and mechanisms are possible. One recent example is a newly observed post-translational regulation mechanism of archaella-dependent motility in the biofilm formation of *Hfx. volcanii*. The mechanism is dependent on the adhesion pilins of the organism and allows for rapid transition from the planktonic to a sessile lifestyle. In the planktonic state, pilins accumulate in the cell membrane and bind to an inhibitor of archaella synthesis, allowing for archaella formation and motility. Upon adhesion of the cells more pilins are incorporated in the adhesion pili, while the inhibitor is released and prevents archaella maintenance (Esquivel & Pohlschröder, 2014).

Transcriptional analyses of pil-2 indicated an induction in adherent cells, but weak expression compared to the other T4P systems of *Hbt. salinarum* R1. Although cotranscription of pil-2 was detected, its functionality is put into question by the presence of an internal stop codon within the genomic sequence of *pilC2* (Losensky *et al.*, 2014). A role of pil-2 in adhesion to plastic and glass surfaces is excluded by the deletion mutant analyses described earlier, while adhesion to

other materials is possible, as well as a potential function under different environmental conditions or in other processes. For instance a function in cell cohesion or stabilization of the complex biofilm architectures is conceivable, even though the primary adhesion is apparently accomplished by the Pil-1 pili. Nevertheless, only one additional surface structure type was observed by TEM besides the archaellum, as concluded from the diameters, and no appendages at all were observed with the double deletion mutant (Losensky *et al.*, 2014).

Contradictory results were obtained with regard to the putative pilin genes *pilA2-4* of the pil-2 locus. No quantitative data was gained for *pilA4* by qRT-PCR, although RT-PCR suggested cotranscription of the seven pil-2 genes. This might be due to an inappropriate qRT-PCR setup, since a standard progam is used for amplification of all targets. Additionally, intrinsic properties of the mRNA like secondary structures or stability influence the transcription analyses (Bustin, 2002; Bustin & Nolan, 2004). Transcription of *pilB2* was weak, which is the initial gene in the polycistronic mRNA. Transcription of the residual genes is potentially below the detection limit with the qRT-PCR setup used. This is substantiated by the fact that transcription of *pilC2* was not detectable, as well. In contrast, the qRT-PCR results suggest the presence of an additional promoter upstream of the genes *pilA3* and *pilA2*, which results in stronger expression of these two genes and allows for detection and quantification. However, the transcription profiles of *pilA2* and *pilA3* argue against an involvement in adhesion and biofilm formation, since they are similar to those of the archaellins, *i.e.* exhibit down-regulations in biofilms.

Conservation of the pil-2 locus among haloarchaeal species was demonstrated by the Southern and the bioinformatics analyses, which raises evolutionary questions. The pil-2 locus represents a complete T4P system, comprising seven genes and a total of 6.7 kbp. Nevertheless, a loss of the pil-2 locus might be expected if it was non-functional, since genome reduction is a dominant mode of evolution (Wolf & Koonin, 2013). On the other hand the existence of multiple T4P and their potential functional versatility may provide advantages for microorganisms under certain conditions (Chimileski & Papke, 2015), although these remain to be defined. This is also true with regard to the putative pilin genes investigated, which were all but one conserved among the halobacterial species, as demonstrated by Southern analyses. Nevertheless, genetic variability was suggested by the diversity of some of the probe hybridization patterns.

In conclusion, a type IV pilus-like mechanism was identified to be crucial for the adhesion of *Hbt. salinarum* R1 to surfaces, which is the first step in biofilm formation of the organism. While it was shown that adhesion is mediated by the Pil-1 pili, the search for the corresponding assembly and potential regulation factors is still in its infancy. Although decisive of the microbial lifestyle, adhesion is only one aspect with respect to the formation of biofilms. A global approach is desirable to gain comprehensive insights into the cellular differentiation during biofilm

formation of *Hbt. salinarum* R1. It will be challenging to uncover other mechanisms and regulation networks in which cell motility and adhesion are integrated.

5. Proteome analysis of *Halobacterium salinarum* R1 biofilms

5.1. Introduction

Microbes often encounter changing environmental conditions in their habitat and need to adapt (Rosenzweig & Adams, 1994). The accommodations go along with profound adjustments and rearrangements at the cellular and molecular level, since the lifestyle changes have profound effects on the transcriptomes and proteomes of microbes (Koerdt *et al.*, 2011; Soppa, 2011).

Halobacterium salinarum R1 and its closely related strain NRC-1 were objects of a number of global studies investigating the consequences of environmental changes on planktonic cells. Microarray analyses of *Halobacterium salinarum* were performed for the investigation of phototrophy (Twellmeyer *et al.*, 2007), anaerobic respiration (Müller & DasSarma, 2005), phosphate limitation (Wende *et al.*, 2009), changes in salinity and temperature (Coker *et al.*, 2007) as well as the responses to UV- and gamma radiation (Baliga *et al.*, 2004; Whitehead *et al.*, 2006). Several proteomic studies have been carried out for the identification of the cytosolic, membrane or low molecular weight proteomes of the *Hbt. salinarum* strains R1 (Klein *et al.*, 2007; Klein *et al.*, 2005; Rietschel *et al.*, 2009; Tebbe *et al.*, 2005) and NRC-1 (Gan *et al.*, 2006; Goo *et al.*, 2003). A quantitative profiling of the *Hbt. salinarum* R1 membrane proteome (Bisle *et al.*, 2006), as well as quantitative analyses comparing aerobic growth in complex versus synthetic medium and aerobic versus anaerobic/phototrophic growth were performed (Tebbe *et al.*, 2009). Also, the effects of changing salt concentrations have been investigated in a quantitative proteomic study of strain NRC-1 (Leuko *et al.*, 2009).

Biofilm formation represents a distinct switch of the microbial lifestyle and cells undergo profound changes to accomplish this (O'Toole *et al.*, 2000). To date global proteomic data on archaeal biofilms is only available in two studies investigating the acidophilic euryarchaeote *Ferroplasma acidarmanus* Fer1 (Baker-Austin *et al.*, 2010) and species of the thermoacidophilic crenarchaeote *Sulfolobus* (*S. solfataricus*, *S. acidocaldarius*, and *S. tokodaii*) (Koerdt *et al.*, 2011). Differential protein abundance profiles have been detected in both studies comparing planktonic and sessile cells. Molecular differentiations are also observed with respect to the haloarchaeon *Halohasta litchfieldiae* [(Mou *et al.*, 2012), formerly referred to as Antarctic isolate t-ADL DL24] that shows different protein patterns and differing protein sets in planktonic and biofilm cells [Diploma thesis G. Losensky, 2011; (Fröls, 2013)]. So far, no comparable data were gained with respect to the molecular differentiation of biofilms formed by *Hbt. salinarum* (Fröls *et al.*, 2012).

Biofilm formation of *Hbt. salinarum* R1 is a process of consecutive events, in which adhesion represents the initial and crucial step, which also marks the fundamental transition from a free

living mode to a sessile lifestyle (see also Chapter 3). It must be assumed that the different phases during biofilm development put specific demands on the physiology of the cells. An extensive adhesion of the cells in the initial phase is only possible if structures mediating this process are synthesized (see also Chapter 4). Also, the distinct architecture observed in mature biofilms depends on these, while other mechanisms must be involved in the synthesis or secretion of extracellular polymeric substances (EPS) that embed the cells. Cell motility is impeded in biofilms, while distinct cellular requirements with regard to the nutrient or energy supply likely originate from living in a biofilm, as well. Almost nothing is known about the molecular changes during biofilm formation of *Hbt. salinarum* R1.

For this reason, proteome analyses of biofilm cells in comparison to planktonic cells were performed. The protein sets of planktonic, as well as initial and mature biofilm cells were determined by mass spectrometry. A quantitation method applicable to the proteome of *Hbt. salinarum* R1 was established. Using this procedure, a large portion of the proteins was quantified and the proteins showing the strongest changes determined. Co-trending proteins were grouped to identify the cellular mechanisms affected in consequence of the biofilm lifestyle. In addition, the transcription of selected genes involved in certain biofilm-related processes was investigated to validate the quantitative proteomic data. The overall goal was to detect biofilm markers showing specific responses at the transcription or protein level during biofilm development.

5.2. Results and discussion

5.2.1. Comparison of protein patterns obtained from planktonic and sessile cells

Cell lysates were prepared from planktonic and sessile *Hbt. salinarum* R1 for a first investigation of the molecular differentiation in biofilms. Protein samples of planktonic cells from the early exponential, late exponential and stationary growth phase, as well as sessile cells harvested after 1 to 15 days, were separated by SDS-PAGE. Two different staining procedures were applied to visualize the proteins, *i.e.* colloidal coomassie and silver staining (Gromova & Celis, 2006). Similar protein patterns were observed with the different samples prepared from planktonic cells (Figure 31A and B). In contrast, the patterns obtained from biofilm samples were fundamentally different from those of the planktonic cells. The differences were already observed after 1 day of biofilm growth, while the 'biofilm pattern' remained virtually constant during the 15 days of development, with a few additional bands appearing.

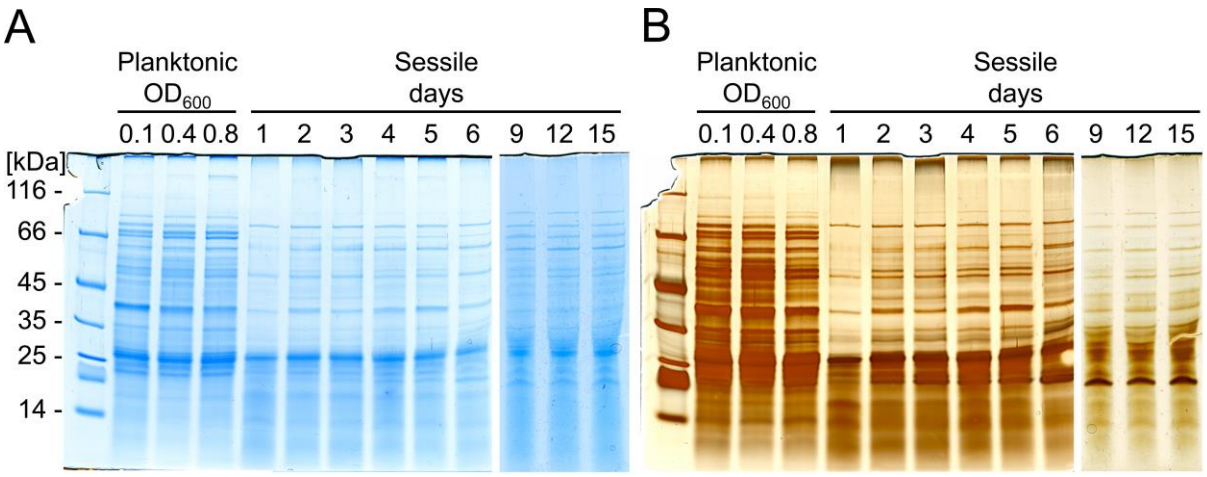

Figure 31 SDS-PAGE of protein samples prepared from lysates of planktonic and sessile cells. **A**, Comparison of protein patterns obtained with planktonic cells grown until early exponential (OD_{600} 0.1), late exponential (0.4) and stationary (0.8) growth phase, as well as sessile biofilm forming cells grown for 1 through 15 days (numbers indicate incubation time in days). 10 µg of proteins were applied per lane. Colloidal coomassie staining. **B**, Silver staining of the gels shown in A.

The reproducibility of the protein patterns was investigated in a second experiment. Several independent cultures, *i.e.* three biological replicates of *Hbt. salinarum* R1 planktonic or sessile cells (I, II, III), were cultivated in parallel and protein samples were prepared and analyzed by SDS-PAGE as before. Biological replicates yielded similar protein patterns (Figure 32A and B), suggesting that the sample preparation was reproducible.

The large differences observed between the protein patterns obtained from planktonic and biofilm samples implied a profound molecular differentiation of *Hbt. salinarum* R1 switching from the planktonic to the sessile biofilm lifestyle. Moreover, an early transition of the cells is suggested, since an altered protein pattern occurs already after one day of biofilm growth. This

is surprising, given the fact that *Hbt. salinarum* R1 has a doubling time of 7.5 hours. The early molecular differentiation coincides with the initial adhesion of the cells and early EPS production observed by microscopic analyses (see also Chapter 3). Similar molecular differentiations on the protein level are seen with planktonic and sessile cells of other bacterial or archaeal species, for instance in *Pseudomonas aeruginosa* (Yu *et al.*, 1990) as well as *Halohasta litchfieldiae* [Diploma thesis G. Losensky, 2011; (Fröls, 2013)] by SDS-PAGE.

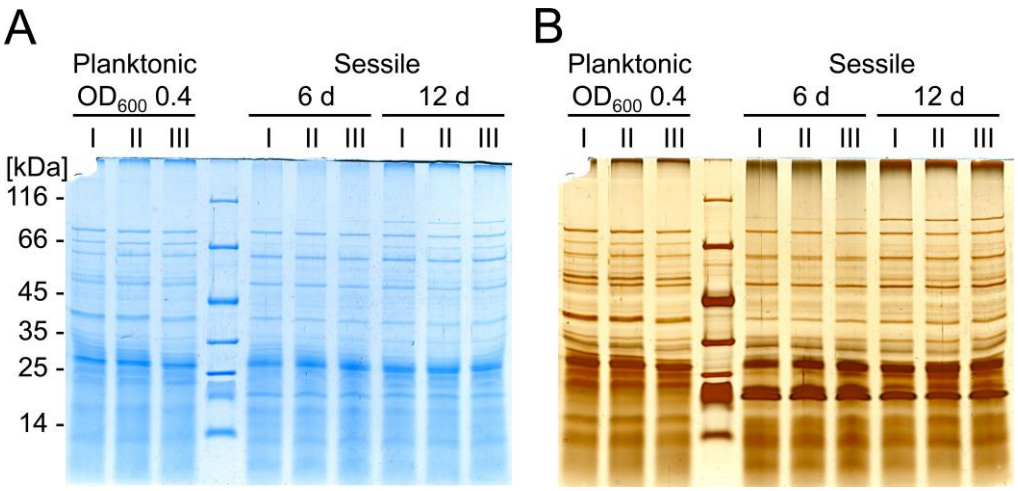

Figure 32 Reproducibility of protein patterns. **A**, Comparison of protein patterns obtained with biological replicates (I, II and III) prepared from planktonic cell samples harvested at the late exponential growth phase (OD_{600} 0.4), as well as sessile cells grown for 6 and 12 days, respectively (6 d and 12 d). Colloidal coomassie staining. 10 µg of proteins were applied per lane. **B**, Silver staining of the gel shown in A.

5.2.2. Identification of the biofilm proteome and quantitation by SWATH-LC/MS/MS

The differences with regard to the protein patterns of planktonic and sessile cells raised the question which proteins accounted for them. Three different biological states were used for the examination of the molecular differentiation in *Hbt. salinarum* R1 biofilms by proteome analyses, namely planktonic cells from the exponential growth phase, as well as sessile cells, after 1 and 15 days of growth, to address the process of biofilm maturation. While the planktonic sample represented a condition under which cells are usually grown in the laboratory, the two different sessile samples constituted distinct developmental stages of *Hbt.* biofilms, *i.e.* initial and mature cells (see also Chapter 3). Since the biofilm cultures were inoculated with planktonic cells of the exponential growth phase, it was interesting to investigate the differences exhibited by initial biofilm cells after only one day of growth.

The proteome analyses were carried out in cooperation with Dr. Christof Lenz (MPI for Biophysical Chemistry, Bioanalytical Mass Spectrometry and University Medical Center, Institute for Clinical Chemistry, Göttingen). An initial qualitative analysis was performed to identify the protein sets of the planktonic and sessile samples by liquid chromatography tandem

mass spectrometry (LC/MS/MS). A common protein preparation technique was used to prepare the samples for the LC/MS/MS analysis, based on tryptic in solution digests, without pre-fractionation or pre-separation of the proteins (also see 2.4.4). The qualitative analysis resulted in the identification of 1553 proteins from planktonic cells, while 1540 and 1528 proteins were identified from the initial and mature biofilm samples, respectively (Figure 33A). Considering the identified proteins, 1456 (89.4%) were detected in all three biological samples, while a number of proteins were identified exclusively in a certain sample or shared by only two of them (Figure 33B). Altogether 1629 different proteins were identified tolerating 1% false discovery rate (FDR), corresponding to a coverage of 63.2% of the *Hbt. salinarum* R1 proteome (Figure 33C). This coverage exceeds the previous maximum coverage (39.5%) achieved in a single global study on strain R1 by a factor of 1.6 (Tebbe *et al.*, 2009). It also slightly surpasses the coverage of the *Hbt. salinarum* NRC-1 PeptideAtlas (62.7%) which accumulates 88 individual experiments (Van *et al.*, 2008).

A

Biological sample	Identified proteins
planktonic	1553
sessile 1 d	1540
sessile 15 d	1528

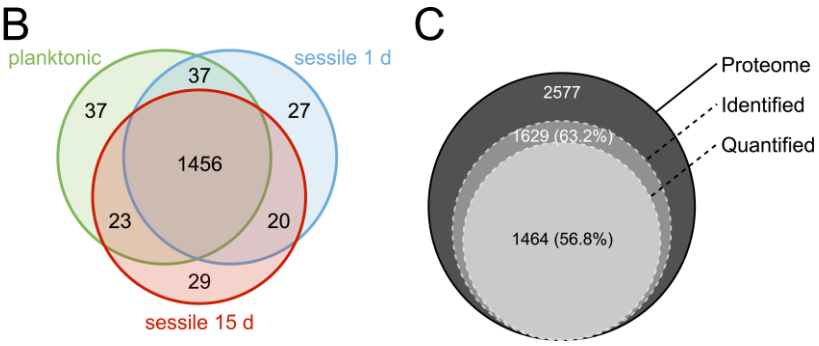

Figure 33 Qualitative proteome analysis of *Hbt. salinarum* R1 planktonic and sessile cells. **A**, Number of proteins identified in the three different biological samples. **B**, Venn diagram illustrating proteins in the three biological samples planktonic (OD_{600} 0.4; green), sessile 1d (grown for 1 day; blue) and sessile 15 d (grown for 15 days; red). Numbers indicate proteins shared by one, two or three of the samples. **C**, Portion of the identified (1629 proteins, corresponding to 63.2% of the proteome) and quantified proteins (1464; 56.8%) in relation to the predicted proteome size (2577 proteins). (Modified from Losensky *et al.*, 2016)

Quantification data was gained for 1464 of the proteins in a global quantitative analysis of the planktonic and sessile samples by SWATH-LC/MS/MS (sequential window acquisition of all theoretical fragment-ion spectra LC/MS/MS). This corresponds to 89.9% quantitation success regarding the identified proteins and an overall quantitation success rate of 56.8% with regard to the predicted *Hbt. salinarum* R1 proteome (Figure 33C). Compared with the few label-free SWATH-MS-based microbiological proteome studies present to date, these are improved results. Earlier studies of *Shewanella oneidensis* biofilms grown on graphite electrodes operating at different electrode potentials yields quantitative SWATH-MS data for 704 proteins (Grobbler *et al.*, 2015), *i.e.* 14.8% of the predicted proteome (Heidelberg *et al.*, 2002). Proteomic profiling of *Bacillus licheniformis* grown in different media results in quantification of 853 proteins

[19.9%, (Veith *et al.*, 2004; Yu *et al.*, 2016), while 1383 proteins (33.5%) are quantified in a study investigating antibiotics stress in *Aeromonas hydrophila* (Lin *et al.*, 2015; Seshadri *et al.*, 2006).

5.2.3. Technical evaluation of the proteome analysis

Several major biophysical parameters of the identified and quantified proteins were ascertained in comparison to the predicted proteome, for an evaluation of the technical quality of the analysis.

The susceptibility of the membrane proteins is an important characteristic of any comprehensive proteomic approach. The theoretical proteome of *Hbt. salinarum* R1 includes 564 proteins predicted to have 1 through 24 transmembrane helices (TMH) by TMHMM server v2.0. In the present study 39.7% of these proteins were identified, while the number of TMH per protein did not correlate with the success of identification or quantitation, respectively (Figure 34A). With respect to the molecular mass, a bias against low masses (< 20 kDa) was observed (Figure 34B, left), which is in accordance with the limited number of tryptic peptides available for small proteins. Moreover, a (small) bias towards proteins with low isolectric point is apparent (Figure 34B, right), which is also reflected by a slightly increased percentage of acidic amino acids (D and E) with regard to the identified and quantified proteins (Figure 34C). The average pI of the theoretical *Hbt. salinarum* R1 proteome is 5.06, while it is shifted to 4.69 and 4.63 considering the totally identified and quantified proteins, respectively.

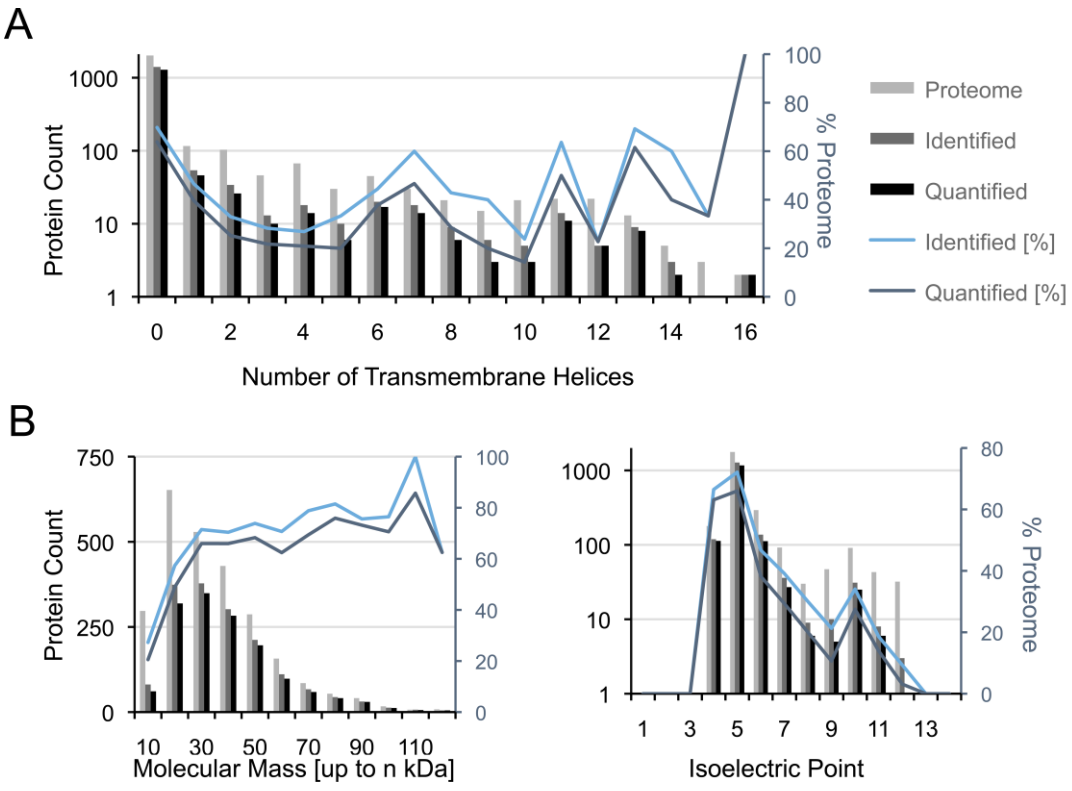

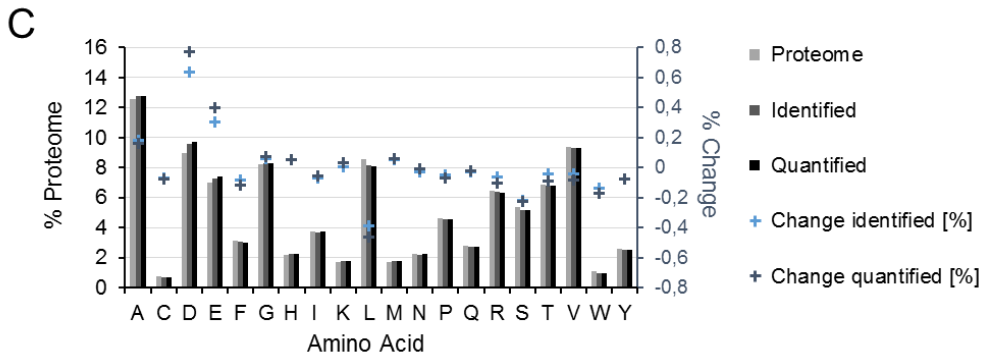

Figure 34 Technical evaluation of the proteome data by ascertainment of biophysical parameters of the *Hbt. salinarum* R1 proteome. **A**, Number of proteins predicted to have 1 through 16 transmembrane helices (light grey) compared to the number of corresponding proteins identified (dark grey) and quantified (black). Graphs illustrate the respective percentage of identified (light blue) and quantified proteins (dark blue) in relation to the predicted proteome. **B**, Left: Distribution of proteins according to their molecular masses indicated in kDa, comparing the whole proteome to the count of identified and quantified proteins. Color code analogous to A. Right: Distribution of proteins based on their isoelectric points (pI), comparing the predicted proteome to the identified and quantified proteins. Color code analogous to A. **C**, Percentage of the amino acids (abbreviated in one letter code) with regard to the proteome, identified and quantified proteins, respectively. Moreover, percentage changes for the identified (light blue crosses) and quantified proteins (dark blue crosses) are indicated. Histogramm color code analogous to A. (Modified from Losensky *et al.*, 2016)

The proteins of extremophilic archaea exhibit a number of special features, such as resistance to thermal and chemical denaturation or protein modifications. In the special case of haloarchaea the proteins are adapted to 3 – 5 molar salt concentrations resulting in acidic proteomes, while a depletion in lysine residues affects trypsination. The proteins are extracted from high salt solutions that can interfere with further procedures (Maupin-Furlow *et al.*, 2012). Therefore, an additional washing step with 80% acetone was implemented in the protein preparation procedure after TCA precipitation and sedimentation. The preparation technique applied in the present work was simple and fast, ensuring minimum error sources and sample variance. The procedure allowed a comprehensive characterization of the *Hbt. salinarum* R1 proteome under the conditions defined here, which is the first investigation of archaeal biofilms using a label-free MS-based proteomic quantitation approach.

5.2.4. Biological evaluation of the proteome analysis

A biological evaluation of the proteome analysis was pursued to address the question of general cellular differentiations comparing the biological samples. Moreover, the identified and quantified proteins were analyzed from a functional point of view, investigating their exposition of the *Hbt. salinarum* R1 proteome.

A non-directed principle component analysis (PCA) was performed to assess the degree of variation between the planktonic and the two biofilm samples (initial and mature). For each of the samples, two biological replicates were analyzed, *i.e.* proteins prepared from independently

grown cultures. In addition, for each biological replicate seven technical replicate analyses were performed. The PCA revealed a clear differentiation between the three biological samples (Figure 35A), with the two largest principle components PC1 and PC2 accounting for a combined 57.2% of differentiation solely due to sample state. The technical and biological replicates of each sample clustered closely. This indicated good reproducibility of the sample preparation as well as the subsequent mass spectrometrical (MS) analyses and was in line with the SDS-PAGE experiment investigating reproducibility. The PCA showed that the three different biological samples were virtually equidistant from one another, confirming their molecular differentiation and suggesting that they represented distinct cellular conditions. The initial biofilm state was almost as distant from the planktonic cells as from the mature biofilm samples. A comparison of planktonic and biofilm cells of either state confirmed the expectations based on the differences observed by SDS-PAGE, while the differences occurring in the SDS gels in the course of biofilm development were rather subtle. However, the PCA suggested a profound molecular differentiation within the development of the biofilms once initiated. This demonstrates that biofilm formation proceeds successively, which is in accordance with the microscopic observations. The results potentially reflect early onset mechanisms in initial biofilm cells, but also long-term effects mediating biofilm maintenance and survival in mature biofilms.

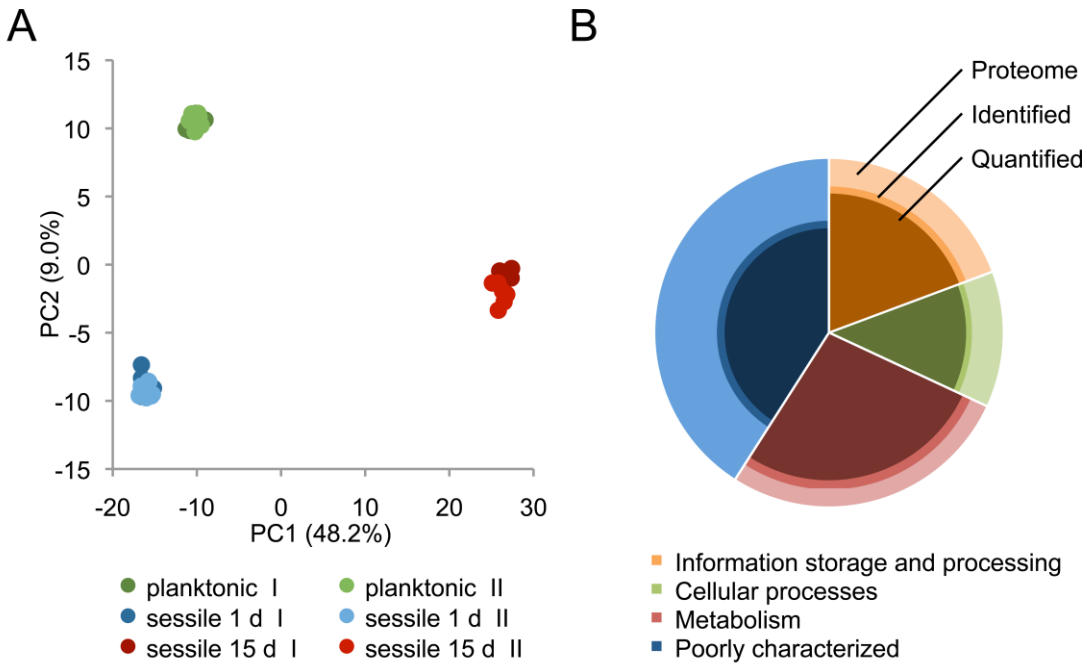

Figure 35 Evaluation of the proteome data from global and functional perspectives. **A**, Principal component analysis of the biological (I and II) and technical replicates of the three biological states, *i.e.* planktonic cells (blue), initial biofilm cells (green) and mature biofilm cells (red). Technical replicates shown in the same color, biological replicates of the same biological state in different shadings. **B**, Functional categorization of the theoretical proteome, identified and quantified proteins according to arCOG (Archaeal Clusters of Orthologous Genes). Pie chart illustrates distribution of the proteins to the four major arCOG categories *Information storage and processing* (orange), *Cellular processes* (green), *Metabolism* (red) and *Poorly characterized* (blue). (Modified from Losensky *et al.*, 2016)

For a functional evaluation of the present *Hbt. salinarum* R1 proteome data the proteins were sorted into functional categories, according to the Archael Cluster of Orthologous Genes (arCOG), which provides a classification system for archaeal genes and improved functional annotations based on 168 archaeal genomes (Makarova *et al.*, 2007). The three major functional categories of proteins with assigned functions*, i.e. Information Storage and Processing*, *Cellular Processes and Signaling* as well as *Metabolism* were represented similarly by the data. Quantitative data was obtained for in average 64.7%, 62.7% and 72.9% of the respective proteins. This implicates a good representation of the *Hbt. salinarum* R1 proteome, with a slightly higher proportion of proteins involved in metabolic processes (Figure 35B). In comparison, proteins falling into the category of *Pooly characterized* proteins appeared underrepresented, with an average of 42.2% identified and 36.5% quantified proteins.

More functional details were gained from the arCOG sub-categories (Table 9). Quantitation success rates higher than 70% were found for 10 out of 20 categories. The highest portions of quantified proteins were achieved with proteins from the three sub-categories *Translation, ribosomal structure and biogenesis* (87.3%), *Energy production and conversion* (86.1%), and *Nucleotide transport and metabolism* (100%). In comparison, only 32.0% and 6% quantitation rates were observed with the sub-categories *Function unknown* and *No arCOG assigned*.

Table 9 Functional categorization of *Hbt. salinarum* R1 proteome, identified and quantified proteins

	[1]Functional category	[1]Relative portion [%]	[1]Predicted proteins total	[2]Identified proteins [%]	[2]SWATH quantitation [%]	[2]Significantly regulated [%]
1. Information storage and processing						
J	Translation, ribosomal structure and biogenesis	5.8	150	90.7	87.3	77.3
K	Transcription	7.1	184	66.3	57.6	42.4
L	Replication, recombination and repair	6.4	165	57.6	49.1	36.4
2. Cellular processes and signaling						
D	Cell cycle control, cell division, chromosome partitioning	0.9	23	56.5	56.5	47.8
M	Cell wall/membrane/envelope biogenesis	2.5	64	79.7	70.3	50.0
N	Cell motility	1.7	44	84.1	72.7	54.5
O	Posttranslational modifications, protein turnover, chaperones	3.3	85	72.9	68.2	55.3
T	Signal transduction mechanisms	2.1	55	81.8	74.5	60.0
U	Intracellular trafficking, secretion and vesicular transport	0.6	15	73.3	53.3	46.7
V	Defense mechanisms	1.5	39	48.7	43.6	28.2
3. Metabolism						
C	Energy production and conversion	4.7	122	91.0	86.1	79.5
E	Amino acid transport and metabolism	5.7	147	88.4	83.0	68.0
F	Nucleotide transport and metabolism	2.4	61	100	100	85.2
G	Carbohydrate transport and metabolism	2.0	52	59.6	53.8	40.4
H	Coenzyme transport and metabolism	4.0	103	84.5	75.7	57.3
I	Lipid transport and metabolism	2.3	59	83.1	76.3	67.8
P	Inorganic ion transport and metabolism	4.3	111	55.9	50.5	38.7
Q	Secondary metabolites transport, biosynthesis and catabolism	1.7	45	68.9	57.8	44.4
4. Poorly characterized						
R	General function prediction only	9.7	250	79.6	71.6	56.8
S	Function unknown	27.3	703	38.1	32.0	23.3
X	No arCOG assigned	3.9	100	9.0	6.0	6.0
	Total	**100**	**2577**	**63.2**	**56.8**	**45.1**

[1] According to a *Hbt. salinarum* R1 extract from the UniProtKB protein sequence database (revision 10/2014) combined with the Archaeal Clusters of Orthologous Genes (arCOG, Makarova *et al.*, 2007, 2015). Source: http://archaea.ucsc.edu/arcogs.
[2] this study (Table modified from Losensky *et al.*, 2016)

5.2.5. Pairwise comparison of the biological samples

The first approach for the identification of molecular processes during biofilm development of *Hbt. salinarum* R1 was based on the relative quantification of the proteins in the different biological samples in a pairwise manner, *i.e.* sessile 1 d versus planktonic, sessile 15 d vs. planktonic, and sessile 15 d vs. sessile 1 d samples. This approach aimed to determine the proteins showing the strongest changes between two distinct biological states.

The statistical calculations of the relative proteomic changes were done in cooperation with Prof. Klaus Jung (Institute for Animal Breeding and Genetics, University of Veterinary Medicine, Hannover). Only proteins with a p-value ≤ 0.05 and an absolute value of the fold change (FC) greater than 2-fold ($log_2FC > 1$ or $log_2FC \leq -1$) were considered significant. Altogether 111 proteins fulfilled the significance criteria comparing initial biofilm cells with planktonic cells. 55 proteins of these showed strongly increased levels in initial biofilms, whereas 56 proteins were decreased (Table 10). Overall 375 proteins were identified in different levels between mature biofilms and planktonic cells, with 192 of these showing an increase and 183 a decrease, whereas even 471 proteins showed significant changes between the mature and initial biofilm state (226 increased and 245 decreased). The relative protein abundance changes ranged between 195-fold increase ($log_2FC = 7.61$) and -22.8-fold decrease ($log_2FC = -4.51$).

Table 10 Relative quantification by pairwise comparison

Samples[1]			Number of proteins with p ≤ 0.05	Significantly increased $log_2FC \geq 1$	Maximum log_2FC	Significantly decreased $log_2FC \leq -1$	Minimum log_2FC
initial	vs.	planktonic	789	55	3.7	56	-3.7
mature	vs.	planktonic	1027	192	7.3	183	-4.5
mature	vs.	initial	1091	226	7.6	245	-3.9

[1] initial, biofilm cells grown for 1 d; mature, biofilm cells grown for 15 d; planktonic, cells from the exponential growth phase (OD_{600} 0.4)

Initial biofilm vs. planktonic cells

Comparing the proteome of initial biofilms with that of planktonic cells, the most obvious increases were observed with proteins involved in energy metabolism and ribosomal proteins. Several proteins involved in carbon-, nucleotide-, and lipid metabolism were less abundant in the initial state, similar to proteins acting in cell motility.

Table 11 Relative quantification initial biofilm vs. planktonic[1]. Abundance changes of selected proteins.

log_2 Fold Change*	Symbol	Annotation	arCOG Category and Function Description	UniProt Accession
-1.13	FlaJ	Archaella biogenesis protein	2, N, Cell motility	B0R4I0
-1.58	FlgB1	Archaellin B1		B0R4I9
-2.20	FlgB3	Archaellin B3		B0R4J1
1.38	ArcA	Arginine deiminase	3, C, Energy production and conversion	B0R9X5
1.30	ArcB	Ornithine carbamoyltransferase		B0R9X3
1.76	ArcC	Carbamate kinase		B0R9X4
0.83	ArcD	Arginine/ornithine antiporter		B0R9X2
3.69	DmsA	Dimethylsulfoxide reductase subunit A (reductase)		B0R488
1.33	DmsB	Dimethylsulfoxide reductase subunit B (e^- transfer)		B0R489
1.19	DmsC	Dimethylsulfoxide reductase subunit C (anchor)		B0R490
2.06	DmsR	HTH-10 family transcription regulator		B0R486
-1.91	NrdA1	Ribonucleoside-diphosphate reductase α subunit	3, F, Nucleotide transport and metabolism	B0R7R5
-2.07	NrdB1	Ribonucleoside-diphosphate reductase β subunit		B0R7R4
-1.64	Gap	Glyceraldehyde-3-phosphate dehydrogenase	3, G, Carbohydrate transport and metabolism	B0R2M2
-2.88	PpsA	Phosphoenolpyruvate synthase		B0R351
-1.18	PpcA	Phosphoenolpyruvate carboxylase		B0R7F9
1.73	PykA	Pyruvate kinase		B0R347
-1.15	Acd2	Acyl-CoA dehydrogenase	3, I, Lipid transport and metabolism	B0R449
-1.84	Acs2	Acyl-CoA synthetase		B0R4M4
-1.00	Acs3	Acyl-CoA synthetase		B0R5D9
-1.10	Acs4	Acyl-CoA synthetase		B0R2S9

[1] A selected portion of the results is shown only. Complete quantitation results are found in Supplementary tables 1. * Fold change (FC), ratio of the respective protein abundance in initial biofilms divided by the abundance in planktonic cells. Positive/negative values, increased/decreased amounts in initial biofilms.

The strongest increase in initial biofilm cells was detected for the subunit DmsA (Table 11) of the *Hbt. salinarum* R1 DMSO reductase, which is an alternative terminal oxidase using substrates like DMSO or TMAO as electron acceptor under anaerobic conditions (Müller & DasSarma, 2005). This was accompanied by higher amounts of the subunits DmsB and C, and of the associated proteins DmsD and E, as well as the corresponding activator DmsR, all encoded by the *dms* operon (Figure 36).

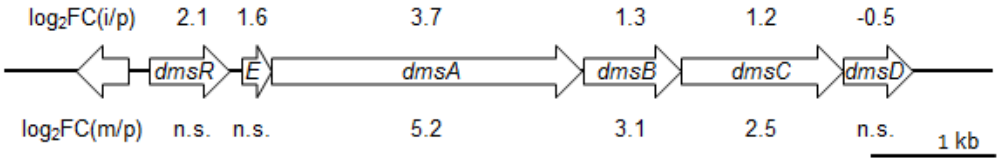

Figure 36 Genetic map of the *Hbt. salinarum* R1 *dms* operon. Genes encode the transcription regulator (*dmsR*), uncharacterized protein (*dmsE*), DMSO reductase subunits A-C (*dmsA-C*) and a chaperone (*dmsD*). Numbers indicate fold change (FC, log_2 scale) of the corresponding protein amounts in initial biofilm cells versus planktonic cells (i/p), respectively, in mature biofilms versus planktonic cells (m/p); n.s., non-significant. (Müller & DasSarma, 2005)

Also, the proteins involved in the fermentative arginine degradation pathway (Arc), an alternative energy conservation mechanism under anaerobic conditions, showed higher abundances in initial biofilms. These proteins are encoded by the operon *arcRACBD* (Ruepp & Soppa, 1996) (Figure 37). The repressor ArcR was only slightly increased. Also several ribosomal proteins displayed strong increases (Supplementary tables 1).

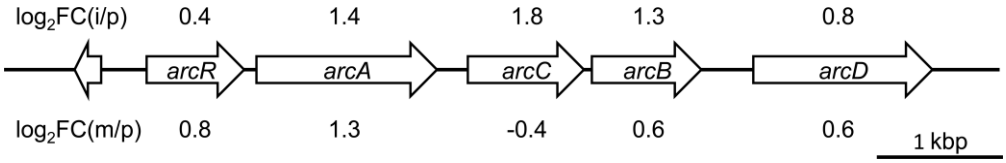

Figure 37 Genetic map of the *Hbt. salinarum* R1 *arc* operon. Genes encode HTH-type transcriptional repressor (*arcR*), arginine deiminase (*arcA*), carbamate kinase (*arcC*), ornithine carbamoyltransferase (*arcB*), and arginine/ornithine antiporter (*arcD*). Numbers indicate fold change (FC, $\log_2$ scale) of the corresponding protein amounts in initial biofilm cells versus planktonic cells (i/p), respectively, in mature biofilms versus planktonic cells (m/p). (Ruepp & Soppa, 1996)

With respect to the central C-metabolism, the enzyme pyruvate kinase (PykA), catalyzing the final step in glycolysis, was strongly increased in initial biofilms (Table 11, p. 85). In contrast, phosphoenolpyruvate synthase (PpsA) which is an essential gluconeogenesis enzyme acting in the opposite direction, showed the second-strongest decrease. This suggests lower cell growth and division in initial biofilms and was accompanied by decreases of two further central C-metabolism enzymes, glyceraldehyde-3-phosphate dehydrogenase (Gap) and PEP carboxylase (PpcA). Strong decreases of subunits of the ribonuleoside-diphosphate reductase, NrdAB1 (Table 11 p. 85), acting in nucleotide metabolism (Torrents, 2014), support this notion.
In addition, several enzymes from the lipid metabolism (Acd2, Acs2-4) were less abundant in initial biofilms. The two archaellins FlgB1 and B3 were found in strongly reduced amounts in the initial state, accompanied by a reduction of the archaella transmembrane protein (FlaJ).

Mature biofilm vs. planktonic cells

The comparison of the proteome of mature biofilms with that of planktonic cells yielded increases of proteins involved in energy-, amino acid-, nucleotide- and lipid metabolism in the mature state. Moreover, proteins acting in gas vesicle formation, signaling and stress response, as well as proteins involved in ion transport were affected similarly. The proteins exhibiting decreased levels in mature biofilms were mainly associated with translation and ribosomes as well as the respiratory chain. Also, the amounts of several proteins involved in amino acid- and nucleotide metabolism, coenzyme biosynthesis and cell motility were reduced.

The strongest increase in mature biofilms was observed for an uncharacterized protein (OE3542R) annotated as 'glutamine-rich alkaline protein' (Table 12). This protein showed the strongest relative change (158 ± 83 -fold) of all proteins detected in the present study.
In silico analyses of OE3542R showed 39% sequence identity to an undefined protein of *Agrobacterium rhizogenes*. Promoter elements (BRE and TATA-Box) were predicted (data not shown). A BLASTn search using the putative OE3542R promoter sequence did not yield similar promoter sequences of any other *Hbt. salinarum* R1 genes. A Hsp20-type molecular chaperone,

Hsp20F, encoded by the downstream ORF, OE3541R, also showed moderately increased protein levels in mature biofilms, suggesting that both ORFs are part of a bicistronic operon.

Table 12 Relative quantification mature biofilm vs. planktonic[1]. Abundance changes of selected proteins.

log_2 Fold Change*	Symbol	Annotation	arCOG Category and Function Description	Uniprot Accession
-1.91	FlgB1	Archaellin B1	2, N, Cell motility	B0R4I9
-2.74	FlgB3	Archaellin B3		B0R4J1
1.43	OE3187R	UspA domain protein	2, T, Signal transduction	B0R5U1
1.06	OE3346R	UspA domain protein		B0R631
1.14	OE3668F	UspA domain protein		B0R6L6
1.30	OE4540R	UspA domain protein		B0R820
1.06	OE5055F	UspA domain protein		B0R9M2
1.59	OE5066R	UspA domain protein		B0R9M8
		Complex I	3, C, Energy production and conversion	
-1.31	NuoB	NADH dehydrogenase subunit B		B0R3U2
		Complex II		
-1.01	SdhB	Succinate dehydrogenase subunit B (Fe-S)		B0R5B6
-1.17	SdhC	Succinate dehydrogenase subunit C (Cyt*b*)		B0R5B8
		Complex III		
-1.38	PetB	Cytochrome *bc*1 complex (Fe-S)		B0R3P8
		Complex IV		
-2.20	CoxA1	Cox-type terminal oxidase subunit I		B0R3V8
1.34	CydA1	Cytochrome *bd* ubiquinol oxidase subunit I		B0R8N5
		Complex V		
-1.72	AtpE	ATP synthase subunit E		B0R758
		Halocyanins		
-1.43	HcpA	Halocyanin HcpA		B0R612
-1.36	HcpF	Halocyanin HcpF		B0R3P0
-1.08	HcpG	Halocyanin HcpG		B0R2Z0
-2.72	CarA	Carbamoyl phosphate synthase small chain	3, E, Amino acid transport and metabolism	B0R6F1
-3.59	CarB	Carbamoyl phosphate synthase large chain		B0R6F0
-3.75	NrdA1	Ribonucleoside-diphosphate reductase α subunit	3, F, Nucleotide transport and metabolism	B0R7R5
-4.51	NrdB1	Ribonucleoside-diphosphate reductase β subunit		B0R7R4
-1.80	NrdJ	Ribonucleoside-diphosphate reductase		B0R617
1.22	PurB	Adenylosuccinate lyase		B0R3B3
1.31	PurC	Phosphoribosylaminoimidazole synthase		B0R6Q0
2.06	PurD	Phosphoribosyl-glycin ligase		B0R5B4
1.44	PurE	N5-carboxyaminoimidazole ribonucleotide mutase		B0R3U0
2.00	PurK	N5-carboxyaminoimidazole ribonucleotide synthase		B0R3T9
1.09	PurM	Phosphoribosylformylglycinamidine cyclo-ligase		B0R4C5
1.87	PurNH	Phosphoribosylglycinamide formyltransferase		B0R3B2
1.23	PurO	IMP Cyclohydrolase		B0R7Q4
-1.06	PurQ	Phosphoribosylformylglycinamidine synthase subunit		B0R6Q5
1.54	PurS	Phosphoribosylformylglycinamidine synthase subunit		B0R6Q6
1.11	AcaB2	Acetyl-CoA C-acyltransferase	3, I, Lipid transport and metabolism	B0R4G6
1.88	Acd2	Acyl-CoA dehydrogenase		B0R449
3.01	Acd3	Acyl-CoA dehydrogenase		B0R528
1.24	Acs2	Acyl-CoA synthetase		B0R4M4
1.19	Acs3	Acyl-CoA synthetase		B0R5D9
1.11	Acs5	Acyl-CoA synthetase		B0R6Z6
1.31	TrkA3	TrkA domain protein (K^+ transport)	3, P, Inorganic ion transport and metabolism	B0R9Q4
3.61	TrkA6	TrkA domain protein (K^+ transport)		B0R6N9
1.45	TrkA7	TrkA domain protein (K^+ transport)		B0R9Q7
3.06	OE2806F	Uncharacterized protein	4, S, Function unknown	B0R581
3.76	OE2872F	Uncharacterized protein		B0R5C1
-4.41	OE3218F	Uncharacterized protein		B0R5W0
7.30	OE3542R	Glutamine-rich alkaline protein		B0R6E4
3.46	OE3545F	Uncharacterized protein		B0R6E6

[1] A selected portion of the results is shown only. Complete quantitation results are found in Supplementary tables 1. * Fold change (FC), ratio of the respective protein abundance in mature biofilms divided by the abundance in planktonic cells. Positive/negative values, increased/decreased amounts in mature biofilms.

The second-strongest increase in mature biofilms was detected for DMSO reductase subunit DmsA, while the subunits B and C of the enzyme also showed higher amounts (also see Figure 36, p. 85). Further proteins involved in energy metabolism exhibiting elevated levels were bacteriorhodopsin (BR) and associated proteins (Blp, Brp and Bap). They are encoded by the *bop* locus (Leong *et al.*, 1988) (Figure 38) and transcription of the gene cluster is induced under low-oxygen conditions with light (Shand & Betlach, 1991).

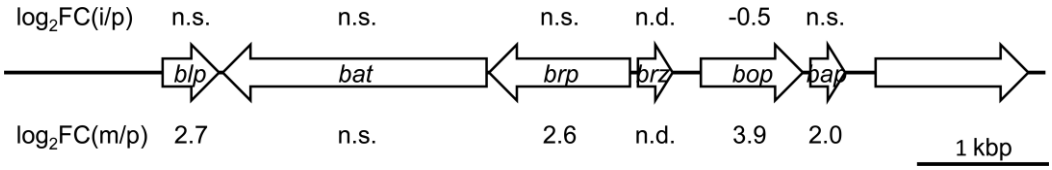

Figure 38 *Hbt. salinarum* R1 *bop* locus. Genes encode bacterioopsin-linked protein (*blp*), bacterioopsin activator (*bat*), bacterioopsin-related protein (*brp*), bacterioopsin-regulating zinc finger protein (*brz*), bacterioopsin (*bop*) and bacterioopsin-associated protein (*bap*). Numbers indicate fold change (FC, $\log_2$ scale) of the corresponding protein amounts in initial biofilm cells versus planktonic cells (i/p), respectively, in mature biofilms versus planktonic cells (m/p); n.s., non-significant; n.d., not detected. (Leong *et al.*, 1988)

Furthermore, all enzymes involved in histidine utilization (Hut) showed increases in mature biofilms compared with planktonic cells (Figure 39). The corresponding *hut* genes are located in a cluster (NCBI). Higher amounts were also observed for enzymes from the nucleotide metabolism, namely acting in purine biosynthesis (Pur) and a number of enzymes involved in lipid metabolism (Table 12, p. 87).

Figure 39 *Hbt. salinarum* R1 histidine utilization (*hut*) gene cluster. Genes encode urocanate hydratase (*hutU*), formimidoylglutamase (*hutG*), imidazolonepropionase (*hutI*) and histidine ammonia-lyase (*hutH*). Numbers indicate fold change (FC, $\log_2$ scale) of the corresponding protein amounts in mature biofilm cells versus planktonic cells (m/p), respectively, in mature biofilms versus initial biofilm cells (m/i). (NCBI).

Similar responses were observed for the gas vesicle regulatory proteins GvpE1 (activator of gas vesicle formation) and GvpD1 (repressing activity) as well as the accessory gas vesicle proteins H1, J1 and K1 all encoded on plasmid pHS1 (Figure 40, p. 89). Furthermore, five universal stress domain-containing proteins (Usp) were significantly more abundant in mature biofilms, similar to three low-affinity K^+ ion transporters (Table 12, p. 87).

Notably over 35% of the proteins exhibiting strong induction in mature biofilms were assigned to the arCOG category *Poorly characterized*. More than ten of these showed strong changes with $\log_2 FC_{m/p} > 2$ and four exhibited $\log_2 FC_{m/p} > 3$ (Table 12).

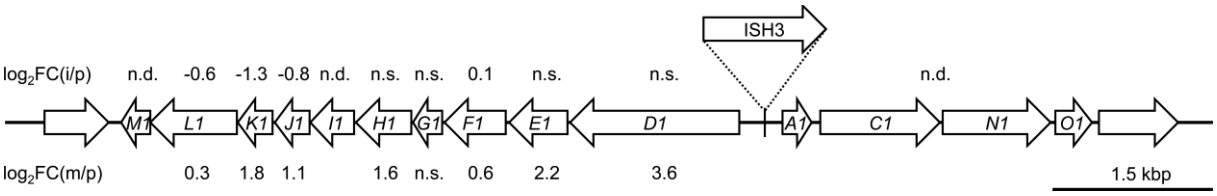

Figure 40 Gene region encoding the gas vesicle proteins on plasmid pHS1. Genes encode proteins GvpA1-M1 (*A1* through *M1*) and insertion element ISH3. Numbers indicate fold change (FC, $\log_2$ scale) of the corresponding protein amounts in initial biofilm cells versus planktonic cells (i/p), respectively, in mature biofilms versus planktonic cells (m/p); n.s., non-significant; n.d., not detected.

The strongest reductions in mature biofilms were observed with ribonucleoside-diphosphate reductase subunits (NrdA1 and B1). The second *Halobacterium* ribonucleoside-diphosphate reductase (NrdJ) was decreased, as well. This was accompanied by reduction of the NrdJ cofactor (cobalamin) biosynthesis machinery (Cbi/Cob), with almost all enzymes involved showing lower amounts in the mature biofilm state (Figure 41).

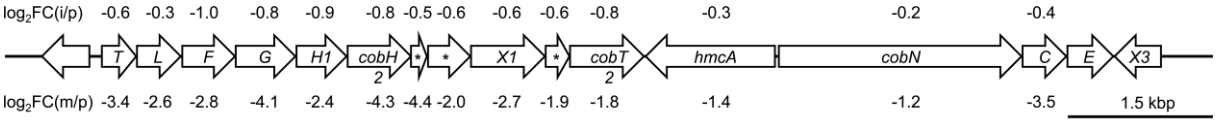

Figure 41 Gene region encoding the cofactor cobalamin biosynthesis machinery. Only a part of the region is shown including several *cbi* genes (letters), *cob* genes (*H2*, *T2* and *M*) and *hmcA*. Asterisks mark genes with unassigned functions. Numbers indicate fold change (FC, $\log_2$ scale) of the corresponding protein amounts in initial biofilm cells versus planktonic cells (i/p), respectively, in mature biofilms versus planktonic cells (m/p).

The major portion of the ribosomal proteins and other proteins associated with translation also showed strong decreases in mature biofilms, with strongest changes determined for ribosomal protein S14 (Supplementary tables 1). Moreover, several proteins involved in amino acid metabolism exhibited similar responses. CarA and B encoding the large and small subunits of the carbamoyl phosphate synthase, involved in arginine as well as pyrimidine biosynthesis (Ashworth *et al.*, 2014), displayed the most pronounced decreases (Table 12, p. 87). Lower levels in the mature biofilm state were also observed for proteins of the respiratory chain (subunits of complexes I, II, III, IV and V, halocyanins), suggesting resting cells. Regarding cell motility, the two archaellins FlgB1 and B3 were strongly reduced, which is in accordance with the sessile lifestyle (Table 12).

Mature biofilm vs. initial biofilm

Among the proteins showing the strongest changes between the mature and initial biofilm stage was a considerable number with unknown functions, *i.e.* assigned to arCOG category *Poorly characterized*. Higher abundances were detected with respect to alternative energy conservation mechanisms and proteins acting in C-metabolism. Also, proteins involved in the amino acid-,

nucleotide- and lipid metabolism exhibited similar responses. Increased amounts in the mature state were also observed for proteins acting in gas vesicle formation, stress response and ion transport. In contrast, many proteins involved in protein biosynthesis and export were strongly reduced in the late biofilm stage. Moreover, several proteins acting in nucleotide metabolism and the biosynthesis of certain coenzymes showed decreases.

About one third (34.9%) of the proteins increased at the late biofilm stage was assigned to the arCOG category *Poorly characterized*, with more than fifteen of them showing strong changes ($log_2FC_{m/i} > 2$). Five uncharacterized conserved proteins (OE1435A1F, OE3545F, OE2443R, and OE2872F) were found with even $log_2FC_{m/i} > 3$ in mature biofilms (Table 13, p. 91), with the strongest change (197 ± 66 -fold) determined for 'glutamine-rich alkaline protein' (OE3542R). This was the strongest relative change of all proteins detected in this study.

Strongly higher abundances were found with bacteriorhodopsin (BR) and its associated proteins, similar to the alternative terminal oxidase subunits DmsA, B and C (Table 13), suggesting anaerobic lifestyle. Moreover, the amounts of several components of the respiratory chain decreased in mature biofilms, namely subunits of the complexes II, III and IV as well as halocyanins (Table 13).

Essential gluconeogenetic C-metabolism enzymes (PpcA and PpsA) were increased in the mature state, suggesting major importance in mature biofilms. In contrast, the amounts of several glycolytic enzymes (Eno and PykA) were reduced. Higher abundances were also observed with enzymes involved in amino acid metabolism, for instance the histidine utilizing (Hut) proteins and components of peptide transporters (Dpp). In addition, proteins acting in nucleotide metabolism, namely purine biosynthesis (Pur) (Supplementary tables 1), were increased, similar to enzymes involved the lipid metabolism (Acs and Acd) (Table 13).

The proteins regulating gas vesicle formation (GvpD1 and GvpE1) exhibited higher abundances in mature biofilms, complemented by higher abundances of the accessory gas vesicle proteins (GvpH1, J1 and K1) (Supplementary tables 1). GvpA, C, N and O1 were not observed due to an ISH3 insertion element in the promoter region (Pfeifer, 2015) (see Figure 40, p. 89). Also, several universal stress proteins (Usp) showed higher abundances in the mature biofilm stage, with OE3187R showing the strongest change. In addition, low affinity potassium ion transport proteins (TrkA3, A6 and A7) were more abundant in mature biofilm cells, similar to the flavin storage and protection protein dodecin (Grininger *et al.*, 2009) (Table 13).

Regarding the proteins decreased in mature biofilms, about one third was assigned to the arCOG category *Poorly characterized*. Several of them showed strong decreases $log_2FC_{m/i} < -2$, with stongest reduction (-15 ± 8 -fold) of an uncharacterized protein (OE3218F) (Table 13).

Table 13 Relative quantification mature vs. initial biofilm[1]. Abundance changes of selected proteins.

log_2 Fold Change*	Symbol	Annotation	arCOG Category and Function Description	UniProt Accession
1.23	OE2097F	UspA domain protein	2, T, Signal transduction	B0R424
2.50	OE3187R	UspA domain protein		B0R5U1
1.13	OE3346R	UspA domain protein		B0R631
1.41	OE4540R	UspA domain protein		B0R820
1.03	OE4544R	UspA domain protein		B0R823
1.37	OE5066R	UspA domain protein		B0R9M8
		Complex II		
-1.39	SdhC	Succinate dehydrogenase subunit C (Cyt*b*)		B0R5B8
		Complex III		
-1.37	PetB	Cytochrome *bc*1 complex (Fe-S)		B0R3P8
		Complex IV		
-2.25	CoxA1	Cox-type terminal oxidase subunit I		B0R3V8
-1.07	CbaA	*Ba3*-type terminal oxidase subunit I		B0R7A7
-1.11	CbaB	*Ba3*-type terminal oxidase subunit II		B0R7A8
1.23	CydA1	Cytochrome *bd* ubiquinol oxidase subunit I	3, C, Energy production and conversion	B0R8N5
		Halocyanins		
-2.14	HcpG	Halocyanin HcpG		B0R2Z0
-1.66	HcpH	Halocyanin HcpH		
1.53	DmsA	Dimethylsulfoxide reductase subunit A (reductase)		B0R488
1.78	DmsB	Dimethylsulfoxide reductase subunit B (e^- transfer)		B0R489
1.34	DmsC	Dimethylsulfoxide reductase subunit C (anchor)		B0R490
4.40	BR	Bacteriorhodopsin		B0R5N9
2.74	Bap	Bacterioopsin-associated protein		B0R5P0
2.62	Blp	Bacterioopsin-linked protein		B0R5N5
2.91	Brp	Bacterioopsin related protein		B0R5N7
1.24	DppA1	ABC-type peptide transporter periplasmic subunit	3, E, Amino acid transport and metabolism	B0R7N9
1.92	DppA2	ABC-type peptide transporter periplasmic subunit		B0R827
2.93	DppA3	ABC-type peptide transporter periplasmic subunit		B0R7P4
1.19	DppF3	ABC-type peptide transporter ATP-binding subunit		B0R7P8
2.23	HutG	Formimidoylglutamase		B0R542
1.59	HutH	Histidine ammonia-lyase		B0R544
2.34	HutI	Imidazolonepropionase		B0R543
3.01	HutU	Urocanate hydratase		B0R541
-1.23	PykA	Pyruvate kinase	3, G, Carbohydrate transport and metabolism	B0R347
-1.04	Eno	Enolase		B0R4Y8
1.75	Gap	Glyceraldehyde-3-phosphate dehydrogenase		B0R2M2
-1.35	KdgK	2-keto-3-deoxygluconate kinase		B0R2S5
2.45	PpsA	Phosphoenolpyruvate synthase		B0R351
2.45	PpcA	Phosphoenolpyruvate carboxylase		B0R7F9
1.11	AcaB2	Acetyl-CoA C-acyltransferase	3, I, Lipid transport and metabolism	B0R4G6
3.03	Acd2	Acyl-CoA dehydrogenase		B0R449
2.60	Acd3	Acyl-CoA dehydrogenase		B0R528
3.08	Acs2	Acyl-CoA synthetase		B0R4M4
2.19	Acs3	Acyl-CoA synthetase		B0R5D9
1.82	Acs4	Acyl-CoA synthetase		B0R2S9
1.33	Acs5	Acyl-CoA synthetase		B0R6Z6
1.54	TrkA3	TrkA domain protein (K^+ transport)	3, P, Inorganic ion transport and metabolism	B0R9Q4
4.28	TrkA6	TrkA domain protein (K^+ transport)		B0R6N9
2.01	TrkA7	TrkA domain protein (K^+ transport)		B0R9Q7
3.22	OE1435A1F	Uncharacterized protein	4, S, Function unknown	B0R315
3.18	OE2443R	Uncharacterized protein		B0R4L9
3.91	OE2872F	Uncharacterized protein		B0R5C1
-3.89	OE3218F	Uncharacterized protein		B0R5W0
7.62	OE3542R	Glutamine-rich alkaline protein		B0R6E4
3.31	OE3545F	Uncharacterized protein		B0R6E6

[1] A selected portion of the results is shown only. Complete quantitation results are found in Supplementary tables 1. * FC, relative ratio of the respective protein abundances in mature biofilms divided by the abundances in initial biofilms. Positive/negative values indicate increased/decreased proteins in mature biofilms.

With regard to nucleotide metabolism ribonucleoside-diphosphate reductase (RNR) subunits NrdA1 and B1, as well as the RNR NrdJ were decreased in mature biofilms. This was

accompanied by a reduction of the enzymes catalyzing cobalamin biosynthesis (Cbi/Cob), which is the cofactor of NrdJ (Torrents *et al.*, 2002) (Supplementary tables 1).

In addition, the amounts of more than forty ribosomal proteins (r-proteins) were significantly reduced in the mature state (Suppl. tables 1), suggesting a reduction of protein biosynthesis in mature biofilms. Coincident with this, similar responses were observed with components of the major protein export pathways (Sec and Tat, Suppl. tables 1).

In summary, the relative quantification of proteins identified proteins altered in abundance. Strong quantity increases in initial or mature biofilm samples suggest biofilm-specific responses. In some cases several functionally related proteins were found in elevated amounts, suggesting a stage-specific relevance (Table 14). Nevertheless, the picture of biofilm formation remained obscure, since only a small portion of the proteins showed pronounced alterations in the relative quantitation, while not all cellular processes were expected to change strongly. Therefore, a more comprehensive overview of the adaptations on the level of proteins is desireable.

Table 14 Overview of the biological processes showing the strongest changes.

	Functional category	Initial biofilm vs. planktonic cells	Mature biofilm vs. planktonic cells	Mature biofilm vs. initial biofilm
Increased			**Cellular processes**	
	Motility		Gvp	Gvp
	Stress response		Usp	Usp
			Metabolism	
	Energy	Arc, Dms	Dms, BR	Dms, BR
	Carbon	Glycolysis		Gluconeogenesis
	Amino acids		Hut	Hut, Dpp
	Nucleotides		Pur	Pur
	Lipids		Acd, Acs	Acd, Acs
	Ions		Trk	Trk
Decreased			**Information**	
	Ribosomes		Rpl, Rps	Rpl, Rps
	Protein export			Sec, Tat
			Cellular processes	
	Motility	Flg, Fla	Flg	
			Metabolism	
	Energy		Respiratory chain	
	Carbon	Gluconeogenesis		Glycolysis
	Amino acids		Car	
	Nucleotides	RNR	RNR	
	Cofactors		Cbi, Cob	Cbi, Cob

5.2.6. Grouping of co-trending proteins

Another quantitative data analysis approach took into account the strength of protein abundance changes as well as the overall trends observed in all three biological states. A grouping of similarly trending protein profiles by a 'Direction Scoring' analysis was performed in cooperation with Prof. Klaus Jung (Institute for Animal Breeding and Genetics, University of Veterinary Medicine, Hannover). As nomenclature, directions written in capitals (UP/DOWN) highlight significant and strong changes ($p < 0.05$ and $\log_2FC > 1$). Only the first character written in capital (Up/Down) indicates significant alterations ($p < 0.05$ and $\log_2FC < 1$). In contrast, small letters (up/down) mark non-significant transitions ($p > 0.05$). Primarily proteins that showed at least two significant changes in all three biological samples, or only one significant but strong shift between two of the states (*i.e.* proteins with a score greater than 2) were examined in the expression profile analysis (Supplementary tables 2).

These criteria were applicable to 882 proteins, corresponding to 34.2% of the proteome, respectively 54.1% of the proteins identified in the study. These proteins were sorted into four major groups (Figure 42A). The so-called Down-Down group (130 proteins) included proteins showing an overall downward trend in the abundance, *i.e.* highest amounts in planktonic cells and lowest in mature biofilms (Figure 42B). Proteins showing an Up-Down pattern (332) had the highest abundance in initial biofilm cells, while the opposite, *i.e.* lowest quantity, was true for members of the Down-Up group (295). Proteins exhibiting Up-Up patterns (125) showed a steady increase with highest abundance in mature biofilms compared to the planktonic lifestyle.

A

Score S	Proteins assigned to group			
	Down - Down	Up - Down	Up - Up	Down - Up
< 1	63	88	43	76
< 2	66	81	61	103
< 3	**65**	**131**	**57**	**120**
< 4	**28**	**47**	**52**	**68**
< 5	**32**	**122**	**12**	**75**
< 7	**5**	**32**	**4**	**32**
∑	**130**	**332**	**125**	**295**

B

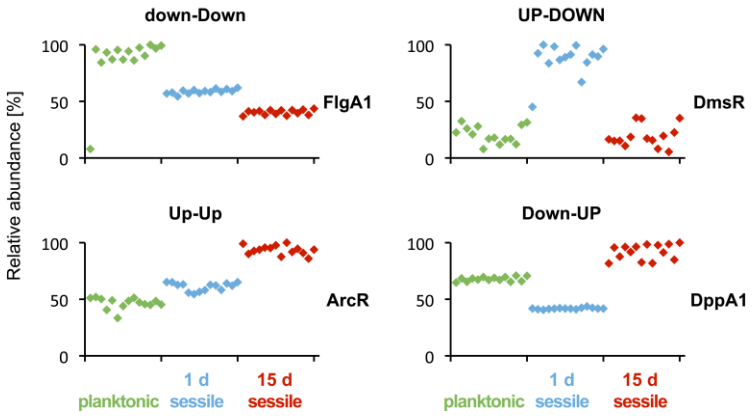

Figure 42 Direction Scoring analysis. **A**, Distribution of proteins with the respective Direction Scores (Score) to the four major groups (Down-Down, Up-Down, Up-Up and Down-Up). Also the total counts of proteins fulfilling the significance criteria assigned to the groups are indicated (∑). **B**, Expression profiles of selected proteins exemplary for the four major groups. Results of the Direction Score analysis are indicated above the plots (nomenclature as explained in the preceding text). Plots illustrate the relative abundance changes of the respective proteins in biological and technical replicates of the investigated sample states (planktonic, green; sessile 1 d, blue; sessile 15 d, red). Profiles shown correspond to archaellin A1 (FlgA1), transcriptional regulator of the DMSO reductase operon (DmsR), transcriptional regulator of the fermentative arginine degradation operon (ArcR) and subunit A1 of a peptide transporter (DppA1).

The biological processes associated with the four major groups of co-trending proteins (Table 15) will be described and discussed in the following section. In some cases complementary proteins were included in the biological interpretation and functional analysis, although they did not fulfill the aforementioned criteria. This was done when these proteins participate in the same processes and show similar trends compared with the proteins primarily identified, or in cases when the respective proteins were of special interest, for instance when their involvement in biofilm formation was known from previous studies.

Table 15 Processes affected by biofilm formation of *Hbt. salinarum* R1

	Function	Down-Down	Up-Down	Up-Up	Down-Up
Information	*DNA repair*	Uvr		Phr	Rad
	Replication		Pol & associates		
	Cell division and shape		FtsZ		FtsZ, MreB
	Transcription and regulators	TfbG, HTH	Rpo, TfbF, HTH, Trh	HTH, Trh	Lrp/AsnC, PadR, HxlR, TrmB
	Ribosome biogenesis	Rpl, Rps	Rpl, Rps		
	Protein biosynthesis, turn-over and export	Sec	Ths, Pan, Sec, Tat		Hsp
Cellular processes	*Motility and adhesion*	Flg, Fla		Pil, Gvp	Fla, Gvp
	Chemotaxis and signal transduction				Che, Htr,Bas, Cos, Mpc
	Stress response			Usp	Usp, Sod
	pH adaptation				Pha
	Glycosylation		Gth, Gtl	Agl	Gth, Gtl
	Energy conversion	Complex I, III, V, Hcp	Complex II, IV (Cba, Cox), V, Hcp, Arc	Complex IV (Cyd), Dms	BR & associates
Metabolism	*Amino acid metabolism*	Car		Hut	Arg, Dpp, Mmc
	Nucleotide metabolism	Pyr, RNR	Pyr	Pur	
	Carbon metabolism		Glycolysis, glycerol		Gluconeogenesis, PP pathway
	Lipid metabolism		Isoprenoids (Hmg)		Fatty acids (Asd, Acs, Aca, Fad)
	Cofactor metabolism	Cbi, Cob, Thi		Moe, Moa	
	Ion transport		Cpx, Sfu, Trk, Phn		Pho, Trk

Abbreviations used in the table are explained in the following text.

Down-Down group

Proteins showing steady decrease throughout biofilm development were involved in translation and ribosome biogenesis, as well as transcription and cell motility. Moreover, energy conservation, namely respiratory chain complexes were affected, accompanied by alterations concerning amino acid and nucleotide metabolism. One fourth of the proteins were annotated as *Poorly characterized*.

>Information processing

Ribosome biogenesis and protein biosynthesis. Several ribosomal proteins (r-proteins) showed a steady decrease. While in some cases their abundance was only slightly reduced in initial biofilms, strong reduction in mature biofilms was observed for almost all of them, with the most pronounced decline determined for r-protein S14. Downward trends were also detected regarding several other proteins associated with translation, for instance a few tRNA-ligases and translation factors, although the changes were mostly moderate. Moreover, the components SecD and SecF of one of the major protein secretion pathways [Sec, (Pohlschröder *et al.*, 1997)] showed decreases during biofilm development, similar to the signal peptidase Sec11. Taken together these findings suggest a lower protein biosynthesis especially in mature biofilms.

DNA repair. Similar responses were observed for the proteins UvrA and D involved in the nucleotide excission UV repair [Uvr, (Crowley *et al.*, 2006)] system. In its natural environment *Hbt. salinarum* encounters DNA-damaging conditions, such as UV-radiation and desiccation (DasSarma *et al.*, 2001). Therefore *Hbt. salinarum* possesses diverse DNA repair systems to maintain its genomic integrity (Capes *et al.*, 2011). Highest abundances of the Uvr proteins in planktonic cells implicate minor importance of this repair mechanism in biofilms.

Transcription. Three predicted HTH domain transcriptional regulators (OE2502R, OE4252R and OE4385F) showed steady decreases. Although their functions are so far unknown, it is conceivable that distinct regulators act at different developmental stages during biofilm formation.

>Cellular processes

Motility. Strong downward tendencies were detected for the two archaellins FlgB1 and B3, which was complemented by moderate decreases of FlgA1 and the accessory archaella protein FlaCE, while the archaella assembly/motor ATPase FlaI showed a decreasing tendency. Lower abundance of archaella in biofilms suggests a repression and underlines the non-motile sessile lifestyle. Especially the strong changes observed with the archaellins are in accordance with the fact that thousands of these proteins are forming the filaments.

>Metabolism

Energy metabolism. A number of proteins involved in the respiratory chain showed steady decreases. Among them were subunits of the NADH dehydrogenase (complex I), cytochrome *bc*1 (complex III), ATP synthase (complex V) and electron transfer halocyanins (Table 16, p. 97). These results suggest a depletion of the aerobic respiration in biofilms, presumably owing to anaerobic conditions.

Amino acid metabolism. Regarding amino acid metabolism, a strong reduction of glutamate dehydrogenase GdhA3 was observed in biofilm cells. Similar changes were the case with alanine dehydrogenase Ocd1, although less severe. Pronounced downward tendencies were detected for the carbamoyl phosphate synthase small and large subunits CarA and B, which are involved in the synthesis of carbamoyl phosphate precursors of arginine as well as pyrimidines (Ashworth *et al.*, 2014). CarAB have previously shown elevated protein amounts under anaerobic conditions (Tebbe *et al.*, 2009). Thus, the observed decrease is due to biofilm differentiation.

Nucleotide metabolism. Furthermore, decreases of the pyrimidine biosynthesis (Pyr) enzymes PyrB, C and I were determined. In addition, both subunits of the oxygen-dependent ribonucleoside-diphosphate reductase (RNR) NrdA1 and B1 showed distinct decreasing patterns. Similar alterations were observed for the cobalamin-dependent RNR, NrdJ (Lundin *et al.*, 2010), accompanied by reduction of the nucleoside-diphosphate kinase Ndk (Ishibashi *et al.*, 2001). Since RNRs are indispensable for replication (Torrents, 2014), lower replication activity in mature biofilms is implicated.

Cofactor metabolism. In accordance with the decrease of NrdJ, marked down-regulations were observed for the enzymes involved in the cofactor cobalamin biosynthesis [Cbi and Cob, (Warren *et al.*, 2002)], especially in mature biofilms. Among them the amounts of CbiG and CobH2 were the most reduced (see also Figure 41, p. 89). In addition, comparable responses were detected for some proteins encoded by ORFs from the same genetic *cbi/cob* locus (OE3218F, OE3219F and OE3224F), which to date have no assigned functions. A similar reduction of Cbi/Cob and NrdAB1 has been observed previously during the transition from aerobic to anaerobic conditions (Tebbe *et al.*, 2009).

>Poorly characterized

Altogether 32 of the 130 proteins within the Down-Down group were uncharacterized proteins, corresponding to 24.6%.

Table 16 Direction Score results of quantified proteins associated with energy conversion.

Symbol	Protein annotation	Accession[1]	Direction[2]	Score
Complex I				
nuoA	NADH dehydrogenase subunit A	B0R3U1	up-down	0.785336112
nuoB	NADH dehydrogenase subunit B	B0R3U2	Down-Down	3
nuoCD	NADH dehydrogenase subunit CD	B0R3U3	Down-Down	2.999999993
nuoH	NADH dehydrogenase subunit H	B0R3U4	Down-Down	2.999999798
nuoI	NADH dehydrogenase subunit I	B0R3U5	up-Down	1.999985778
nuoL	NADH dehydrogenase subunit L	B0R3U9	up-Down	1.949401882
nuoN	NADH dehydrogenase subunit N	B0R3V1	Down-down	1.991715826
Complex II				
sdhA	Succinate dehydrogenase subunit A (flavin)	B0R5B5	Up-Down	3
sdhB	Succinate dehydrogenase subunit B (Fe-S)	B0R5B6	down-Down	1.999984692
sdhC	Succinate dehydrogenase subunit C (Cyt*b*)	B0R5B8	Up-DOWN	5
Complex III				
petA	Cytochrome *bc1* complex (Fe-S)	B0R3P9	down-Down	1.999967823
petB	Cytochrome *bc1* complex (Cyt*b*)	B0R3P8	down-DOWN	3.999928643
petD	Cytochrome *bc1* complex (Cyt*b/c*)	B0R3P7	Down-Down	2.999999998
Complex IV				
coxA1	Cox-type terminal oxidase subunit I	B0R3V8	up-DOWN	3.999989666
cbaA	*Ba3*-type terminal oxidase subunit I	B0R7A7	Up-DOWN	5
cbaB	*Ba3*-type terminal oxidase subunit II	B0R7A8	Up-DOWN	4.999999998
cbaD[3]	*Ba3*-type terminal oxidase subunit III	B0R7A9	Up-Down	2.999995774
cydA1	Cytochrome *bd* ubiquinol oxidase subunit I	B0R8N5	up-UP	3.999976889
Complex V				
atpA	ATP synthase subunit A	B0R755	Down-Down	3
atpB	ATP synthase subunit B	B0R754	Up-Down	2.999999998
atpC	ATP synthase subunit C	B0R757	Up-Down	2.999997904
atpD	ATP synthase subunit D	B0R751	Up-Down	2.999999997
atpE	ATP synthase subunit E	B0R758	DOWN-Down	4.999999998
atpF	ATP synthase subunit F	B0R756	Up-Down	2.999999998
atpH	ATP synthase subunit H	B0R761	Down-Down	2.999998006
atpI	ATP synthase subunit I	B0R760	Up-Down	2.999999992
atpK	ATP synthase subunit K	B0R759	Up-Down	2.999999804
Halocyanins				
hcpA	Halocyanin HcpA	B0R612	Down-Down	2.999857913
hcpB[3]	Halocyanin HcpB	B0R7A9	Up-Down	2.999995774
hcpE	Halocyanin HcpE	B0R3Q1	Up-Down	2.999999989
hcpF	Halocyanin HcpF	B0R3P0	Down-Down	2.999999998
hcpG	Halocyanin HcpG	B0R2Z0	UP-DOWN	6.999999998
hcpH	Halocyanin HcpH	B0R456	up-DOWN	3.999876742
DMSO reductase				
dmsR	Transcriptional regulator	B0R486	UP-DOWN	7
dmsA	Dimethylsulfoxide reductase subunit A (reductase)	B0R488	UP-UP	6.999999998
dmsB	Dimethylsulfoxide reductase subunit B (e^- transfer)	B0R489	UP-UP	6.999999999
dmsC	Dimethylsulfoxide reductase subunit C (anchor)	B0R490	UP-UP	6.999999913
dmsD	Tat proofreading chaperone	B0R491	Down-Up	2.997856358
Arg fermentation				
arcA	Arginine deiminase	B0R9X5	UP-Down	4.999998427
arcB	Ornithine carbamoyltransferase	B0R9X3	UP-Down	4.999999998
arcC	Carbamate kinase	B0R9X4	UP-DOWN	6.999999998
arcD	Arginine/ornithine antiporter	B0R9X2	Up-Down	2.999999998
arcR	Transcriptional regulator	B0R9X6	Up-Up	3
Bacteriorhodopsin				
blp	Bacterioopsin-linked protein	B0R5N5	up-UP	3.999891912
bat	Bacterioopsin activator	B0R5N6	down-up	0.448280718
brp	Bacteriorhodopsin related protein	B0R5N7	down-UP	3.999955223
bop	Bacterioopsin	B0R5N9	Down-UP	4.999999506
bap	Bacterioopsin-associated protein	B0R5P0	down-UP	3.999621196

[1] UniProtKB accession number; [2] nomenclature as explained in the text, color code: highest respective protein abundance in planktonic cells (green), initial biofilms (blue) and mature biofilms (red), non-significant alterations shown in grey; [3] *cbaD* and *hcpB* genes are fused in the archaeon.

Up-Down group

Highest abundances in initial biofilms were seen for ribosomal proteins and a number of additional proteins associated with the translation and modification of tRNAs, and also with proteins involved in protein turnover and export. In addition, the transcription machinery and various transcription regulators indicated similar responses, as did the proteins involved in replication and cell division. Moreover, energy conversion mechanisms, central carbon metabolism, nucleotide biosynthesis and some ion transport components were affected, similar to proteins acting in lipid metabolism and glycosylation.

>Information processing

Ribosome biogenesis and protein biosynthesis. 41 of the 58 ribosomal proteins present in *Hbt. salinarum* R1 were assigned to the Up-Down group (Figure 43). While for many of them the changes in initial biofilms were moderate, the transitions from initial to mature biofilms often showed strong reductions. Among them S28e and L10e exhibited the strongest alterations. Also, a number of proteins connected with translation, *i.e.* translation factors, tRNA ligases and tRNA modifying enzymes showed similar patterns. This was accompanied by several proteins involved in protein turnover (Shukla, 2006), chaperones like GrpE and Hsp20A, as well as the thermosome subunits (GroEL homologs) Ths1 and 3. Moreover, components of the proteasome (Chamieh *et al.*, 2008), like the regulatory subunits Pan1 and Pan2 or PsmB showed similar responses. This was also the case regarding SecY and TatA involved in the two major protein export mechanisms [Sec and Tat, (Bolhuis, 2002)].

Similar to the ribosomal and protein biosynthesis proteins assigned to the Down-Down group, these findings implicate a reduced translational activity in mature biofilms. However, the highest abundances in initial biofilms detected for many of the proteins suggest a most active translation apparatus already in the early phase of biofilm growth, leading to the fundamentally different protein patterns observed between planktonic and biofilm cells.

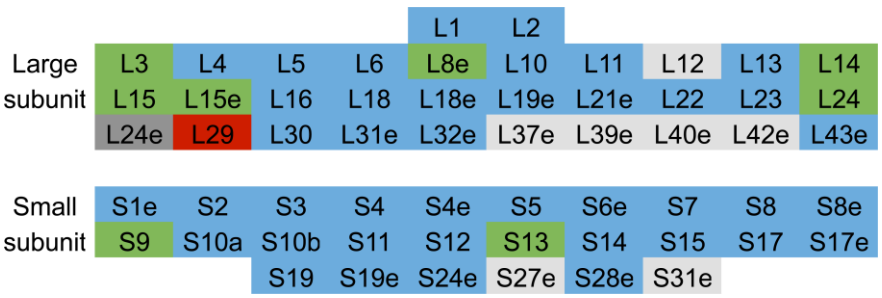

Figure 43 Highest abundances of the large and small subunit ribosomal proteins. Color code: Highest abundance of the respective proteins in planktonic cells (green), biofilms grown for 1 day (blue) and 15 days (red), respectively. Proteins lacking quantitative data are shown in dark grey. Undetectable proteins are shown in light grey.

Transcription. Almost all subunits of the DNA-directed RNA polymerase (Rpo) displayed Up-Down patterns, which was also detected for several transcription factors from diverse regulator families. Regarding the basal transcription machinery, transcription initiation factor TfbF was the only factor exhibiting a distinct profile (UP-DOWN). Quantitative data was only gained for two other basal factors, *i.e.* TfbG (Down-Down) and TATA-box binding protein TbpE (up-Up).

TATA-box binding proteins (TBP) and transcription initiation factors (TFB) are necessary for the recruitment of RNA polymerase to promoter regions during transcription initiation (Thomm, 1996). The above mentioned TFB and TBP were the only basal transcription factors with significant alterations in the present study, although there are six different TBP (A through F, with TBP A, B, C and D encoded by multiple gene copies) and eight TFB (A through H) in *Hbt. salinarum* R1 (www.halolex.mpg.de). Incomplete identification of the TFB/TBP was also the case in previous studies, probably owing to the abundance of the basal transcription factors. Only TbpE and TfbG, which are both chomosomally encoded, were frequently identified (Gan *et al.*, 2006; Leuko *et al.*, 2009; Tebbe *et al.*, 2009). Quantitative analyses in *Hbt. salinarum* PHH1 showed that the transcription level of *tbpE* is 8-fold higher compared to the other TBP encoding genes (Teufel *et al.*, 2008). Moreover, TbpE is the major TATA-box binding factor under standard conditions and the only chromosomally encoded and universally present TBP in strains of *Hbt. salinarum*, while TfbF is supposed to be the dominant TFB in exponentially growing cells (Facciotti *et al.*, 2010). It has been suggested that different combinations of the various TBP and TFB proteins in *Hbt. salinarum* initiate transcription in reaction to different growth conditions, similar to the sigma factor regulated transcriptional responses in bacteria (Baliga *et al.*, 2000). Differential expression of the *tfb* genes was observed after cold and heat shock in strains of *Hbt. salinarum* (Bleiholder *et al.*, 2012). The hypothesis is supported by the differential responses of the TBP and TFB proteins detected in consequence of biofilm formation in the present study. In a previous report investigating the role of TFBs in the global gene regulatory network of *Hbt. salinarum* NRC-1, TfbF correlates with the expression of ribosomal protein encoding genes, while TfbG correlates with that of the archaella (Facciotti *et al.*, 2007). Both observations are supportet by the present study. TfbF showed an Up-Down response, similar to most ribosomal proteins, whereas Down-Down patterns were observed for TfbG and diverse archaella associated proteins. These observations connect TfbF with the cellular activity and TfbG with motility of the cells.

The strongest alterations among the transcriptional regulators were observed for the PadR family regulator PadR1, which is the equivalent to the *Hbt. salinarum* NRC-1 regulator RosR (reactive oxygen species regulator). RosR is required for reactive oxygen species resistance in

this strain (Sharma *et al.*, 2012). Two genes encoding a putative ribonuclease HI (OE1400F) and TfbG are located adjacent to the gene *padR1*, both showing steady reduction in biofilm cells.

The two regulators PadR2 and SirR were both moderately induced in the initial biofilm stage and still slightly more abundant in mature biofilms compared to planktonic cells, while the Lrp/AsnC family transcription regulator Trh3 showed a marked reduction in the mature stage, comparable to a predicted HTH domain regulator (OE3125R). The gene *trh3* is located adjacent of the carbamoyl phosphate synthase genes *carAB*, acting in amino acid metabolism, which both showed strongly decreasing levels in biofilms. This proposes an involvement of Trh3 in the regulation of *carAB* and supports previous reports (Ashworth *et al.*, 2014). The function of the other regulators that showed similar patterns is elusive.

Replication and cell division. Proteins involved in DNA-replication (Berquist *et al.*, 2007; Makarova & Koonin, 2013) exhibited mostly Up-Down patterns. Sometimes a clearly reduced amount in mature biofilms was observed (Table 17). Similar patterns were detected for several cell division proteins (FtsZ1, 2 and 3) (Faguy & Doolittle, 1998) and chromosome partition proteins (Smc and Sph2). In addition, several enzymes involved in the pyrimidine biosynthesis (Pyr) exhibited Up-Down responses. In contrast, two other proteins involved in cell division (FtsZ4 and the MreB/Mbl homolog OE1259R) showed slightly decreased levels in the initial biofilm state, while a clear induction in mature biofilm cells was the case (Down-Up patterns).

Table 17 Direction Score results of quantified proteins associated with replication.

Symbol	Protein annotation	Accession[1]	Direction[2]	Score
fen	Flap endonuclease 1	B0R5F5	Up-Down	2.99998825
ginS	DNA replication factor	B0R5P2	Up-DOWN	4.99999999
gyrA	DNA gyrase subunit A	B0R4D5	Up-Down	2.99999999
gyrB	DNA gyrase subunit B	B0R4D4	Up-DOWN	4.99999993
mcm	ATP-dependent DNA helicase	B0R796	up-DOWN	3.99999194
nucS	Endonuclease NucS	B0R6T6	UP-DOWN	6.99999651
pcn	DNA polymerase sliding clamp	B0R7F7	Up-Down	2.99999999
polB	DNA polymerase II small subunit	B0R7U1	down-up	0.81251150
polD2	DNA polymerase II large subunit	B0R7M9	Up-Down	3
priL	DNA primase large subunit	B0R7F5	up-DOWN	3.99997930
priS	DNA primase small subunit	B0R5P1	Up-Down	2.99999563
recJ1	Single-stranded-DNA-specific exonuclease	B0R7M5	Up-Down	2.99999978
rfcL	Replication factor C large subunit (clamp loader)	B0R601	Up-Down	2.99999967
rfcS	Replication factor C small subunit (clamp loader)	B0R7H7	Up-Down	2.99999999
rpa3	Replication protein A	B0R776	Up-Down	2.99999905
topA	DNA topoisomerase 1	B0R363	Up-DOWN	4.99999989

[1] UniProtKB accession number; [2] nomenclature as explained in the text, color code: highest respective protein abundance in planktonic cells (green), initial biofilms (blue) and mature biofilms (red), non-significant alterations shown in grey

Slight increases of replication proteins in initial biofilm cells indicate an increased cellular activity. This is in agreement with the more active translation, as well as higher abundances of several proteins associated with cell division at this stage. However, it is in contrast to the

reduction of ribonucleoside-diphosphate reductases (RNR), which are indispensable for replication (Torrents, 2014). Since *Hbt. salinarum* cells are polyploid (Breuert *et al.*, 2006), a reduction of the genome copy number is possible, but this was not yet investigated.
Decreases of RNR in mature biofilms suggest a reduced cellular activity and cell division at this stage, *i.e.* potentially resting cells, which is in agreement with other changes observed regarding protein biosynthesis, transcription, nucleotide metabolism, cell division and energy conversion. However, it is in contrast to increased amounts of the cell division proteins FtsZ4 and OE1259R.

>Cellular processes

Glycosylation. Up-Down tendencies were also observed with several predicted glycosyltransferases (Table 18), like the type 1 glycosyltransferases Gth2, 3 and 6 as well as the type 2 glycosyltransferase Gtl6. In contrast, the two glycosyltransferases (Gth8 and Gtl4) exhibited Down-Up patterns, with highest abundances in mature biofilms.

Table 18 Direction Score results of proteins (potentially) associated with glycosylation

Symbol	Protein annotation	Accession[1]	Direction[2]	Score
Predicted glycosyltransferases				
gth2	Probable glycosyltransferase, type 1	B0R3R3	up-Down	1.99788147
gth3	Probable glycosyltransferase, type 1	B0R3B0	UP-down	3.99063803
gth4	Probable glycosyltransferase, type 1	B0R2J5	down-up	0.81588114
gth5	Probable glycosyltransferase, type 1	B0R2J7	up-down	0.92598929
gth6	Probable glycosyltransferase, type 1	B0R8G0	Up-Down	2.99999995
gth7	Probable glycosyltransferase, type 1	B0R4S4	down-up	0.09825757
gth8	Probable glycosyltransferase, type 1	B0R4P2	DOWN-UP	6.99998185
gtl3	Probable glycosyltransferase, type 2	B0R6Z3	up-down	0.93571441
gtl4	Probable glycosyltransferase, type 2	B0R324	Down-UP	4.99999635
gtl5	Probable glycosyltransferase, type 2	B0R307	Down-up	1.99766738
gtl6	Probable glycosyltransferase, type 2	B0R4F7	Up-DOWN	4.99999831
Archaeal glycosylation pathway proteins				
aglB	Dolichyl oligosaccharide-protein glycotransferase	B0R4T2	Down-DOWN	4.99999999
aglF1	Sugar nucleotidyltransferase	B0R8F7	down-Up	1.98022126
aglF2	Sugar nucleotidyltransferase	B0R4S0	Down-up	0.49655884
aglG	Glycosyltransferase	B0R4T1	down-down	0.77884955
aglJ	Dolichyl-phosphate hexosyltransferase	B0R4R8	up-Up	1.99998132
aglM1	UDP-glucose 6-dehydrogenase	B0R4R5	Up-Up	3
aglM2	UDP-glucose 6-dehydrogenase	B0R8F6	Up-DOWN	4.99999945
aglQ	AglQ family protein	B0R4S3	Up-up	1.95559777

[1] UniProtKB accession number; [2] nomenclature as explained in the text, color code: highest respective protein abundance in planktonic cells (green), initial biofilms (blue) and mature biofilms (red), non-significant alterations shown in grey

Extracellular polymeric substances (EPS) are a major trait of biofilms (Flemming & Wingender, 2010) and glycosyltransferases as well as sugar-modifying enzymes play important roles in the synthesis of EPS glycoconjugates and exopolysaccharides, as demonstrated in bacterial biofilms (Koo *et al.*, 2010; Lebeer *et al.*, 2009). Thus, the involvement of the aforementioned enzymes in the synthesis of considerable amounts of extracellular glycoconjugates within the biofilms of *Hbt. salinarum* R1 (see also Chapter 3) is possible, but this needs to be proven by gene deletion

and complementation analyses, as performed in *Sulfolobus* species (Koerdt *et al.*, 2012; Orell *et al.*, 2013b).

A similar Up-Down pattern was observed with AglM2 (Table 18, p. 101) acting in the archaeal glycosylation pathway [Agl, (Kandiba & Eichler, 2015)], while other proteins involved in the Agl pathway displayed variable trends. Upward tendencies were observed with AglM1, AglJ, and AglQ.

Agl is the major mechanism for protein modification by glycans in *Hbt. salinarum* (Eichler *et al.*, 2013). It was demonstrated in different archaeal species that the Agl pathway acts for instance in the modification of the cell surface glycoproteins (S-layer protein) as well as archaellins and pilins (Meyer *et al.*, 2015; Pohlschröder & Esquivel, 2015).

>Metabolism

Energy metabolism. Regarding energy metabolism, several subunits of respiratory chain complexes also showed Up-Down responses (Table 16, p. 97). This was found with subunits of succinate dehydrogenase (complex II), *ba*3-type terminal oxidase (complex IV), cox-type terminal oxidase (alternative complex IV) and ATP synthase (complex V). Additionally, several electron transfer halocyanins (HcpB, E, G and H) (Falb *et al.*, 2005) showed similar patterns. These results suggest an adjustment of the respiratory chain in biofilm cells of *Hbt. salinarum* R1.

Also, enzymes catalyzing the fermentative arginine degradation (Arc) showed comparable Up-Down patterns, *i.e.* ArcA-D (Figure 44). This alternative energy conversion pathway is encoded by the operon *arcRACBD* (see also Figure 37, p. 86) (Ruepp & Soppa, 1996). The corresponding repressor (ArcR) exhibited a different profile (Up-Up). However, activation of the Arc pathway in initial biofilm cells is indicated, whereas it decreases at the mature biofilm stage.

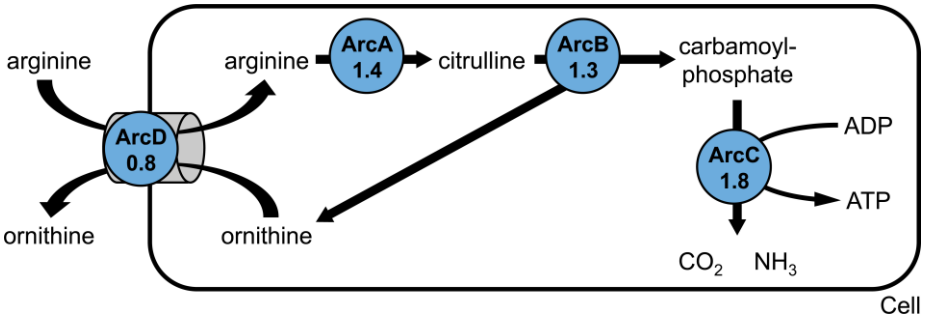

Figure 44 Schematic representation of the fermentative arginine degradation pathway. Enzymes involved are the arginine-ornithine antiporter (ArcD), arginine deiminase (ArcA), ornithine carbamoyltransferase (ArcB) and carbamate kinase (ArcC). Numbers indicate regulation factors (in $\log_2$ scale) of the respective enzymes in initial biofilm cells compared to planktonic cells.

Carbon metabolism. A number of central C-metabolism enzymes (Falb *et al.*, 2008) displayed Up-Down patterns, as well, *e.g.* glycerol metabolizing enzymes like glycerol dehydrogenase (GldA1), glycerol-3-phosphate dehydrogenase (GlpA1, B and C) and glycerol kinase (GlpK). This is interesting, since biofilm formation of the bacterial species *Bacillus subtilis* is promoted by glycerol via histidine kinase signaling (Shemesh & Chai, 2013). A similar role of glycerol in *Hbt. salinarum* R1 biofilms is conceivable, which is substantiated by the presence of a number of histidine and other kinases in the proteome, several of which showed upward trends in biofilms. Glycerol is abundant in the natural habitat of *Hbt. salinarum* where it is produced *e.g.* by the halophilic green algae *Dunaliella* as compatible solute (DasSarma & DasSarma, 2001).

Comparable Up-Down responses were detected for 2-keto-3-deoxygluconate kinase (KdgK), involved in the semi-phosphorylated Entner-Doudoroff (ED) pathway, which is a modified variant of the classical ED pathway for glucose degradation common in haloarchaea (Bräsen *et al.*, 2014; Hochstein, 1974; Verhees *et al.*, 2003). In addition, further glycolysis enzymes (Falb *et al.*, 2008) like triosephosphate isomerase (TpiA) and enolase (Eno) showed similar responses, as well as pyruvate kinase (PykA) which catalyzes the last and irreversible step of glycolysis. Thus, the glycolytic pathway seems to be most active in initial biofilms.
In comparison, subunits of the pyruvate-ferredoxin oxidoreductase, pyruvate dehydrogenase as well as the enzymes acting in the citric acid cycle showed minor changes only, underlining their permanent importance in the central metabolism.

Lipid metabolism. Up-Down alterations were also observed with enzymes acting in the mevalonate pathway required for the synthesis of membrane lipids and bacterioruberins (Smit & Mushegian, 2000). Most of these enzymes showed weak changes, except for the initial enzyme of the pathway, *i.e.* hydroxymethylglutaryl-CoA synthase (HmgB; Up-DOWN).
One can speculate that a molecular rearrangement of the biofilm cells, which was indicated by transcriptional and translational processes after one day already, might also affects lipids, *e.g.* the biofilm lifestyle might lead to an alteration of the cellular envelope. Such phenomena are observed in the eukaryotic species *Candida albicans* and the bacterial species *Pseudomonas aeruginosa* where the lipid compositions of planktonic and biofilm cell membranes deviate considerably (Benamara *et al.*, 2014; Lattif *et al.*, 2011). In *C. albicans* the lipid composition had an effect on the ability to form biofilms, while in *P. aeruginosa* the lipid composition even varied between biofilm cells of different ages. For archaeal cell membranes the composition has not yet been investigated in biofilms, but it is possible that alterations occur.

Ion transport. Diverse proteins involved in metal ion transport also exhibited Up-Down patterns, for instance the iron transport system [Sfu, (Angerer *et al.*, 1992)] component SfuA

and two proteins involved in Fe^{3+}-hydroxamat transport (OE4576F and OE4593R). The predicted copper transport ATPase Cpx (Srivastava & Kowshik, 2013) did not display significant changes in initial biofilms, but was reduced in the mature state.

On one hand metals play important roles in the physiology of the cells, *e.g.* with regard to electron transport processes or as cofactors of enzymes, while on the other hand they can also exert toxic consequences on microorganisms (Srivastava & Kowshik, 2013). This explains the diverse regulatory effects observed with different metal metabolism proteins, which presumably aim at maintenance of metal ion homeostasis. Metals can have effects on biofilm formation, as well, which was previously shown, *e.g.* in *P. aeruginosa* (Banin *et al.*, 2005) and *Hbt. salinarum* R1 (unpublished results S. Völkel & S. Fröls; Master thesis S. Völkel, 2015), while biofilms can also improve toxic metal resistance of cells (Flemming & Wingender, 2010).

>Poorly characterized

25.9% of the proteins assigned to the Up-Down group were uncharacterized proteins (*e.g.* OE1239F, OE2191F, OE3639F, OE3849F, OE6188R and OE6191F) or proteins with a general function prediction only. Some of these proteins exhibited pronounced UP-DOWN patterns, like AhbC and D involved in heme synthesis (Storbeck *et al.*, 2010).

Up-Up group

Continuous increased protein amounts were observed with a number of tRNA-modifying enzymes as well as diverse transcriptional regulators and chromosome/chromatin associated proteins. Moreover, proteins related to the cell envelope and motility, alike factors involved in signaling and stress response showed similar variations. In addition, energy metabolism as well as amino acid and nucleotide metabolism were affected. About one fourth of the proteins falling in the Up-Up group were *Poorly characterized* proteins.

>Information processing

Ribosome biogenesis and protein biosynthesis. A single ribosomal protein (Rpl29) was found to show an upward trend in biofilms (Figure 43), similar to several tRNA modifying enzymes, like tRNA-ligases.

Transcription. More than ten transcriptional regulators from various transcriptional regulator families were assigned to the group, with pronounced changes determined for three predicted HTH-10 family regulators (OE1263F, OE2253F and OE6196R), similar to the Lrp/AsnC family transcription regulator Trh6. To date nothing is known about their function, but they are of special interest due to their constant increases throughout biofilm development.

Moreover, three GNAT (Gcn5-related *N*-acetyltransferase) family proteins (OE1291R, OE1974R and OE3300F) increased steadily, regarding OE1291R and OE1974R especially in mature biofilm samples. Similar responses were observed for the archaeal histone HstA and a nonhistone chromosomal protein (OE4509F).

OE1291R and OE1974R contain pfam13673 multidomains known from proteins with N-acetyltransferase functions, which play roles in chromatin remodeling during transcription in yeast (Han *et al.*, 2008). However, the existence of transcriptional regulation by histone modification (acetylation/ deacetylation) is an open question in Archaea (Peeters *et al.*, 2015). Only genetic analyses in *Hfx. volcanii* have proven that the histone deacetylase *hdaI* is essential for viability (Altman-Price & Mevarech, 2009). The *hdaI* homolog of *Hbt. salinarum* R1 (OE1221F) is located next to the H3/H4 fusion histone encoding gene *hstA* (OE1220F), similar to the location of this gene in *Hfx. volcanii*. The corresponding proteins (Hda1 and HstA) showed constant increases in biofilm cells, similar to the protein MC1 (OE4509F), which mediates DNA compaction and bending (Reeve, 2003). Slight up-regulation under anaerobic phototrophic conditions was detected for HstA only (Tebbe *et al.*, 2009), indicating a biofilm-

specific reaction of the other aforementioned histone associated proteins, possibly involved in regulation of the molecular differentiation.

DNA repair. Moreover, three proteins (Phr1-3) associated with the *Hbt. salinarum* photoreactivation repair [Phr, (Takao *et al.*, 1989)] pathway of UV-damaged DNA showed constant increases during biofilm development, *i.e.* highest abundances in mature biofilms. This is in contrast to the aforementioned decrease of the Uvr mechanism involved in the dark repair of UV lesions (Crowley *et al.*, 2006), and suggests major importance of the Phr pathway in biofilms.

>Cellular processes

Motility. *Hbt. salinarum* R1 contains two gas vesicle protein (Gvp) encoding operons located on the plasmids pHS1 (p-vac region; see also Figure 40, p. 89) and pHS3 (c-vac region) (Englert *et al.*, 1992). Mainly proteins encoded by the p-vac were detected in the present study showing highest amounts in mature biofilms, namely the accessory gas vesicle proteins GvpFHJKL1 (Table 19). The transcriptional activator, GvpE1, was enhanced in the mature state, similar to GvpD1 counteracting GvpE. In contrast, the proteins GvpACNO1 were not detectable, due to an ISH3 insertion element in the promoter of the respective *gvpACNO1* transcription unit, also encoding the main structural proteins GvpA and GvpC (Pfeifer, 2015). For this reason *Hbt. salinarum* strain R1 is gas vesicle negative, in contrast to strain DSM3754 that contains gas vesicles in mature biofilm cells (Fröls *et al.*, 2012). The results are in agreement with the fact, that gas vesicles are usually used to cope with stress conditions (*e.g.* with respect to oxygen or nutrients) that also occur in the mature biofilms.

Table 19 Direction Score results of gas vesicle proteins (Gvp)

Symbol[1]	Protein annotation	Accession[2]	Direction[3]	Score
gvpM1	Gas vesicle protein	B0R8K4	n.q.	
gvpL1	Gas vesicle protein	B0R8K5	Down-Up	2.99999996
gvpK1	Gas vesicle protein	B0R8K6	DOWN-UP	7
gvpJ1	Gas vesicle protein	B0R8K7	Down-UP	4.99999998
gvpI1	Gas vesicle protein	B0R8K8	n.d.	
gvpH1	Gas vesicle protein	B0R8K9	up-UP	3.99923338
gvpG1	Gas vesicle protein	B0R8L0	n.q	
gvpF1	Gas vesicle protein	B0R8L1	Up-Up	2.99999953
gvpE1	Transcription activator GvpE	B0R8L2	up-UP	3.99996538
gvpD1	Regulatory protein GvpD	B0R8L3	down-UP	3.99999177
gvpA1	Gas vesicle protein	B0R8L5	n.d.	
gvpC1	Gas vesicle protein	B0R8L6	n.d.	
gvpN1	Gas vesicle protein	B0R8L7	n.d.	
gvpO1	Gas vesicle protein	B0R8L8	n.d.	

[1]Genes *gvpD-M1* and *gvpACNO1* located on pHS1 (p-vac), only gene products of the p-vac region are shown; [2] UniProtKB accession number; [3] nomenclature as explained in the text, color code: highest respective protein abundance in planktonic cells (green), initial biofilms (blue) and mature biofilms (red), non-significant alterations shown in grey; n.d., not detectable; n.q., not quantifiable.

The protein GvpO2 was the only exception, showing continuous decrease, *i.e.* highest amounts in planktonic cells. It was one out of five pHS3-encoded Gvp detected and the only one that showed significant changes.

Stress response and signal transduction. Similar upward tendencies were also determined for three universal stress proteins [Usp, (Nachin *et al.*, 2005)] containing UspA domains (OE3162F, OE3668F and OE5066R) (see also Table 20, p. 111). Moreover, the serine/threonine kinase PrkA1, as well as two histidine kinases (Ark and OE2964F) exhibited upward trends, while different patterns (Down-Up), but also highest abundances in mature biofilms, were detected for several additional kinases (KinA1, OE3462R, OE4283R, PrkA2 and Rio1).
Kinases can be involved in signal cascades. A role for a serine/threonine kinase (PknB) during development of *Staphylococcus aureus* biofilms is known (Hussain *et al.*, 2006), while control of archaellation of *Sulfolobus acidocaldarius* also depends on two serine/threonine kinases (Saci1193 and Saci1694) (Reimann *et al.*, 2012).

Adhesion. It was shown recently that *Hbt. salinarum* R1 is able to adhere to surfaces mediated by type IV-like pili (Losensky *et al.*, 2014). However, the identity of the filament subunits (pilins) remained unknown (see also Chapter 4). Quantitative data for some of the putative pilin candidates previously identified by a bioinformatical search was gained in the SWATH/LC/MS/MS analysis. The two candidate pilins PilA6 (OE1501F) and PilA8 (OE2586F) showed up-UP and down-UP patterns, respectively, with highest abundances in mature biofilm samples. In comparison, PilA7 yielded a (non-significant) up-down pattern, but its protein abundance tended to be distinctly increased at the initial biofilm stage. Interestingly, the genes *pilA6* and *pilA7* showed prominent transcript profiles with highest amounts in initial biofilm cells (see also Chapter 4.2.6). The uncharacterized conserved protein encoded by the ORF OE3292F exhibited an up-UP pattern, as well. Although it contains an archaeal class III (type IV pilin-like) signal peptide, the predicted protein appears to be too large (70 kDa) for a pilin, since pilins are usually rather small proteins [< 20 kDa, (Giltner *et al.*, 2012)].

>Metabolism

Energy metabolism. All subunits, DmsABC, of the dimethylsulfoxide (DMSO) reductase were more abundant in initial and even higher in mature biofilms. This was accompanied by strong increase of the HTH-10 regulator DmsR, the putative activator of the DMSO reductase operon (*dms*) (Müller & DasSarma, 2005). The enzyme represents an alternative terminal oxidase using electron acceptors like DMSO or TMAO (Müller & DasSarma, 2005). Also, proteins (MoaBE,

MoeA1-2) acting in biosynthesis of its molybdenum cofactor (Müller & DasSarma, 2005) showed moderate upward trends during biofilm development.

Moreover, subunit CydA1 of an alternative terminal oxidase (complex IV analogon) was the only component of the respiratory chain exhibiting an upward trend during biofilm formation (Table 16, p. 97), in contrast to the Down/Up-Down patterns observed with other respiratory chain complexes. It was demonstrated previously that this *d*-type cytochrome oxidase is markedly up-regulated under anaerobic conditions in *Hbt. salinarum* NRC-1, alike the *dms* genes. These findings underline an adjustment of the respiratory chain in biofilm cells, in response to anaerobic conditions.

Amino acid metabolism. With regard to amino acid metabolism a number of proteins exhibited up-UP patterns, *i.e.* non-significant changes in initial biofilms but strong induction in the mature biofilm state. Of these the strongest alterations were observed for the proteins HutG, H and U, involved in histidine utilization [Hut, (Bender, 2012), Figure 45], which are encoded by an operon (see also Figure 39, p. 88)

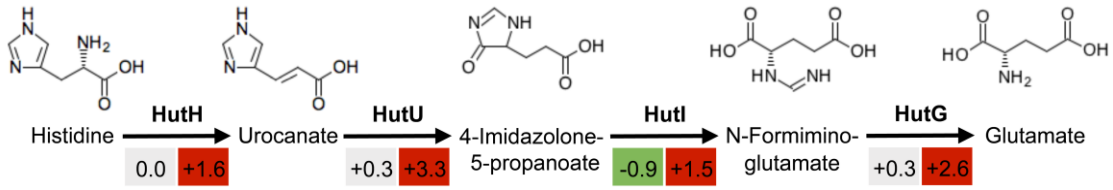

Figure 45 Histidine utilization pathway. The reactions are catalyzed by the enzymes histidine ammonia-lyase (HutH), Urocanase (HutU), Imidazolonepropionase (HutI) and Formimidoylglutamase (HutG). Numbers indicate fold change (in $\log_2$ scale) of the respective enzymes in initial (left box) and mature (right box) biofilms compared to the planktonic state. Color code displays higher amounts in initial biofilms (blue), mature biofilms (red) or planktonic cells (green) and non-significant changes (grey). (Kyoto Encyclopedia of Genes and Genomes, www.genome.jp/kegg)

Nucleotide metabolism. Most enzymes participating in purine biosynthesis [Pur, (Brown *et al.*, 2011)] also showed constant increase throughout biofilm development (Figure 46, p. 109), with PurD, PurNH and PurK exhibiting the strongest effects.

Up-regulation of genes involved in purine biosynthesis was also observed in bacterial *Bacillus cereus* biofilms. It has been shown, that exponential cells of this species are decorated with extracellular DNA (eDNA), which is no longer the case upon deletion of the *purA* gene. Moreover, indication has been found that eDNA acts as adhesin and is required for biofilm formation of *B. cereus* (Vilain *et al.*, 2009), while the role of eDNA observed in biofilms of *Hbt. salinarum* R1 is unknown (see also Chapter 3).

Cofactor metabolism. Increases of the Pur proteins are in contrast to enzymes involved in the biosynthesis of thiamine (ThiB, C and I), which were mainly decreased in biofilms. Since both

biosynthesis pathways are coupled (Figure 46), the results suggest that only the thiamine branch is shut down in biofilms (Brown *et al.*, 2011). Decreased amounts of the thiamine synthesis machinery was also observed under anaerobic conditions (Tebbe *et al.*, 2009). Thiamine is for instance cofactor of the E1 component of the pyruvate dehydrogenase complex, which did not undergo major changes in biofilms.

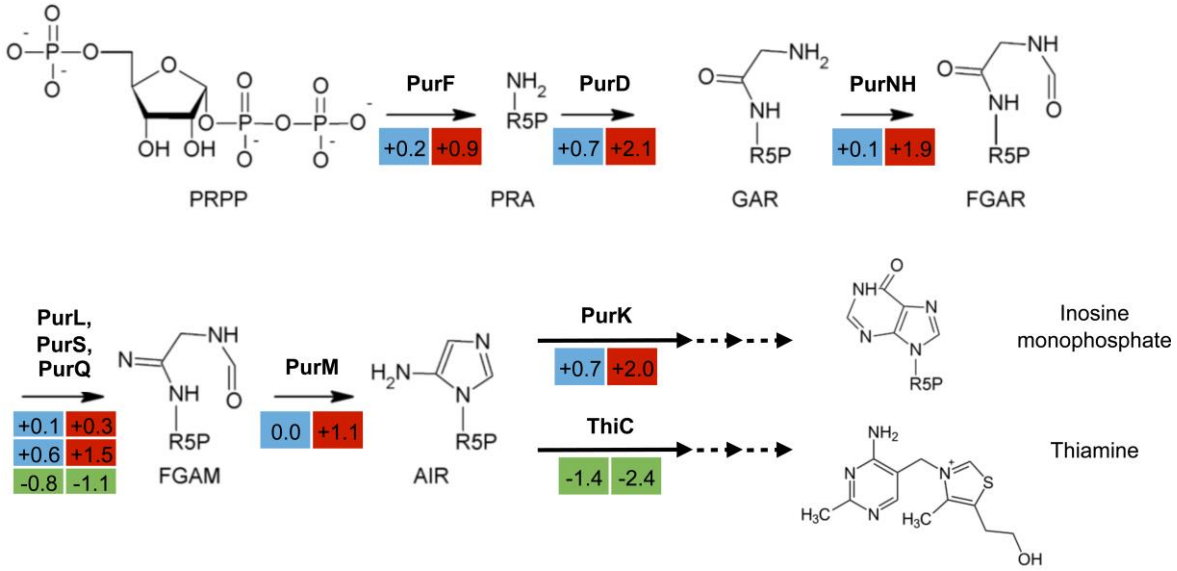

Figure 46 Initial steps in the *de novo* biosynthesis of purines and thiamine. The first steps catalyzed by the enzymes PurF, PurD, PurNH, PurL, PurS, PurQ and PurM are common to both biosynthesis pathways. Purine synthesis is resumed by PurK, while the thiamine branch is carried on by ThiC. Numbers indicate fold change (in $\log_2$ scale) of the respective enzymes in initial (left box) and mature (right box) biofilms compared to the planktonic state. Color code displays higher amounts in initial biofilms (blue), mature biofilms (red) or planktonic cells (green). Broken arrows indicate synthesis steps omitted. Abbreviations: PRPP, phosphoribosyl pyrophosphate; PRA, 5-phospho-β-D-ribosylamine; GAR, glycinamide ribonucleotide; FGAR, N-Formylglycinamide ribonucleotide; FGAM, 5'-Phosphoribosylformylglycinamidine; AIR, Aminoimidazole ribotide. (Modified from Brown *et al.*, 2011)

>Poorly characterized

35 of the 125 proteins assigned to the Up-Up group (28%) had only a general function prediction or unknown functions. Nevertheless, some of these proteins showed pronounced upward trends, such as two uncharacterized proteins (OE3545F and OE2806F) or a predicted metal-binding protein (OE1376R).

Down-Up group

Lowest abundances in the initial biofilm state and increases at the mature stage were observed for a few proteins associated with translation and protein turnover. Moreover, several GNAT acetyltransferases and transcriptional regulators from different regulator families showed similar responses. Additionally, proteins involved in motility and chemotaxis as well as cell signaling and stress response were assigned to the group. Comparable alterations were found with proteins acting in energy conservation and enzymes involved in the central C-metabolism. Also, amino acid and lipid metabolism as well as ion transport were affected. Almost one third of the proteins within the Down-Up group were *Poorly characterized* proteins.

>Information processing

DNA repair. Proteins involved in DNA double-strand break repair (Rad50 and RadA) yielded Down-Up patterns (Delmas *et al.*, 2009), while further proteins involved in the pathway (RadB, Mre11 or NurA) did not show strong alterations but similar tendencies. Homologous recombination has the potential to promote genetic diversification and to increase the resistance against unstable environmental conditions, as demonstrated in *Pseudomonas aeruginosa* biofilms (Boles *et al.*, 2004). Polyploidy of *Halobacterium* represents a potential mechanism favoring gene diversification and the acquisition of new functions, as well (Breuert *et al.*, 2006).

Transcription. Several GNAT family acetyltransferases were sorted into the Down-Up group, with OE1722R, OE4260R and OE4543R showing the strongest alterations. A potential role of GNAT family acetyltransferases is discussed on p. 105.

Furthermore, a number of transcriptional regulators from various families followed Down-Up responses. The Lrp/AsnC family transcription regulators AsnC, OE3711R and Trh5 were most abundant in mature biofilms, whereas a PadR family regulator (OE2108F) had the highest abundance in planktonic cells. In comparison, the changes observed with a HxlR family regulator (OE2047R) and a TrmB family regulator (OE3081F) were less pronounced.
The Lrp/AsnC family is a major family of transcriptional regulators found in haloarchaea. More than ten genes encoding members of the family are found in *Hbt. salinarum* R1, while the genes that they regulate are currently unknown. This is also true for the PadR family, with eight homologs in *Hbt. salinarum* R1, and the other aforementioned transcriptional regulators.

>Cellular processes

Stress response. The two superoxide dismutases Sod1 and Sod2 exhibited similar Down-Up changes, alike a number of putative universal stress proteins [Usp, (Siegele, 2005)], containing

UspA domains (OE2097F, OE3187R, OE3346R, OE4540R, OE4544R and OE5254F) (Table 20). Dodecin, a binding and protection protein of flavin derivatives like FMN and FAD (Grininger *et al.*, 2009), exhibited also a distinct DOWN-UP response.

DNA damage as well as damage of other biomolecules like lipids, proteins and carbohydrates is caused by reactive oxygen species (ROS). ROS are a byproduct of aerobic respiration and can also be increased by UV, radiation or desiccation (Rastogi *et al.*, 2010). For the detoxification of ROS *Hbt. salinarum* possesses a network of dismutases, peroxidase and catalase enzymes (Kaur *et al.*, 2010). In contrast to the peroxidase/catalase KatG, a putative peroxidase and the superoxide dismutases Sod1 and Sod2 were present in higher amounts in mature biofilm cells, with Sod2 showing the strongest increase. This is in contrast to the observations made with regard to the proteins of the respiratory chain, which are reduced in *Hbt. salinarum* R1 biofilms and replaced by other mechanisms. Since respiratory chains are the main source of ROS (Imlay & Fridovich, 1991), the corresponding detoxification mechanisms should go in parallel with these. However, spatial proximity of the cells within biofilms might result in the accumulation of ROS, and the observed response might be part of a general stress response in biofilms.

The universal stress proteins (Usp), several of which exhibited constant increases throughout biofilm development, support this notion. Usp act in manifold cellular processes concerning stress response, DNA repair, adhesion and motility in *E. coli* (Siegele, 2005). In addition, biofilm formation of *Porphyromonas gingivalis* cells was impaired upon inactivation of an Usp encoding gene (Chen *et al.*, 2006), and Usp occur in elevated amounts in *Sulfolobus solfataricus* biofilms (Koerdt *et al.*, 2011). *Hbt. salinarum* R1 possesses a repertoire of 17 Usp encoding genes, with so far unassigned functions. The plethora of Usp and their differential expression suggests similar processes in halobacterial biofilms.

Table 20 Direction Score results of putative universal stress proteins.

Symbol	Protein annotation	Accession[1]	Direction[2]	Score
OE1911R	UspA domain protein, nucleotide-binding	B0R3R6	Up-Up	2.99999999
OE2097F	UspA domain protein, nucleotide-binding	B0R424	DOWN-UP	6.99999999
OE2269F	UspA domain protein, nucleotide-binding	B0R4B3	n.d.	
OE3162F	UspA domain protein, nucleotide-binding	B0R5S6	Up-Up	2.99999785
OE3187R	UspA domain protein, nucleotide-binding	B0R5U1	DOWN-UP	6.99999992
OE3346R	UspA domain protein, nucleotide-binding	B0R631	down-UP	3.99997574
OE3466R	UspA domain protein, nucleotide-binding	B0R6A1	Up-Down	2.99999999
OE3668F	UspA domain protein, nucleotide-binding	B0R6L6	Up-Up	3
OE4338R	UspA domain protein, nucleotide-binding	B0R7R7	n.d	
OE4540R	UspA domain protein, nucleotide-binding	B0R820	down-UP	3.99999499
OE4541F	UspA domain protein, nucleotide-binding	B0R821		
OE4544R	UspA domain protein, nucleotide-binding	B0R823	Down-UP	5
OE4045F	UspA domain protein, nucleotide-binding	B0R9L4	n.d.	
OE5055F	UspA domain protein, nucleotide-binding	B0R9M2	up-up	0.76554868
OE5066R	UspA domain protein, nucleotide-binding	B0R9M8	up-UP	3.99994830
OE5089F	UspA domain protein, nucleotide-binding	B0R9P4	Down-down	1.99995391
OE5254F	UspA domain protein, nucleotide-binding	B0R9Z6	Down-Up	2.99821544

[1] UniProtKB accession number; [2] nomenclature as explained in the text, colors: highest respective protein abundance in planktonic cells (green), initial biofilms (blue) and mature biofilms (red), non-significant alterations shown in grey; n.d. not detected.

Motility. With regard to cell motility, the archaella assembly protein FlaJ showed a distinct DOWN-UP pattern, with its highest abundance in mature biofilm cells, while the archaella accessory protein FlaH and the prearchaellin peptidase FlaK showed weak changes and highest amounts in mature biofilms (Patenge *et al.*, 2001).

These findings are in contrast to the downward trends observed with other archaella poteins especially regarding the archaellins, but this might be explained by the fact that biofilm dispersal occurs at the late stage. How archaella are regulated in *Hbt. salinarum* R1 biofilms is elusive. In bacteria several mechanisms are known hindering motility during biofilm development. For instance in *Bacillus subtilis* the rotation of the flagella is inhibited by the protein EpsE, acting as a clutch on the flagellar rotor and mediating a rapid loss of motility in the initial biofilm phase (Guttenplan *et al.*, 2010). The expression of the flagellar basal body and filaments is repressed by a transcriptional regulator at the mature biofilm stage (Guttenplan & Kearns, 2013).

Chemotaxis and signal transduction. The chemotaxis proteins [Che, (Rudolph & Oesterhelt, 1996)] CheA, CheR, CheW1 and CheY yielded significant Down-Up patterns (Table 21). In addition, signal transducer proteins (Schlesner *et al.*, 2012) like BasT, CosT and MpcT showed comparable alterations (Table 21, p. 112). This was similar to the transducer proteins Htr6, Htr9, Htr13 and Htr18. Moreover, the phototaxis-mediating sensory rhodopsin I (SopI), and its corresponding sensory rhodopsin I transducer (Htr-I) detecting orange and UV light (Ferrando-May *et al.*, 1993) exhibited similar profiles.

Hbt. salinarum R1 possesses a network of chemotaxis and signal transducer proteins to sense and to respond to environmental signals, such as light, oxygen, amino acids or membrane potential changes (Schlesner *et al.*, 2012). Their Down-Up patterns suggest minor importance for these proteins in the initial biofilm phase, when the cells switch to the sessile lifestyle, while the increasing protein levels at the mature stage might be associated with cells recovering taxis, respectively motility, as a prerequisite for a possible biofilm dispersal.

Table 21 Direction Score results of chemotaxis and signal transduction proteins.

Symbol	Protein annotation	Accession[1]	Direction[2]	Score
Chemotaxis proteins				
cheA	Chemotaxis protein	B0R4J9	Down-Up	3
cheB	Chemotaxis response regulator	B0R4K0	down-Up	1.99868435
cheC2	Taxis cluster protein	B0R4J8	up-Up	1.99988878
cheC3	Taxis cluster protein	B0R4J7	Up-DOWN	4.99976755
cheD	Probable chemoreceptor glutamine deamidase	B0R4J6	down-up	0.42685029
cheF1	Taxis protein	B0R4J3	Up-Up	2.99999985
cheF2	Taxis protein	B0R4J4	Down-Up	2.99999948
cheR	Chemotaxis protein methyltransferase	B0R4J5	Down-Up	3
cheW1	Purine-binding taxis protein CheW	B0R4K2	Down-Up	2.99999975
cheW2	Purine-binding taxis protein CheW	B0R4H6	Down-up	1.99290482
cheY	Chemotaxis protein (response regulator)	B0R4K1	Down-Up	3

Signal transduction associated proteins				
htr1	Sensory rhodopsin I transducer	B0R632	Down-Up	2.99999999
sop1	Sensory rhodopsin I	B0R6B0	up-Down	1.99994862
htr2	Sensory rhodopsin II transducer	B0R6B1	up-DOWN	3.99999998
sop2	Sensory rhodopsin II	B0R633	Down-Up	2.99999999
htr4	Transducer protein	B0R470	Up-Down	2.99999999
htr6	Transducer protein	B0R461	Down-Up	2.99999927
htr7	Transducer protein	B0R6A6	down-down	0.05524224
htr8	Transducer protein	B0R5T0	up-Up	1.99997882
htr9	Transducer protein	B0R5I3	down-Up	1.99304748
htr12	Transducer protein	B0R5L8	Up-Down	2.99999999
htr13	Transducer protein	B0R4N9	down-Up	1.99998421
htr15	Transducer protein	B0R4I7	Down-Down	3
htr16	Transducer protein	B0R3S6	n.d.	
htr17	Transducer protein	B0R688	up-down	0.8018625
htr18	Transducer protein	B0R474	down-UP	3.99997218
basB	Transduction system substrate-binding protein	B0R6I5	down-Up	1.99999215
basT	Transducer protein (amino acids)	B0R6I4	Down-UP	4.99999999
car	Cytoplasmic transducer protein (arginine)	B0R9Z1	up-up	0.34389912
cosB	Transduction system substrate-binding protein	B0R6A8	Down-Up	3
cosT	Transducer protein (compatible solutes)	B0R6A7	Down-Up	2.99999999
mpcT	Membrane potential change transducer protein	B0R367	Down-UP	5

[1] UniProtKB accession number; [2] nomenclature as explained in the text, color code: highest respective protein abundance in planktonic cells (green), initial biofilms (blue) and mature biofilms (red), non-significant alterations shown in grey

>Metabolism

Energy metabolism. Down-Up patterns were observed for the light-driven proton pump bacteriorhodopsin (BR, Table 16, p. 97) and related proteins (Sharma *et al.*, 2007), which showed moderate decrease in initial and increase in mature biofilms (see also Figure 38, p. 88). Bacteriorhodopsin (BR) represents an important mechanism for energy conversion under anaerobic conditions and light (Shand & Betlach, 1991; Tarasov *et al.*, 2011). An increase of BR connected proteins has been also observed under anaerobic/phototrophic conditions (Tebbe *et al.*, 2009). These results, along with the other changes in energy metabolism described before, clearly demonstrate a stepwise activation of alternative energy conversion mechanisms during the biofilm development of *Hbt. salinarum* R1.

Carbon metabolism. A number of enzymes involved in central C-metabolism showed similar patterns, like the two initial enzymes of the glycolytic pathway, glyceraldehyde dehydrogenase (Gap) and phosphoglycerate kinase (Pgk). Moreover, phosphoenolpyruvate carboxylase (PpcA) and phosphoenolpyruvate synthase (PpsA), which acts as the key enzyme in the gluconeogenesis pathway, as well as fructose-1,6-bisphosphatase (Fbp) showed similar responses. Fbp links gluconeogenesis to the oxidative pentose phosphate (PP) pathway, which is indispensable for *e.g.* ribonucleotide synthesis, with Fbp acting irreversibly in this direction (Falb *et al.*, 2008; Soderberg, 2005). Also, another key enzyme of the PP pathway, Gnd (Bräsen *et al.*, 2014; Falb *et al.*, 2008), was slightly more abundant in planktonic cells compared to the biofilm state. These findings suggest that the ATP-consuming gluconeogenesis and PP pathway are mainly used in planktonic cells, maybe owing to better energy supply in these cells. Since

none of these enzymes showed a significant change upon the transition from aerobic to anaerobic phototrophic growth (Tebbe *et al.*, 2009), the results suggest biofilm-specific responses.

Amino acid metabolism. Many proteins and enzymes involved in amino acid transport and metabolism were assigned to the Down-Up group, adding up to 13.6% of the proteins within this group. The most obvious changes were observed with DppA1, 2 and 3, which are the substrate-binding components of three ABC-type di-/oligopeptide transport systems (Monnet, 2003). Several peptidases showed similar responses (*e.g.* Cxp and OE1613R). Among the amino acid metabolizing enzymes, the strongest alterations were detected for the homoserine dehydrogenase (Hom), cystathionine synthase/lyase (MetB2), threonine aldolase (Ita) and threonine synthase (ThrC1). These are functionally related enzymes, since homoserine is a precursor for threonine and methionine biosynthesis (Falb *et al.*, 2008).
Generally, the changes observed with regard to amino acid metabolism reflect the fact that *Hbt. salinarum* R1 grows on amino acids (Gonzalez *et al.*, 2009). In accordance with this, the components of the chemotactic signal transduction system for branched-chain and sulfur-containing amino acids (BasBT) exhibited similar trends.

Lipid metabolism. Down-Up patterns were also found with enzymes associated with the propionyl-CoA pathway (Table 22, p. 115), linking degradation of branched chain amino acids and also odd-chain fatty acids to the central C-metabolism (Falb *et al.*, 2008; Yabuta *et al.*, 2015), *i.e.* subunits of the methylmalonyl-CoA mutase (MmcA1, A2 and B) and propionyl-CoA carboxylase (PpcA2 and B1). Several other enzymes involved in fatty acid metabolism (Dibrova *et al.*, 2014) exhibited similar patterns, namely three out of six acyl-CoA dehydrogenases (Acd2, 4 and 6) and four out of five acyl-CoA synthetases (Acs1-4) present in *Hbt. salinarum* R1. This was also true for the acetyl-CoA acetyltransferases (AcaB1 and B2), enoyl-CoA hydratases (FadA1 and A2) and 2-hydroxyacyl-CoA dehydrogenases (Hbd1 and 2). Most of these enzymes were less abundant in initial biofilms than in planktonic cells and a number of them showed marked increases in mature biofilms, suggesting a role for the corresponding pathway. This is surprising, since there are no reports on fatty acid oxidation by *Hbt. salinarum* R1 to date. Therefore, fatty acid oxidation for the purpose of energy production is unlikely. Possibly the enzymes work in the opposite direction, namely fatty acid biosynthesis in a manner proposed by Dibrova *et al.* (2014) to stabilize the cell membrane or membrane-bound energy-transducing enzymes like BR or Dms (Dibrova *et al.*, 2014; Hendler *et al.*, 2003). Nevertheless, this would be in contrast to biofilms of *P. aeruginosa*, where energy consuming lipid formation is systematically reduced in anaerobically grown biofilms (Tielen *et al.*, 2013).

Table 22 Direction Score results of proteins associated with fatty acid metabolism

Symbol	Protein annotation	Accession[1]	Direction[2]	Score
acaB1	Acetyl-CoA C-acetyltransferase	B0R3X4	Down-Up	2.99985033
acaB2	Acetyl-CoA C-acetyltransferase	B0R4G6	down-UP	3.99988547
acaB3	Acetyl-CoA C-acetyltransferase	B0R6Z2	Up-Up	2.99997144
acd1	Acyl-CoA dehydrogenase	B0R379	Up-Down	5
acd2	Acyl-CoA dehydrogenase	B0R449	DOWN-UP	7
acd3	Acyl-CoA dehydrogenase	B0R528	up-UP	3.99997978
acd4	Acyl-CoA dehydrogenase	B0R3X6	Down-Up	3
acd5	Acyl-CoA dehydrogenase	B0R5Q2	up-Down	1.99961285
acd6	Acyl-CoA dehydrogenase	B0R803	Down-up	1.99995491
acs1	Acyl-CoA synthetase	B0R3G8	Down-Up	3
acs2	Acyl-CoA synthetase	B0R4M4	DOWN-UP	7
acs3	Acyl-CoA synthetase	B0R5D9	DOWN-UP	7
acs4	Acyl-CoA synthetase	B0R2S9	DOWN-UP	6.99999999
acs5	Acyl-CoA synthetase	B0R6Z6	down-UP	3.99999964
fadA1	Enoyl-CoA hydratase	B0R6X0	Down-Up	4.99996849
fadA2	Enoyl-CoA hydratase	B0R3C3	DownUp	2.99998936
hbd1	3-hydroxyacyl-CoA dehydrogenase	B0R3X8	Down-Up	3
hbd2	3-hydroxyacyl-CoA dehydrogenase	B0R5C0	DOWN-UP	7
mmcA1	Methylmalonyl-CoA mutase subunit	B0R3V4	down-UP	3.99994213
mmcA2	Methylmalonyl-CoA mutase subunit	B0R3GS	Down-Up	2.99999981
mmcB	Methylmalonyl-CoA mutase subunit	B0R3X0	Down-UP	5
pccA2	Propionyl-CoA carboxylase carboxyltransferase component	B0R5T7	Down-Up	3
pccB2	Propionyl-CoA carboxylase carboxyltransferase component	B0R3T1	DOWN-UP	7
pccB2	Propionyl-CoA carboxylase carboxyltransferase component	B0R5T5	Down-down	1.99764706

[1] UniProtKB accession number; [2] nomenclature as explained in the text, color code: highest respective protein abundance in planktonic cells (green), initial biofilms (blue) and mature biofilms (red), non-significant alterations shown in grey.

Ion transport. Down-Up profiles were determined for the Trk domain proteins TrkA2, 3, 6 and 7 (Table 23) involved in potassium ion transport (Mongodin *et al.*, 2005), while two other Trk proteins (TrkA4 and 5) showed different patterns. Changes in initial biofilms were moderate with regard to most Trk type K^+ transporters, but some of them were strongly increased in the mature state (TrkA3, 6 and 7).

Table 23 Direction Score results of putative potassium ion transport proteins.

Symbol	Protein annotation	Accession[1]	Direction[2]	Score
trkA1	K^+ transport system TrkA domain protein	B0R2T9	n.d	
trkA2	K^+ transport system TrkA domain protein	B0R9L7	down-Up	1.99994715
trkA3	K^+ transport system TrkA domain protein	B0R9Q4	Down-UP	4.99999974
trkA4	K^+ transport system TrkA domain protein	B0R9S5	Down-Down	2.99999999
trkA5	K^+ transport system TrkA domain protein	B0R597	Up-Down	2.99999991
trkA6	K^+ transport system TrkA domain protein	B0R6N9	Down-UP	4.99999999
trkA7	K^+ transport system TrkA domain protein	B0R9Q7	Down-UP	4.99999999
trkA8	K^+ transport system TrkA domain protein	B0RA22	n.d	

[1] UniProtKB accession number; [2] nomenclature as explained in the text, color code: highest respective protein abundance in planktonic cells (green), initial biofilms (blue) and mature biofilms (red), non-significant alterations shown in grey

Trk transporters are important for osmoregulation (Vieira-Pires *et al.*, 2013) and *trkA6* transcription is strongly induced in *Hbt. salinarum* NRC-1 under low salinity conditions (Coker *et al.*, 2007), which suggests altered osmoregulation in the biofilm samples investigated. However, no significant evaporation of water from the culture media was detected over the two

weeks of incubation (data not shown). The observations are favored by the absence of the K^+ transporters encoded by the *kdpABC* operon, which was not detected in the present work. It was shown that Kdp is involved in K^+ homeostasis and induced under potassium limitation and desiccation conditions (Strahl & Greie, 2008). However, a deficiency of Kdp due to the SWATH/LC/MS/MS technique employed is possible.

Similar Down-Up responses were the case with regard to the phosphate uptake regulators PhoU3 and PhoU4 (Wende *et al.*, 2009), which was accompanied by a strong increase of the putative substrate binding protein PstS1 of the phosphate ABC-type transport system Pst1 (Furtwängler *et al.*, 2010). In contrast, components (PhnC, D and E) of the ABC-type phosphate/phosphonate transport [Phn, (Gebhard *et al.*, 2006; Metcalf & Wanner, 1991)] system were clearly reduced in mature biofilms.
Phosphate is often a growth limiting nutrient but indispensable for survival of microorganisms and can have effects on biofilm formation, which was reported for *Pseudomonas aureofaciens* (Monds *et al.*, 2001). Furthermore, it was shown for *Pseudomonas aeruginosa* that biofilm formation is controlled by phosphate signaling, assisted by the PstS subunit of a Pst phosphate transporter, which has dual functions in phosphate uptake and also regarding the control of biofilm formation (Neznansky *et al.*, 2014).

pH adaptation. The proteins PhaB1, D2 and E involved in pH-adaptation [Pha, (Falb *et al.*, 2005)] showed similar Down-Up patterns, but only weak changes, while PhaG showed slight and constant decrease. This suggests no major need for pH-adaptation in the biofilms, which was supported by pH measurements showing only a slight shift towards weak alkaline (pH 7.4 - 8.0) conditions in the course of the experiment (data not shown).

>Poorly characterized

Altogether 93 of the 295 proteins of the Down-Up group, corresponding to 31.5%, belonged to the categories *General function prediction only* or *Function unknown*. From these, distinct DOWN-UP patterns were detected, *e.g.* for the predicted substrate-binding protein TmpC, a DUF21/CBS domain protein (OE5193F), a SIMPL domain protein (OE4633F), as well as three further uncharacterized proteins (OE2618R, OE2041R and OE4069R) and three putative oxidoreductases (OE1719R, OE4021F and OE4695F) from the short-chain dehydrogenase/ reductase family [SDR, (Kallberg *et al.*, 2010)]. In addition, the predicted 'glutamine-rich alkaline protein' (OE3542R) was marginally reduced in initial biofilms, while strongly increased amounts were detected in the mature biofilm state.

In summary, the 'Direction Scoring' analysis led to the assignment of four major groups of co-trending proteins. Functionally related proteins appeared in the same group in many instances, suggesting relevance of certain pathways with regard to the molecular differentiation in initial or mature biofilms. The identified biological processes presented in Table 15 (p. 94) provide an overview of biofilm differentiation in *Hbt. salinarum* R1.

5.2.7. Validation of the proteomic data of selected proteins

A validation of the quantitative (SWATH-LC/MC/MC) proteomic data by qRT-PCR was persued. For this purpose RNA was extracted from similar biological samples as used in the MS analysis, *i.e.* planktonic cells in the exponential growth phase, as well as initial and mature biofilm cells grown for 1 and 15 days, respectively. For some target genes additional samples were investigated, *i.e.* early exponential and stationary growth phase, as well as biofilms grown for 6 days. The qRT-PCR analyses were carried out as described in 2.4.16. Selected genes encoding representative proteins from each of the four major groups of differentially abundant proteins were investigated. Moreover, genes involved in energy metabolism were tested. The transcripts of sessile cells were quantified in comparison to the planktonic cells from the exponential growth phase, to test whether they showed similar profiles in response to biofilm formation as the corresponding protein abundances.

Table 24 Validation of the proteomic data by qRT-PCR.

Group	Symbol[1]	Proteomic				Transcriptional				Valid[2]
		initial/plankton		mature/plankton		initial/plankton		mature/plankton		
		Ratio	SD	Ratio	SD	Ratio	SD	Ratio	SD	
Down-Down	***carA***	**-1.11**	±0.38	**-2.71**	±0.39	**1.85**	±0.08	**-5.99**	±0.08	-
	cbiG	**-0.75**	±0.08	**-4.14**	±0.34	**-1.24**	±0.23	**-5.16**	±0.55	+
	nrdA1	**-1.91**	±0.19	**-3.75**	±0.24	**-4.44**	±0.13	**-12.12**	±0.21	+
Up-Down	***dmsR***	**2.06**	±0.64	**-0.33**	±0.87	**1.20**	±0.19	**-4.55**	±0.93	+
	pykA	**1.73**	±0.11	**0.49**	±0.12	**-0.80**	±0.16	**-2.14**	±0.33	-
	rps13	**1.46**	±0.16	**-0.05**	±0.14	**0.33**	±0.09	**-3.60**	±0.17	+
Up-Up	***lrpA2***	**0.36**	±0.20	**0.76**	±0.17	**0.51**	±0.07	**-1.20**	±0.08	-
	OE1974R	**0.50**	±0.45	**3.52**	±0.29	**1.47**	±0.15	**2.74**	±0.19	+
	OE4416R	**1.87**	±0.39	**3.06**	±0.34	**0.65**	±0.12	**0.81**	±0.08	+
Down-Up	**OE2097F**	**-1.04**	0.11	**0.20**	0.05	**2.51**	0.08	**0.38**	0.08	-
	OE3073R	**-1.23**	±0.75	**1.89**	±0.10	**-0.41**	±0.12	**0.76**	±0.12	+
	OE3542R	**-0.32**	±0.89	**7.30**	±0.61	**-0.77**	±0.10	**2.07**	±0.08	+

All values are indicated in $\log_2$ scale. [1]Symbols: *carA*, Carbamoyl phosphate synthase small chain; *cbiG*, Cobalt-precorrin 5A hydrolase; *nrdA1*, Ribonucleoside-diphosphate reductase alpha subunit; *dmsR*, Predicted transcriptional regulator of DMSO reductase operon; *pykA*, Pyruvate kinase; *rps13*, 30S ribosomal protein S13; *lrpA2*, Lrp/AsnC family transcription regulator; OE1974R, GNAT family acetyltransferase; OE4416R, Uncharacterized conserved protein; OE2097F, UspA domain protein; OE3073R, Dodecin; OE3542, Glutamine-rich alkaline protein.

[2]Valid: Indicates whether proteome analysis is reflected by transcription analysis (+) or not (-).

Down-Down group

With regard to the Down-Down group two of the three target genes tested showed a similar trend on transcript level as on the level of proteins, *i.e.* lowest amounts were observed in the mature biofilm state (Table 24, p. 118). The *cbiG* and *nrdA1* mRNA was reduced in initial biofilms compared to the planktonic state (mRNA $logFC_{i/p}$ = -1.24 and -4.44, respectively), which confirmed the protein abundances (protein $logFC_{i/p}$ = -0.75 and -1.91). This was also noticed comparing the decreased transcript (mRNA $logFC_{m/p}$ = -5.16 and -12.12) and protein amounts (protein $logFC_{m/p}$ = -4.14 and -3.75) of *cbiG* and *nrdA1* in mature biofilm cells, while in case of *nrdA1* the mRNA response was extremely enhanced. In contrast, *carA* showed an Up-Down response in transcription (mRNA $logFC_{i/p}$ = 1.9 and $logFC_{m/p}$ = -6.0), which was different from the Down-Down pattern observed with regard to the corresponding proteins. Nevertheless, the outcome was the same for transcription and translation, *i.e.* lowest levels in the mature biofilm state.

Up-Down group

With respect to the Up-Down group, *dmsR* and *rps13* showed similar responses on both transcript and protein level, although they exhibited partially differences with regard to the magnitude of the changes observed (Table 24). The *rps13* mRNA was not notably more abundant in initial biofilms compared to planktonic cells (mRNA $logFC_{i/p}$ = 0.33), whereas the corresponding change in the amount of protein was more pronounced (protein $logFC_{i/p}$ = 1.46). In mature biofilm cells the situation was reversed compared to the planktonic state, *i.e.* a strong decrease of the transcript (mRNA $logFC_{m/p}$ = -3.6) but no change of the protein abundance ($logFC_{m/p}$ = -0.05). Similar observations were made for *dmsR* transcripts and the corresponding proteins. In contrast, *pykA* mRNA showed a steady decrease comparing initial and mature biofilms to the planktonic state (mRNA $logFC_{i/p}$ = -0.8 and $logFC_{m/p}$ = -2.14), whereas amounts of the protein PykA were highest in initial biofilms (protein $logFC_{i/p}$ = 1.73).

Up-Up group

Regarding the Up-Up group, the predicted GNAT family acetyltransferase (OE1974R) and the uncharacterized conserved protein (OE4416R) both exhibited protein profiles fitting with the translation changes (Table 24). In contrast, the transcriptional regulator *lrpA2* exhibited Up-Down changes in transcript level, *i.e.* the *lrpA2* mRNA showed slight increase in initial biofilms (mRNA $logFC_{i/p}$ = 0.51), while in mature biofilm cells a clear decrease was observed (mRNA $logFC_{m/p}$ = -1.2) in comparison to planktonic cells.

Down-Up group

Concerning the Down-Up group, dodecin (OE3073R) and 'glutamine-rich alkaline protein' (OE3542R) transcript and protein levels showed similar trends (Table 24, p. 118). The increase of the OE3542R protein amount in mature biofilms (protein $logFC_{m/p} = 7.3$) strongly surpassed the corresponding change observed on transcript level (mRNA $logFC_{m/p} = 2.1$). A more detailed analysis of the amount of OE3542R transcript yielded a very strong increase in stationary planktonic cells (mRNA $logFC_{m/p} = 6.48 \pm 0.36$) suggesting no biofilm-specific up-regulation. In comparison, the UspA domain protein (OE2097F) showed an opposing transcript response exhibiting strong induction in initial biofilms (mRNA $logFC_{i/p} = 2.51$) and a slight increase in the mature biofilm state (mRNA $logFC_{m/p} = 0.38$).

Energy conversion systems

Furthermore, transcripts of several genes involved in different energy conversion systems of *Hbt. salinarum* R1 (*arcC*, *dmsA* and *bop*) were investigated, to test whether the changes observed on protein level were biofilm-specific or represented general reactions of the cells in response to their cellular condition, respectively the growth phase.

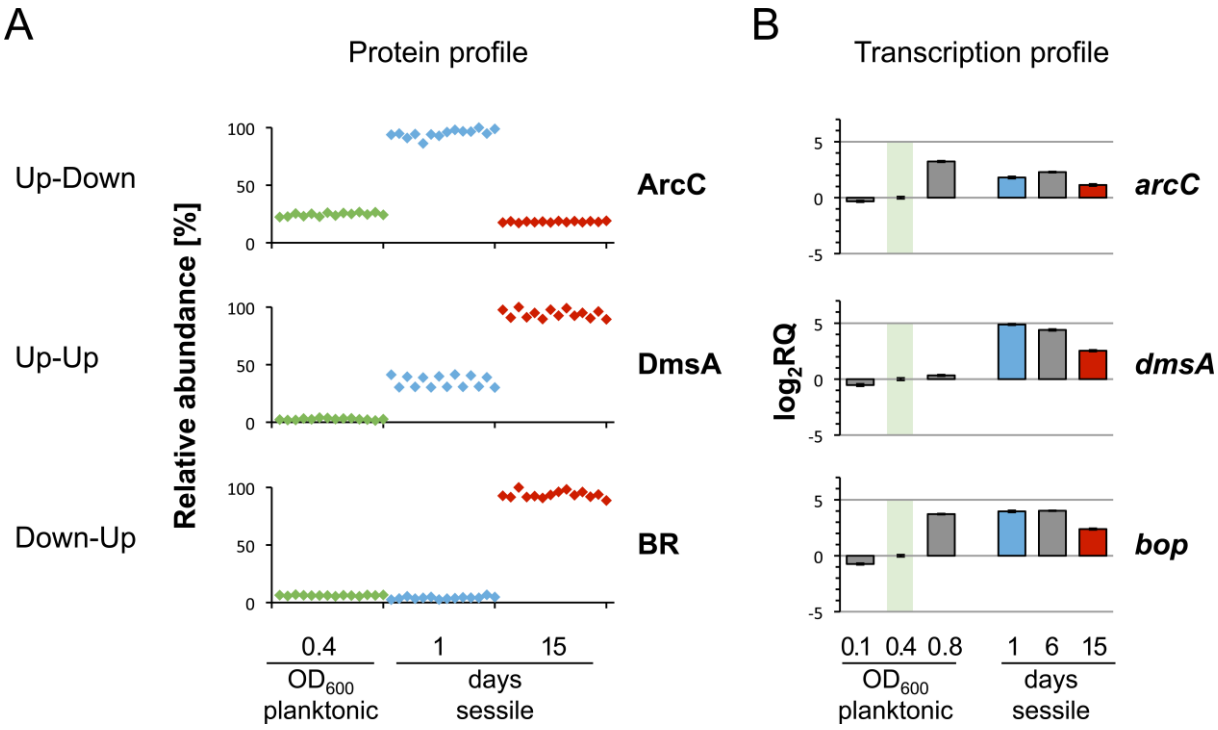

Figure 47 Protein and transcription profiles of representative genes involved in energy conversion. **A**, Relative response [%] of the respective proteins in biological and technical replicates of the investigated sample states (planktonic, green; sessile 1 d, blue; sessile 15, red). Respective protein groups are indicated (Up-Down, Up-Up and Down-Up). Carbamate kinase (ArcC) represents the Up-Down group, DMSO reductase subunit A (DmsA) the Up-Up group and bacteriorhodopsin (BR) the Down-Up group. **B**, Relative quantification (RQ) of the transcription of the corresponding genes (*arcC*, *dmsA*, and *bop*) encoding the proteins shown in (A). Three different planktonic samples, *i.e.* cells from the early exponential (OD_{600} 0.15), late exponential (0.4) and stationary (0.8) growth phase, as well as sessile cells

harvested from biofilms grown for different incubation times, *i.e.* 1 day (1), 6 days (6) and 15 days (15) were investigated. Bars represent fold change of the respective gene transcription compared to the OD_{600} 0.4 sample, shown in log_2 scale.

With regard to *arcC*, a higher transcript level was observed in the early biofilm phases, followed by a reduction at the mature stage (Figure 47B). This was in accordance with the Up-Down pattern deduced from the proteomic data (Figure 47A). However, even higher *arcC* transcript amounts were observed in stationary planktonic cells, ruling out a biofilm-specific response and implicating growth phase or oxygen status-dependent effects.

An extremely increased transcript level of *dmsA* was observed in initial biofilms, which was still markedly higher during the later biofilm stages. In comparison, virtually no transcript changes were detected throughout the planktonic samples. Although activation of the *dms* operon is common under anaerobic conditions (Müller & DasSarma, 2005), it might represent a biofilm-specific response. This interpretation is supportet by the magnitude of increase of the *dmsA* mRNA in biofilms. The question whether DMSO or related compounds were present in the medium was not addressed. DMSO was not supplemented to the medium, but might derive from degradation of sulfur-containing amino acids. With regard to the natural habitat of *Halobacterium*, DMSO is a common chemical compound resulting from biotic and abiotic processes (Griebler & Slezak, 2001). Thus, an association of DMSO respiration with the sessile lifestyle might be reasonable. In some aquatic regions DMSO respiration might represent the only possibility for energy conservation.

Transcripts of the *bop* gene were much more abundant in stationary planktonic cells and almost unchanged in the biofilm samples grown for 1 or 6 days, respectively, while the level at the mature biofilm stage was still markedly higher. Strong transcript increases of *bop* in the initial biofilm phase were in contrast to the reduced protein amounts at this stage. Since the *bop* transcript level in initial biofilms is almost the same as in stationary phase cells, it likely represents a growth phase-dependent response.

Taken together, examples were found in every group, which showed similar profiles regarding their transcript and protein abundances, underlining the proteome data and suggesting that these candidates might serve as biofilm markers in *Hbt. salinarum* R1. However, other examples showed different responses on both levels of gene expression investigated, implicating mRNA-intrinsic properties or potentially additional regulatory mechanisms.

6. Conclusions and perspectives

The present work joins previous studies on microbial biofilm formation as well as investigations of profound lifestyle changes in microorganisms. A comprehensive description of biofilm formation by *Hbt. salinarum* R1 was achieved. The introductory microscopic analyses provided a detailed overview of the temporal and spatial sequence of events during biofilm development. Also first insights into the complex architecture of the multicellular communities were gained, *e.g.* with regard to the presence of EPS containing glycoconjugates and eDNA. However, given the complexity of previously studied biofilms of other species, it can be assumed that what was observed in the present study represented only the tip of the iceberg. Future studies in this direction are expected to uncover more components of the EPS and gain more informations on their synthesis as well as their structure and function relationship in the sophisticated three-dimensional biofilm network. The process of biofilm formation as observed here in *Hbt. salinarum* R1 and in previous biofilm studies suggests a general procedure.

The adhesion in *Hbt. salinarum* R1 is based on a well-known microbial theme, *i.e.* type IV pili-like cell surface structures. First components involved in the assembly of the *Hbt. salinarum* R1 adhesion pili were identified, as well as further promising candidates. However, not all factors involved are specified yet, requiring further investigations. Especially the pilin composition of the *Hbt. salinarum* R1 adhesion pili is of interest. How adhesion is achieved by use of these modules and what molecular interactions occur are still open questions. To date, various functions of type IV pili-like structures have been described, but the molecular basis of their versatility demands future examinations.

A label-free SWATH-LC/MS/MS-based quantitative proteome analysis method was established to investigate the proteomes of planktonic and biofilm cells of *Hbt. salinarum* R1. Using this method enabled us to describe the molecular differentiation and the biological processes underlining the switch from planktonic to sessile lifestyle in *Hbt. salinarum* R1 biofilms. The questions of biofilm initiation as well as biofilm maturation were addressed by comparing the respective proteomes. Various processes were observed to undergo alterations in biofilm cells and are associated with certain biological states (Figure 48, p. 123). In many instances, like transcription and translation, cell motility or alternative energy conversion mechanisms the insights appear plausible. While for instance the energy metabolic changes within the biofilms of *Hbt. salinarum* R1 were described in detail; the significance of other processes affected, *e.g.* adhesion, glycosylation, stress response and signal transduction, as well as nucleotide or lipid metabolism require further investigations. Also, the large portion of uncharacterized proteins showing distinct alterations in biofilms reflects the need for further examinations. This is also true for the diverse transcriptional regulators showing specific responses. The generation of

gene deletion mutants in combination with a phenotypic characterization of the biofilms will provide insights into the function of the respective proteins.

The quantitative proteomics method used here should also be applicable to investigate other cellular lifestyle changes or the effects of environmental parameters, like temperature, radiation or metals on biofilm formation. With regard to some effects observed, the investigation of additional cellular states like stationary phase cells is desireable, to evaluate whether mature biofilms represent a 'resting condition' of the cells. The present work using SWATH-LC/MS/MS represents the first one in archaea.

This thesis has shed light on multifaceted molecular processes taking place in *Hbt. salinarum* R1 during biofilm development. The results obtained are a starting point for future studies to elucidate the cellular mechanisms and regulation networks contributing to biofilm formation.

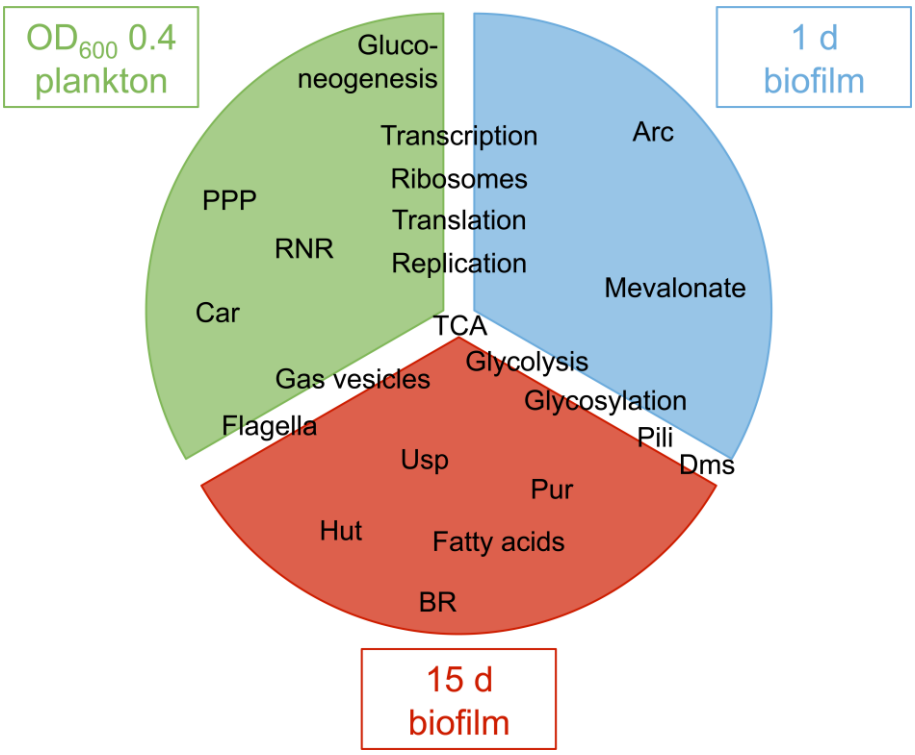

Figure 48 Overview of the proteins respectively processes associated with certain biological states. Proteins/processes connected with distinct states, *i.e.* plankton (green), initial biofilms (blue) and mature biofilms (red) were found. Proteins/processes associated with two states are placed in the space between the two respective sectors. The citric acid cycle (TCA) did not undergo major changes and therefore is assigned to the center of all three states. Abbreviations indicate: Arc, fermentative arginine degradation; BR, bacteriorhodopsin; Car, carbamoyl phosphate synthase; Dms, DMSO reductase; Hut, histidine utilization; PPP, pentose phosphate pathway; Pur, purine biosynthesis; RNR, ribonucleoside-diphosphate reductase; Usp, universal stress proteins.

Literature

Alam, M., & Oesterhelt, D. (1984). Morphology, function and isolation of halobacterial flagella. *J Mol Biol,* **176**(4), 459-475.

Albers, S. V., & Jarrell, K. F. (2015). The archaellum: how Archaea swim. *Front Microbiol,* **6**, 23.

Albers, S. V., & Pohlschröder, M. (2009). Diversity of archaeal type IV pilin-like structures. *Extremophiles,* **13**(3), 403-410.

Albers, S. V., Szabo, Z., & Driessen, A. J. (2003). Archaeal homolog of bacterial type IV prepilin signal peptidases with broad substrate specificity. *J Bacteriol,* **185**(13), 3918-3925.

Altman-Price, N., & Mevarech, M. (2009). Genetic evidence for the importance of protein acetylation and protein deacetylation in the halophilic archaeon *Haloferax volcanii*. *J Bacteriol,* **191**(5), 1610-1617.

An, Y. H., & Friedman, R. J. (1998). Concise review of mechanisms of bacterial adhesion to biomaterial surfaces. *J Biomed Mater Res,* **43**(3), 338-348.

Andrei, A. S., Banciu, H. L., & Oren, A. (2012). Living with salt: metabolic and phylogenetic diversity of archaea inhabiting saline ecosystems. *FEMS Microbiol Lett,* **330**(1), 1-9.

Angerer, A., Klupp, B., & Braun, V. (1992). Iron transport systems of *Serratia marcescens*. *J Bacteriol,* **174**(4), 1378-1387.

Anton, J., Meseguer, I., & Rodriguez-Valera, F. (1988). Production of an Extracellular Polysaccharide by *Haloferax mediterranei*. *Appl Environ Microbiol,* **54**(10), 2381-2386.

Ashworth, J., Plaisier, C. L., Lo, F. Y., Reiss, D. J., & Baliga, N. S. (2014). Inference of expanded Lrp-like feast/famine transcription factor targets in a non-model organism using protein structure-based prediction. *PLoS One,* **9**(9), e107863.

Baker-Austin, C., Potrykus, J., Wexler, M., Bond, P. L., & Dopson, M. (2010). Biofilm development in the extremely acidophilic archaeon '*Ferroplasma acidarmanus*' Fer1. *Extremophiles,* **14**(6), 485-491.

Baliga, N. S., Bjork, S. J., Bonneau, R., Pan, M., Iloanusi, C., Kottemann, M. C., . . . DiRuggiero, J. (2004). Systems level insights into the stress response to UV radiation in the halophilic archaeon *Halobacterium* NRC-1. *Genome Res,* **14**(6), 1025-1035.

Baliga, N. S., Goo, Y. A., Ng, W. V., Hood, L., Daniels, C. J., & DasSarma, S. (2000). Is gene expression in *Halobacterium* NRC-1 regulated by multiple TBP and TFB transcription factors? *Mol Microbiol,* **36**(5), 1184-1185.

Bang, C., & Schmitz, R. A. (2015). Archaea associated with human surfaces: not to be underestimated. *FEMS Microbiol Rev,* **39**(5), 631-648.

Banin, E., Vasil, M. L., & Greenberg, E. P. (2005). Iron and *Pseudomonas aeruginosa* biofilm formation. *Proc Natl Acad Sci U S A,* **102**(31), 11076-11081.

Bardy, S. L., Mori, T., Komoriya, K., Aizawa, S., & Jarrell, K. F. (2002). Identification and localization of flagellins FlaA and FlaB3 within flagella of *Methanococcus voltae*. *J Bacteriol,* **184**(19), 5223-5233.

Barns, S. M., Delwiche, C. F., Palmer, J. D., & Pace, N. R. (1996). Perspectives on archaeal diversity, thermophily and monophyly from environmental rRNA sequences. *Proc Natl Acad Sci U S A,* **93**(17), 9188-9193.

Bellack, A., Huber, H., Rachel, R., Wanner, G., & Wirth, R. (2011). *Methanocaldococcus villosus* sp. nov., a heavily flagellated archaeon that adheres to surfaces and forms cell-cell contacts. *Int J Syst Evol Microbiol,* **61**(Pt 6), 1239-1245.

Benamara, H., Rihouey, C., Abbes, I., Ben Mlouka, M. A., Hardouin, J., Jouenne, T., & Alexandre, S. (2014). Characterization of membrane lipidome changes in

Pseudomonas aeruginosa during biofilm growth on glass wool. *PLoS One,* **9**(9), e108478.
Bender, R. A. (2012). Regulation of the histidine utilization (hut) system in bacteria. *Microbiol Mol Biol Rev,* **76**(3), 565-584.
Benjamini, Y., & Hochberg, Y. (1995). Controlling the false discovery rate: a practical and powerful approach to multiple testing. *Journal of the Royal Statistical Society B*(57), 289-300.
Berquist, B. R., DasSarma, P., & DasSarma, S. (2007). Essential and non-essential DNA replication genes in the model halophilic Archaeon, *Halobacterium sp.* NRC-1. *BMC Genet,* **8**, 31.
Berry, J. L., & Pelicic, V. (2015). Exceptionally widespread nanomachines composed of type IV pilins: the prokaryotic Swiss Army knives. *FEMS Microbiol Rev,* **39**(1), 134-154.
Beznosov, S. N., Piatibratov, M. G., & Fedorov, O. V. (2007). Multicomponent nature of *Halobacterium salinarum* flagella. *Mikrobiologiia,* **76**(4), 494-501.
Bisle, B., Schmidt, A., Scheibe, B., Klein, C., Tebbe, A., Kellermann, J., . . . Oesterhelt, D. (2006). Quantitative profiling of the membrane proteome in a halophilic archaeon. *Mol Cell Proteomics,* **5**(9), 1543-1558.
Bleiholder, A., Frommherz, R., Teufel, K., & Pfeifer, F. (2012). Expression of multiple tfb genes in different *Halobacterium salinarum* strains and interaction of TFB with transcriptional activator GvpE. *Arch Microbiol,* **194**(4), 269-279.
Boles, B. R., Thoendel, M., & Singh, P. K. (2004). Self-generated diversity produces "insurance effects" in biofilm communities. *Proc Natl Acad Sci U S A,* **101**(47), 16630-16635.
Bolhuis, A. (2002). Protein transport in the halophilic archaeon *Halobacterium sp.* NRC-1: a major role for the twin-arginine translocation pathway? *Microbiology,* **148**(Pt 11), 3335-3346.
Bolstad, B. M., Irizarry, R. A., Astrand, M., & Speed, T. P. (2003). A comparison of normalization methods for high density oligonucleotide array data based on variance and bias. *Bioinformatics,* **19**(2), 185-193.
Bouwer, E. J., & Zehnder, A. J. (1993). Bioremediation of organic compounds--putting microbial metabolism to work. *Trends Biotechnol,* **11**(8), 360-367.
Bradford, M. M. (1976). A rapid and sensitive method for the quantitation of microgram quantities of protein utilizing the principle of protein-dye binding. *Anal Biochem,* **72**, 248-254.
Bräsen, C., Esser, D., Rauch, B., & Siebers, B. (2014). Carbohydrate metabolism in Archaea: current insights into unusual enzymes and pathways and their regulation. *Microbiol Mol Biol Rev,* **78**(1), 89-175.
Breuert, S., Allers, T., Spohn, G., & Soppa, J. (2006). Regulated polyploidy in halophilic archaea. *PLoS One,* **1**, e92.
Brochier-Armanet, C., Boussau, B., Gribaldo, S., & Forterre, P. (2008). Mesophilic Crenarchaeota: proposal for a third archaeal phylum, the Thaumarchaeota. *Nat Rev Microbiol,* **6**(3), 245-252.
Brown, A. M., Hoopes, S. L., White, R. H., & Sarisky, C. A. (2011). Purine biosynthesis in archaea: variations on a theme. *Biol Direct,* **6**, 63.
Bryant, M. P., Wolin, E. A., Wolin, M. J., & Wolfe, R. S. (1967). *Methanobacillus omelianskii*, a symbiotic association of two species of bacteria. *Arch Mikrobiol,* **59**(1), 20-31.
Bustin, S. A. (2002). Quantification of mRNA using real-time reverse transcription PCR (RT-PCR): trends and problems. *J Mol Endocrinol,* **29**(1), 23-39.
Bustin, S. A., & Nolan, T. (2004). Pitfalls of quantitative real-time reverse-transcription polymerase chain reaction. *J Biomol Tech,* **15**(3), 155-166.
Capes, M. D., Coker, J. A., Gessler, R., Grinblat-Huse, V., DasSarma, S. L., Jacob, C. G., . . . DasSarma, S. (2011). The information transfer system of halophilic archaea. *Plasmid,* **65**(2), 77-101.

Chaban, B., Voisin, S., Kelly, J., Logan, S. M., & Jarrell, K. F. (2006). Identification of genes involved in the biosynthesis and attachment of *Methanococcus voltae* N-linked glycans: insight into N-linked glycosylation pathways in Archaea. *Mol Microbiol,* **61**(1), 259-268.

Chamieh, H., Guetta, D., & Franzetti, B. (2008). The two PAN ATPases from *Halobacterium* display N-terminal heterogeneity and form labile complexes with the 20S proteasome. *Biochem J,* **411**(2), 387-397.

Chen, W., Honma, K., Sharma, A., & Kuramitsu, H. K. (2006). A universal stress protein of *Porphyromonas gingivalis* is involved in stress responses and biofilm formation. *FEMS Microbiol Lett,* **264**(1), 15-21.

Chimileski, S., Dolas, K., Naor, A., Gophna, U., & Papke, R. T. (2014a). Extracellular DNA metabolism in *Haloferax volcanii*. *Front Microbiol,* **5**, 57.

Chimileski, S., Franklin, M. J., & Papke, R. T. (2014b). Biofilms formed by the archaeon *Haloferax volcanii* exhibit cellular differentiation and social motility, and facilitate horizontal gene transfer. *BMC Biol,* **12**, 65.

Chimileski, S., & Papke, R. T. (2015). Getting a hold on archaeal type IV pili: an expanding repertoire of cellular appendages implicates complex regulation and diverse functions. *Front Microbiol,* **6**, 362.

Chomczynski, P., & Sacchi, N. (2006). The single-step method of RNA isolation by acid guanidinium thiocyanate-phenol-chloroform extraction: twenty-something years on. *Nat Protoc,* **1**(2), 581-585.

Cohen-Krausz, S., & Trachtenberg, S. (2002). The structure of the archeabacterial flagellar filament of the extreme halophile *Halobacterium salinarum* R1M1 and its relation to eubacterial flagellar filaments and type IV pili. *J Mol Biol,* **321**(3), 383-395.

Coker, J. A., DasSarma, P., Kumar, J., Muller, J. A., & DasSarma, S. (2007). Transcriptional profiling of the model Archaeon *Halobacterium sp.* NRC-1: responses to changes in salinity and temperature. *Saline Systems,* **3**, 6.

Crowley, D. J., Boubriak, I., Berquist, B. R., Clark, M., Richard, E., Sullivan, L., . . . McCready, S. (2006). The uvrA, uvrB and uvrC genes are required for repair of ultraviolet light induced DNA photoproducts in *Halobacterium sp.* NRC-1. *Saline Systems,* **2**, 11.

DasSarma, S., & DasSarma, P. (2001). Halophiles *eLS*: John Wiley & Sons, Ltd.

DasSarma, S., Kennedy, S. P., Berquist, B., Victor Ng, W., Baliga, N. S., Spudich, J. L., . . . Hood, L. (2001). Genomic perspective on the photobiology of *Halobacterium* species NRC-1, a phototrophic, phototactic, and UV-tolerant haloarchaeon. *Photosynth Res,* **70**(1), 3-17.

Davey, M. E., & O'Toole G, A. (2000). Microbial biofilms: from ecology to molecular genetics. *Microbiol Mol Biol Rev,* **64**(4), 847-867.

Delmas, S., Shunburne, L., Ngo, H. P., & Allers, T. (2009). Mre11-Rad50 promotes rapid repair of DNA damage in the polyploid archaeon *Haloferax volcanii* by restraining homologous recombination. *PLoS Genet,* **5**(7), e1000552.

DeLong, E. F. (1998). Everything in moderation: archaea as 'non-extremophiles'. *Curr Opin Genet Dev,* **8**(6), 649-654.

Dennis, P. P., & Shimmin, L. C. (1997). Evolutionary divergence and salinity-mediated selection in halophilic archaea. *Microbiol Mol Biol Rev,* **61**(1), 90-104.

Dibrova, D. V., Galperin, M. Y., & Mulkidjanian, A. Y. (2014). Phylogenomic reconstruction of archaeal fatty acid metabolism. *Environ Microbiol,* **16**(4), 907-918.

Ding, Y., Lau, Z., Logan, S. M., Kelly, J. F., Berezuk, A., Khursigara, C. M., & Jarrell, K. F. (2015). The Effects of Growth Conditions on Archaellation and N-Glycosylation in *Methanococcus maripaludis*. *Microbiology*.

Dominiak, D. M., Nielsen, J. L., & Nielsen, P. H. (2011). Extracellular DNA is abundant and important for microcolony strength in mixed microbial biofilms. *Environ Microbiol,* **13**(3), 710-721.

Dufrêne, Y. F. (2015). Sticky microbes: forces in microbial cell adhesion. *Trends Microbiol,* **23**(6), 376-382.
Ebert, K., Goebel, W., & Pfeifer, F. (1984). Homologies between heterogeneous extrachromosomal DNA populations of *Halobacterium halobium* and four new isolates. *Mol. Gen. Genet.*(194), 91–97.
Eichler, J., Arbiv, A., Cohen-Rosenzweig, C., Kaminski, L., Kandiba, L., & Konrad, Z. (2013). N-glycosylation in *Haloferax volcanii*: adjusting the sweetness. *Front Microbiol,* **4**, 403.
Elleuche, S., Schafers, C., Blank, S., Schroder, C., & Antranikian, G. (2015). Exploration of extremophiles for high temperature biotechnological processes. *Curr Opin Microbiol,* **25**, 113-119.
Englert, C., Kruger, K., Offner, S., & Pfeifer, F. (1992). Three different but related gene clusters encoding gas vesicles in halophilic archaea. *J Mol Biol,* **227**(2), 586-592.
Esquivel, R. N., & Pohlschröder, M. (2014). A conserved type IV pilin signal peptide H-domain is critical for the post-translational regulation of flagella-dependent motility. *Mol Microbiol,* **93**(3), 494-504.
Esquivel, R. N., Schulze, S., Hippler, M., & Pohlschroder, M. (2016). Identification of *Haloferax volcanii* pilin N-glycans with diverse roles in pilus-biosynthesis, adhesion and microcolony formation. *J Biol Chem*.
Esquivel, R. N., Xu, R., & Pohlschröder, M. (2013). Novel archaeal adhesion pilins with a conserved N terminus. *J Bacteriol,* **195**(17), 3808-3818.
Evans, D. J., Allison, D. G., Brown, M. R., & Gilbert, P. (1991). Susceptibility of *Pseudomonas aeruginosa* and *Escherichia coli* biofilms towards ciprofloxacin: effect of specific growth rate. *J Antimicrob Chemother,* **27**(2), 177-184.
Facciotti, M. T., Pang, W. L., Lo, F. Y., Whitehead, K., Koide, T., Masumura, K., . . . Baliga, N. S. (2010). Large scale physiological readjustment during growth enables rapid, comprehensive and inexpensive systems analysis. *BMC Syst Biol,* **4**, 64.
Facciotti, M. T., Reiss, D. J., Pan, M., Kaur, A., Vuthoori, M., Bonneau, R., . . . Baliga, N. S. (2007). General transcription factor specified global gene regulation in archaea. *Proc Natl Acad Sci U S A,* **104**(11), 4630-4635.
Faguy, D. M., & Doolittle, W. F. (1998). Cytoskeletal proteins: the evolution of cell division. *Curr Biol,* **8**(10), R338-341.
Falb, M., Muller, K., Konigsmaier, L., Oberwinkler, T., Horn, P., von Gronau, S., . . . Oesterhelt, D. (2008). Metabolism of halophilic archaea. *Extremophiles,* **12**(2), 177-196.
Falb, M., Pfeiffer, F., Palm, P., Rodewald, K., Hickmann, V., Tittor, J., & Oesterhelt, D. (2005). Living with two extremes: conclusions from the genome sequence of *Natronomonas pharaonis*. *Genome Res,* **15**(10), 1336-1343.
Falkowski, P. G., Fenchel, T., & Delong, E. F. (2008). The microbial engines that drive Earth's biogeochemical cycles. *Science,* **320**(5879), 1034-1039.
Ferrando-May, E., Krah, M., Marwan, W., & Oesterhelt, D. (1993). The methyl-accepting transducer protein HtrI is functionally associated with the photoreceptor sensory rhodopsin I in the archaeon *Halobacterium salinarium*. *EMBO J,* **12**(8), 2999-3005.
Flemming, H. C., & Wingender, J. (2010). The biofilm matrix. *Nat Rev Microbiol,* **8**(9), 623-633.
Fröls, S. (2013). Archaeal biofilms: widespread and complex. *Biochem Soc Trans,* **41**(1), 393-398.
Fröls, S., Ajon, M., Wagner, M., Teichmann, D., Zolghadr, B., Folea, M., . . . Albers, S. V. (2008). UV-inducible cellular aggregation of the hyperthermophilic archaeon *Sulfolobus solfataricus* is mediated by pili formation. *Mol Microbiol,* **70**(4), 938-952.

Fröls, S., Dyall-Smith, M., & Pfeifer, F. (2012). Biofilm formation by haloarchaea. *Environ Microbiol,* **14**(12), 3159-3174.
Furtwängler, K., Tarasov, V., Wende, A., Schwarz, C., & Oesterhelt, D. (2010). Regulation of phosphate uptake via Pst transporters in *Halobacterium salinarum* R1. *Mol Microbiol,* **76**(2), 378-392.
Gaci, N., Borrel, G., Tottey, W., O'Toole, P. W., & Brugere, J. F. (2014). Archaea and the human gut: new beginning of an old story. *World J Gastroenterol,* **20**(43), 16062-16078.
Gan, R. R., Yi, E. C., Chiu, Y., Lee, H., Kao, Y. C., Wu, T. H., . . . Ng, W. V. (2006). Proteome analysis of *Halobacterium sp.* NRC-1 facilitated by the biomodule analysis tool BMSorter. *Mol Cell Proteomics,* **5**(6), 987-997.
Gebhard, S., Tran, S. L., & Cook, G. M. (2006). The Phn system of *Mycobacterium smegmatis*: a second high-affinity ABC-transporter for phosphate. *Microbiology,* **152**(Pt 11), 3453-3465.
Gerl, L., Deutzmann, R., & Sumper, M. (1989). Halobacterial flagellins are encoded by a multigene family. Identification of all five gene products. *FEBS Lett,* **244**(1), 137-140.
Gerl, L., & Sumper, M. (1988). Halobacterial flagellins are encoded by a multigene family. Characterization of five flagellin genes. *J Biol Chem,* **263**(26), 13246-13251.
Ghosh, A., & Albers, S. V. (2011). Assembly and function of the archaeal flagellum. *Biochem Soc Trans,* **39**(1), 64-69.
Gillet, L. C., Navarro, P., Tate, S., Rost, H., Selevsek, N., Reiter, L., . . . Aebersold, R. (2012). Targeted data extraction of the MS/MS spectra generated by data-independent acquisition: a new concept for consistent and accurate proteome analysis. *Mol Cell Proteomics,* **11**(6), O111 016717.
Giltner, C. L., Nguyen, Y., & Burrows, L. L. (2012). Type IV pilin proteins: versatile molecular modules. *Microbiol Mol Biol Rev,* **76**(4), 740-772.
Gonzalez, O., Gronau, S., Pfeiffer, F., Mendoza, E., Zimmer, R., & Oesterhelt, D. (2009). Systems analysis of bioenergetics and growth of the extreme halophile *Halobacterium salinarum*. *PLoS Comput Biol,* **5**(4), e1000332.
Goo, Y. A., Yi, E. C., Baliga, N. S., Tao, W. A., Pan, M., Aebersold, R., . . . Ng, W. V. (2003). Proteomic analysis of an extreme halophilic archaeon, *Halobacterium sp.* NRC-1. *Mol Cell Proteomics,* **2**(8), 506-524.
Griebler, C., & Slezak, D. (2001). Microbial activity in aquatic environments measured by dimethyl sulfoxide reduction and intercomparison with commonly used methods. *Appl Environ Microbiol,* **67**(1), 100-109.
Grininger, M., Staudt, H., Johansson, P., Wachtveitl, J., & Oesterhelt, D. (2009). Dodecin is the key player in flavin homeostasis of archaea. *J Biol Chem,* **284**(19), 13068-13076.
Grobbler, C., Virdis, B., Nouwens, A., Harnisch, F., Rabaey, K., & Bond, P. L. (2015). Use of SWATH mass spectrometry for quantitative proteomic investigation of *Shewanella oneidensis* MR-1 biofilms grown on graphite cloth electrodes. *Syst Appl Microbiol,* **38**(2), 135-139.
Gromova, I., & Celis, J. E. (2006). Protein Detection in Gels by Silver Staining: A Procedure Compatible with Mass-Spectrometry. In J. E. Celis, N. Carter, T. Hunter, K. Simons, J. V. Small, & D. Shotton (Eds.), *Cell Biology: A Laboratory Handbook. 3rd Edition.* Elsevier. Academic Press.
Gruber, C., Legat, A., Pfaffenhuemer, M., Radax, C., Weidler, G., Busse, H. J., & Stan-Lotter, H. (2004). *Halobacterium noricense* sp. nov., an archaeal isolate from a bore core of an alpine Permian salt deposit, classification of *Halobacterium* sp. NRC-1 as a strain of H. salinarum and emended description of *H. salinarum*. *Extremophiles,* **8**(6), 431-439.

Gupta, R. S., Naushad, S., & Baker, S. (2015). Phylogenomic analyses and molecular signatures for the class Halobacteria and its two major clades: a proposal for division of the class Halobacteria into an emended order Halobacteriales and two new orders, Haloferacales ord. nov. and Natrialbales ord. nov., containing the novel families Haloferacaceae fam. nov. and Natrialbaceae fam. nov. *Int J Syst Evol Microbiol,* **65**(Pt 3), 1050-1069.

Guttenplan, S. B., Blair, K. M., & Kearns, D. B. (2010). The EpsE flagellar clutch is bifunctional and synergizes with EPS biosynthesis to promote *Bacillus subtilis* biofilm formation. *PLoS Genet,* **6**(12), e1001243.

Guttenplan, S. B., & Kearns, D. B. (2013). Regulation of flagellar motility during biofilm formation. *FEMS Microbiol Rev,* **37**(6), 849-871.

Hall-Stoodley, L., Costerton, J. W., & Stoodley, P. (2004). Bacterial biofilms: from the natural environment to infectious diseases. *Nat Rev Microbiol,* **2**(2), 95-108.

Hamedi, J., Mohammadipanah, F., & Ventosa, A. (2013). Systematic and biotechnological aspects of halophilic and halotolerant actinomycetes. *Extremophiles,* **17**(1), 1-13.

Han, Q., Lu, J., Duan, J., Su, D., Hou, X., Li, F., . . . Huang, B. (2008). Gcn5- and Elp3-induced histone H3 acetylation regulates hsp70 gene transcription in yeast. *Biochem J,* **409**(3), 779-788.

Hänsch, G. L. (2012). Host Defence against Bacterial Biofilms: "Mission Impossible"? *ISRN Immunology, 2012*(Article ID 853123).

Harrison, J. J., Ceri, H., & Turner, R. J. (2007). Multimetal resistance and tolerance in microbial biofilms. *Nat Rev Microbiol,* **5**(12), 928-938.

Hartman, A. L., Norais, C., Badger, J. H., Delmas, S., Haldenby, S., Madupu, R., . . . Eisen, J. A. (2010). The complete genome sequence of *Haloferax volcanii* DS2, a model archaeon. *PLoS One,* **5**(3), e9605.

Hartmann, R., & Oesterhelt, D. (1977). Bacteriorhodopsin-mediated photophosphorylation in *Halobacterium halobium*. *Eur J Biochem,* **77**(2), 325-335.

Hartmann, R., Sickinger, H. D., & Oesterhelt, D. (1980). Anaerobic growth of halobacteria. *Proc Natl Acad Sci U S A,* **77**(7), 3821-3825.

Heidelberg, J. F., Paulsen, I. T., Nelson, K. E., Gaidos, E. J., Nelson, W. C., Read, T. D., . . . Fraser, C. M. (2002). Genome sequence of the dissimilatory metal ion-reducing bacterium *Shewanella oneidensis*. *Nat Biotechnol,* **20**(11), 1118-1123. doi:10.1038/nbt749

Henche, A. L., Ghosh, A., Yu, X., Jeske, T., Egelman, E., & Albers, S. V. (2012a). Structure and function of the adhesive type IV pilus of *Sulfolobus acidocaldarius*. *Environ Microbiol,* **14**(12), 3188-3202.

Henche, A. L., Koerdt, A., Ghosh, A., & Albers, S. V. (2012b). Influence of cell surface structures on crenarchaeal biofilm formation using a thermostable green fluorescent protein. *Environ Microbiol,* **14**(3), 779-793.

Hendler, R. W., Barnett, S. M., Dracheva, S., Bose, S., & Levin, I. W. (2003). Purple membrane lipid control of bacteriorhodopsin conformational flexibility and photocycle activity. *Eur J Biochem,* **270**(9), 1920-1925.

Hendrickson, E. L., Liu, Y., Rosas-Sandoval, G., Porat, I., Soll, D., Whitman, W. B., & Leigh, J. A. (2008). Global responses of *Methanococcus maripaludis* to specific nutrient limitations and growth rate. *J Bacteriol,* **190**(6), 2198-2205.

Henneberger, R., Moissl, C., Amann, T., Rudolph, C., & Huber, R. (2006). New insights into the lifestyle of the cold-loving SM1 euryarchaeon: natural growth as a monospecies biofilm in the subsurface. *Appl Environ Microbiol,* **72**(1), 192-199.

Hochstein, L. I. (1974). The metabolism of carbohydrates by extremely halophilic bacteria: glucose metabolism via a modified Entner-Doudoroff pathway. *Can J Microbiol,* **20**(8), 1085-1091.

Houwink, A. L. (1956). Flagella, gas vacuoles and cell-wall structure in *Halobacterium halobium*; an electron microscope study. *J Gen Microbiol,* **15**(1), 146-150.

Huber, H., Hohn, M. J., Rachel, R., Fuchs, T., Wimmer, V. C., & Stetter, K. O. (2002). A new phylum of Archaea represented by a nanosized hyperthermophilic symbiont. *Nature,* **417**(6884), 63-67.

Hussain, H., Branny, P., & Allan, E. (2006). A eukaryotic-type serine/threonine protein kinase is required for biofilm formation, genetic competence, and acid resistance in *Streptococcus mutans*. *J Bacteriol*, **188**(4), 1628-1632.

Ibars, J. R., Moreno, D. A., & Ranninger, C. (1992). Microbial corrosion of stainless steel. *Microbiologia,* **8**(2), 63-75.

Imlay, J. A., & Fridovich, I. (1991). Assay of metabolic superoxide production in *Escherichia coli*. *J Biol Chem,* **266**(11), 6957-6965.

Ishibashi, M., Tokunaga, H., Hiratsuka, K., Yonezawa, Y., Tsurumaru, H., Arakawa, T., & Tokunaga, M. (2001). NaCl-activated nucleoside diphosphate kinase from extremely halophilic archaeon, *Halobacterium salinarum*, maintains native conformation without salt. *FEBS Lett,* **493**(2-3), 134-138

Jaakkola, S. T., Zerulla, K., Guo, Q. G., Liu, Y., Ma, H. L., Yang, C. H., . . . Oksanen, H. M. (2014). Halophilic Archaea Cultivated from Surface Sterilized Middle-Late Eocene Rock Salt Are Polyploid. *PLoS One,* **9**(10).

Jachlewski, S., Jachlewski, W. D., Linne, U., Brasen, C., Wingender, J., & Siebers, B. (2015). Isolation of Extracellular Polymeric Substances from Biofilms of the Thermoacidophilic Archaeon *Sulfolobus acidocaldarius*. *Front Bioeng Biotechnol,* **3**, 123.

Jarrell, K. F., Ding, Y., Meyer, B. H., Albers, S. V., Kaminski, L., & Eichler, J. (2014). N-linked glycosylation in Archaea: a structural, functional, and genetic analysis. *Microbiol Mol Biol Rev,* **78**(2), 304-341.

Jarrell, K. F., Ding, Y., Nair, D. B., & Siu, S. (2013). Surface appendages of archaea: structure, function, genetics and assembly. *Life (Basel),* **3**(1), 86-117.

Jarrell, K. F., Stark, M., Nair, D. B., & Chong, J. P. (2011). Flagella and pili are both necessary for efficient attachment of *Methanococcus maripaludis* to surfaces. *FEMS Microbiol Lett,* **319**(1), 44-50.

Jung, K., Friede, T., & Beissbarth, T. (2011). Reporting FDR analogous confidence intervals for the log fold change of differentially expressed genes. *BMC Bioinformatics,* **12**, 288.

Jung, K., Poschmann, G., Podwojski, K., Eisenacher, M., Kohl, M., Pfeiffer, K., . . . Stephan, C. (2009). Adjusted Confidence Intervals for the Expression Change of Proteins Observed in 2-Dimensional Difference Gel Electrophoresis. *J Proteomics Bioinform*(2), 078-087.

Kallberg, Y., Oppermann, U., & Persson, B. (2010). Classification of the short-chain dehydrogenase/reductase superfamily using hidden Markov models. *FEBS J,* **277**(10), 2375-2386.

Kalmokoff, M. L., Jarrell, K. F., & Koval, S. F. (1988). Isolation of flagella from the archaebacterium *Methanococcus voltae* by phase separation with Triton X-114. *J Bacteriol,* **170**(4), 1752-1758.

Kandiba, L., & Eichler, J. (2015). Deciphering a pathway of *Halobacterium salinarum* N-glycosylation. *Microbiologyopen,* **4**(1), 28-40.

Kandler, O., & Konig, H. (1998). Cell wall polymers in Archaea (Archaebacteria). *Cell Mol Life Sci,* **54**(4), 305-308.

Katoh, K., & Standley, D. M. (2014). MAFFT: iterative refinement and additional methods. *Methods Mol Biol,* 1079, 131-146.

Kaur, A., Van, P. T., Busch, C. R., Robinson, C. K., Pan, M., Pang, W. L., . . . Baliga, N. S. (2010). Coordination of frontline defense mechanisms under severe oxidative stress. *Mol Syst Biol,* **6**, 393.

Khoury, A. E., Lam, K., Ellis, B., & Costerton, J. W. (1992). Prevention and control of bacterial infections associated with medical devices. *ASAIO J,* **38**(3), M174-178.

Kim, K. K., Park, H. Y., Park, W., Kim, I. S., & Lee, S. T. (2005). *Microbacterium xylanilyticum* sp. nov., a xylan-degrading bacterium isolated from a biofilm. *Int J Syst Evol Microbiol,* **55**(Pt 5), 2075-2079.

Kish, A., Kirkali, G., Robinson, C., Rosenblatt, R., Jaruga, P., Dizdaroglu, M., & DiRuggiero, J. (2009). Salt shield: intracellular salts provide cellular protection against ionizing radiation in the halophilic archaeon, *Halobacterium salinarum* NRC-1. *Environmental Microbiology,* **11**(5), 1066-1078.

Klein, C., Aivaliotis, M., Olsen, J. V., Falb, M., Besir, H., Scheffer, B., . . . Oesterhelt, D. (2007). The low molecular weight proteome of *Halobacterium salinarum*. *Journal of Proteome Research,* **6**(4), 1510-1518.

Klein, C., Garcia-Rizo, C., Bisle, B., Scheffer, B., Zischka, H., Pfeiffer, F., . . . Oesterhelt, D. (2005). The membrane proteome of *Halobacterium salinarum*. *Proteomics,* **5**(1), 180-197.

Koch, M. K., & Oesterhelt, D. (2005). MpcT is the transducer for membrane potential changes in *Halobacterium salinarum*. *Mol Microbiol,* **55**(6), 1681-1694.

Koerdt, A., Godeke, J., Berger, J., Thormann, K. M., & Albers, S. V. (2010). Crenarchaeal biofilm formation under extreme conditions. *PLoS One,* **5**(11), e14104.

Koerdt, A., Jachlewski, S., Ghosh, A., Wingender, J., Siebers, B., & Albers, S. V. (2012). Complementation of *Sulfolobus solfataricus* PBL2025 with an alpha-mannosidase: effects on surface attachment and biofilm formation. *Extremophiles,* **16**(1), 115-125.

Koerdt, A., Orell, A., Pham, T. K., Mukherjee, J., Wlodkowski, A., Karunakaran, E., . . . Albers, S. V. (2011). Macromolecular Fingerprinting of *Sulfolobus* Species in Biofilm: A Transcriptomic and Proteomic Approach Combined with Spectroscopic Analysis. *Journal of Proteome Research,* **10**(9), 4105-4119.

Koo, H., Xiao, J., Klein, M. I., & Jeon, J. G. (2010). Exopolysaccharides produced by *Streptococcus mutans* glucosyltransferases modulate the establishment of microcolonies within multispecies biofilms. *J Bacteriol,* **192**(12), 3024-3032.

Koonin, E. V., Mushegian, A. R., Galperin, M. Y., & Walker, D. R. (1997). Comparison of archaeal and bacterial genomes: computer analysis of protein sequences predicts novel functions and suggests a chimeric origin for the archaea. *Mol Microbiol,* **25**(4), 619-637.

Koonin, E. V., & Wolf, Y. I. (2008). Genomics of bacteria and archaea: the emerging dynamic view of the prokaryotic world. *Nucleic Acids Res,* **36**(21), 6688-6719.

Kottemann, M., Kish, A., Iloanusi, C., Bjork, S., & DiRuggiero, J. (2005). Physiological responses of the halophilic archaeon *Halobacterium* sp. strain NRC1 to desiccation and gamma irradiation. *Extremophiles,* **9**(3), 219-227.

Kozubal, M. A., Romine, M., Jennings, R., Jay, Z. J., Tringe, S. G., Rusch, D. B., . . . Inskeep, W. P. (2013). Geoarchaeota: a new candidate phylum in the Archaea from high-temperature acidic iron mats in Yellowstone National Park. *ISME J,* **7**(3), 622-634.

Krogh, A., Larsson, B., von Heijne, G., & Sonnhammer, E. L. (2001). Predicting transmembrane protein topology with a hidden Markov model: application to complete genomes. *J Mol Biol,* **305**(3), 567-580.

Kupper, J., Marwan, W., Typke, D., Grunberg, H., Uwer, U., Gluch, M., & Oesterhelt, D. (1994). The flagellar bundle of *Halobacterium salinarium* is inserted into a distinct polar cap structure. *J Bacteriol,* **176**(16), 5184-5187.

Lambert, J. P., Ivosev, G., Couzens, A. L., Larsen, B., Taipale, M., Lin, Z. Y., . . . Gingras, A. C. (2013). Mapping differential interactomes by affinity purification coupled with data-independent mass spectrometry acquisition. *Nat Methods,* **10**(12), 1239-1245.

Lapaglia, C., & Hartzell, P. L. (1997). Stress-Induced Production of Biofilm in the Hyperthermophile *Archaeoglobus fulgidus*. *Appl Environ Microbiol,* **63**(8), 3158-3163.

Lassak, K., Ghosh, A., & Albers, S. V. (2012a). Diversity, assembly and regulation of archaeal type IV pili-like and non-type-IV pili-like surface structures. *Res Microbiol,* **163**(9-10), 630-644.

Lassak, K., Neiner, T., Ghosh, A., Klingl, A., Wirth, R., & Albers, S. V. (2012b). Molecular analysis of the crenarchaeal flagellum. *Mol Microbiol,* **83**(1), 110-124.

Lattif, A. A., Mukherjee, P. K., Chandra, J., Roth, M. R., Welti, R., Rouabhia, M., & Ghannoum, M. A. (2011). Lipidomics of *Candida albicans* biofilms reveals phase-dependent production of phospholipid molecular classes and role for lipid rafts in biofilm formation. *Microbiology,* **157**(Pt 11), 3232-3242.

Lebeer, S., Verhoeven, T. L., Francius, G., Schoofs, G., Lambrichts, I., Dufrene, Y., . . . De Keersmaecker, S. C. (2009). Identification of a Gene Cluster for the Biosynthesis of a Long, Galactose-Rich Exopolysaccharide in Lactobacillus rhamnosus GG and Functional Analysis of the Priming Glycosyltransferase. *Appl Environ Microbiol,* **75**(11), 3554-3563.

Leong, D., Pfeifer, F., Boyer, H., & Betlach, M. (1988). Characterization of a second gene involved in bacterio-opsin gene expression in a halophilic archaebacterium. *J Bacteriol,* **170**(10), 4903-4909.

Leuko, S., Raftery, M. J., Burns, B. P., Walter, M. R., & Neilan, B. A. (2009). Global protein-level responses of *Halobacterium salinarum* NRC-1 to prolonged changes in external sodium chloride concentrations. *Journal of Proteome Research,* **8**(5), 2218-2225.

Lin, X., Lin, L., Yao, Z., Li, W., Sun, L., Zhang, D., . . . Lin, W. (2015). An integrated quantitative and targeted proteomics reveals fitness mechanisms of Aeromonas hydrophila under oxytetracycline stress. *Journal of Proteome Research,* **14**(3), 1515-1525.

Losensky, G. (2011). Untersuchungen auf Proteinebene zur Biofilmbildung halophiler Archaea. Diploma thesis, Technische Universität Darmstadt, Darmstadt Germany.

Losensky, G., Fröls, S., Jung, K., Pfeifer, F., Urlaub, H., & Lenz, C. (2016). Shedding light on biofilm formation of *Halobacterium salinarum* R1 by SWATH-LC/MS/MS analysis of planktonic and sessile cells. *Proteomics*, Submitted February 2016, under revision.

Losensky, G., Vidakovic, L., Klingl, A., Pfeifer, F., & Frols, S. (2014). Novel pili-like surface structures of *Halobacterium salinarum* strain R1 are crucial for surface adhesion. *Front Microbiol,* **5**, 755.

Lundin, D., Gribaldo, S., Torrents, E., Sjoberg, B. M., & Poole, A. M. (2010). Ribonucleotide reduction - horizontal transfer of a required function spans all three domains. *BMC Evol Biol,* **10**, 383.

Makarova, K. S., & Koonin, E. V. (2013). Archaeology of eukaryotic DNA replication. *Cold Spring Harb Perspect Biol,* **5**(11), a012963.

Makarova, K. S., Sorokin, A. V., Novichkov, P. S., Wolf, Y. I., & Koonin, E. V. (2007). Clusters of orthologous genes for 41 archaeal genomes and implications for evolutionary genomics of archaea. *Biol Direct,* **2**, 33.

Mandelli, F., Miranda, V. S., Rodrigues, E., & Mercadante, A. Z. (2012). Identification of carotenoids with high antioxidant capacity produced by extremophile microorganisms. *World J Microbiol Biotechnol,* **28**(4), 1781-1790.

Maupin-Furlow, J. A., Humbard, M. A., & Kirkland, P. A. (2012). Extreme challenges and advances in archaeal proteomics. *Curr Opin Microbiol,* **15**(3), 351-356.

Meng, J., Xu, J., Qin, D., He, Y., Xiao, X., & Wang, F. (2014). Genetic and functional properties of uncultivated MCG archaea assessed by metagenome and gene expression analyses. *ISME J,* **8**(3), 650-659.

Metcalf, W. W., & Wanner, B. L. (1991). Involvement of the *Escherichia coli* phn (psiD) gene cluster in assimilation of phosphorus in the form of phosphonates, phosphite, Pi esters, and Pi. *J Bacteriol,* **173**(2), 587-600.

Meyer, B. H., Birich, A., & Albers, S. V. (2015). N-Glycosylation of the archaellum filament is not important for archaella assembly and motility, although N-Glycosylation is essential for motility in *Sulfolobus acidocaldarius*. *Biochimie,* **118**, 294-301.

Moissl, C., Rachel, R., Briegel, A., Engelhardt, H., & Huber, R. (2005). The unique structure of archaeal 'hami', highly complex cell appendages with nano-grappling hooks. *Mol Microbiol,* **56**(2), 361-370.

Moissl, C., Rudolph, C., & Huber, R. (2002). Natural communities of novel archaea and bacteria with a string-of-pearls-like morphology: molecular analysis of the bacterial partners. *Appl Environ Microbiol,* **68**(2), 933-937.

Molin, S., & Tolker-Nielsen, T. (2003). Gene transfer occurs with enhanced efficiency in biofilms and induces enhanced stabilisation of the biofilm structure. *Curr Opin Biotechnol,* **14**(3), 255-261.

Monds, R. D., Silby, M. W., & Mahanty, H. K. (2001). Expression of the Pho regulon negatively regulates biofilm formation by *Pseudomonas aureofaciens* PA147-2. *Mol Microbiol,* **42**(2), 415-426.

Mongodin, E. F., Nelson, K. E., Daugherty, S., Deboy, R. T., Wister, J., Khouri, H., . . . Rodriguez-Valera, F. (2005). The genome of *Salinibacter ruber*: convergence and gene exchange among hyperhalophilic bacteria and archaea. *Proc Natl Acad Sci U S A,* **102**(50), 18147-18152.

Monnet, V. (2003). Bacterial oligopeptide-binding proteins. *Cell Mol Life Sci,* **60**(10), 2100-2114.

Moreau, Y., Aerts, S., De Moor, B., De Strooper, B., & Dabrowski, M. (2003). Comparison and meta-analysis of microarray data: from the bench to the computer desk. *Trends Genet,* **19**(10), 570-577.

Mou, Y. Z., Qiu, X. X., Zhao, M. L., Cui, H. L., Oh, D., & Dyall-Smith, M. L. (2012). *Halohasta litorea* gen. nov. sp. nov., and *Halohasta litchfieldiae* sp. nov., isolated from the Daliang aquaculture farm, China and from Deep Lake, Antarctica, respectively. *Extremophiles,* **16**(6), 895-901.

Mukhopadhyay, B., Johnson, E. F., & Wolfe, R. S. (2000). A novel pH2 control on the expression of flagella in the hyperthermophilic strictly hydrogenotrophic methanarchaeaon *Methanococcus jannaschii*. *Proc Natl Acad Sci U S A,* **97**(21), 11522-11527.

Müller, D. W., Meyer, C., Gurster, S., Kuper, U., Huber, H., Rachel, R., . . . Bellack, A. (2009). The Iho670 fibers of *Ignicoccus hospitalis*: a new type of archaeal cell surface appendage. *J Bacteriol,* **191**(20), 6465-6468.

Müller, J. A., & DasSarma, S. (2005). Genomic analysis of anaerobic respiration in the archaeon *Halobacterium* sp. strain NRC-1: dimethyl sulfoxide and trimethylamine N-oxide as terminal electron acceptors. *J Bacteriol,* **187**(5), 1659-1667.

Myszka, K., & Czaczyk, K. (2009). Characterization of adhesive exopolysaccharide (EPS) produced by *Pseudomonas aeruginosa* under starvation conditions. *Curr Microbiol,* **58**(6), 541-546.

Nachin, L., Nannmark, U., & Nystrom, T. (2005). Differential roles of the universal stress proteins of *Escherichia coli* in oxidative stress resistance, adhesion, and motility. *J Bacteriol,* **187**(18), 6265-6272.

Nair, D. B., Uchida, K., Aizawa, S., & Jarrell, K. F. (2014). Genetic analysis of a type IV pili-like locus in the archaeon *Methanococcus maripaludis*. *Arch Microbiol,* **196**(3), 179-191.

Nasir, A., Kim, K. M., & Caetano-Anolles, G. (2014). Global patterns of protein domain gain and loss in superkingdoms. *PLoS Comput Biol,* **10**(1), e1003452.

Nath, A. (2015). Insights into the sequence parameters for halophilic adaptation. *Amino Acids*. doi:10.1007/s00726-015-2123-x

Näther, D. J., Rachel, R., Wanner, G., & Wirth, R. (2006). Flagella of *Pyrococcus furiosus*: multifunctional organelles, made for swimming, adhesion to various surfaces, and cell-cell contacts. *J Bacteriol,* **188**(19), 6915-6923.

Nelson-Sathi, S., Dagan, T., Landan, G., Janssen, A., Steel, M., McInerney, J. O., . . . Martin, W. F. (2012). Acquisition of 1,000 eubacterial genes physiologically transformed a methanogen at the origin of Haloarchaea. *Proc Natl Acad Sci U S A,* **109**(50), 20537-20542.

Nelson-Sathi, S., Sousa, F. L., Roettger, M., Lozada-Chavez, N., Thiergart, T., Janssen, A., . . . Martin, W. F. (2015). Origins of major archaeal clades correspond to gene acquisitions from bacteria. *Nature,* **517**(7532), 77-80.

Nesvizhskii, A. I. (2007). Protein identification by tandem mass spectrometry and sequence database searching. *Methods Mol Biol,* **367**, 87-119.

Neznansky, A., Blus-Kadosh, I., Yerushalmi, G., Banin, E., & Opatowsky, Y. (2014). The *Pseudomonas aeruginosa* phosphate transport protein PstS plays a phosphate-independent role in biofilm formation. *FASEB J,* **28**(12), 5223-5233.

Ng, W. V., Kennedy, S. P., Mahairas, G. G., Berquist, B., Pan, M., Shukla, H. D., . . . DasSarma, S. (2000). Genome sequence of *Halobacterium* species NRC-1. *Proc Natl Acad Sci U S A,* **97**(22), 12176-12181.

Nicolaus, B., Manca, M. C., Romano, I., & Lama, L. (2003). Production of an exopolysaccharide from two thermophilic archaea belonging to the genus *Sulfolobus*. *FEMS Microbiology Letters,* **109**(2-3), 203–206.

Niquette, P., Servais, P., & Savoir, R. (2001). Bacterial dynamics in the drinking water distribution system of Brussels. *Water Res,* **35**(3), 675-682.

Noffke, N., Christian, D., Wacey, D., & Hazen, R. M. (2013). Microbially induced sedimentary structures recording an ancient ecosystem in the ca. 3.48 billion-year-old Dresser Formation, Pilbara, Western Australia. *Astrobiology,* **13**(12), 1103-1124.

Norton, C. F., & Grant, W. D. (1988). Survival of Halobacteria within Fluid Inclusions in Salt Crystals. *Journal of General Microbiology,* **134**, 1365-1373

Nunoura, T., Takaki, Y., Kakuta, J., Nishi, S., Sugahara, J., Kazama, H., . . . Takami, H. (2011). Insights into the evolution of Archaea and eukaryotic protein modifier systems revealed by the genome of a novel archaeal group. *Nucleic Acids Res,* **39**(8), 3204-3223.

O'Toole, G., Kaplan, H. B., & Kolter, R. (2000). Biofilm formation as microbial development. *Annu Rev Microbiol,* **54**, 49-79.

Offre, P., Spang, A., & Schleper, C. (2013). Archaea in biogeochemical cycles. *Annu Rev Microbiol,* **67**, 437-457.

Orell, A., Frols, S., & Albers, S. V. (2013a). Archaeal biofilms: the great unexplored. *Annu Rev Microbiol,* **67**, 337-354.

Orell, A., Peeters, E., Vassen, V., Jachlewski, S., Schalles, S., Siebers, B., & Albers, S. V. (2013b). Lrs14 transcriptional regulators influence biofilm formation and cell motility of Crenarchaea. *ISME J,* **7**(10), 1886-1898.

Oren, A. (1999). Bioenergetic aspects of halophilism. *Microbiol Mol Biol Rev, 63*(2), 334-348.

Oren, A. (2002). Diversity of halophilic microorganisms: environments, phylogeny, physiology, and applications. *J Ind Microbiol Biotechnol,* **28**(1), 56-63.

Oren, A. (2008). Microbial life at high salt concentrations: phylogenetic and metabolic diversity. *Saline Systems,* **4**, 2.

Oren, A. (2013). Life at high salt concentrations, intracellular KCl concentrations, and acidic proteomes. *Front Microbiol,* **4**, 315.

Parsek, M. R., & Singh, P. K. (2003). Bacterial biofilms: an emerging link to disease pathogenesis. *Annu Rev Microbiol,* **57**, 677-701.

Patenge, N., Berendes, A., Engelhardt, H., Schuster, S. C., & Oesterhelt, D. (2001). The fla gene cluster is involved in the biogenesis of flagella in *Halobacterium salinarum*. *Mol Microbiol,* **41**(3), 653-663.

Peeters, E., Driessen, R. P., Werner, F., & Dame, R. T. (2015). The interplay between nucleoid organization and transcription in archaeal genomes. *Nat Rev Microbiol,* **13**(6), 333-341.
Pfeifer, F. (2015). Haloarchaea and the formation of gas vesicles. *Life (Basel),* **5**(1), 385-402.
Pfeifer, F., & Blaseio, U. (1989). Insertion elements and deletion formation in a halophilic archaebacterium. *J Bacteriol,* **171**(9), 5135-5140.
Pfeifer, F., Blaseio, U., & Ghahraman, P. (1988). Dynamic plasmid populations in *Halobacterium halobium*. *J Bacteriol,* **170**(8), 3718-3724.
Pfeiffer, F., Broicher, A., Gillich, T., Klee, K., Mejia, J., Rampp, M., & Oesterhelt, D. (2008a). Genome information management and integrated data analysis with HaloLex. *Arch Microbiol,* **190**(3), 281-299.
Pfeiffer, F., Schuster, S. C., Broicher, A., Falb, M., Palm, P., Rodewald, K., . . . Oesterhelt, D. (2008b). Evolution in the laboratory: the genome of *Halobacterium salinarum* strain R1 compared to that of strain NRC-1. *Genomics,* **91**(4), 335-346.
Pohlschröder, M., & Esquivel, R. N. (2015). Archaeal type IV pili and their involvement in biofilm formation. *Front Microbiol,* **6**, 190.
Pohlschröder, M., Ghosh, A., Tripepi, M., & Albers, S. V. (2011). Archaeal type IV pilus-like structures--evolutionarily conserved prokaryotic surface organelles. *Curr Opin Microbiol,* **14**(3), 357-363.
Pohlschröder, M., Prinz, W. A., Hartmann, E., & Beckwith, J. (1997). Protein translocation in the three domains of life: variations on a theme. *Cell,* **91**(5), 563-566.
Pyatibratov, M. G., Beznosov, S. N., Rachel, R., Tiktopulo, E. I., Surin, A. K., Syutkin, A. S., & Fedorov, O. V. (2008). Alternative flagellar filament types in the haloarchaeon *Haloarcula marismortui*. *Can J Microbiol,* **54**(10), 835-844.
Rastogi, R. P., Richa, Kumar, A., Tyagi, M. B., & Sinha, R. P. (2010). Molecular mechanisms of ultraviolet radiation-induced DNA damage and repair. *J Nucleic Acids, 2010*, 592980.
Reeve, J. N. (2003). Archaeal chromatin and transcription. *Mol Microbiol,* **48**(3), 587-598.
Reimann, J., Lassak, K., Khadouma, S., Ettema, T. J., Yang, N., Driessen, A. J., . . . Albers, S. V. (2012). Regulation of archaella expression by the FHA and von Willebrand domain-containing proteins ArnA and ArnB in *Sulfolobus acidocaldarius*. *Mol Microbiol,* **86**(1), 24-36.
Rietschel, B., Arrey, T. N., Meyer, B., Bornemann, S., Schuerken, M., Karas, M., & Poetsch, A. (2009). Elastase digests: new ammunition for shotgun membrane proteomics. *Mol Cell Proteomics,* **8**(5), 1029-1043.
Rinker, K. D., & Kelly, R. M. (1996). Growth Physiology of the Hyperthermophilic Archaeon *Thermococcus litoralis*: Development of a Sulfur-Free Defined Medium, Characterization of an Exopolysaccharide, and Evidence of Biofilm Formation. *Appl Environ Microbiol,* **62**(12), 4478-4485.
Rivera, M. C., Jain, R., Moore, J. E., & Lake, J. A. (1998). Genomic evidence for two functionally distinct gene classes. *Proc Natl Acad Sci U S A,* **95**(11), 6239-6244.
Rosenzweig, R. F., & Adams, J. (1994). Microbial adaptation to a changeable environment: cell-cell interactions mediate physiological and genetic differentiation. *Bioessays,* **16**(10), 715-717.
Rothschild, L. J., & Mancinelli, R. L. (2001). Life in extreme environments. *Nature,* **409**(6823), 1092-1101.
Rudolph, J., & Oesterhelt, D. (1995). Chemotaxis and phototaxis require a CheA histidine kinase in the archaeon *Halobacterium salinarium*. *EMBO J,* **14**(4), 667-673.
Rudolph, J., & Oesterhelt, D. (1996). Deletion analysis of the che operon in the archaeon *Halobacterium salinarium*. *J Mol Biol,* **258**(4), 548-554.
Ruepp, A., & Soppa, J. (1996). Fermentative arginine degradation in *Halobacterium salinarium* (formerly *Halobacterium halobium*): genes, gene products, and transcripts of the arcRACB gene cluster. *J Bacteriol,* **178**(16), 4942-4947.

Schägger, H., & von Jagow, G. (1987). Tricine-sodium dodecyl sulfate-polyacrylamide gel electrophoresis for the separation of proteins in the range from 1 to 100 kDa. *Anal Biochem,* **166**(2), 368-379.

Schink, B. (1997). Energetics of syntrophic cooperation in methanogenic degradation. *Microbiol Mol Biol Rev,* **61**(2), 262-280.

Schlesner, M., Miller, A., Besir, H., Aivaliotis, M., Streif, J., Scheffer, B., . . . Oesterhelt, D. (2012). The protein interaction network of a taxis signal transduction system in a halophilic archaeon. *BMC Microbiol,* **12**, 272.

Schlesner, M., Miller, A., Streif, S., Staudinger, W. F., Muller, J., Scheffer, B., . . . Oesterhelt, D. (2009). Identification of Archaea-specific chemotaxis proteins which interact with the flagellar apparatus. *BMC Microbiol,* **9**, 56.

Schmittgen, T. D., & Livak, K. J. (2008). Analyzing real-time PCR data by the comparative C(T) method. *Nat Protoc,* **3**(6), 1101-1108.

Schneider, K. L., Pollard, K. S., Baertsch, R., Pohl, A., & Lowe, T. M. (2006). The UCSC Archaeal Genome Browser. *Nucleic Acids Res,* **34**(Database issue), D407-410.

Schopf, S., Wanner, G., Rachel, R., & Wirth, R. (2008). An archaeal bi-species biofilm formed by *Pyrococcus furiosus* and *Methanopyrus kandleri*. *Arch Microbiol,* **190**(3), 371-377.

Schultz, J., Milpetz, F., Bork, P., & Ponting, C. P. (1998). SMART, a simple modular architecture research tool: identification of signaling domains. *Proc Natl Acad Sci U S A,* **95**(11), 5857-5864.

Selevsek, N., Chang, C. Y., Gillet, L. C., Navarro, P., Bernhardt, O. M., Reiter, L., . . . Aebersold, R. (2015). Reproducible and consistent quantification of the Saccharomyces cerevisiae proteome by SWATH-mass spectrometry. *Mol Cell Proteomics,* **14**(3), 739-749.

Seneviratne, C. J., Wang, Y., Jin, L., Wong, S. S., Herath, T. D., & Samaranayake, L. P. (2012). Unraveling the resistance of microbial biofilms: has proteomics been helpful? *Proteomics,* **12**(4-5), 651-665.

Seshadri, R., Joseph, S. W., Chopra, A. K., Sha, J., Shaw, J., Graf, J., . . . Heidelberg, J. F. (2006). Genome sequence of *Aeromonas hydrophila* ATCC 7966T: jack of all trades. *J Bacteriol,* **188**(23), 8272-8282.

Shahapure, R., Driessen, R. P., Haurat, M. F., Albers, S. V., & Dame, R. T. (2014). The archaellum: a rotating type IV pilus. *Mol Microbiol,* **91**(4), 716-723.

Shahmohammadi, H. R., Asgarani, E., Terato, H., Saito, T., Ohyama, Y., Gekko, K., . . . Ide, H. (1998). Protective roles of bacterioruberin and intracellular KCl in the resistance of *Halobacterium salinarium* against DNA-damaging agents. *J Radiat Res*, **39**(4), 251-262.

Shand, R. F., & Betlach, M. C. (1991). Expression of the bop gene cluster of *Halobacterium halobium* is induced by low oxygen tension and by light. *J Bacteriol,* **173**(15), 4692-4699.

Sharma, A. K., Walsh, D. A., Bapteste, E., Rodriguez-Valera, F., Ford Doolittle, W., & Papke, R. T. (2007). Evolution of rhodopsin ion pumps in haloarchaea. *BMC Evol Biol,* **7**, 79.

Sharma, K., Gillum, N., Boyd, J. L., & Schmid, A. (2012). The RosR transcription factor is required for gene expression dynamics in response to extreme oxidative stress in a hypersaline-adapted archaeon. *BMC Genomics,* **13**, 351.

Shemesh, M., & Chai, Y. (2013). A combination of glycerol and manganese promotes biofilm formation in *Bacillus subtilis* via histidine kinase KinD signaling. *J Bacteriol,* **195**(12), 2747-2754.

Shibata, M., Hariya, T., Hatao, M., Ashikaga, T., & Ichikawa, H. (1999). Quantitative polymerase chain reaction using an external control mRNA for determination of gene expression in a heterogeneous cell population. *Toxicol Sci,* **49**(2), 290-296.

Shukla, H. D. (2006). Proteomic analysis of acidic chaperones, and stress proteins in extreme halophile *Halobacterium* NRC-1: a comparative proteomic approach to study heat shock response. *Proteome Sci,* **4**, 6.
Siegele, D. A. (2005). Universal stress proteins in *Escherichia coli*. *J Bacteriol,* **187**(18), 6253-6254.
Smit, A., & Mushegian, A. (2000). Biosynthesis of isoprenoids via mevalonate in Archaea: the lost pathway. *Genome Res,* **10**(10), 1468-1484.
Smyth, G. K. (2004). Linear models and empirical bayes methods for assessing differential expression in microarray experiments. *Stat Appl Genet Mol Biol,* **3**, Article3.
Soderberg, T. (2005). Biosynthesis of ribose-5-phosphate and erythrose-4-phosphate in archaea: a phylogenetic analysis of archaeal genomes. *Archaea,* **1**(5), 347-352.
Soppa, J. (2011). Functional genomic and advanced genetic studies reveal novel insights into the metabolism, regulation, and biology of Haloferax volcanii. Archaea, 2011, 602408. doi:10.1155/2011/602408
Soto, G. E., & Hultgren, S. J. (1999). Bacterial adhesins: common themes and variations in architecture and assembly. *J Bacteriol,* **181**(4), 1059-1071.
Southern, E. M. (1975). Detection of specific sequences among DNA fragments separated by gel electrophoresis. *J Mol Biol,* **98**(3), 503-517.
Spang, A., Saw, J. H., Jorgensen, S. L., Zaremba-Niedzwiedzka, K., Martijn, J., Lind, A. E., . . . Ettema, T. J. (2015). Complex archaea that bridge the gap between prokaryotes and eukaryotes. *Nature,* **521**(7551), 173-179.
Srivastava, P., & Kowshik, M. (2013). Mechanisms of metal resistance and homeostasis in haloarchaea. *Archaea, 2013*. doi:10.1155/2013/732864
Stams, A. J., & Oude Elferink, S. J. (1997). Understanding and advancing wastewater treatment. *Curr Opin Biotechnol,* **8**(3), 328-334.
Stan-Lotter, H., & Fendrihan, S. (2015). Halophilic Archaea: Life with Desiccation, Radiation and Oligotrophy over Geological Times. *Life (Basel),* **5**(3), 1487-1496.
Stewart, P. S., & Franklin, M. J. (2008). Physiological heterogeneity in biofilms. *Nat Rev Microbiol,* **6**(3), 199-210.
Storbeck, S., Rolfes, S., Raux-Deery, E., Warren, M. J., Jahn, D., & Layer, G. (2010). A novel pathway for the biosynthesis of heme in Archaea: genome-based bioinformatic predictions and experimental evidence. *Archaea, 2010*. doi:10.1155/2010/175050
Strahl, H., & Greie, J. C. (2008). The extremely halophilic archaeon *Halobacterium salinarum* R1 responds to potassium limitation by expression of the K+-transporting KdpFABC P-type ATPase and by a decrease in intracellular K+. *Extremophiles,* **12**(6), 741-752.
Sutherland, I. W. (2001). The biofilm matrix--an immobilized but dynamic microbial environment. *Trends Microbiol,* **9**(5), 222-227.
Switzer, R. C., 3rd, Merril, C. R., & Shifrin, S. (1979). A highly sensitive silver stain for detecting proteins and peptides in polyacrylamide gels. *Anal Biochem,* **98**(1), 231-237.
Syutkin, A. S., Pyatibratov, M. G., & Fedorov, O. V. (2014a). Flagella of halophilic archaea: differences in supramolecular organization. *Biochemistry (Mosc),* **79**(13), 1470-1482.
Syutkin, A. S., Pyatibratov, M. G., Galzitskaya, O. V., Rodriguez-Valera, F., & Fedorov, O. V. (2014b). *Haloarcula marismortui* archaellin genes as ecoparalogs. *Extremophiles,* **18**(2), 341-349.
Szabó, Z., Sani, M., Groeneveld, M., Zolghadr, B., Schelert, J., Albers, S. V., . . . Driessen, A. J. (2007a). Flagellar motility and structure in the hyperthermoacidophilic archaeon *Sulfolobus solfataricus*. *J Bacteriol,* **189**(11), 4305-4309.
Szabó, Z., Stahl, A. O., Albers, S. V., Kissinger, J. C., Driessen, A. J., & Pohlschroder, M. (2007b). Identification of diverse archaeal proteins with class III signal peptides cleaved by distinct archaeal prepilin peptidases. *J Bacteriol,* **189**(3), 772-778.

Takai, K., & Nakamura, K. (2011). Archaeal diversity and community development in deep-sea hydrothermal vents. *Curr Opin Microbiol,* **14**(3), 282-291.
Takao, M., Kobayashi, T., Oikawa, A., & Yasui, A. (1989). Tandem arrangement of photolyase and superoxide dismutase genes in *Halobacterium halobium*. *J Bacteriol,* **171**(11), 6323-6329.
Tarasov, V., Schwaiger, R., Furtwangler, K., Dyall-Smith, M., & Oesterhelt, D. (2011). A small basic protein from the brz-brb operon is involved in regulation of bop transcription in *Halobacterium salinarum*. *BMC Mol Biol,* **12**, 42.
Tarasov, V. Y., Pyatibratov, M. G., Tang, S. L., Dyall-Smith, M., & Fedorov, O. V. (2000). Role of flagellins from A and B loci in flagella formation of *Halobacterium salinarum*. *Mol Microbiol,* **35**(1), 69-78.
Tebbe, A., Klein, C., Bisle, B., Siedler, F., Scheffer, B., Garcia-Rizo, C., . . . Oesterhelt, D. (2005). Analysis of the cytosolic proteome of *Halobacterium salinarum* and its implication for genome annotation. *Proteomics,* **5**(1), 168-179.
Tebbe, A., Schmidt, A., Konstantinidis, K., Falb, M., Bisle, B., Klein, C., . . . Oesterhelt, D. (2009). Life-style changes of a halophilic archaeon analyzed by quantitative proteomics. *Proteomics,* **9**(15), 3843-3855.
Teufel, K., Bleiholder, A., Griesbach, T., & Pfeifer, F. (2008). Variations in the multiple tbp genes in different *Halobacterium salinarum* strains and their expression during growth. *Arch Microbiol,* **190**(3), 309-318.
Thoma, C., Frank, M., Rachel, R., Schmid, S., Nather, D., Wanner, G., & Wirth, R. (2008). The Mth60 fimbriae of *Methanothermobacter thermoautotrophicus* are functional adhesins. *Environ Microbiol,* **10**(10), 2785-2795.
Thomm, M. (1996). Archaeal transcription factors and their role in transcription initiation. *FEMS Microbiol Rev,* **18**(2-3), 159-171.
Tielen, P., Rosin, N., Meyer, A. K., Dohnt, K., Haddad, I., Jansch, L., . . . Jahn, D. (2013). Regulatory and metabolic networks for the adaptation of *Pseudomonas aeruginosa* biofilms to urinary tract-like conditions. *PLoS One,* **8**(8), e71845.
Torrents, E. (2014). Ribonucleotide reductases: essential enzymes for bacterial life. *Front Cell Infect Microbiol, 4*, 52.
Torrents, E., Aloy, P., Gibert, I., & Rodriguez-Trelles, F. (2002). Ribonucleotide reductases: divergent evolution of an ancient enzyme. *J Mol Evol,* **55**(2), 138-152.
Tripepi, M., Esquivel, R. N., Wirth, R., & Pohlschroder, M. (2013). *Haloferax volcanii* cells lacking the flagellin FlgA2 are hypermotile. *Microbiology,* **159**(Pt 11), 2249-2258.
Tripepi, M., Imam, S., & Pohlschroder, M. (2010). *Haloferax volcanii* flagella are required for motility but are not involved in PibD-dependent surface adhesion. *J Bacteriol,* **192**(12), 3093-3102.
Tripepi, M., You, J., Temel, S., Onder, O., Brisson, D., & Pohlschroder, M. (2012). N-glycosylation of *Haloferax volcanii* flagellins requires known Agl proteins and is essential for biosynthesis of stable flagella. *J Bacteriol,* **194**(18), 4876-4887.
Twellmeyer, J., Wende, A., Wolfertz, J., Pfeiffer, F., Panhuysen, M., Zaigler, A., . . . Oesterhelt, D. (2007). Microarray analysis in the archaeon *Halobacterium salinarum* strain R1. *PLoS One,* **2**(10), e1064.
Tych, K. M., Hoffmann, T., Batchelor, M., Hughes, M. L., Kendrick, K. E., Walsh, D. L., . . . Dougan, L. (2015). Life in extreme environments: single molecule force spectroscopy as a tool to explore proteins from extremophilic organisms. *Biochem Soc Trans,* **43**(2), 179-185.
van de Vossenberg, J. L., Driessen, A. J., & Konings, W. N. (1998). The essence of being extremophilic: the role of the unique archaeal membrane lipids. *Extremophiles,* **2**(3), 163-170.
Van, P. T., Schmid, A. K., King, N. L., Kaur, A., Pan, M., Whitehead, K., . . . Baliga, N. S. (2008). *Halobacterium salinarum* NRC-1 PeptideAtlas: toward strategies for

targeted proteomics and improved proteome coverage. *Journal of Proteome Research,* **7**(9), 3755-3764.
van Wolferen, M., Ajon, M., Driessen, A. J., & Albers, S. V. (2013). Molecular analysis of the UV-inducible pili operon from *Sulfolobus acidocaldarius*. *Microbiologyopen,* **2**(6), 928-937.
Veith, B., Herzberg, C., Steckel, S., Feesche, J., Maurer, K. H., Ehrenreich, P., . . . Gottschalk, G. (2004). The complete genome sequence of *Bacillus licheniformis* DSM13, an organism with great industrial potential. *J Mol Microbiol Biotechnol,* **7**(4), 204-211.
Ventosa, A., & Nieto, J. J. (1995). Biotechnological applications and potentialities of halophilic microorganisms. *World J Microbiol Biotechnol,* **11**(1), 85-94.
Verhees, C. H., Kengen, S. W., Tuininga, J. E., Schut, G. J., Adams, M. W., De Vos, W. M., & Van Der Oost, J. (2003). The unique features of glycolytic pathways in Archaea. *Biochem J,* **375**(Pt 2), 231-246.
Vidakovic, L. (2014). Zelladhäsion und Biofilmbildung von *Halobacterium salinarum*: Herstellung und Charakterisierung von Deletionsmutanten. Master thesis, Technische Universität Darmstadt, Darmstadt, Germany.
Vieira-Pires, R. S., Szollosi, A., & Morais-Cabral, J. H. (2013). The structure of the KtrAB potassium transporter. *Nature,* **496**(7445), 323-328.
Vilain, S., Pretorius, J. M., Theron, J., & Brozel, V. S. (2009). DNA as an adhesin: *Bacillus cereus* requires extracellular DNA to form biofilms. *Appl Environ Microbiol,* **75**(9), 2861-2868.
Voisin, S., Houliston, R. S., Kelly, J., Brisson, J. R., Watson, D., Bardy, S. L., . . . Logan, S. M. (2005). Identification and characterization of the unique N-linked glycan common to the flagellins and S-layer glycoprotein of *Methanococcus voltae*. *J Biol Chem,* **280**(17), 16586-16593.
Völkel, S. (2015). Einfluss von Schwermetallionen auf haloarchaeale Biofilme. Master thesis, Technische Universität Darmstadt, Darmstadt, Germany.
Wang, C., Lee, J., Deng, Y., Tao, F., & Zhang, L. H. (2012). ARF-TSS: an alternative method for identification of transcription start site in bacteria. *Biotechniques,* **52**(4). doi:10.2144/000113858
Wang, S., Liu, X., Liu, H., Zhang, L., Guo, Y., Yu, S., . . . Ma, L. Z. (2015). The exopolysaccharide Psl-eDNA interaction enables the formation of a biofilm skeleton in *Pseudomonas aeruginosa*. *Environ Microbiol Rep,* **7**(2), 330-340.
Wang, Y. A., Yu, X., Ng, S. Y., Jarrell, K. F., & Egelman, E. H. (2008). The structure of an archaeal pilus. *J Mol Biol,* **381**(2), 456-466.
Warren, M. J., Raux, E., Schubert, H. L., & Escalante-Semerena, J. C. (2002). The biosynthesis of adenosylcobalamin (vitamin B12). *Nat Prod Rep,* **19**(4), 390-412.
Wende, A., Furtwangler, K., & Oesterhelt, D. (2009). Phosphate-dependent behavior of the archaeon *Halobacterium salinarum* strain R1. *J Bacteriol,* **191**(12), 3852-3860.
Whitchurch, C. B., Tolker-Nielsen, T., Ragas, P. C., & Mattick, J. S. (2002). Extracellular DNA required for bacterial biofilm formation. *Science,* **295**(5559), 1487.
Whitehead, K., Kish, A., Pan, M., Kaur, A., Reiss, D. J., King, N., . . . Baliga, N. S. (2006). An integrated systems approach for understanding cellular responses to gamma radiation. *Mol Syst Biol,* **2**, 47.
Woese, C. R., & Fox, G. E. (1977). The concept of cellular evolution. *J Mol Evol, 10*(1), 1-6.
Woese, C. R., Kandler, O., & Wheelis, M. L. (1990). Towards a natural system of organisms: proposal for the domains Archaea, Bacteria, and Eucarya. *Proc Natl Acad Sci U S A,* **87**(12), 4576-4579.
Wolf, Y. I., & Koonin, E. V. (2013). Genome reduction as the dominant mode of evolution. *Bioessays,* **35**(9), 829-837.

Yabuta, Y., Kamei, Y., Bito, T., Arima, J., Yoneda, K., Sakuraba, H., . . . Watanabe, F. (2015). Functional and structural characteristics of methylmalonyl-CoA mutase from *Pyrococcus horikoshii*. *Biosci Biotechnol Biochem,* **79**(5), 710-717.

Yu, G. H., Yuan, J. P., & Zhong, N. S. (1990). Pulmonary Pseudomonas infections. *Zhonghua Nei Ke Za Zhi*, **29**(2), 94-97, 126.

Yu, W., Chen, Z., Shen, L., Wang, Y., Li, Q., Yan, S., . . . He, N. (2016). Proteomic profiling of *Bacillus licheniformis* reveals a stress response mechanism in the synthesis of extracellular polymeric flocculants. *Biotechnol Bioeng,* **113**(4), 797-806.

Yu, X., Goforth, C., Meyer, C., Rachel, R., Wirth, R., Schroder, G. F., & Egelman, E. H. (2012). Filaments from *Ignicoccus hospitalis* show diversity of packing in proteins containing N-terminal type IV pilin helices. *J Mol Biol,* **422**(2), 274-281.

Yu, Y. Q., Gilar, M., Lee, P. J., Bouvier, E. S., & Gebler, J. C. (2003). Enzyme-friendly, mass spectrometry-compatible surfactant for in-solution enzymatic digestion of proteins. *Anal Chem,* **75**(21), 6023-6028.

Zerulla, K., Chimileski, S., Nather, D., Gophna, U., Papke, R. T., & Soppa, J. (2014). DNA as a Phosphate Storage Polymer and the Alternative Advantages of Polyploidy for Growth or Survival. *PLoS One,* **9**(4).

Zerulla, K., & Soppa, J. (2014). Polyploidy in haloarchaea: advantages for growth and survival. *Frontiers in Microbiology, 5*.

Zhu, W., Smith, J. W., & Huang, C. M. (2010). Mass spectrometry-based label-free quantitative proteomics. *J Biomed Biotechnol, 2010.* doi:10.1155/2010/840518

Zillig, W., Palm, P., Reiter, W. D., Gropp, F., Puhler, G., & Klenk, H. P. (1988). Comparative evaluation of gene expression in archaebacteria. *Eur J Biochem,* **173**(3), 473-482.

Zolghadr, B., Klingl, A., Koerdt, A., Driessen, A. J., Rachel, R., & Albers, S. V. (2010). Appendage-mediated surface adherence of *Sulfolobus solfataricus*. *J Bacteriol,* **192**(1), 104-110.

Zolghadr, B., Weber, S., Szabo, Z., Driessen, A. J., & Albers, S. V. (2007). Identification of a system required for the functional surface localization of sugar binding proteins with class III signal peptides in *Sulfolobus solfataricus*. *Mol Microbiol,* **64**(3), 795-806.

Zuker, M. (2003). Mfold web server for nucleic acid folding and hybridization prediction. *Nucleic Acids Res,* **31**(13), 3406-3415.

Appendix

Table S1 Results of the search for putative pilins in the proteome of *Hbt. salinarum* R1 using FlaFind 1.2.

Symbol*	Gene number	Annotation	Length [aa]	Fla Find[1]	Cleavage motif[2]	No. of TMH[2]	DUF1628[3]	NetNGlyc[4]	Comments[5]
pilA1	**OE1186A1F**	**DUF1628 protein**	**122**	**+**	**RAVS**	**1**	**+**	**3**	***Hfx. pilA4***
pilA2	**OE1334R**	**Uncharacterized protein**	**122**	**+**	**RGQA**	**1**	**–**	**1**	**pil-2 locus**
pilA3	**OE1336R**	**Uncharacterized protein**	**225**	**+**	**RGQA**	**1**	**–**	**2**	**pil-2 locus**
pilA4	**OE1340R**	**Uncharacterized protein**	**240**	**+**	**RGQS**	**1**	**–**	**1**	**pil-2 locus**
pilA5	**OE1476R**	**Uncharacterized protein**	**136**	**+**	**RGLL**	**1**	**–**	**0**	
pilA6	**OE1501F**	**Uncharacterized protein**	**129**	**+**	**RAAT**	**2**	**–**	**0**	
hcpH	OE2157F	Halocyanin HcpH	149	+	RAFL	1	–	n.d.	
htr18	OE2195F	Transducer protein Htr18	816	+	KAAV	2	–	n.d.	
	OE2233F	Uncharacterized protein	80	+	RAAA	2	–	n.d.	
	OE2330R	Uncharacterized protein	366	+	RAFL	1	–	n.d.	
flgB1	OE2397F	Archaellin B1	193	+	RGQV	1	–	n.d.	B locus
flgB2	OE2398F	Archaellin B2	196	+	RGQV	1	–	n.d.	B locus
flgB3	OE2399F	Archaellin B3	193	+	RGQV	1	–	n.d.	B locus
	OE2444F	Uncharacterized protein	270	+	KGAI	2	–	n.d.	
	OE2456F	DUF2061 protein	69	+	KAAS	1	–	n.d.	
flgA1	OE2469F	Archaellin A1	196	+	RGQV	1	–	n.d.	A locus
flgA2	OE2470F	Archaellin A2	194	+	RGQV	1	–	n.d.	A locus
pilA7	**OE2531F**	**Uncharacterized protein**	**326**	**+**	**RGLL**	**1**	**–**	**0**	
pilA8	**OE2586F**	**Uncharacterized protein**	**394**	**+**	**DAMV**	**1**	**–**	**6**	
flgX	OE2695F	Flagellin X	207	+	RGQV	1	–	n.d.	
	OE3163F	DUF2892 protein	69	+	DALA	2	–	n.d.	
	OE3292F	Uncharacterized protein	666	+	RGVT	1	–	n.d.	
	OE3744R	Probable cell surface glycoprotein	1363	+	RAVA	1	–	n.d.	
pilA9	**OE3768F**	**Uncharacterized protein**	**173**	**+**	**RAAT**	**1**	**+**	**0**	***Hfx. pilA5***
	OE3937R	Uncharacterized protein	89	+	RGAV	2	–	n.d.	
pilA10	**OE3996R**	**DUF1628 protein**	**153**	**–**	**(RGSA)**	**1**	**+**	**0**	***Hfx. pilA3***
	OE4043R	Uncharacterized protein	195	+	RGLA	1	–	n.d.	
pilA11	**OE4050F**	**DUF1628 protein**	**125**	**–**	**(RATS)**	**1**	**+**	**1**	***Hfx. pilA2***
	OE4382R	Uncharacterized protein	92	+	KAVM	2	–	n.d.	
	OE4421B1F	Uncharacterized protein	64	+	RGAL	2	–	n.d.	
	OE4523F	Uncharacterized protein	266	+	RAAV	2	–	n.d.	
	OE4682A1R	Uncharacterized protein	252	+	DAVS	1	–	n.d.	
	OE4748F	Uncharacterized protein	393	+	KALI	1	–	n.d.	
csg	OE4759F	Cell surface glycoprotein (S-layer)	852	+	RAVL	2	–	n.d.	
kdpF	OE5051A1F	K^+-transporting ATPase subunit F	234	+	EAVL	1	–	n.d.	
gvpM2	OE5112R	Gas vesicle protein	73	+	DGAV	1	–	n.d.	
	OE5248F	Uncharacterized protein	545	+	RAAI	2	–	n.d.	
pilA12	**OE6130F**	**DUF1628 protein**	**163**	**+**	**RGVS**	**1**	**+**	**2**	***Hfx. pilA3***

* Gene symbols of putative pilins (bold) are based on the ascending gene numbers. [1] Plus, positive FlaFind 1.2 results, *i.e.* presence of type IV pilin-like signatures; hyphen, negative results. [2] Predicted by FlaFind 1.2, motifs in brackets assigned manually. [3] According to HaloLex (www.halolex.mpg.de); plus, DUF1628 present; hyphen, no DUF1628. [4] Number of potential N-glycosylation sites predicted by NetNGlyc 1.0 Server; n.d., not determined. [5] Based on BLASTp search against *Hbt. salinarum* R1 and *Haloferax* sp., respectively.

Figure S1 Multiple protein sequence alignment of the *Hbt. salinarum* R1 archaellins (Flg) and putative pilins (Pil). Gene numbers and symbols are indicated. Also exemplaric adhesion pilins of *Haloferax volcanii* (HVOA0633) and *Sulfolobus acidocaldarius* (Saci2314) are shown. (http://mafft.cbrc.jp/alignment/server)

Abbreviations

%	percent
°C	degrees Celcius
A	Ampere
AO	Acridine orange
arCOG	archaeal Clusters of Orthologous Genes
ARF-TSS	Adaptor- and radioactivity-free determination of transcriptional start sites
BLAST	Basic Local Alignment Search Tool
bp	base pairs
BRE	transcription factor B recognition element
cDNA	complementary DNA
CLSM	confocal laser scanning microscopy
ConA	Concanavalin A
C_T	cycle of threshold
C-terminus	carboxy-terminus
Da	Dalton
DNA	desoxyribonucleic acid
ddH_2O	double deionized water
Δ gene	gene deletion
DIA	data-independent acquisition
DIG	digoxigenin
DMSO	dimethyl sulfoxide
e.g.	*exempli gratia* (for example)
eDNA	extracellular DNA
EPS	extracellular polymeric substances
et al.	*et alii* (and others)
FC	fold change
FDR	false discovery rate
g	gram
gDNA	Genomic DNA
h	hour
Hbt. salinarum	*Halobacterium salinarum*
Hfx. volcanii	*Haloferax volcanii*
HGT	horizontal gene transfer
i.e.	*id est* (that is)
KEGG	Kyoto Encyclopedia of Genes and Genomes
L	liter
LAU/mm2	light absorbing units per square millimeter
LC-MS/MS	Liquid chromatography tandem mass spectrometry
m	meter
M	molar
min	minute
m/z	mass per charge
MOPS	3-(N-Morpholino)-propane sulfonic acid
mRNA	messenger RNA
MS	mass spectrometry
NCBI	National Center for Biotechnology Information
nLC	nano liquid chromatography

nm	nanometer
nt	nucleotide
N-terminus	amino-terminus
OD_{600}	optical density at 600 nm
ORF	open reading frame
p.	page
P. aeruginosa	*Pseudomonas aeruginosa*
PAA	polyacrylamide
PC	principle component analysis
PCA	principle component analysis
PCM	phase contrast microscopy
PCR	Polymerase chain reaction
PI	Propidium iodide
qRT-PCR	Quantitative reverse transcription PCR
RNA	ribonucleic acid
ROS	reactive oxygen species
rpm	rounds per minute
r-protein	ribosomal protein
RQ	relative quantification
rRNA	ribosomal RNA
RT-PCR	Reverse transcription PCR
s	second
S. acidocaldarius	*Sulfolobus acidocaldarius*
S. solfataricus	*Sulfolobus solfataricus*
S. tokodaii	*Sulfolobus tokodaii*
SD	standard deviation
SDS-PAGE	Sodium dodecyl sulfate polyacrylamide gel electrophoresis
SEM	scanning electron microscopy
Suppl.	Supplementary
SWATH	Sequential window acquisition of all theoretical fragment ion spectra
T4P	type IV pili
TCA	trichloroacetic acid
TEM	transmission electron microscopy
TMAO	trimethylamine oxide
TMH	transmembrane helix
TOF	time of flight
TSS	transcription start site
U	unit
UniProtKB	UniProt Knowledgebase
UV	ultra-violet
V	Volt
v/v	volume per volume
w/v	weight per volume

Curriculum vitae

Personal information

Name	Gerald Losensky
Date of birth	28th August 1985
Place of birth	Groß-Umstadt, Germany

Academic history

2011 – 2016	Doctorate at the Technische Universität Darmstadt, Department of Biology
	Workgroup: Microbiology and Archaea
	Advisors: Prof. Dr. Felicitas Pfeifer and Dr. Sabrina Fröls
	Project title: "Shedding light on adhesion and biofilm formation of *Halobacterium salinarum* R1"
2011	Diploma thesis at the Technische Universität Darmstadt, Department of Biology
	Workgoup: Microbiology and Archaea
	Advisors: Prof. Dr. Felicitas Pfeifer and Dr. Sabrina Fröls
	Project title: "Untersuchungen auf Proteinebene zur Biofilmbildung halophiler Archaea"
2006 – 2011	Study of Biology at the Technische Universität Darmstadt
	Thematic priority: Microbiology, Biochemistry, Cell, Radiation and Developmental Biology
	Degree: Diplom-Biologe

Educational history

1998 – 2005	Max-Planck-Schule (Grammar school), Groß-Umstadt
	Advanced courses: Biology and Mathematics
	Degree: Allgemeine Hochschulreife (Abitur)

Danksagung

An erster Stelle bedanke ich mich bei Frau Prof. Dr. Felicitas Pfeifer, für die Möglichkeit, diese Arbeit in ihrer Arbeitsgruppe anfertigen zu dürfen, bei deren Ausgestaltung mir alle Freiheiten gelassen wurden. Ich bedanke mich darüber hinaus für ihre Unterstützung und die wertvollen wissenschaftlichen Ratschläge.

Mein besonderer Dank gilt Dr. Sabrina Fröls, die mich so lange hervorragend betreut und „ertragen“ hat. Danke, dass Du mir während meiner gesamten Doktorandenzeit mit Rat und Tat zur Seite standest, mich immer motiviert hast und vielen, vielen Dank für die äußerst angenehme Zusammenarbeit im „Biofilmhauptquartier“.

Bei PD Dr. Arnulf Kletzin bedanke ich mich für die Hilfe bei allerlei Problemen, die vielen hilfreichen Tipps und dafür, dass er sich als zweiter Referent dieser Arbeit bereit erklärt hat.

Ein großes Dankeschön geht an unsere „gute Seele“ Gisela Schaffert, die im Hintergrund die Fäden spinnt und alles irgendwie organisiert bekommt. Vielen Dank auch für die stets angenehme tea- bzw. Müsli-time.

Vielen Dank an Dr. Christof Lenz und Prof. Klaus Jung, für die erfolgreiche Kooperation im Rahmen des Proteomprojekts.

Besten Dank an die „lieben Kollegen“ und Ehemaligen aus dem Biofilmlabor, allen voran meinen Doktorbruder Johannes Born, sowie Sabrina Völkel und Lucia Vidakovic, mit denen ich die längste Zeit im Labor verbracht habe. Das Arbeitsumfeld bei uns war stets super und ich bin immer gerne auf die Arbeit gekommen. Daran hatte auch die Nachbar-AG mit Dennis Petrasch, Uwe Pöll, „Haasi“, „Rühli“ und Renate Fröhlich großen Anteil. Des Weiteren möchte ich mich bei den gesamten AGs Pfeifer und Kletzin mitsamt den Technischen Assistentinnen, Spülfrauen und allen Ehemaligen bedanken, die irgendwann mal mit mir „die Laborbank gedrückt“ haben.

Vielen Dank auch an die Kollegen aus den AGs Simon und Göringer. Danke für die geborgten Chemikalien und die angenehmen Unterhaltungen im Labor, zwischen Tür und Angel, auf dem Flur oder im Pausenraum.

Ich bedanke mich ganz herzlich bei Jeanette, die mich immer unterstützt und ihren Schreibtisch mit mir geteilt hat.

Mein großer Dank gilt auch meiner Familie. Ich bedanke mich bei meiner Mutter für die fortwährende Unterstützung und Motivation. Danke Dani und Steffen, dass ihr immer an mich geglaubt und mich angespornt habt.

Ehrenwörtliche Erklärung

Die vorliegende Arbeit wurde unter der Leitung von Frau Prof. Dr. Felicitas Pfeifer im Fachbereich Biologie, Fachgebiet Mikrobiologie und Archaea, der Technischen Universität Darmstadt in der Zeit von November 2011 bis Mai 2016 angefertigt.

Ein Teil der vorliegenden Arbeit wurde in der Arbeitsgruppe von Prof. Dr. Henning Urlaub und Dr. Christof Lenz im Universitätsklinikum Göttingen, Abteilung Klinische Chemie und am Max-Planck-Institut für Biophysikalische Chemie, Abteilung Bioanalytische Massenspektrometrie im Rahmen einer Kooperation durchgeführt.

Ich erkläre hiermit ehrenwörtlich, dass ich die vorliegende Arbeit entsprechend den Regeln guter wissenschaftlicher Praxis selbstständig und ohne unzulässige Hilfe Dritter angefertigt habe.

Sämtliche aus fremden Quellen direkt oder indirekt übernommenen Gedanken sowie sämtliche von Anderen direkt oder indirekt übernommenen Daten, Techniken und Materialien sind als solche kenntlich gemacht. Die Arbeit wurde bisher bei keiner anderen Hochschule zu Prüfungszwecken eingereicht.

Darmstadt, den 12.05.2016

Gerald Losensky